NASA CR-121126

# INVESTIGATION OF NOISE SUPPRESSION BY SONIC INLETS FOR TURBOFAN ENGINES

## Volume I: Program Summary

D6-40855

July 1973

by F. Klujber, J. C. Bosch,
R. W. Demetrick, and W. L. Robb

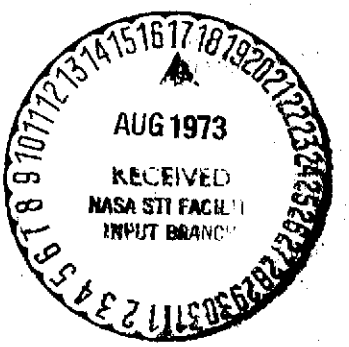


BOEING COMMERCIAL AIRPLANE COMPANY

prepared for

NATIONAL AERONAUTICS AND SPACE ADMINISTRATION

NASA Lewis Research Center
Contract NAS3-15574

| 1. Report No. | 2. Government Accession No. | 3. Recipient's Catalog No. |
|---|---|---|
| NASA CR-121126 | | |

| 4. Title and Subtitle | 5. Report Date |
|---|---|
| INVESTIGATION OF NOISE SUPPRESSION BY SONIC INLETS FOR TURBOFAN ENGINES—Volume I: Program Summary | July 1973 |
| | 6. Performing Organization Code |
| 7. Author(s) | 8. Performing Organization Report No. |
| F. Dlujber, J. C. Bosch, R. W. Demetrick, and W. L. Robb | D6-40855 |
| | 10. Work Unit No. |
| 9. Performing Organization Name and Address | 11. Contract or Grant No. |
| Boeing Commercial Airplane Company<br>P. O. Box 3707<br>Seattle, Washington 98124 | NAS3-15574 |
| | 13. Type of Report and Period Covered |
| 12. Sponsoring Agency Name and Address | Contractor report |
| National Aeronautics and Space Administration<br>Washington, D.C. 20546 | 14. Sponsoring Agency Code |

15. Supplementary Notes

NASA Project Manager, J. P. Lewis

16. Abstract

Results of a current program (NAS3-15574) for sonic inlet technology development are presented. This program includes configuration and mechanical design selection of concepts, aerodynamic design description of the models, and results of test evaluation. Several sonic inlet concepts were tested and compared for aerodynamic and acoustic performance. Results of these comparative evaluations are presented. Near-field measurements were taken inside several of the inlet models. Results of these tests are discussed with respect to the effect of Mach number gradients on noise attenuation and rotor shock wave attenuation, and boundary layer effects on noise propagation. The test facilities and experimental techniques employed are described briefly.

| 17. Key Words (Suggested by Author(s)) | 18. Distribution Statement |
|---|---|
| Sonic inlet<br>Inlet performance<br>Noise attenuation | Unclassified—unlimited |

| 19. Security Classif. (of this report) | 20. Security Classif. (of this page) | 21. No. of Pages | 22. Price* |
|---|---|---|---|
| Unclassified | Unclassified | 220 | |

*For sale by the National Technical Information Service, Springfield, Virginia 22151

# INVESTIGATION OF NOISE SUPPRESSION BY SONIC INLETS FOR TURBOFAN ENGINES

BY: F. KLUJBER,
J. C. BOSCH, R. W. DEMETRICK, AND W. L. ROBB

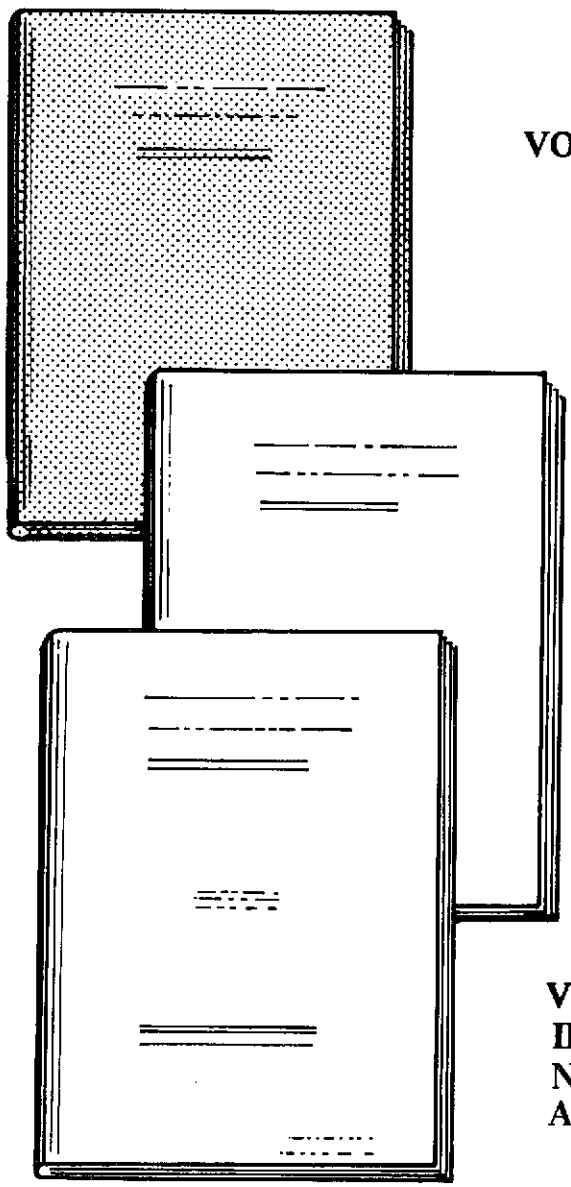

## VOLUME I: PROGRAM SUMMARY

CR-121126 D6-40855

## VOLUME II: APPENDIXES

CR-121127 D6-40855-1

A. MECHANICAL DESIGN STUDY AND TEST CONFIGURATION SELECTION

B. DETAIL DESIGN OF MODELS

C. INSTRUMENTATION DETAILS

D. DATA ANALYSIS PROCEDURE

E. CONCEPT SCREENING.

## VOLUME III: AN EXPERIMENTAL INVESTIGATION OF THE INTERNAL NOISE FIELD OF TWO MODEL AXISYMMETRIC SONIC INLETS

CR-121128 D6-40818

# CONTENTS

# 1.0 SUMMARY

This report summarizes the results of work conducted by The Boeing Company under NASA contract NAS3-15574, "Investigation of Noise Suppression of Sonic Inlets for Turbofan Engines".

The program incorporated analytical and experimental investigations to establish a design technology base for sonic inlets for STOL propulsion system inlet noise reduction. The objective of the program was to identify a practical inlet design, utilizing the concept of choking for inlet noise reduction. This inlet noise reduction requirement stems from the demonstrated low aft arc noise level that has been achieved by the augmentor wing propulsion system concept. As a result, the dominant noise source is that radiated forward by the engine fan. Preliminary analyses indicated a required inlet noise suppression of 20 to 30 PNdB at a 500-ft sideline distance. By the demonstration of the objective inlet noise level reduction, the augmentor wing STOL airplane noise could be reduced below 95 PNdB at a 500-ft sideline. This program has demonstrated that the noise level objectives can be achieved and even exceeded by sonic inlets, with aerodynamic losses substantially lower than previous sonic inlet program results indicated. This performance was demonstrated with a realistic inlet length and without the use of sophisticated flow control devices.

The investigation was accomplished by analytical and mechanical design studies and experimental investigation of sonic inlet models on a fan rig test facility in an anechoic chamber.

The program was initiated with a sonic inlet configuration and concept selection study. Preliminary mechanical design layouts were made of several promising sonic inlet concepts. The inlet concepts were studied in two separate groups, consisting of single-passage inlets (throat undivided) and multipassage inlets (throat subdivided). All concepts were evaluated in terms of performance, mechanical design, and operational characteristics, and potential problem areas were identified. On the basis of this concept screening study, two single-passage and two multipassage inlets were selected for preliminary test evaluation. These were:

- Translating centerbody
- Contracting cowl wall
- Retractable radial vane
- Double-articulated radial vane

A schematic representation of each of these concepts is shown on figure 1.

The four selected inlet models were designed for test evaluation. The basic design weight flows for all configurations at full scale were as follows:

| | | |
|---|---|---|
| Approach | = | 402 lb/sec |
| Takeoff | = | 515 lb/sec |
| Maximum Cruise | = | 475 lb/sec |

These were based on engine criteria used for system design and evaluation studies of jet STOL aircraft.

The design procedures were similar for both of the single-passage inlets, with throat and diffuser exit areas defined by the engine airflow requirements; the prime variables were length (L/D, inlet length to fan diameter ratio) and diffuser area distribution. These variables were initially selected on a trial-and-error basis and evaluated with the aid of a computerized potential flow program combined with a boundary layer program. Surface Mach number, boundary layer shape factors, and boundary layer thickness were calculated and plotted as a function of diffuser length. The criterion used for inlet optimization was the attainment of minimum length without boundary layer separation or excessive boundary layer thickness.

The multipassage inlet models were designed by the use of a free-stream axisymmetric radial equilibrium turbomachinery design program. Standard NACA airfoil shapes were used in the airfoil selections. The basic design objective for the multipassage inlets was to attain uniform radial Mach number distribution.

Two configurations were designed for the translating centerbody concept, one with an L/D = 1.3, and the other with an L/D = 1. For each of the other inlet models, one test configuration was designed with an L/D = 1. All models were fabricated and tested for the approach power weight flow range. This was considered the most critical operating region for performance comparison.

The tests were conducted in an anechoic chamber utilizing a 12-in.-diameter fan test vehicle (fig. 2). The wall between the test chamber and the anechoic room is acoustically impermeable, ensuring that measurements taken in the acoustic chamber were not influenced by fan aft-radiated noise. Acoustic measurements were taken by a microphone array on a 10-ft radius at 10° intervals. Aerodynamic data were also acquired during testing for evaluation of inlet recovery, distortion, and throat Mach number.

Overall results of these tests are shown in figure 3. All performance parameters are shown in terms of inlet normalized Mach numbers ($M_N$).* Inlet noise reduction, inlet total pressure recovery,

*Normalized Mach number was introduced to eliminate large deviations in calculated Mach numbers for the different test configurations due to the effective flow area differences in configurations from the design area values. For the choked condition the Mach number for all configurations was defined as unity.

and flow distortion are shown for the models tested. Based on the results of these tests, two configurations were selected for final evaluation. The L/D = 1 translating centerbody inlet was chosen for the single-passage and the radial vane sonic inlet for the multipassage type.

Design modifications were made on these models as deemed necessary to improve performance prior to final testing. Detailed inlet exit-plane flow profile measurements were performed. A limited amount of distortion simulation was performed by cross-wind blowing on these static tests. The models were tested in takeoff and cruise configurations in addition to the approach configuration.

The test results for the final models are shown on figures 4 and 4a. The following conclusions can be drawn from these results:

- A sonic inlet can be designed to produce inlet noise reduction in the range of 25 to 30 PNdB with less than 2% inlet recovery loss on approach and less than 1% in takeoff and cruise operation. Inlet flow distortion effects remain within acceptable limits for satisfactory engine/inlet compatibility.

- Inlet noise reduction in excess of 40 PNdB is possible with sonic inlets, with increased performance loss.

- Single-passage inlets are superior to multipassage inlets in terms of inlet recovery. The trend in terms of total pressure distortion is reversed.

- It has been demonstrated that using the latest available design technology, sonic inlets can be designed within an L/D limit of unity consistent with the objective of this program.

- Fan operating line and stall margin investigations have shown that no significant effect of stall margin change has occurred as a result of flow distortion created by sonic inlets (fig. 4a).

A translating centerbody inlet has been tested with acoustic lining. The lining effectiveness is shown on figure 5. The tests have shown that some inlet throat Mach number reduction can be achieved using acoustic lining. The benefits depend on the particular noise reduction level desired.

Concurrently with the concept selection effort, near-field noise measurements were taken inside sonic inlets to gain some understanding of the noise attenuation mechanisms involved with large Mach number gradients such as those existing at or near sonic flow conditions. The experimental approach was chosen for lack of analytical tools in this technology area.

The objectives of these experiments were to provide some insights into potential problem areas that could prevent the achievement of the ambitious goals set for the program. Of specific interest were Mach number gradient effects on noise attenuation, shock wave propagation through the sonic throat, and noise leakage through the boundary layer. Another point of interest was noise generated by the sonic plane.

A specially constructed probe for the measurement of noise and static pressure measurement in the free stream was built. Two contracting cowl wall inlets were evaluated. The near-field instrument probe and typical survey location for these tests are shown on figure 6. Results of these experiments were extremely useful in making design decisions for the rest of the program, and the information obtained is considered unique. Significant conclusions of these experiments are summarized below:

- Increasing the inlet throat Mach number from about 0.5 to 1.0 resulted in an increasing noise attenuation at blade passing frequency (figs. 7 and 8).

- The rate of decay of the blade passing tone was found to be less on the centerline than near the outer wall. This was attributed to the radial Mach number gradient in the throat area (figs. 9 and 10).

- The multiple pure tone ("buzz-saw") noise, which was only observed at fan blade speeds above the sonic velocity, did not propagate through the inlet throat plane (fig. 11).

- No evidence was found of noise leakage at blade passing frequency through the inlet throat boundary layer (fig. 12).

- No significant noise generation by the sonic plane was observed (fig. 13).

This program has demonstrated significant improvement over earlier programs in both acoustic and aerodynamic performance for sonic or high Mach number inlets. Because of this, it is believed that sonic inlet technology can be applied in a wide variety of applications in aircraft inlet noise reduction. Other gas turbine engine installations may also benefit from the technology and performance potential demonstrated in this program for sonic inlets.

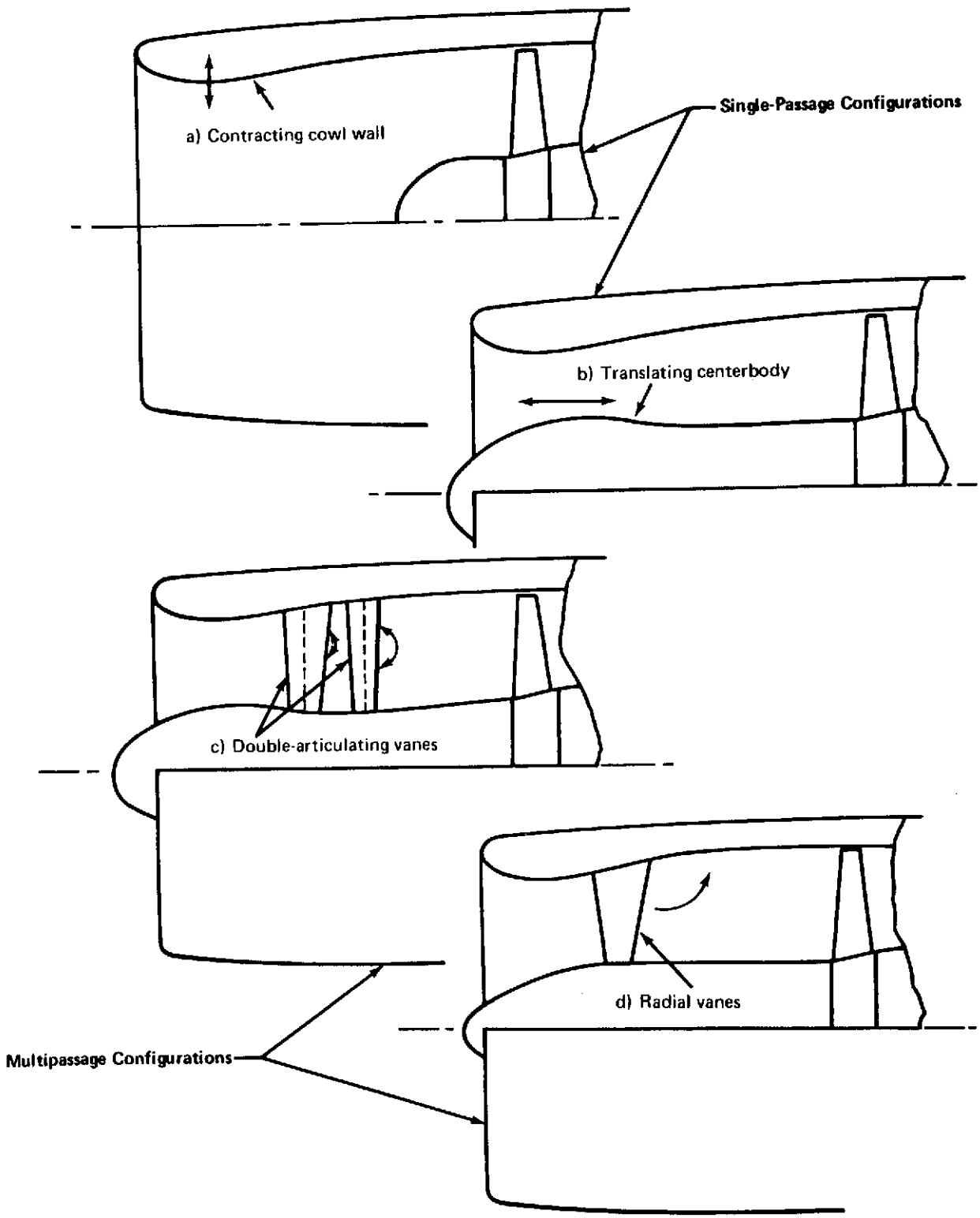


*FIGURE 1.—INLET TEST CONFIGURATIONS—APPROACH MODE*

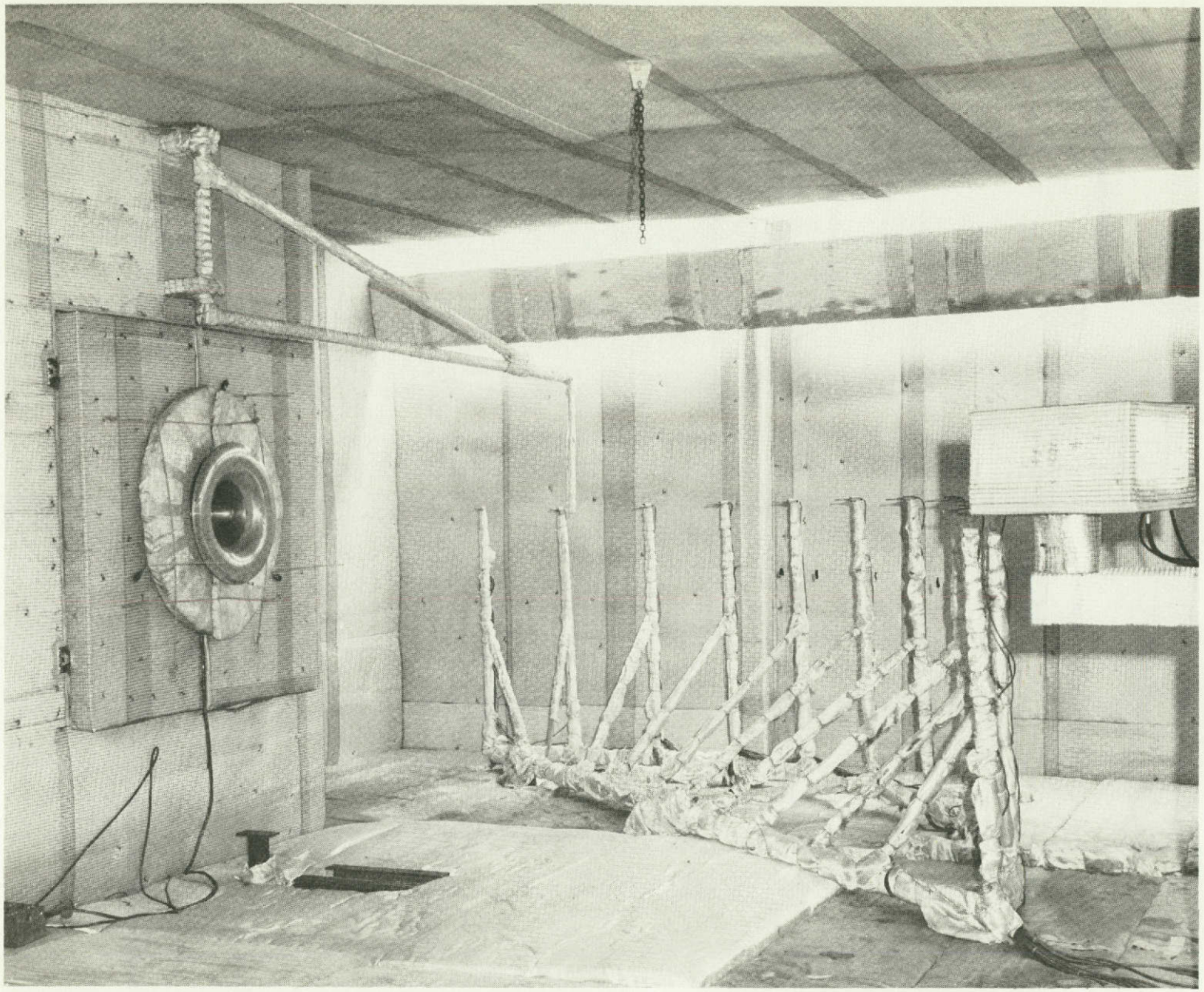

*FIGURE 2.–ANECHOIC ROOM WITH MODEL AND BELLMOUTH INSTALLED*

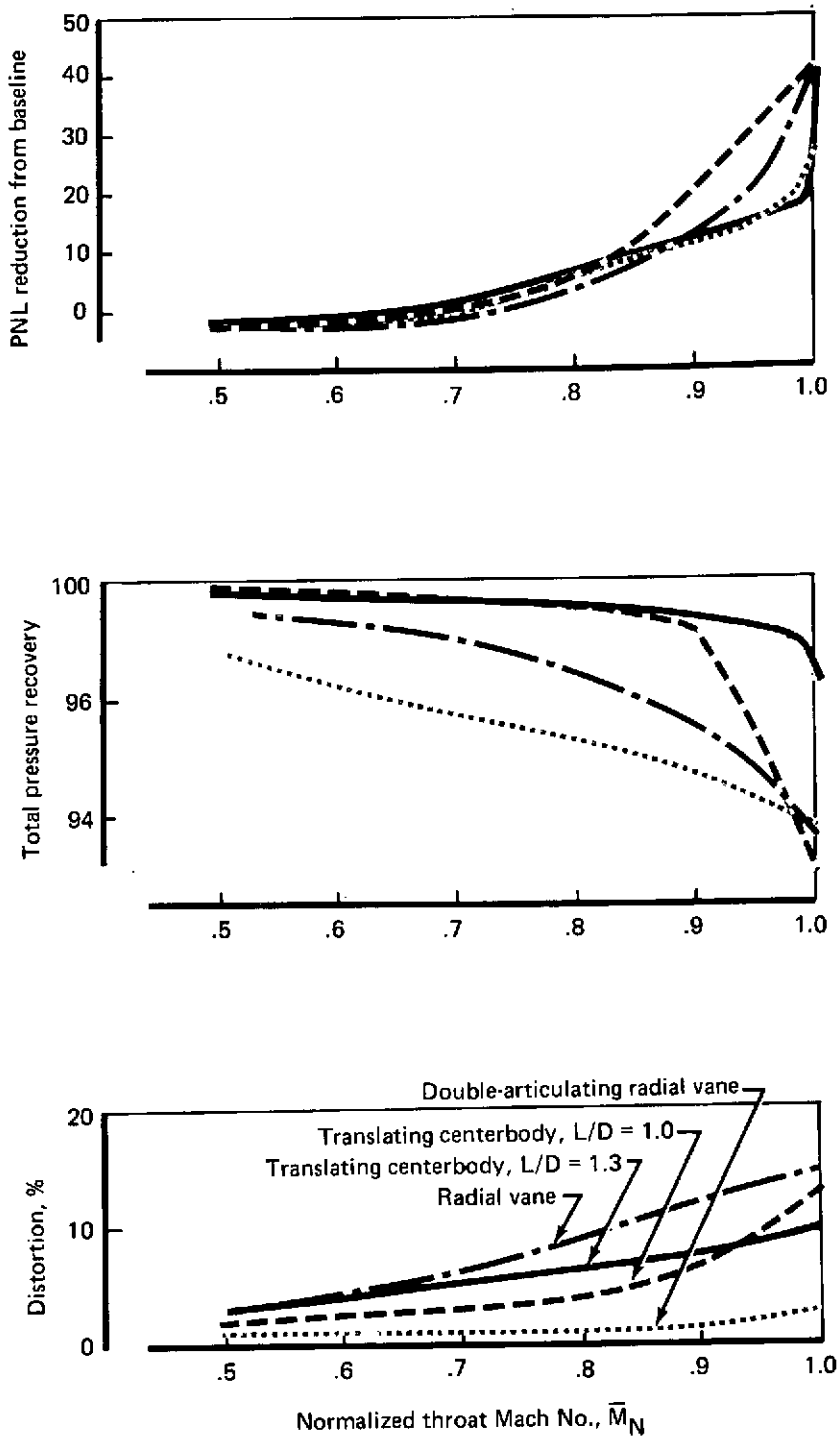


*FIGURE 3.–COMPARISONS OF TRANSLATING CENTERBODY WITH MULTIPASSAGE INLETS (APPROACH)*

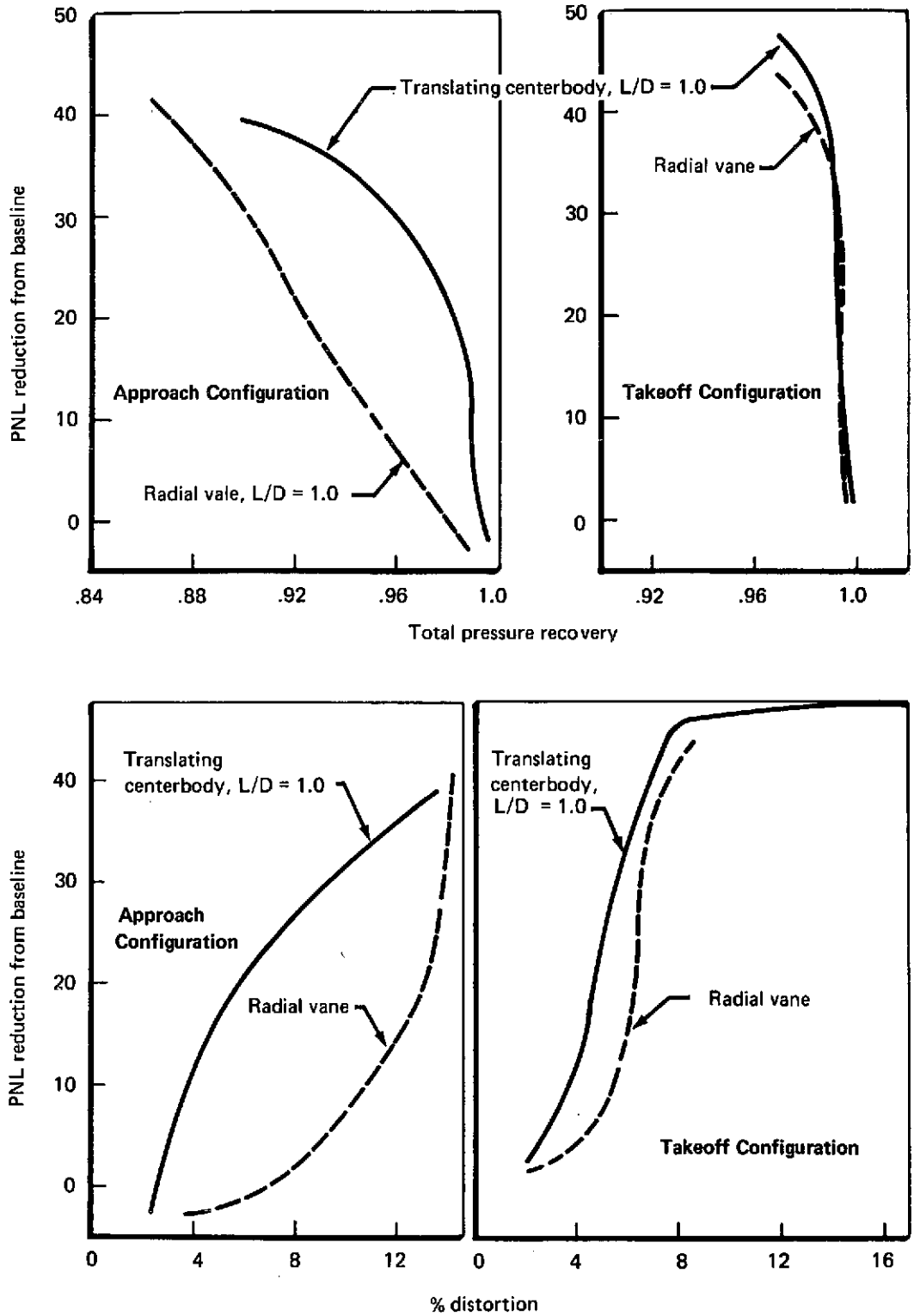


*FIGURE 4.–COMPARISONS OF TRANSLATING CENTERBODY VS RADIAL VANE INLETS (APPROACH AND TAKEOFF)*

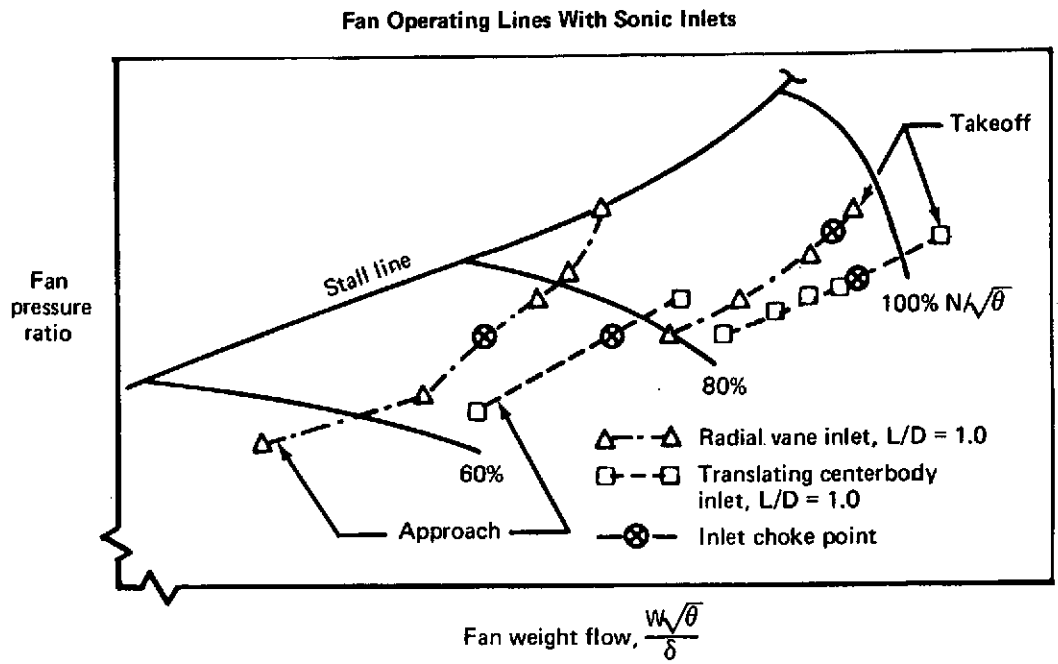


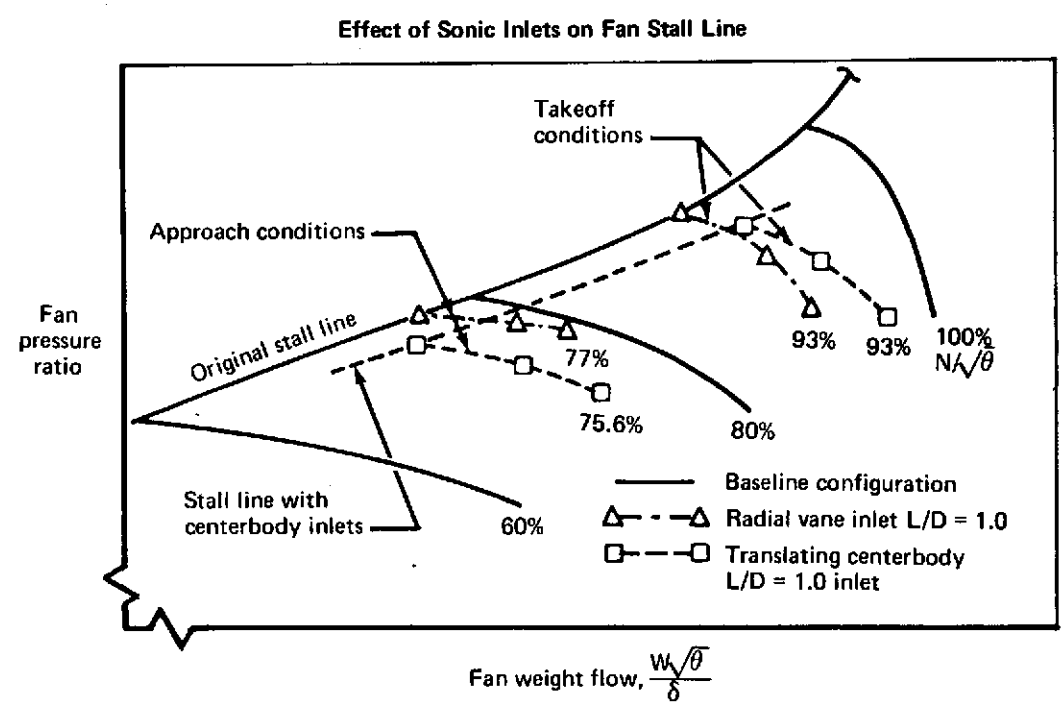


*FIGURE 4A.—FAN OPERATING LINES AND FAN STALL LINE WITH SONIC INLETS*

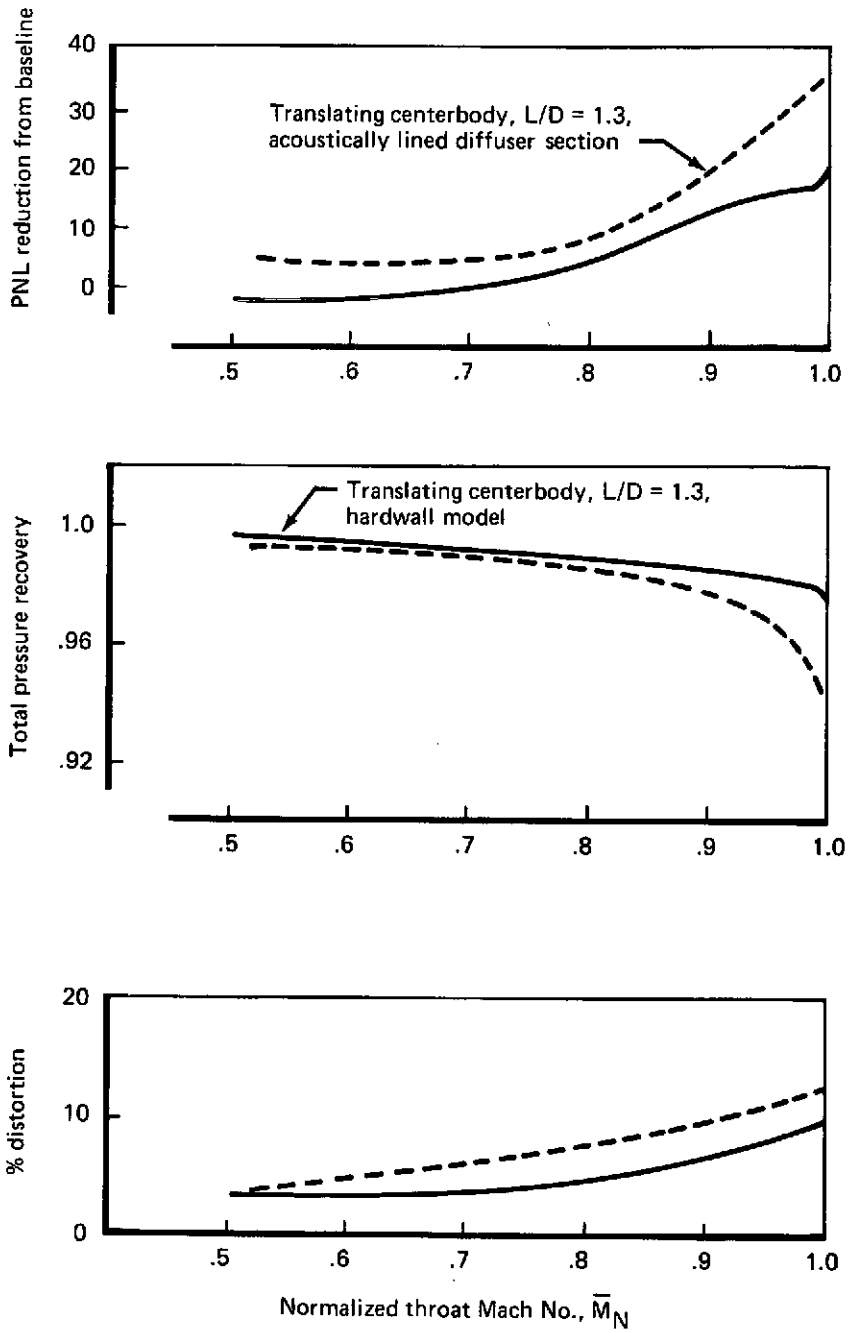


*FIGURE 5.—EFFECTS OF ACOUSTIC LINING ON THE L/D = 1.3 TRANSLATING CENTERBODY (APPROACH)*

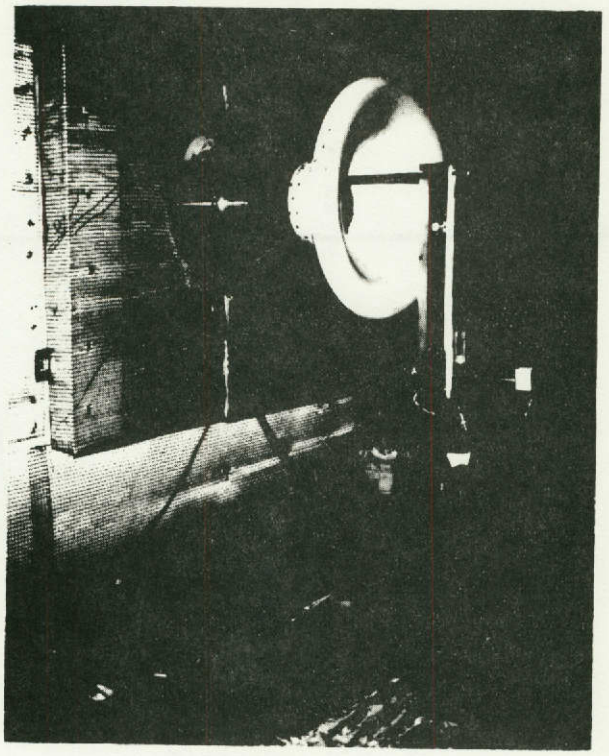

Test Setup

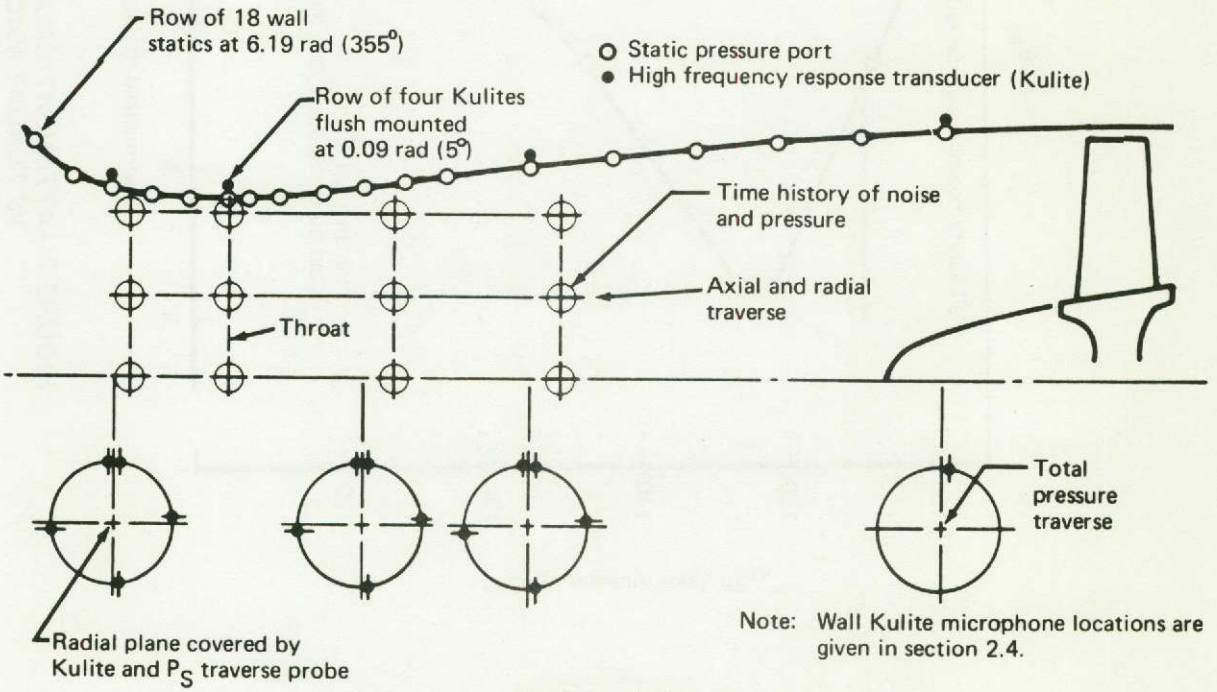


Instrumentation

*FIGURE 6.–TEST SETUP AND INSTRUMENTATION*

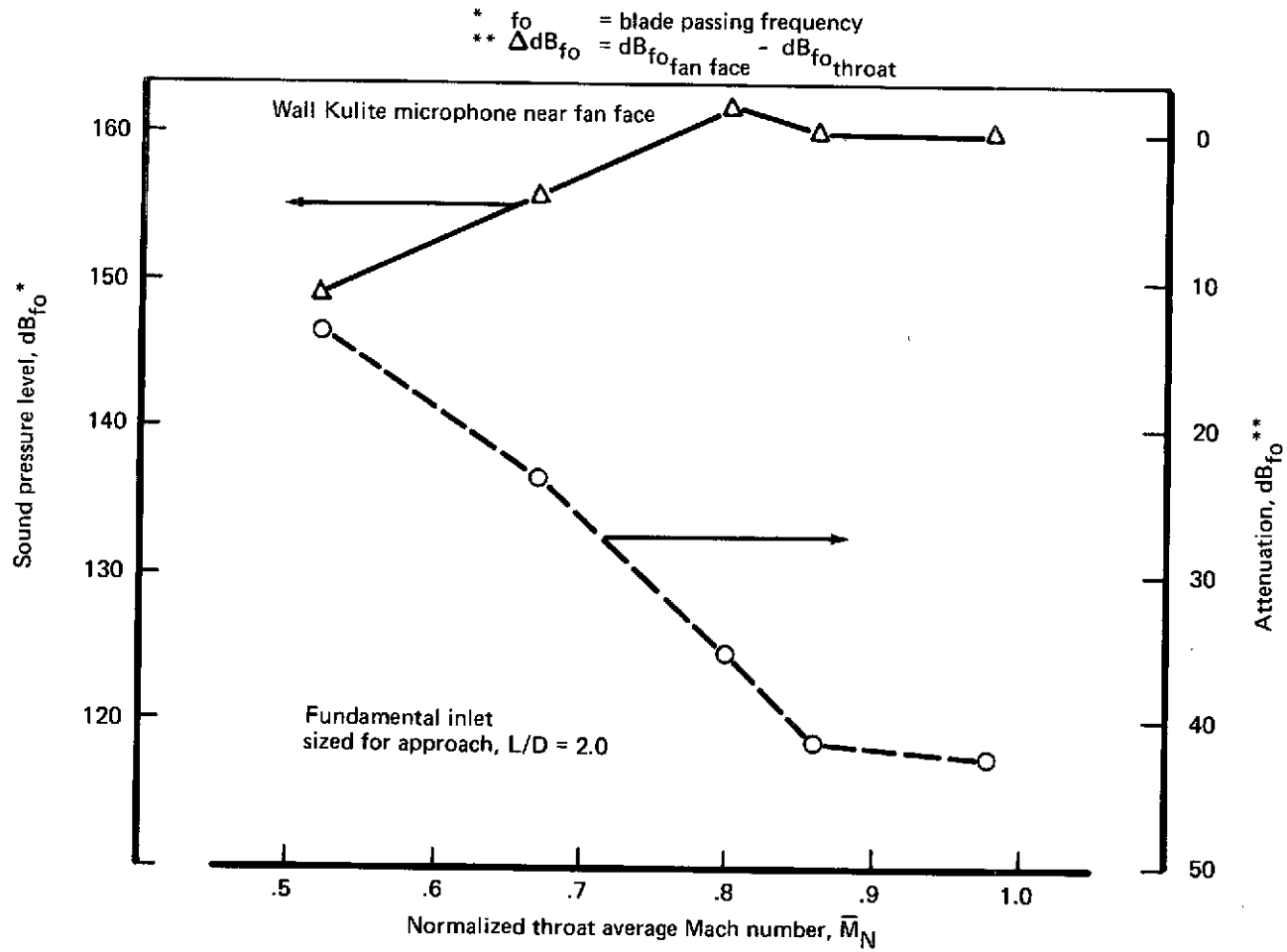


*FIGURE 7.–ATTENUATION AT BLADE PASSING FREQUENCY VS THROAT MACH NUMBER (APPROACH)*

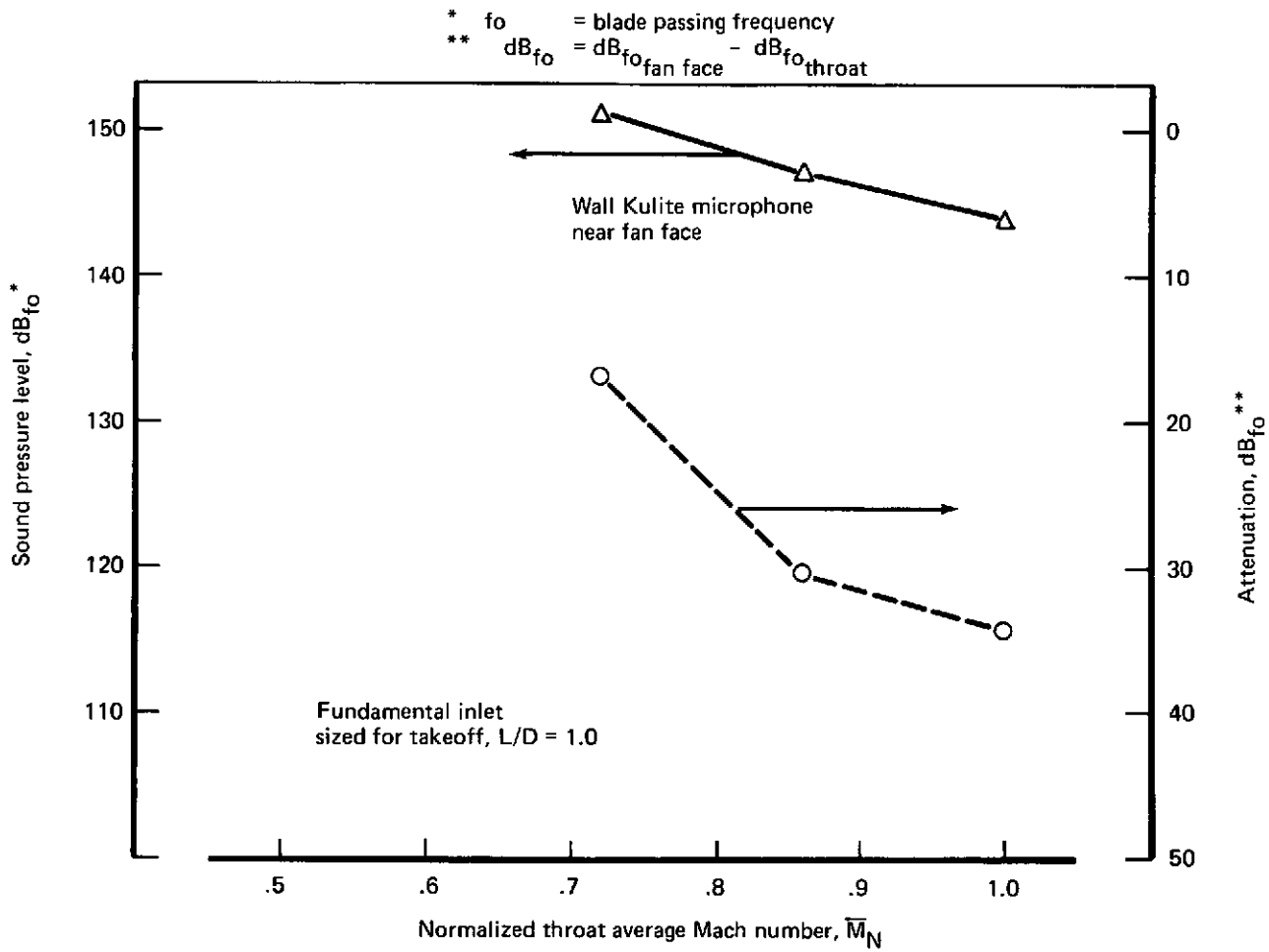


*FIGURE 8.—ATTENUATION AT BLADE PASSING FREQUENCY VS THROAT MACH NUMBER (TAKEOFF)*

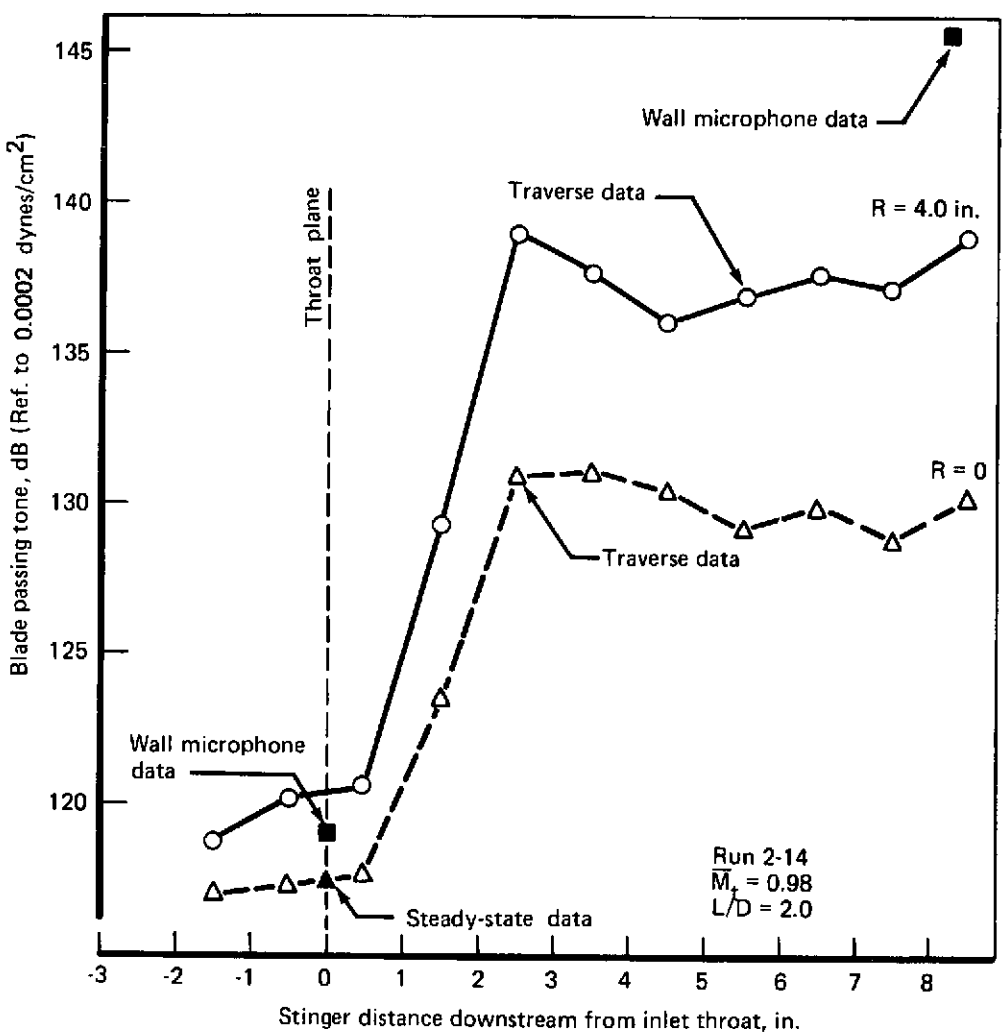


*FIGURE 9.–AXIAL DISTRIBUTION OF BLADE PASSING TONE IN APPROACH INLET*

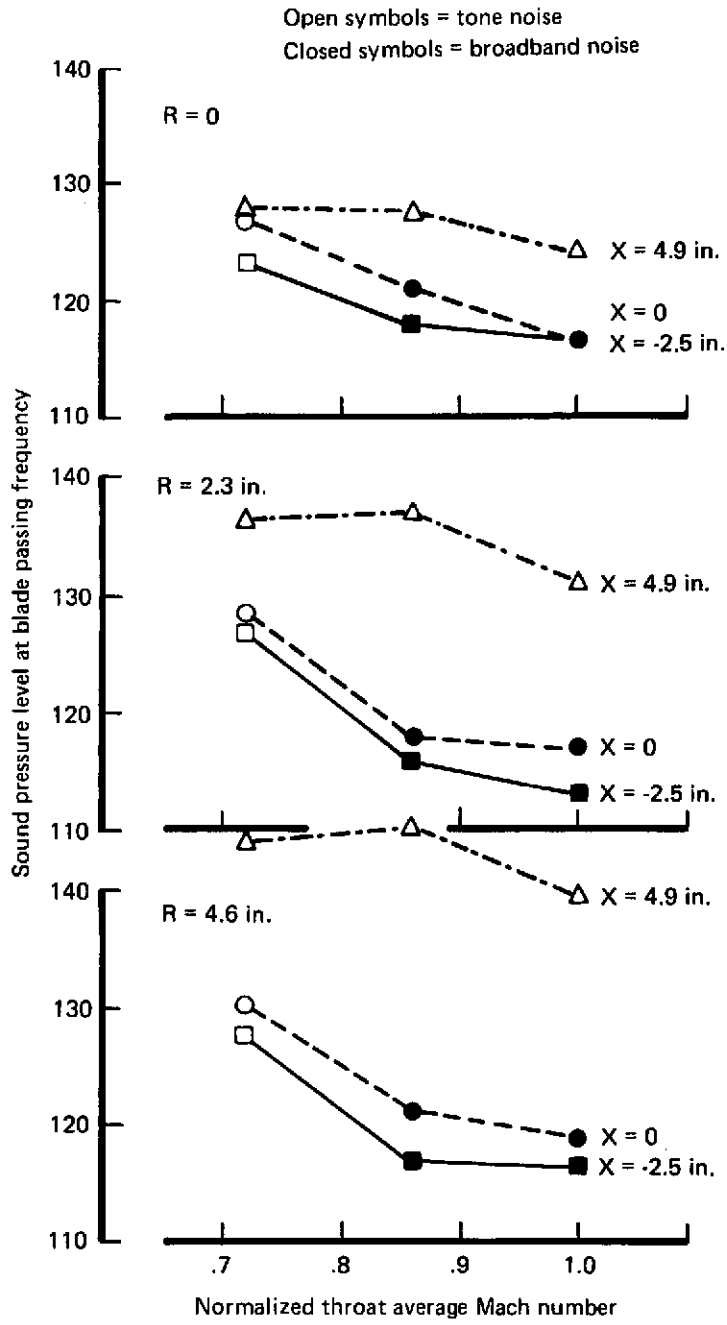


*FIGURE 10.–BLADE PASSING TONE VS THROAT MACH NUMBER IN TAKEOFF INLET*

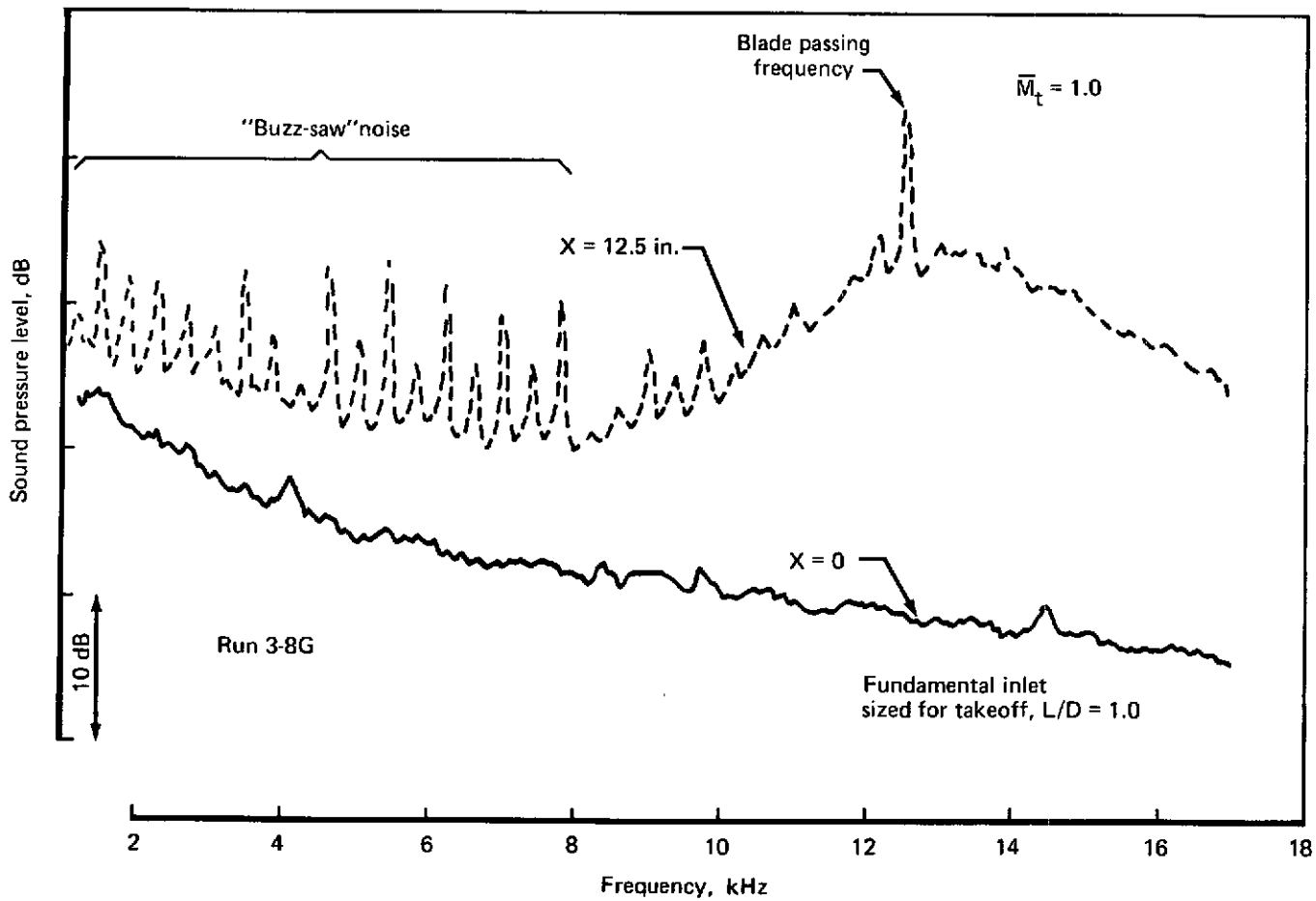


*FIGURE 11.–NEAR-FIELD, WALL KULITE NOISE SPECTRA IN TAKEOFF INLET*

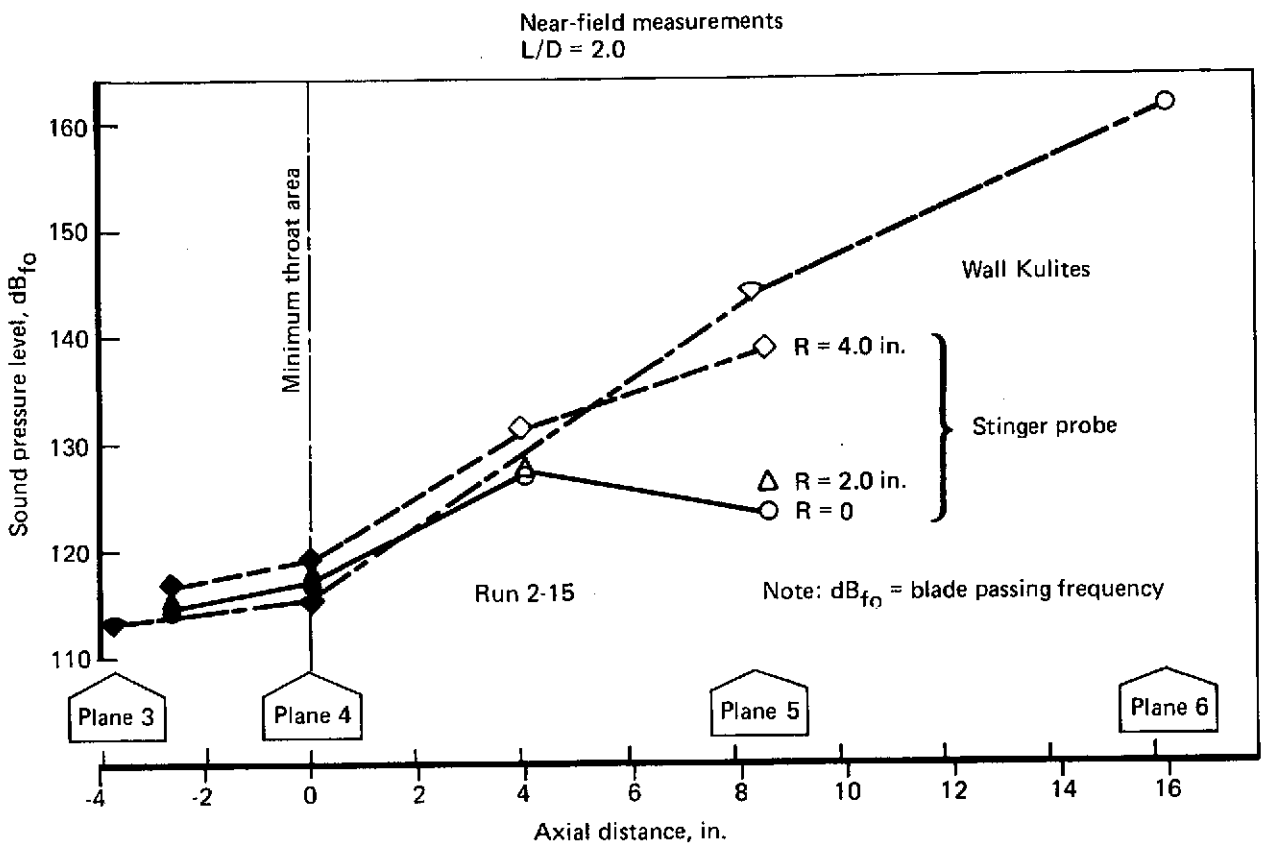


*FIGURE 12.–BLADE PASSING TONE VS AXIAL DISTANCE IN APPROACH INLET*

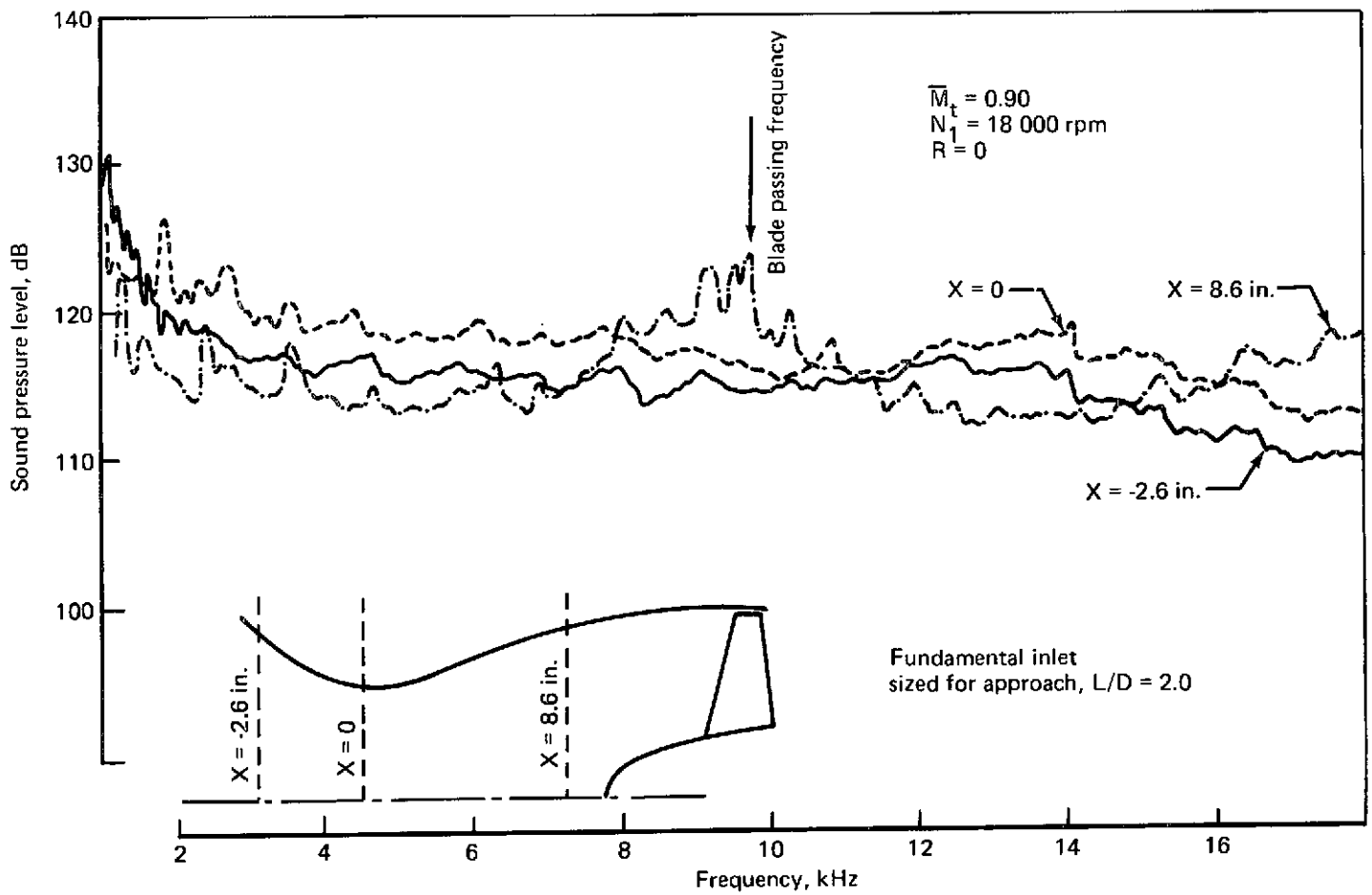


*FIGURE 13.—NEAR-FIELD NOISE SPECTRA INSIDE FUNDAMENTAL APPROACH INLET*

# 2.0 INTRODUCTION

Sonic inlet noise and performance potential has been under investigation for the past several years. Appendix E, volume II of this report summarizes the results of past investigations. These programs covered a large number of investigations and a variety of configurations and experimental techniques. They have demonstrated the basic feasibility of sonic inlets and the potential for large inlet noise reductions by inlet choking, thus contributing significantly to sonic inlet technology. However, some limitations exist in the results of earlier experiments. Satisfactory attention was provided to the aerodynamic design details on full-scale sonic inlet engine tests conducted, but in most cases configuration constraints were imposed to make use of existing hardware, resulting in compromised performance. Acoustic data from engine tests were usually affected by other engine noise sources. Most of the scale model tests lacked the aerodynamic design detail and adequate instrumentation for the evaluation of the aerodynamic performance potential of the different configurations.

The task of identifying a sonic inlet for a practical airplane application requires more than the mere demonstration of feasibility. Configuration concepts have to be compared and evaluated in terms of their aerodynamic and noise performance, mechanical design feasibility, and overall system considerations. The technology data base gained from past program results was inadequate for these types of studies.

This program, conducted under a NASA Lewis contract, had the objective of expanding the technology base for sonic inlets. In the area of aerodynamic performance, pressure recovery of the different inlet concepts had to be established for comparison studies. Flow distortion and inlet/engine compatibility trades required the determination of the distortion characteristics of different sonic inlet concepts. Finally, the noise potential of different inlets had to be demonstrated.

These tasks were accomplished by mechanical design studies of sonic inlets for concept selection, design, and testing of inlets utilizing the latest available technology in all areas. The tests were conducted in an anechoic chamber to separate aft radial noise from inlet noise. Measurements were taken to establish detailed acoustic and aerodynamic performance of all inlets tested.

Significant improvement in sonic inlet technology has been achieved by this effort.

# 3.0 INLET DESIGN DESCRIPTION

Two groups of inlet concepts were studied during the test program: a single-passage type and a multipassage type. The configurations were selected from these two groups for test evaluation on the basis of a mechanical design and model selection study (appendix A, volume II). Concepts were compared to weigh their relative merits in terms of design, performance, and operational characteristics. Four designs were selected for test evaluation: a contracting cowl and a translating centerbody design for the single-passage type, and a radial vane and double-articulated vane design for the multipassage type (fig. 14). All designs were optimized for minimum length and satisfactory predicted performance.

## 3.1 SINGLE-PASSAGE TEST CONFIGURATIONS

Two contracting cowl wall inlets were designed using L/D = 1.0 (takeoff) and L/D = 2.0 (approach). Because these two inlets were used mainly to study aerodynamic noise mechanisms, the length was conservatively selected to avoid uncertain aerodynamic performance. The L/D = 2.0 model was extensively instrumented to correlate the experimental flow properties with the theoretical analysis used during the design. The instrumentation included a line of static taps, running the full length of the inlet; boundary layer rakes; and total pressure rakes at the fan face. The test configuration of this inlet is shown in figure 14a.

Detailed analysis of this inlet is presented in volume II, appendix B. The translating centerbody inlet was first designed using L/D = 1.3 and then subsequently using L/D = 1.0, which was the design selected for extensive tests in the latter part of the program. The instrumentation for this inlet was similar to that for all models tested over the latter part of the program. A sketch of the configuration is shown in figure 14b.

The inlet designed using L/D = 1.3 was tested both as initially designed and later with three different configurations of acoustic lining added on the inner surface. This test series and a detailed model description are given in volume II, appendix B.

## 3.2 MULTIPASSAGE TEST CONFIGURATIONS

During the early part of the program both a radial vane inlet and a double-articulated vane inlet were tested. Later, most of the work was done with the radial vane inlet, which was considered the better of the two configurations.

The double-articulated vane inlet test configuration is presented on figure 14c. The throat was produced by a row of inlet guide vanes which turned the flow. Immediately downstream, a second row of blades returned the flow to an axial direction. The instrumentation used with this configuration consisted of static pressures on the wall in the throat region, a traverse probe between the vane rows, and a total pressure traverse wave rake at the exit.

The radial vane inlet, shown in figure 14d, employed 36 radial vanes to produce a sonic throat which would be removed by "stowing" during cruise operation. The instrumentation used for this configuration included guide-vane-channel static taps as well as a longitudinal row of statics from the lip to the fan face. Total pressure rakes were located at the fan face.

A complete list of configurations tested, together with a brief description and the identification of the particular test run number, is presented in table 1. The figure number showing the inlet geometry and test configuration is presented in appendix B, volume II.

## 3.3 MECHANICAL DESIGN CONFIGURATION STUDIES

Design studies of both single-passage and multipassage full-scale inlet configurations were conducted. Preliminary evaluations were made to select candidate configurations for the screening test program. Following the screening tests, two inlets were selected for final test on the basis of structural integrity, foreign object damage and ingestion, anti-icing, sensing and control systems, mechanical actuation, subsystem integration, and engine/aircraft constraints. In addition to aiding in the configuration selection, the purpose of these studies was to identify problem areas and constraints and determine possible approaches to the solution of these problems.

Sonic inlets were categorized as single-passage or multipassage. A single-passage inlet was considered as any inlet which had a throat which did not subdivide the flow streamlines into separate flow paths. Multipassage inlets were considered as those in which the throat annulus area was separated into more than one flow passage.

Figures 15 and 16 are summaries of the major characteristics of the various sonic inlet concepts studied. These summaries serve as a guide toward evaluating each inlet concept according to the application proposed. These mechanical design studies, along with aerodynamic studies, were used in selecting the sonic inlet models that were tested.

Two different types of single-passage inlets, translating centerbody and variable cowl wall inlets, were studied. The characteristics of each are summarized in figure 15.

*TABLE 1.—LIST OF MODELS*

| Model no. | L/D | Run no. | Description |
|---|---|---|---|
| 0 | 2.0 | 1 | Baseline configuration; straight constant-diameter duct with long bellmouth fitted |
| 1 | 2.0 | 2 | Fundamental (contracting cowl) inlet; approach configuration with long bellmouth fitted |
| 2 | 1.0 | 3 | Fundamental (contracting cowl) inlet; takeoff configuration with long bellmouth fitted |
| 3 | 1.3 | 4<br>5 | Translating centerbody inlet; approach configuration with long bellmouth fitted<br>Takeoff configuration with long bellmouth fitted |
| 3A | 1.3 | 101 | Model 3, approach configuration with acoustic lining added to internal surfaces |
| 3B | 1.3 | 102 | Model 3, approach configuration with acoustic lining added to internal cowl surface and diffuser section of centerbody only |
| 3C | 1.3 | 10 | Model 8, approach configuration with acoustic lining added to diffuser section only |
| 4 | 1.0 | <br>6<br>8<br>11<br>12 | Translating centerbody inlet; approach configuration<br>Long bellmouth fitted<br>Flight lip fitted<br>Flight lip fitted (part of run), short bellmouth (remainder)<br>Takeoff configuration with short bellmouth fitted |
| 5A | 1.0 | 7 | Radial vane inlet; approach configuration with long bellmouth fitted |
| 5B | 1.0 | 13<br>14 | Radial vane inlet; approach configuration with short bellmouth fitted<br>Takeoff configuration with short bellmouth fitted |
| 6 | 1.0 | 9 | Double-articulated vane inlet; approach configuration<br>Short bellmouth fitted (part of run)<br>Flight lip fitted (remainder of run) |

For the multipassage inlets, mechanical design feasibility was studied for the following concepts:

Variable sweep or radial vanes
Translating parallel vanes
Translating radial vanes
Expanding radial vanes
Translating radial vanes and centerbody
Translating external ring
Translating ring and centerbody
Articulated radial vanes

Figure 16 gives a summary of these concepts. A detailed description is provided in volume II, appendix A.

# 4.0 TEST SETUP AND PROCEDURE

The test program was conducted in the Boeing anechoic acoustic test facility (fig. 17). The basic feature of this facility is that forward- and aft-radiated noise are separated. For this program, testing was done in the "forward mode," in which aft-radiated noise was excluded from the acoustic chamber, so that inlet noise reduction produced by sonic inlets could be measured without the interference of aft arc noise.

## 4.1 TEST VEHICLE

A sketch showing the 12-in.-diameter fan fitted with a bellmouth inlet is presented in figure 18, and a photograph of the anechoic chamber showing the microphone array is presented in figure 19.

The fan and turbine were directly coupled and could be remotely controlled by both air supply pressure and fuel flow rate to the turbine combustor. Maximum continuous fan operating capability was:

- Mass flow rate: 28 lb/sec (bellmouth inlet)
- Pressure ratio: 1.5
- RPM: 29 400
- Number of blades: 32 rotor; 27 stator

A translating cone was used to vary the fan loading (fig. 18). The fan exhausted radially throughout the full circumference into the fan drive cell, and the exhaust escaped to atmosphere through an overhead stack. The fan inlet bellmouth protruded through the wall into the anechoic chamber (fig. 19), where the far-field forward arc measurements were made.

## 4.2 ACOUSTIC CHAMBER

The anechoic chamber was lined with material which provided an acoustic absorption coefficient of better than 0.95 (above 1000 Hz). The room was 33 ft long along the rig axis; 35 ft, 6 in. wide; and 11 ft high. An air vent in the roof, suitably insulated from external noise, allowed atmospheric air to enter the chamber.

## 4.3 INSTRUMENTATION AND DATA ACQUISITION SYSTEM

Near-field nosie measurements were made using flush-mounted Kulite transducers located on the internal cowl surface and with the probe installation shown in figure 20. The cantilevered stinger probe which supported an aft-facing transducer on its tip was inserted from the bellmouth and could be traversed longitudinally and radially. The location of the probe tip was accurately measured automatically. Also close to the probe tip were two static pressure ports, connected to an externally mounted pressure transducer, that measured static pressure in the stream.

Far-field noise measurements were made with the microphone array shown in figure 19. The microphones were 1/4-in. (B&K) condenser type.

Total pressure measurements were made within the inlet to determine the boundary layer conditions and the mainstream losses. The rotating rake located at the fan face comprised four arms of seven probes each and could be rotated in 10° increments. Boundary layer total pressure measurements were also made using rakes of closely pitched probes.

A photograph (fig. 21) shows a partial buildup of the test equipment where the inlet and rotating rake assembly were about to be joined to the 12-in.-diameter fan rig.

## 4.4 TEST PROCEDURE

The inlets were operated at various throat Mach number levels by operating the fan at the proper rpm level to obtain the necessary air flow rate. Backloading on the fan was held constant throughout the normal Mach number region of investigation on each inlet model.

All pressure readings on the test vehicle were read simultaneously by a system of chop valves and transducers with a pressure scanning device. The diffuser exit plane of each inlet model was surveyed with either a total pressure probe or rake. These surveys were made to determine total pressure recovery and flow distortion for each inlet model. All test rig parameters were recorded by an automatic digital recording system and printed out in the form of punched paper tape. This tape was input to a computer which converted all parameters to engineering units and made such calculations as air flow, Mach numbers, pressure recovery, etc.

All acoustic data were recorded simultaneously on multichannel magnetic tape. This included the far-field microphones, flush-mounted microphones on the inlet duct walls, and a fixed position of the midstream stinger microphone whenever it was used. Reduction of acoustic data during the test operation was limited to one or two select microphones for monitoring purposes only.

## 4.5 CROSS-WIND TEST SETUP

To demonstrate the effect of flow distortion on inlet noise, the special cross-wind generator shown in figure 22 was installed. Air was fed through six 4-in.-diameter flexible pipes from a high-pressure supply via specially built silencers. The velocity at the pipe exit was 100, 200, and 300 ft/sec for the cross-wind test points.

# 5.0 RESULTS AND DISCUSSION

The aerodynamic performance has been measured in terms of area-weighted average total pressure recovery and total pressure distortion at the fan face station of the diffuser. All pressure measurements have been nondimensionalized by the acoustic chamber pressure. Appendix C, volume II gives a detailed description of the instrumentation and test procedures and shows the points on each model at which measurements were taken. Besides fan face total pressure measurements, the static pressure distribution was also measured, and these are presented in the form of Mach number distribution where necessary for the discussion. Also, boundary layer total pressure rakes were used in various parts of the program; these results were used during the study to help explain various aerodynamic effects.

Far-field noise data were recorded at 10 microphone locations on a 10-ft radius arc. All data were reduced by a 1/3 octave band data reduction system. These data were then scaled to a 32-bladed, 53-in.-diameter fan. To condense the final results, one angle was chosen to represent the noise characteristics. A survey of the data showed that blade passing frequency SPL and PNL maximums mostly occurred at 50° from inlet centerline, and that the noise differentials were in most cases evenly distributed over the range of directivity angles. It was therefore concluded that the noise data recorded at the 50° location were representative of the acoustic performance at all other angles and would be used for further inlet analysis and comparisons. Scaled PNL differentials from baseline versus inlet throat Mach number, inlet recovery, and inlet fan face distortion provided the relevant parameters for comparison of the various inlet concepts.

## 5.1 SINGLE-PASSAGE INLETS

### 5.1.1 Aerodynamic Performance–Single-Passage Inlets

#### 5.1.1.1 Approach Configuration

Two basic single-passage inlet configurations for the approach flight condition were selected: the contracting cowl wall and the translating centerbody. Three models were designed, built, and tested. The configurations and test run numbers are defined in table 2.

Figures 23 through 26 show the inlet total pressure recovery and distortion versus the throat average Mach number for these models. The throat Mach number was calculated from the measured airflow and the geometric throat area, assuming an area coefficient of 1.0. The contracting cowl model (run 2) had a maximum recovery at choke of 0.978 with a minimum distortion of 8.2%. The

*TABLE 2.–SINGLE-PASSAGE CONFIGURATIONS (APPROACH)*

| Model no. | Run no. | L/D | Type | Figure no. |
|---|---|---|---|---|
| 1 | 2 | 2 | Contracting cowl | 23, 27, 30 |
| 3 | 4 | 1.3 | Translating centerbody | 24, 31 |
| 4 | 6 | 1.0 | Translating centerbody | 25, 28, 32 |
| 4 | 11 | 1.0 | Translating centerbody | 26, 29, 33 |

1.3 L/D translating centerbody model (run 4) had a maximum recovery at choke of 0.980 with a distortion of 9.9%. The other approach model, L/D = 1.0 (runs 6 and 11), had a recovery of 0.965 with a distortion of 8.5%. This model was tested in both phases of the program, and figures 25 and 26 show good agreement for both recovery and distortion. The tests differed in some respects (different bellmouths, different total pressure measurement methods) but the model was unchanged.

Figure 27, 28, and 29 show the surface Mach number based on measured static pressure along the inlet length. Each figure covers a range of throat Mach numbers from low (approximately 0.5) to choke. In each model the data show the maximum surface Mach number at choke to be over 1.0, nearly 1.2 on run 11 (fig. 29). This is an indication that at the choke conditions the flow goes supersonic downstream of the geometric throat.

Figures 30 through 33 are the fan face total pressure profiles for each test point of each run for the approach single-passage inlet models. Figure 30 (contracting cowl wall L/D = 2 model) shows no evidence of inlet separation at any throat Mach number condition. The 1.3 centerbody profiles (fig. 31) also do not show any evidence of flow separation. Figures 32 and 33 (L/D = 1.0 centerbody model) show that the flow was separated on the cowl at the high flow condition. The shorter L/D = 1.0 inlets had lower recovery values when the profiles indicated flow separation than the models that showed no sign of flow separation.

5.1.1.2 Takeoff Configuration

The single-passage inlets were also evaluated for the takeoff condition. Three different models were tested (table 3).

*TABLE 3.–SINGLE-PASSAGE CONFIGURATIONS (TAKEOFF)*

| Model no. | Run no. | L/D | Type | Figure no. |
|---|---|---|---|---|
| 2 | 3 | 1.0 | Contracting cowl wall | 34, 38 |
| 3 | 5 | 1.3 | Translating centerbody | 35, 39 |
| 4 | 12 | 1.0 | Translating centerbody | 36, 37, 40 |

Figures 34, 35, and 36 show the total pressure recovery and distortion vs the average throat Mach number. The contracting cowl wall, L/D = 1 (run 3), has a recovery of 0.986, slightly better than the L/D = 1.3 translating centerbody inlet (run 5) value of 0.985. The other inlet (L/D = 1.0 translating centerbody, run 12) had the best recovery, 0.990. The distortion values had the same relationship, with the shortest translating centerbody inlet being 5.5% as compared to about 10% for the other two. These results point out that the translating centerbody designs have a better throat Mach number distribution, contributing to higher recovery and lower distortion. The throat average Mach number for the translating centerbody models was higher than for the contracting cowl wall design.

Figure 37 is the surface Mach number distribution for the L/D = 1.0 translating centerbody model (run 12). The other takeoff models did not have sufficient wall static pressure instrumentation to calculate their surface Mach numbers. As for the approach models, the maximum cowl Mach number was greater than 1.0 (Mach 1.12 near the throat).

Figures 38, 39, and 40 show the fan face radial total pressure profiles for the three takeoff configurations. Only the L/D = 1.0 translating centerbody model (run 12) shows any flow separation or near separation. In this case the hub boundary layer was the thickest and at choke appears close to separation.

### 5.1.1.3 Inlet Lip Effect On Performance

Three different inlet entrance configurations were used in this program: a long bellmouth, used to accurately determine the airflow; a short bellmouth; and a simulated flight lip geometry. Figure 41 is a schematic of the three configurations along with the recovery vs the normalized throat Mach number. The simulated flight lip has the best performance, as the shorter length upstream of the throat

had the thinnest boundary layer growth, resulting in a higher overall recovery. The two bellmouth configurations had nearly the same performance, the shorter bellmouth having better performance than the long bellmouth.

Because most of the boundary layer on the bellmouth was laminar and therefore thin, the overall effect on recovery was not significantly affected by the three lip configurations. To fully evaluate the bellmouth effects, more detailed throat boundary layer measurements would be necessary. This type of instrumentation and evaluation was beyond the scope of this program.

### 5.1.2 Acoustic Performance—Single-Passage Inlets

#### 5.1.2.1 SPL Directivity and Spectra—12-In. Fan Model—Data Presentation

The baseline (model 0, straight duct) was tested over the entire range of approach and takeoff fan speeds. Figure 42 shows the model blade passing frequency noise directivity and the 1/3 octave band noise spectrum at 50° from inlet centerline for the approach range of fan speed settings. The noise distribution in the 0° to 90° quadrangle is similar for both low fan speed (13 910 rpm) and high fan speed (23 410 rpm) settings. The maximum blade passing frequency noise level occurs at the 50° location microphone for both conditions. The noise increase due to fan speed variation was evenly distributed in the quadrangle (+8 to 10 dB).

Figures 43 through 58 show the 12-in. fan blade passing frequency directivity and the 50° SPL spectra for all models tested in approach and takeoff configuration. The noise characteristics are shown for two throat Mach number settings in each case. Data corresponding to low throat Mach number settings, i.e., below Mach 0.7, were representative of a condition where small Mach number noise reduction occurred. Data corresponding to high throat Mach number settings, i.e., above Mach 0.7, were representative of a condition where a large Mach number noise reduction was observed. In general the Mach number effect reduced the blade passing frequency by 20 to 40 dB. The noise reduction was generally not very dependent on directivity. The noise reduction was more dependent on frequency—higher noise reduction was observed for frequencies over 5000 Hz than below that frequency. In most cases the fan blade passing frequency peak was not visible on the high throat Mach number SPL spectrum. It is believed that the noise in some frequency band was decreased below the test arena noise floor. The noise floor is 50-55 dB. Most inlet blade passing directivity and SPL spectra fitted the description given above; a few presented some peculiarities.

Figure 44 shows the blade passing frequency directivity and the 50° SPL spectra for the translating centerbody inlet (model 3) in approach condition. Noise characteristics are shown at low (M = 0.492) and high (M = 0.824) throat Mach number settings. The Mach number effect reduced the blade passing frequency by a maximum of 43 dB at the 40° location and by a minimum of 19 dB at

the 10° location. The noise reduction was clearly directivity dependent, with greater noise reduction between angles 30° and 80° than at lower angles.

Figure 45 shows the blade passing frequency directivity and the 50° SPL spectra for the centerbody inlet with acoustic lining added to internal surfaces (model 3A). Noise characteristics are shown at low (M = 0.497) and high (M = 0.781) throat Mach number settings. The combination of lining and high Mach number resulted in reducing the blade passing frequency by a maximum of 10 dB at the 0° location and by a minimum of 5 dB at the 10° location. These reductions were less than those obtained with the same inlet unlined (see fig. 44). In addition, the low-frequency (from 2.5 Hz to 5.6 Hz) sound pressure levels were increased by 0 to 11 dB. These results were due to poor aerodynamic performance caused by the lining in the inlet. Detailed description of this is in section 5.3 of this report.

Figure 54 shows blade passing frequency noise directivity for the 10-ft radius baseline model and the 1/3 octave band noise spectrum at 50° from inlet centerline for the takeoff range of fan speed settings. The noise distribution in the 0° to 90° quadrangle was similar for both low fan speed (17 780 rpm) and high fan speed (23 410 rpm) settings. The maximum blade passing frequency noise level occurred around the 50° location for both conditions. Only slight noise variations were observed at blade passing frequency for the rpm variation. The broadband noise increased by 3 to 10 dB.

#### 5.1.2.2 SPL Directivity and Spectra–Scaled Data

Figures 59 through 75 show the full-scale blade passing frequency noise directivity and the 50° SPL spectra for all models tested in approach and takeoff configurations. The frequency spectrum for full scale is that of the model ratioed down by the diameter ratio. The full-scale SPLs were then obtained by adding 10 $\log_{10}$ of the weight flow ratio to the scale model SPL. The scaling procedure is described in detail in appendix D, volume II. The 1/3 octave band blade passing frequency SPL directivity is not identical to that of the 12-in. fan model because it is presented on a 500-ft sideline instead of a 10-ft radius. The observations made about the 12-in. model remain, nevertheless, applicable to the full-scale directivity characteristics and will not be repeated here. Due to the distance extrapolation the SPL are often shown below the noise floor.

#### 5.1.2.3 PNL Directivity–Scaled Data

Figures 76 through 92 show the PNL directivity at 500-ft sideline for all models tested in approach and takeoff configurations. PNL directivity is shown for two throat Mach number settings in each case. Data corresponding to low throat Mach number settings, i.e.: below Mach 0.7, are representative of conditions where small or no Mach number noise reduction occurred. Data corresponding to high throat Mach number settings, i.e., above Mach 0.7, are representative of conditions where large

Mach number noise reduction was observed. Except for the baseline, all PNL directivity characteristics were similar in shape. In general, the maximum PNL occurred at the 50° location. The Mach number effect reduced the PNL by 20 to 40 PNdB. No consistent dependence of PNL reduction on directivity was observed. This observation justifies the use of the 50° location noise spectrum characteristics for comparisons in later discussions.

#### 5.1.2.4 Approach Configurations–Single-Passage Inlets

Figure 93 shows the 500-ft sideline PNL versus fan rpm (scaled-up data) for the baseline (model 0) in approach and takeoff configurations. The baseline is the basis of comparison for deriving the PNL reduction curves shown on figures 94 through 109. The number labeling each data point is the condition reference within the run. All data are scaled up, except when otherwise stated.

Figure 94 shows model 1 contracting cowl wall (L/D = 2.0 with long bellmouth) noise characteristics versus fan speed and throat Mach number. The noise started to decrease around throat Mach 0.6 to reach a 32-PNdB maximum observed PNL reduction from baseline at throat Mach 0.84. The minimum observed level at this point was 67.5 PNdB.

Figure 95 shows model 3 (translating centerbody inlet, L/D = 1.3 with long bellmouth) noise characteristics versus fan speed and throat Mach number. The PNL was slightly higher than baseline (+2 PNdB) up to throat Mach number = 0.63. This noise increase at low speed was the result of wake interactions from the struts, which did not exist in the baseline model. The maximum PNL reduction observed was 34 PNdB at Mach 0.86 corresponding to a 66-PNdB level.

Figure 96 shows noise characteristics of model 4 (translating centerbody inlet, L/D = 1.0 with long bellmouth). Noise started to decrease at Mach 0.7 to reach a 39-PNdB maximum PNL reduction at Mach 1.0 corresponding to a 61-PNdB level.

Figure 97 shows noise characteristics of model 4 tested with the simulated flight lip. Here the noise started to decrease at Mach 0.6 and reached a maximum PNdB reduction of 34 PNdB at Mach 0.94, but a noise increase occurred around that Mach number. The noise spectrum observed dynamically on a scope showed instabilities with SPL in most frequency bands oscillating. This type of instability occurred with various degrees of magnitude in all inlets, but it was most evident in the single-passage inlets. Short recurrences of the phenomenon were visible on the real-time analysis equipment. Due to the 32 seconds time average used for reducing the data, the phenomenon was generally not apparent on the 1/3 octave band SPL spectrum unless, as in this case, it was of a long enough duration. This phenomenon was believed to have been caused by flow instabilities in the inlet, but detailed studies of this were beyond the scope of this program.

Figure 98 shows model 4 noise results as tested with a short bellmouth. The noise level decreased after the Mach number reached 0.73, and a 42-PNdB maximum PNL reduction was reached at the maximum Mach number test condition. At this point the noise level was 56.5 PNdB.

#### 5.1.2.5 Takeoff Configurations—Single-Passage Inlets

Figure 99 shows model 2 (contracting cowl wall, L/D = 1.0 with bellmouth) noise reduction characteristics. Noise decreased for Mach numbers above 0.7. The lowest level observed was 67 PNdB at Mach 0.86.

Figure 100 shows the noise characteristics of inlet model 3 (translating centerbody, L/D = 1.3) tested with a bellmouth. The perceived noise level decreased from Mach 0.65 until approximately Mach 0.8, where the level was 57 PNdB. No more noise reduction was observed beyond Mach 0.9. This was most probably due to the fact that such a low noise level was down to the test installation floor noise.

Figure 101 shows the noise characteristics of model 4 tested with the short bellmouth. This model was 3 to 4 PNdB quieter than baseline at low throat Mach numbers. The noise decreased 47 PNdB for Mach 1.0. The lowest noise level was 54 PNdB, down to the floor noise.

#### 5.1.2.6 Inlet Lip Effect on Noise

The three inlet lip shapes tested with model 4 in approach configuration are compared on figure 102. PNL versus fan rpm and PNL reduction versus throat Mach number are shown. The curves are very similar for the long and short bellmouth. The flight lip led to a steeper noise reduction curve up to Mach 0.94, where the noise increased due to the instability phenomenon described in section 5.1.2.4.

## 5.2 MULTIPASSAGE INLETS

Two basic multipassage inlet concepts were investigated, the radial vane inlet and the double-articulated vane inlet. Test configurations were as shown in table 4.

*TABLE 4.—MULTIPASSAGE CONFIGURATIONS (APPROACH)*

| Model no. | Run no. | Inlet configuration | Figure number |
|---|---|---|---|
| 5A | 7 | Radial vane | 103, 108, 111 |
| 5B | 13 | Redesigned radial vane | 105, 106, 110, 114 |
| 6 | 9 | Double-articulated vane | 104, 107, 109, 111, 112, 113 |

### 5.2.1 Aerodynamic Performance—Multipassage Models

#### 5.2.1.1 Approach Configuration

Figures 103, 104, and 105 show the recovery and distortion versus average throat Mach number for the radial vane model (run 7), the double-articulated vane model (run 9), and the redesigned radial vane model (run 13), respectively. The average throat Mach number was calculated from the corrected weight flow and the geometric throat area, assuming an area coefficient of unity. Highest recovery of the radial vane inlet model (run 7, fig. 103) at choke was 0.954, with corresponding radial distortion of 6.2%. In the redesigned radial vane inlet model (run 13, fig. 105) the highest recovery at choke was 0.939, with the corresponding radial distortion of 13.5%. Lower recovery of the redesigned radial vane inlet model may be due to the four support struts in the diffuser. The double-articulated vane inlet (run 9, fig. 104) had highest recovery at choked condition of 0.916, with corresponding radial distortion of 2.8%.

Figure 106 shows the measured centerbody and cowl surface Mach number distribution of the redesigned radial vane inlet model (run 13). Average throat Mach numbers from 0.5 to choke are shown. The highest surface Mach numbers on both the cowl and centerbody for all test conditions were reached at the geometric throat. At the choke condition, supersonic velocity (Mach 1.1) was observed on the centerbody surface, while the maximum cowl surface velocity was Mach 0.9. The supersonic velocity on the centerbody surface is believed to be due to the continuously accelerating flow passage design upstream of the throat. A small amount of flow diffusion designed into the centerbody surface upstream of the throat would eliminate the supersonic velocity on the centerbody.

Figure 107 shows the cowl surface velocity distribution in the double-articulated vane inlet cascade channel. Average throat Mach numbers from 0.5 to choke are shown. The maximum cowl

surface velocity is subsonic, and it occurs at the same front vane chord position for all test conditions. The maximum average throat Mach number was 0.942 as compared to the corresponding maximum 0.95 Mach number on the cowl surface in the cascade channel. It is concluded that sonic velocity and maximum weight flow were reached at an aerodynamic throat of an area smaller than the design geometric throat.

Figures 108 and 109 show the fan face average total pressure profiles for the radial vane inlet (run 7) and the redesigned radial vane inlet (run 13), respectively. The radial vane inlet (run 7, fig. 108) indicates some performance deficiencies in the centerbody region. The redesigned radial vane inlet (run 13, fig. 109) indicates possible flow reversal at the centerbody, but this cannot be substantiated due to possible inherent errors in the centerbody wall static pressure measurement. Figure 110 shows the fan face average total pressure profiles for the double-articulated vane inlet (run 9). Higher recovery losses at choked conditions near the centerbody are attributed to the higher solidity of the vanes near the hub.

Figure 111 shows the vane wake total pressure profiles at the diffuser exit of the radial vane inlet (run 7) and the double-articulated vane inlet (run 9). Normalized average throat Mach numbers from 0.5 to choke are shown. At each Mach number, the pressure recovery profiles with the highest circumferential distortion are compared. The double-articulated vane inlet displayed higher wake distortion than the radial vane inlet, and the distortion increased with increasing average throat Mach number.

Figure 112 shows the radial distribution of the double-articulated vane inlet design and measured front vane flow turning angle (run 9). The first row of vanes acts as a row of nozzles accelerating the flow similarly to a turbine blade flow passage. The 5° overturning of the wake flow with respect to the design flow turning angle is caused by Prandtl-Meyer expansion of the flow downstream of the front vanes. Turning angle measurements were available as online data with two-digit accuracy, which explains why many of the data points were of the same turning angle magnitude.

Figure 113 shows the radial distribution of the double-articulated vane inlet front vane exit flow Mach number. Normalized average throat Mach numbers from 0.5 to choke are represented. The double-articulated vanes were designed for radially uniform noise reduction by means of a radially uniform Mach number at the exit of the front vanes. Prism probe velocity measurements in the front vane exit plane indicate lower than design exit velocities near the cowl surface.

#### 5.2.1.2 Takeoff Configuration

Only one configuration, the redesigned radial vane inlet (run 14), was tested.

Figure 114 shows the inlet average total pressure recovery and distortion versus the average throat Mach number. The highest recovery at choke was 0.983, with corresponding distortion of 12.9%, as compared to the highest recovery at choke of 0.939 and distortion of 13.5% in the approach configuration.

Figure 115 shows the measured centerbody and cowl surface Mach number distribution. Average throat Mach numbers of 0.48, 0.74, and 0.86 (choke condition) are shown. Due to the skewed throat position in the takeoff configuration it is difficult to establish a precise throat location. Flow is slightly supersonic on both the cowl and centerbody surfaces, but the velocities are very close to each other.

Figure 116 shows the fan face total pressure profiles. No flow separation is indicated by the profiles.

### 5.2.2 Acoustic Performance–Multipassage Inlets

Two basic types of multipassage inlets were investigated, the radial vane inlet (model 5) and the double-articulated vane inlet, L/D = 1.0 (model 6).

#### 5.2.2.1 Approach Configurations

Figure 117 shows the noise performance of model 5A (radial vane inlet, L/D = 1.0). This inlet was up to 4 PNdB noisier than the baseline at low Mach numbers. This noise increase can be explained by blade wake interactions, which did not exist in the baseline. The noise then decreased as the Mach number effect took place in the throat. The lowest noise level observed was 67 PNdB at Mach 0.835, corresponding to a 37-PNdB reduction from baseline.

Figure 118 shows the noise performance of model 5B (redesigned radial vane inlet). As mentioned above, the presence of vanes in the inlet creates additional wake interaction noise. As a result the noise level is higher than baseline for Mach numbers less than 0.65, when no Mach number effect occurred. The noise decreased at higher Mach numbers. A 64-PNdB level was observed at Mach 0.75. This corresponded to a 41-PNdB reduction from baseline.

Figure 119 shows the noise performance of model 6 (double-articulated vane inlet). At low Mach numbers this inlet was noisier than the baseline by 2 to 3 PNdB due to vane wake interactions. For throat Mach numbers higher than 0.7 the lowest noise level observed was 68 PNdB, corresponding to a 34-PNdB reduction from baseline at Mach 0.94.

#### 5.2.2.2 Takeoff Configurations

Figure 120 shows the noise data for model 5B (radial vane inlet) in takeoff configuration. This inlet was quieter than baseline over the range of Mach numbers tested. This may have been due to increased throat Mach number in lower rpm region. Noise reduction was 2 to 4 PNdB for Mach numbers up to 0.65, then increased to a maximum reduction of 43 PNdB at throat Mach number = 0.865. The noise level was then 59 PNdB.

## 5.3 ACOUSTIC LINING TESTS

The noise reduction effectiveness of acoustic lining in a choked inlet was evaluated using the approach configuration of the translating centerbody, L/D = 1.3, sonic inlet. The lining configuration consisted of 0.038-in. polyimide sheet with flow resistance of 58 rayls at 155 dB, over 0.1-in. deep honeycomb material with 1/8-in. cell size. The target frequency at throat Mach 0.9 was 12 kHz, corresponding to the blade passage frequency.

The first lined configuration was designed with acoustic treatment covering nearly the full length of the inlet (fig. 121). Test data obtained on this first configuration indicated substantial performance deterioration. The poor performance was attributed to the effect of friction coefficient increase in the high Mach number region of the inlet. Therefore, two subsequent configurations were tested (figs. 122 and 123). These configurations were obtained by covering the lining with hard epoxy resin in the throat region. The covered area was sanded to restore it to the original smooth finish. Test configurations were as shown in table 5.

*TABLE 5.—LINED CONFIGURATIONS*

| Model no. | Run no. | Lining configuration | Figure no. |
|---|---|---|---|
| 3 | 4.xxx | Hardwall (no acoustic lining) | |
| 3A | 101.xxx | Lined cowl and centerbody | 121 |
| 3B | 102.xxx | Lined cowl, centerbody lined in the diffuser | 122 |
| 3C | 10.xxx | Cowl and centerbody lining in the diffuser only | 123 |

### 5.3.1 Aerodynamic Performance

Figures 124, 125, and 126 show average total pressure recovery and distortion versus the average throat Mach number for each lined model. Each data point is numbered on the curves to identify it with the data key. The average throat Mach number was calculated using the corrected weight flow and the geometric throat area using an area coefficient of unity.

Figure 127 shows the fan face average total pressure recovery profiles of the fully lined inlet. The lowest recovery profiles are along the cowl, and the profiles deteriorate with increasing normalized throat Mach number due to the increased friction losses of the lined surfaces.

Figure 128 shows the recovery profiles for the data points taken with the lined cowl and centerbody lined only in the diffuser. This configuration had the poorest of all recovery profiles, indicating flow separation along the cowl.

Figure 129 shows the recovery profiles of the diffuser-only lined configuration. The profiles reveal no flow separation and only minimal profile deterioration along the cowl.

Figure 130 shows the average total pressure recovery and radial distortion versus the normalized throat Mach number for each configuration.

Figure 131 shows the total pressure recovery profiles at the fan face and at a plane midway between the throat and the fan face in the diffuser. The total pressure recovery profiles are compared at nearest available test condition to 0.9 normalized throat Mach number.

Fully lined cowl and centerbody configuration showed 1% recovery decrease below that of the hardwall inlet at 0.5 normalized throat Mach number and 2% decrease at 0.9 normalized throat Mach number, while the distortion increased by 2% and 6%, respectively. Further increase in the corrected weight flow caused the recovery to drop from 0.965 to 0.905, indicating flow separation. The total pressure recovery profile measured in the diffuser confirmed the flow separation on the hub, but the corresponding fan face profile indicated that the flow had reattached to the surface. The recovery of this inlet at 0.9 normalized throat Mach number was 0.963 as compared to 0.984 for the hardwall inlet.

The inlet configuration with fully lined cowl and centerbody lining only in the diffuser resulted in total pressure recovery of 0.953 and distortion of 18%. Since the recovery of this inlet was lower than that of the fully lined configuration, it was concluded that separation on the cowl, as indicated from the pressure recovery profile in the diffuser, is more detrimental to inlet performance than separation on the centerbody.

A final test was run with the lining on cowl and centerbody only in the diffuser. Total pressure recovery was only 0.4% below that of the hardwall inlet over the range of normalized throat Mach number from 0.5 to 0.95. The total pressure recovery profile in the diffuser indicated incipient separation on the cowl. At the fan face, the total pressure recovery profile is fully attached on both surfaces, but the boundary layer is somewhat thicker for the lined inlet case, especially on the cowl surface.

Because of the deterioration of the recovery profile at the fan face, caused by the increased skin friction of the lined inlet, the maximum weight flow that could be passed through the diffuser lined inlet was 1.2% less than for the hardwall inlet. The total pressure recovery profiles associated with the hardwall model showed no indication of flow separation on either the cowl or the centerbody, and the average total pressure recovery at 0.9 normalized throat Mach number was 0.984 as compared to 0.980 for the best lined inlet configuration tested, the inlet with lining only in the diffuser.

### 5.3.2 Acoustic Performance—Lined Inlets

Figures 132, 133, and 134 show the noise characteristics of the three lined inlet models. For consistency the inlets are compared here with the baseline inlet, although it was of a different configuration. Noise performance of the treated inlet is compared with that of the unlined inlet in section 5.5.2.1. Model 3A (fig. 132) had lining added to all internal surfaces and presented flow problems that resulted in little noise reduction. Model 3B (fig. 133) was tested with acoustic lining added to the internal cowl surface only. Model 3C (fig. 134) had acoustic lining added to the diffuser section only, and had good noise reduction.

## 5.4 DISTORTION EFFECTS

### 5.4.1 Distortion Simulation Methods

The second phase of this program was partially directed toward inlet distortion simulation and its associated aerodynamic and acoustic performance effects. Fan face instrumentation in the form of a 28-pickup, four-arm rotating rake was incorporated in the test setup to measure the total pressure distribution at 10° increments. A computer program was used to obtain fan face total pressure distribution maps for each test point. Simulated flow distortion was done by using low-pressure air blown normal to the inlet air flow at the face of the bellmouth. Six 4-in. air pipes were located at the bottom portion of the bellmouth. A silencing chamber was installed on the air pipes to keep the air injection noise to a minimum. Experimentation with the number of pipes, their orientation to the bellmouth, and the blowing rate was done to arrive at a range of fan face distortions up to 20% with acceptable

blowing air noise. Two throat Mach numbers (approximately 0.68 and 0.90) were investigated. Distortion at each of these Mach numbers was measured with crosswind values of zero, 100, 200, and 300 ft/sec. Two models in the approach and takeoff configurations were evaluated. See figure 135 for the crosswind blowing setup.

### 5.4.2 Aerodynamic Performance–Distortion Effects

#### 5.4.2.1 Approach Configurations

The two approach configurations were the translating centerbody, L/D = 1.0 (model 4, run 11), and the modified radial vane inlet, L/D = 1.0 (model 5B, run 13).

Figures 136 and 137 are the fan face total pressure distributions for the translating centerbody inlet at an average throat Mach number of 0.66 at zero and 100-ft/sec air injection. Figure 136 shows some bottom sector total pressure loss caused by the presence of the six air pipes, even through no air was being injected at this run. The distortion increases from 2.6% to 4.6% when the cross wind is increased to 100 ft/sec. The lowest total pressure occurred at the bottom of the inlet, coinciding with the location of the blowing pipes. The average recovery decreased from 0.993 to 0.986 as the crosswind is increased to 100 ft/sec. Both patterns were symmetrical from one side to the other with all the distortion coming from differences of the top and bottom sectors, as expected. Figures 138 and 139 are of the same inlet configuration at a near-choked throat condition. Here a comparison of a "clean" inlet (no air pipes) and the 100-ft/sec air injection was made. The overall distortion change was small, 11.4% compared to 9.3% for the "clean" inlet.

Figures 140 through 143 show the radial vane model (run 13) at low and high throat Mach numbers at 0- and 100-ft/sec crosswind. Table 6 is a summary of the distortion effects.

The radial vane model distortion maps show the pressure distribution to be more even than for the centerbody inlet. While the distortion values are about the same level (10% at 100 ft/sec), the pressure contour lines are spread out over the entire lower 180° of the annulus for the radial vane models, whereas the single-passage inlets have local low-pressure regions in the bottom center location only.

#### 5.4.2.2 Takeoff Configurations

Figure 135 shows the distortion versus the normalized Mach number for the translating centerbody takeoff configuration at the various crosswind conditions. For the takeoff area configurations, in each zero crosswind case the crosswind injection pipes were installed, and this caused a low-pressure region in the lower section of the inlet.

*TABLE 6.–DISTORTION EFFECTS (APPROACH)*

| Point no. | $\bar{M}_T$ | Crosswind velocity | Overall distortion | Overall recovery | Figure no. |
|---|---|---|---|---|---|
| 13.014 | 0.735 | Zero | 6.75% | 0.977 | 140 |
| 13.015 | 0.735 | 100 ft/sec | 6.58% | 0.975 | 141 |
| 13.018 | 0.910 | Zero | 10.78% | 0.945 | 142 |
| 13.019 | 0.910 | 100 ft/sec | 11.70% | 0.941 | 143 |

The translating centerbody inlet (figs. 144 and 145) at the low throat Mach number (0.690) shows a definite increase in the distortion and a decrease in recovery when the crosswind was increased from zero to 100 ft/sec. The fan face total pressure maps show that the entire bottom section of the inlet was affected. The low-pressure region caused by the crosswind extended from the cowl to the centerbody surface. This is in contrast to the higher throat Mach number cases (figs. 146 and 147, Mach ~ 0.9) where the flow near the centerbody seems unaffected by the 100-ft/sec crosswind.

The radial vane model at the low throat Mach number (figs. 148 and 149) shows only a small increase in distortion, 4.6% to 5.8%, when the crosswind was increased from zero to 100 ft/sec. The flow near the centerbody seems unchanged, and the only difference in the fan face maps is near the cowl surface of the bottom sector of the inlets. At the higher throat Mach number, the increase in crosswind has even less effect on the distortion patterns. The overall distortion stays approximately the same at 10%, and the recovery shows only slight reduction for the 100-ft/sec crosswind (figs. 150 and 151). A summary of the takeoff distortion data is shown in table 7.

In general, the distortion studies for both the approach and takeoff configurations showed that the multipassage models were less affected by the crosswind than the single-passage inlets and that the high throat Mach number cases were less sensitive to the induced flow disturbances than were the low throat Mach number cases from an aerodynamic point of view.

### 5.4.3 Acoustic Performance–Distortion Effects

#### 5.4.3.1 Approach Configuration

Figure 152 shows the distortion and noise characteristics for model 4 (centerbody, L/D = 1.0) in approach condition. Fan face distortion increased with blowing rate for the two Mach number

*TABLE 7.–DISTORTION EFFECTS (TAKEOFF)*

| Point no. | $\bar{M}_T$ | Crosswind velocity | Overall distortion | Overall recovery | Figure no. | Model |
|---|---|---|---|---|---|---|
| 12.014 | 0.690 | Zero | 4.5% | 0.993 | 144 | Model 4 translating centerbody L/D = 1.0 |
| 12.015 | 0.690 | 100 ft/sec | 7.1% | 0.982 | 145 | |
| 12.018 | 0.875 | Zero | 9.1% | 0.977 | 146 | |
| 12.019 | 0.875 | 100 ft/sec | 15.3% | 0.957 | 147 | |
| 14.013 | 0.67 | Zero | 4.64% | 0.991 | 148 | Model 5B radial vane redesign L/D = 1.0 |
| 14.014 | 0.66 | 100 ft/sec | 5.76% | 0.986 | 149 | |
| 14.018 | 0.915 | Zero | 10.19% | 0.960 | 150 | |
| 14.019 | 0.885 | 100 ft/sec | 9.3% | 0.957 | 151 | |

conditions tested. The effect on noise radiation was small over the range of cross blowing speeds for Mach 0.66. At a high Mach number, 0.92, the effect was small at 100-ft/sec blowing rate (+0.5 PNdB). Noise increased by 9 PNdB between 100 ft/sec and 300 ft/sec blowing rate.

Figure 153 shows the distortion and noise characteristics for model 5B in approach configuration. A small (0.5 PNdB) increase was observed for 100-ft/sec blowing rate at a low Mach number, 0.735. Noise increased by another 2 PNdB when the blowing rate was increased up to 300 ft/sec. At a high throat Mach number setting, M = 0.91, the noise increased by 6 PNdB for 100-ft/sec blowing rate and by another 5 PNdB between 100 and 300 ft/sec.

### 5.4.3.2 Takeoff Configuration

Figure 154 shows the distortion and noise characteristics for model 4 (centerbody L/D = 1.0) in takeoff configuration. A small (0.5 PNdB) increase was observed for 100-ft/sec blowing rate at a low Mach number, 0.69. Noise increased by another 2.5 PNdB when the blowing rate was increased to 300 ft/sec. At a high throat Mach number setting, M = 0.875, the noise increased by 7 PNdB for 100-ft/sec blowing rate and by another 6.5 PNdB between 100 and 250 ft/sec.

Figure 155 shows the distortion and noise characteristics for model 5B (radial vane inlet) in takeoff configuration. A 2-PNdB increase was observed for 100-ft/sec blowing rate at a low Mach number,

0.67. Noise increased by another 2 PNdB when the blowing rate was increased to 300 ft/sec. At a high throat Mach number setting, M = 0.885, the noise increased by 7 PNdB for 100-ft/sec blowing rate and by another 5.5 PNdB between 100 and 250 ft/sec.

Results of crosswind distortion tests showed that the single-passage and multipassage inlet noise characteristics were similarly affected by internal fan face distortion. Generally the effect was greater for a high throat Mach number condition (inlet choked). The noise reduction loss resulting from cross-blowing at 100 ft/sec and high throat Mach number was around 7 PNdB for all inlets and conditions. For blowing rates above 100 ft/sec the radial vane inlet showed less distortion and a slightly smaller noise increase.

## 5.5 COMPARISONS

In the preceding discussion, aerodynamic and acoustic results have been presented on an individual configuration basis to provide a comprehensive survey of all the test data. To satisfy the program objectives, i.e., to identify the most effective sonic inlet concept from the designs selected for analysis and testing, a comparison of inlet performance in terms of total pressure recovery and distortion and noise reduction was necessary.

Average throat Mach number has been used as the independent variable in many parts of the preceding discussion. This quantity was derived from the measured weight flow and throat geometric area, assuming no total pressure losses up to the throat plane. Owing to boundary layer growth and slight changes in axial location of the effective aerodynamic throat, with inlet configuration and airflow, this definition of a mean throat Mach number provided inaccurate, making correlation of results somewhat confusing (e.g., fig. 23 shows model 3 choking at $\bar{M} = 0.84$, whereas fig. 25 shows model 4 choking at $\bar{M} = 1.0$). To provide a more representative variable on which comparisons could be made, a quantity called "normalized Mach number" was defined. This was based on the assumption that the average throat Mach number was 1.0 when inlet airflow was a maximum (choked condition) and all other airflow quantities for a given inlet were ratioed to that maximum. From the airflow quantities the A/A* values were calculated and the associated Mach number, called "normalized Mach number," was used in the following comparisons.

### 5.5.1 Aerodynamic Performance Comparisons

#### 5.5.1.1 Definition of Parameters

*Inlet distortion.*—This is defined as $(P_{T_{max}} - P_{T_{min}})/\bar{P}_T$, the maximum total pressure being taken from the midstream readings of the rotating rake or the traversing probe. The minimum total

pressure was taken to be the lowest pressure measured by a pressure pickup nearest the wall. This minimum pressure used would be higher than the lowest boundary layer pressure, which was actually the surface static pressure.

*Inlet recovery.*—The inlet fan face recovery calculation was the average of the exit total pressures divided by the acoustic chamber ambient pressure. The exit total pressure average was measured by the 10-position traverse probe or the 28-pickup, four-arm rake or, in the case of the first vane models, a 9-pickup wake probe. When the rotating rake was used, readings were taken each 10° resulting in a total pressure average calculated from 252 individual pressures.

### 5.5.1.2 Approach Configurations

Seven different approach configurations were evaluated, and the aerodynamic performance is compared on figures 156, 157, and 158. The total pressure recovery versus average throat Mach number for the approach condition is presented on figure 156. As mentioned above, it is difficult to compare these results using the mass-derived average throat Mach number, so the same results are presented on figure 157 as a function of normalized throat Mach number. Figure 158 shows distortion versus normalized throat Mach number.

Figure 157 shows that the multipassage inlets have lower recovery than the single-passage type. Comparing the recovery at $\bar{M}_N = 0.95$, the double-articulated vane inlet had a recovery of 0.92, and the radial vane inlet a recovery of 0.927, whereas the translating centerbody inlet with the short bellmouth installed (the short bellmouth was more representative of flight conditions than the long bellmouth) gave a recovery of 0.98. The distortion for the same series of models is plotted against normalized Mach number on figure 158 and shows a distortion of 6.8% for the translating centerbody inlet compared to 13.3% for the radial vane inlet (both fitted with short bellmouth). The double-articulated vane inlet gave a distortion of 2.8%. It was found from pressure profile measurements in the diffuser that the boundary layer on the cowl surface had separated near the vanes on the radial vane inlet, causing the severe distortion level. When the long bellmouth was fitted (run 7) the distortion level was 4.8%, indicating that unless separation occurred the multipassage inlet gave generally better distortion levels than the single-passage type.

### 5.5.1.3 Takeoff Configurations

The throat location and area of the takeoff translating centerbody models were more difficult to determine than those of the approach models, because the minimum cowl radius was not at the same station as the maximum centerbody radius. This makes the normalized Mach number parameter even more useful in comparing the aerodynamic performance of these four takeoff configuration models. Figure 159 is the total pressure recovery versus the measured throat Mach number, showing the spread

of the choked Mach number values (0.86 to 1.0). Figures 160 and 161 are the recovery and distortion plotted versus the normalized Mach number. The contracting cowl wall, L/D = 1.0 inlet and the translating centerbody, L/D = 1.3 inlet have the best recovery (0.988) at choke. The distortion comparison shows that the contracting cowl wall is 9.5%, approximately 3% lower than that of the translating centerbody, L/D = 1.3 inlet.

The translating centerbody, L/D = 1.0 inlet had lower recovery, 0.968, compared to 0.986 for the L/D = 1.3 translating centerbody at choke. Up to a throat Mach number of approximately 0.8, these two inlets were equal; then the L/D = 1.0 inlet began to separate on the centerbody as can be seen from the total pressure profiles of figure 40. At the choke Mach number the distortion is 17%. This high distortion is due to the low total pressure associated with the centerbody separation.

The radial vane inlet (run 14) had the lowest choke recovery (0.953) but had good performance (above 0.98) up to a relatively high throat Mach number of 0.95. The maximum choke distortion of this inlet was 10.8%.

From these comparisons of the two different translating centerbody inlets it is apparent that in the range of interest of 25 PNdB noise reduction, performance of both inlets is satisfactory.

### 5.5.1.4 Final Configurations

A comparison of the aerodynamic performance of the single-passage inlet (translating centerbody) and the multipassage inlet (radial vane) is shown in table 8.

*TABLE 8.–AERODYNAMIC PERFORMANCE COMPARISON*

| $M_N = 1.0$ | | | | | | |
|---|---|---|---|---|---|---|
| Inlet type | Flight condition | Maximum total pressure recovery | Minimum overall distortion | Run no. | L/D | Figure no. |
| Translating centerbody | Approach | 0.955 | 11.2% | 11 | 1.0 | 157, 158 |
| Translating centerbody | Takeoff | 0.968 | 17% | 12 | 1.0 | 160,161 |
| Radial vane | Approach | 0.914 | 14% | 13 | 1.0 | 157, 158 |
| Radial vane | Takeoff | 0.953 | 10.8% | 14 | 1.0 | 160, 161 |

The single-passage inlets in both the approach and takeoff configurations had higher total pressure recovery than the multipassage inlets. The distortion values for the multipassage inlets at choke for the approach configuration were higher than for the single-passage model. The takeoff models showed the opposite trend.

#### 5.5.1.5 Fan Operation With Sonic Inlets

Figure 162 shows the operating line for two sonic inlets superimposed on the baseline fan map. These operating lines show that changes in fan operating points were very gradual even after the inlet choke point, where the recovery versus throat Mach number took a vertical drop. The choke points are shown for each test run. The radial vane inlet in the approach configuration showed a gradual ascendance to the stall line; however, the highest test points were of unrealistically low recovery points for real inlet-engine operation. All other operating lines exhibited a near-normal operating line representative of constant exhaust nozzle area setting with conventional inlets.

Figure 163 shows stall line changes due to flow distortion created by two sonic inlets. The radial vane inlet showed no effect on the fan stall line, but the centerbody inlet reduced the stall margin by a small amount. This difference between the two different inlets could be attributed to the difference in radial flow distortion created by the inlets.

### 5.5.2 Acoustic Performance Comparisons

In this section, all the inlets tested are compared in approach and takeoff configuration. The 500-ft sideline PNL reduction from baseline at 50° from inlet centerline is plotted against normalized throat Mach number, inlet recovery, and fan face distortion.

#### 5.5.2.1 Approach Configurations

*Single-passage inlets.*—Figure 164 shows the PNL reduction from baseline versus normalized throat Mach number for the three types of single-passage inlets. The L/D = 1 inlet was better than the L/D = 1.3 centerbody inlet over the whole range of Mach numbers. It was also better than the contracting cowl inlet at a high throat Mach number (M = 0.85).

Figure 165 shows PNL reduction versus inlet recovery. Figure 166 shows PNL reduction versus percent fan face distortion. It can be seen that the model 4 inlet had better or equal recovery and distortion than the two others up to 25 PNdB reduction. Table 9 summarizes the normalized throat Mach number, inlet recovery, and fan face distortion for 25 PNdB noise reduction.

*TABLE 9.–ACOUSTIC PERFORMANCE–SINGLE-PASSAGE INLETS (APPROACH)*

| Model no. | PNdB | $M_N$ | Recovery | Distortion |
|---|---|---|---|---|
| 1 | 25 | 1.0 | 0.978 | 7.6% |
| 3 | 25 | 1.0 | 0.974 | 8.7% |
| 4 | 25 | 0.915 | 0.975 | 9.8% |

*Multipassage inlets.*–Figure 167 shows PNL reduction versus normalized throat Mach number for the radial vane inlet fitted with a long bellmouth (model 5A), a short bellmouth (model 5B), and the double-articulated inlet.

Figure 168 shows PNL reduction versus recovery and figure 169 shows PNL reduction versus fan face distortion for these same three inlets. The model 5B inlet (radial vane with short bellmouth) showed better noise reduction than the two other inlets when compared on the basis of throat Mach number. Table 10 summarizes the normalized throat Mach number, inlet recovery, and fan face distortion for the 25-PNdB reduction target.

*TABLE 10.–ACOUSTIC PERFORMANCE–MULTIPASSAGE INLETS (APPROACH)*

| Model no. | PNdB | $M_N$ | Recovery | Distortion |
|---|---|---|---|---|
| 5A | 25 | 1.00 | 0.92 | 6.2% |
| 5B | 25 | 0.975 | 0.913 | 13.8% |
| 6 | 25 | 1.00 | 0.910 | 2.3% |

*Acoustically treated inlets.*–Figure 170 shows PNL reduction from baseline versus normalized throat Mach number for the three lined inlet tests and for the untreated version (model 3). It can be seen that model 3C (lining in diffuser section only) resulted in a noise level 0 to 7 PNdB lower than the unlined model for Mach 0.5 to 0.8. The gain was due to lining effect. At throat Mach numbers from 0.8 to 1.0, the lining allowed for a 0.05 throat Mach number reduction for the same noise as compared with the unlined case.

### 5.5.2.2 Takeoff Configurations

*Single-passage inlets.*—Figure 171 shows PNL reduction from baseline versus normalized throat Mach number for the model 2, 3, and 4 inlets. Figure 172 shows PNL reduction versus recovery and figure 173 shows PNL reduction versus fan face distortion for the same three inlets. Model 4 (centerbody, L/D = 1.0, with short bellmouth) was consistently better than the two other inlets. Table 11 summarizes the normalized throat Mach number, inlet recovery, and fan face distortion for the 25-PNdB reduction target.

*TABLE 11.—ACOUSTIC PERFORMANCE—SINGLE-PASSAGE INLETS (TAKEOFF)*

| Model no. | PNdB | $M_N$ | Recovery | Distortion |
|---|---|---|---|---|
| 2 | 25 | 0.91 | 0.988 | 7.5% |
| 3 | 25 | 0.85 | 0.991 | 8.8% |
| 4 | 25 | 0.795 | 0.992 | 5.1% |

*Multipassage inlets.*—Figure 174 shows the PNL reduction from baseline versus normalized throat Mach number for model 5B. This inlet configuration was the original radial vane inlet with the vanes removed to simulate takeoff configuration. Figure 175 shows the PNL reduction versus recovery and figure 176 shows PNL reduction versus fan face distortion for the same inlet.

Table 12 summarizes the normalized throat Mach number, inlet recovery, and fan face distortion obtained from the curve for the 25-PNdB reduction target.

*TABLE 12.—ACOUSTIC PERFORMANCE—MULTIPASSAGE INLETS (TAKEOFF)*

| Model no. | PNdB | $M_N$ | Recovery | Distortion |
|---|---|---|---|---|
| 5B | 25 | 0.65 | 0.992 | 6.4% |

### 5.5.2.3 Final Configurations

PNL reduction from baseline is plotted versus normalized throat Mach number (fig. 177), versus inlet recovery (fig. 178), and versus fan face distortion (fig. 179) for the two final inlet configurations in approach condition. The two inlets showed very comparable noise reduction characteristics versus Mach number. When compared on the basis of inlet recovery and percent fan face distortion, the centerbody inlet concept showed a definite advantage over the radial vane concept. The same two inlets were compared on the basis of PNL reduction versus normalized throat Mach number (fig. 180), versus inlet recovery (fig. 181), and versus fan face distortion (fig. 182) in takeoff configuration. Here the centerbody inlet showed a better noise reduction versus Mach number, comparable noise reduction performance versus inlet recovery, and better PNL reduction versus fan face distortion.

Table 13 summarizes the characteristics of both inlets for the 25-PNdB reduction target.

*TABLE 13.–ACOUSTIC PERFORMANCE COMPARISON*

| Inlet concept | Model no. | L/D | PNL reduction | Normalized Mach no. | Inlet recovery | Fan face distortion |
|---|---|---|---|---|---|---|
| Centerbody | 4 | 1.0 | 25 | 0.97 | 0.967 | 7.8% |
| Radial vane | 5B | 1.0 | 25 | 0.97 | 0.911 | 13.6% |
| Centerbody | 4 | 1.0 | 25 | 0.795 | 0.992 | 5.2% |
| Radial vane | 5B | 1.0 | 25 | 0.865 | 0.992 | 6.4% |

# 6.0 CONCLUSIONS

Results of this program lead to the following conclusions:

- A sonic inlet can be designed to produce inlet noise reduction in the range of 25 to 30 PNdB with less than 3% inlet recovery loss on approach and less than 1% in takeoff and cruise operation. Inlet flow distortion effects remain within acceptable limits for satisfactory engine inlet compatibility.

- Inlet noise reduction in excess of 40 PNdB is possible by sonic inlets with increased performance loss.

- Single-passage inlets are superior in terms of inlet recovery to multipassage inlets. The trend in terms of total pressure distortion is reversed.

- It has been demonstrated that, using the latest available design technology, sonic inlets can be designed within an L/D limit of unity consistent with the objective of this program.

- Increasing the inlet throat Mach number from about 0.5 to 1.0, resulted in an increasing noise attenuation at blade passing frequency.

- The rate of decay of the blade passing tone was found to be less on the centerline than near the outer wall. This was attributed to the radial Mach number gradient in the throat area.

- The multiple pure tone ("buss-saw") noise, which was only observed at fan blade speeds above the sonic velocity, did not propagate through the inlet throat plane.

- No evidence was found of noise leakage at blade passing frequency through the inlet throat boundary layer.

- No significant noise generation by the sonic plane was observed.

- Spectral comparison of the noise for the baseline and sonic inlet indicated that attenuation effectiveness is to some extent a function of frequency. Pure tones of high frequency and high-frequency broadband noise are more effectively attenuated than low-frequency noise.

- Noise directivity measurements taken in the acoustic chamber, with adequate inlet sidewall insulation and other noise sources minimized, indicate that the noise is effectively reduced at all angles in the forward arc.

This program has demonstrated significant improvement over earlier programs in both acoustic and aerodynamic performance for sonic or high Mach number inlets. Because of this, it is believed that sonic inlet technology can be applied in a wide variety of applications in aircraft inlet noise reduction. Other gas turbine engine installations may also benefit from the technology and performance potential demonstrated in this program for sonic inlets.

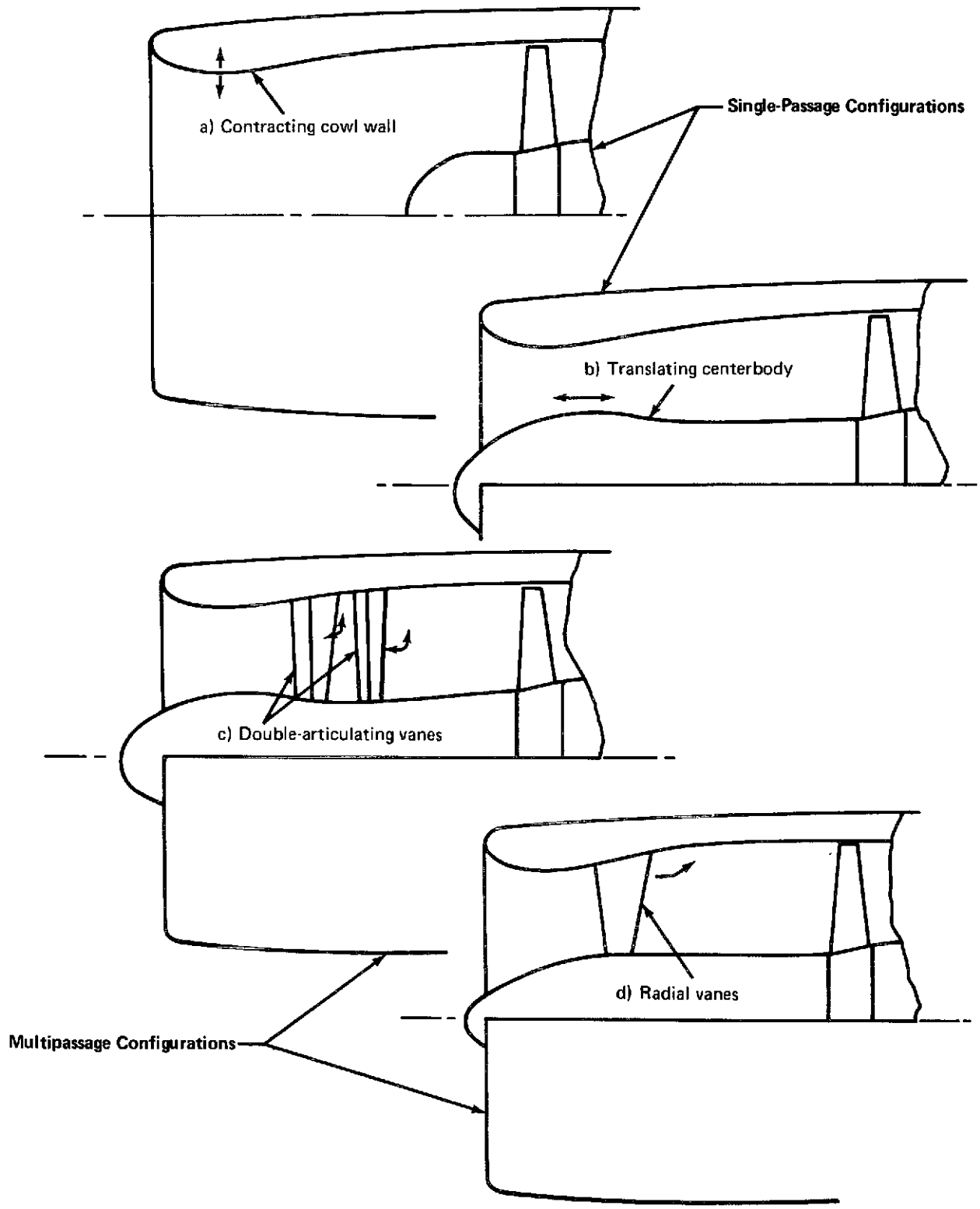


*FIGURE 14.—INLET TEST CONFIGURATIONS—APPROACH MODE*

| Design Consideration | | Translating Centerbody |
|---|---|---|
| | | 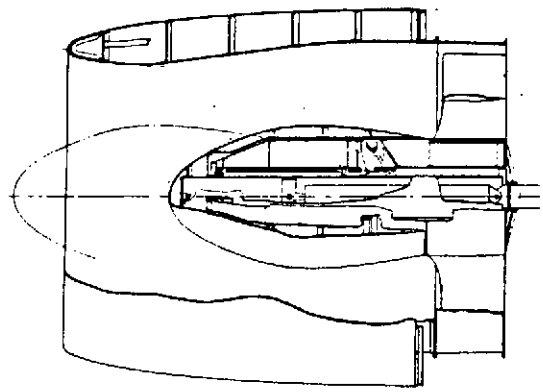 See figure A-11, volume II |
| Basic design | Lines | Good area progression profile with maximum cowl wall diffusion angle of 7.5°and L/D of 1.4; external lines not affected |
| | Structure | Conventional skin and frame outer cowl with centerbody support integrated with engine inlet guide vane design |
| | Mechanism | Actuator-driven centerbody translating on slide blocks and tracks |
| | Seals | Static seals only |
| | Range of application | Larger area changes can be achieved at the expense of increased inlet length and/or diffusion angle |
| Actuation | Power source | Engine bleed air for two-position pneumatic system; hydraulic for multiple position |
| | Type of actuation | Pneumatic piston for two position; hydraulic piston for multiple position |
| | Load and stroke | Load ≈3500 lb; stroke = 27.0 in. |
| | Synchronization | None required |
| | Failsafe potential | Careful venting of plug and/or locking devices required to counteract adverse pressure loads |
| Control | Two position | Electrical signal to air control valve |
| | Multiple position | Electronic input to electromechanical transfer valve nulled by linearly variable differential transducer position feedback with position selected as a function of engine rpm and total pressure at the fan face 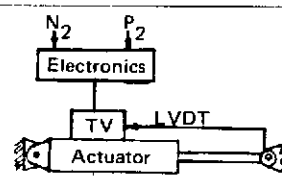  |
| Weight estimate (lb) | | Basic cowl 174.0<br>Translating centerbody 55.0<br>IGV modification 34.0<br>Centerbody support structure 89.0<br>Actuation and control 22.0<br>Anti-icing system 65.0<br>Total inlet 439.0<br>Engine penalty 40.0<br>Total 479.0<br>Comparative weight of 707-320B nonsonic inlet = 220 lb (scaled) |
| Smoothness | | Imperfections limited to joint between centerbody and support structure |
| Bird strike | | Hazard no greater than current inlets |
| Anti-icing system | | Outer cowl leading edge comparable to existing inlets; telescopic routing to centerbody leading edge required |
| Acoustic treatment | | Wall treatment more effective |

*FIGURE 15.—EVALUATION CHART—SINGLE THROAT SONIC INLETS*

| Design Consideration | | Variable Cowl Wall |
|---|---|---|
| | | 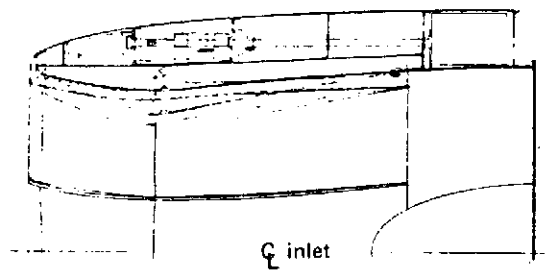 See figure A-12, volume II |
| Basic design | Lines | Good area progression profile at cruise; 11° diffusion angle during approach; L/D = 1.35 |
| | Structure | Conventional skin and frame outer surface with combination closure pan and leaf support beams on inner surface |
| | Mechanism | Eight sets of two leaves with link connected to track-mounted unison ring or driven by individual actuators; option: replace eight sets of two leaves with eight leaves with controlled flexure for throat variation |
| | Seals | Approximately 700 in. of leaf edge requires variable degree of sealing |
| | Range of application | Has advantage of maximum area change with minimum diameter change at outer surface |
| Actuation | Power source | Engine bleed air for two-position pneumatic system; hydraulics for multiple position |
| | Type of actuation | Four ball screws, gear box driven from air motor, driving unison ring or eight individual actuators |
| | Load and stroke | Load ≈ 20,000 lb; stroke = 5.4 in. |
| | Synchronization | Flex shaft between gear boxes for unison ring drive or common input to transfer valves on independent actuators having linearly variable differential transducer position feedback |
| | Failsafe potential | Pressure loads are adverse |
| Control | Two position | Electrical signal to air control valve |
| | Multiple position | Electronic input to electromechanical transfer valves nulled by linearly variable differential transducer position feedback with position selected as a function of engine rpm and total inlet pressure at the fan face 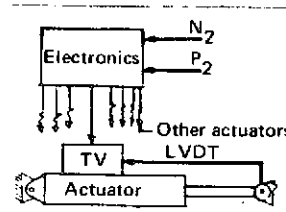 |
| Weight estimate (lb) | | Basic cowl 168.0<br>Nose dome 10.0<br>Variable leaves 104.0<br>Actuation and control 105.0<br>Anti-icing system 56.0<br>Total inlet 443.0<br>Engine penalty 41.0<br>Total 484.0<br>Comparative weight of 707-320B nonsonic inlet = 220 lb (scaled) |
| Smoothness | | Leaf support beams protrude into airstream during cruise; longitudinal and circumferential joints around leaves; variable gap in surface continuity at aft end of leaves 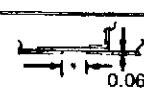 *Approach ≈ 0.80; cruise = 0.02 |
| Bird strike | | Leaf damage could cause failures that result in leaf ingestion (throat variation using leaves with controlled flexure would minimize this hazard) |
| Anti icing system | | Leading edge anti icing is readily accomplished; leaf jamming is a possibility |
| Acoustic treatment | | Wall treatment less effective |

*FIGURE 15.—Concluded*

| Design Consideration | | Rotating Radial Vanes (1) |
|---|---|---|
| | | 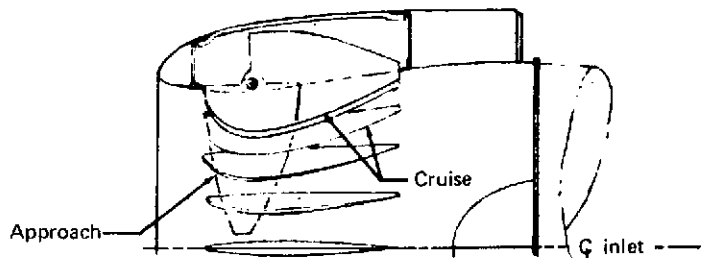 See figure A-1, volume II |
| Basic design | Lines | Good area progression; vane and actuation stowage influences shape of exterior lines; L/D = 1.05 |
| | Structure | Conventional skin and frame cowl with longitudinal stiffening and support in area of vane penetration |
| | Mechanism | Actuator-driven unison ring driving links to rotating vanes |
| | Seals | 30.0 in. of seal required around each vane; relatively simple for cruise-only seal, complex otherwise |
| | Range of application | Larger area changes can be achieved by adding vanes and cowl compromise |
| Actuation | Power source | Engine bleed air for two-position; pneumatic system hydraulic pump for multiple position |
| | Type of actuation | Pneumatic or hydraulic piston |
| | Load and stroke | Load ≈ 2400 lb; stroke = 8.9 in. |
| | Synchronization | Mechanical load limit or position feedback control |
| | Failsafe potential | Pressure loads tend to move vanes toward open throat position; balance point not established |
| Control | Two position | |
| | Multiple position | Electronic input to electromechanical transfer valve nulled by a linearly variable differential transducer position feedback with position selected as a function of engine rpm and total pressure at the fan face |
| Weight estimate (lb) | | Basic cowl 236.0<br>Nose dome 10.0<br>Radial vanes 74.0<br>Actuation and control 96.0<br>Anti-icing system 78.0<br>Total inlet 494.0<br>Engine penalty 48.0<br>Total 542.0 |
| Smoothness | | Exposed slots in cowl wall during approach (can be minimized or eliminated with added complexity) |
| Bird strike | | Shock-absorbing linkage or beef-up required |
| Anti-icing system | | Complicated multiple routing to vanes |
| Performance concerns | Leakage | Minimum at cruise; a concern in other positions |
| | Angle-of-attack sensitivity | Comparable to current inlets |
| | Distortion | Radial wakes (circumferential distortion) |
| | Diffusion angle | 7.5° (good) |
| | Vane airfoil | T/C = 0.14; taper ratio = 6/1 (add vanes to decrease) (T/C = thickness/chord) |
| | Flow passage Mach no. mismatch | Minimal |
| | Cruise flow restrictions | Vanes protrude in flow path |
| Acoustic potential | | Has potential of flow choking and lining of vanes and cowl wall |

*FIGURE 16.—EVALUATION CHART—MULTIPLE THROAT SONIC INLETS*

| Design Consideration | | Translating Parallel Vanes (2) |
|---|---|---|
| | | 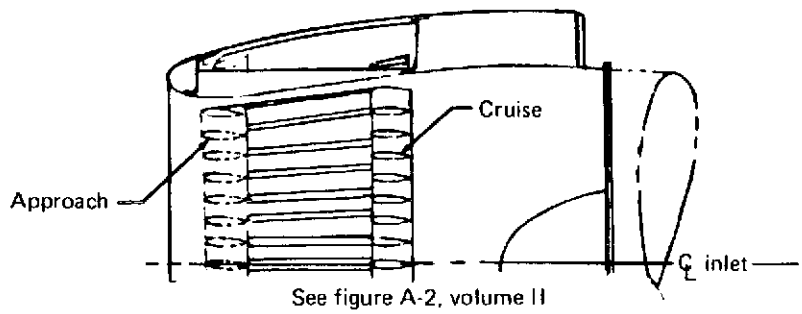 See figure A-2, volume II |
| Basic design | Lines | Vane support and actuation could influence shape of external lines; L/D 1.1 |
| | Structure | Conventional skin and frame cowl with longitudinal bridging in area of vane penetration |
| | Mechanism | Vanes attached to actuator-driven unison ring |
| | Seals | Difficult and complex seal design required for vane penetration slot closure |
| | Range of application | Limited by the amount of diffuser expansion possible for vane stowage; diffusion angle or inlet length and vane translation would increase |
| Actuation | Power source | Same as (1) |
| | Type of actuation | Same as (1) |
| | Load and stroke | Load ≈ 800 lb; stroke = 22.4 in. |
| | Synchronization | Same as (1) |
| | Failsafe potential | Friction forces will probably counteract pressure forces, and vanes will remain in position last called for if actuation fails |
| Control | Two position | |
| | Multiple position | Same as (1) |
| Weight estimate (lb) | | Basic cowl 184.0<br>Nose dome 10.0<br>Vanes 43.0<br>Actuation and control 58.0<br>Anti-icing system 59.0<br>Total inlet 390.0<br>Engine penalty 37.0<br>Total 427.0 |
| Smoothness | | Open slots in cowl wall during approach; smoothness at cruise will be a function of how well a difficult seal design problem is resolved |
| Bird strike | | Shock-absorbing support plus vane beef-up required |
| Anti-icing system | | Complicated routing to multiple translating vanes |
| Performance concerns | Leakage | Function of seal design at cruise; concern in other positions |
| | Angle-of-attack sensitivity | Same as (1) |
| | Pressure recovery | Same as (1) |
| | Distortion | Complicated distortion pattern |
| | Diffusion angle | Same as (1) |
| | Vane airfoil | T/C = 0.167 |
| | Flow passage Mach no. mismatch | Vanes adjacent to cowl could be a problem |
| | Cruise flow restrictions | Stowed vanes create a second throat |
| Acoustic potential | | Same as (1) |

*FIGURE 16.—Continued*

| Design Consideration | | Translating Radial Vanes (3) |
|---|---|---|
| | | 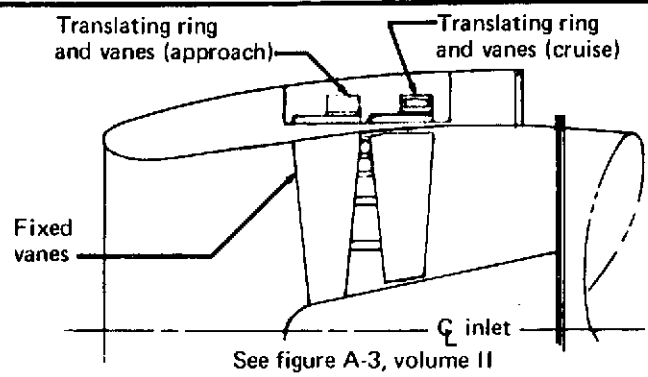 See figure A-3, volume II |
| Basic design | Lines | External lines could be affected as in (2); L/D = 1.1 |
| | Structure | Same as (2) |
| | Mechanism | Same as (2) |
| | Seals | Vane penetration sealing similar to (2); not quite as difficult |
| | Range of application | Same limitations as (2) |
| Actuation | Power source | Same as (1) |
| | Type of actuation | Same as (1) |
| | Load and stroke | Load ≈ 600 lb; stroke = 10.0 in. |
| | Synchronization | Same as (1) |
| | Failsafe potential | Same as (2) |
| Control | Two position | |
| | Multiple position | Same as (1) |
| Weight estimate (lb) | | Basic cowl 248.0<br>Nose dome 12.0<br>Radial vanes 67.0<br>Actuation and control 60.0<br>Anti-icing system 64.0<br>Total inlet 451.0<br>Engine penalty 45.0<br>Total 496.0 |
| Smoothness | | Same as (2) |
| Bird strike | | Same as (2) |
| Anti-icing system | | Same as (2) |
| Performance concerns | Leakage | Similar to (2) |
| | Angle-of-attack sensitivity | Same as (1) |
| | Pressure recovery | Same as (1) |
| | Distortion | Same as (1) |
| | Diffusion angle | Same as (1) |
| | Vane airfoil | T/C = 0.16 |
| | Flow passage Mach no. mismatch | Same as (1) |
| | Cruise flow restrictions | Same as (2) |
| Acoustic potential | | Same as (1) |

*FIGURE 16.—Continued*

| Design Consideration | | Expanding Radial Vanes (4) |
|---|---|---|
| | | 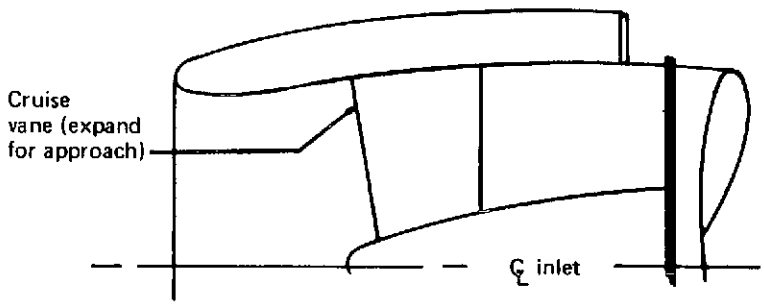 See figure A-4, volume II |
| Basic design | Lines | Good area progression; L/D = 1.2 |
| | Structure | Conventional skin and frame cowl |
| | Mechanism | Vane panels hinged for expansion and spring loaded to the collapsed cruise position |
| | Seals | Required at vane ends |
| | Range of application | Same limitations as (2) |
| Actuation | Power source | Engine bleed air |
| | Type of actuation | Pneumatic diaphrams and spring returns |
| | Load and stroke | Load ≈ 450 lb vane; stroke = 1.6 in. |
| | Synchronization | None; vane expansion will vary with ability to provide uniform airflow |
| | Failsafe potential | Vanes go to cruise position with loss of pneumatic power |
| Control | Two position | Electrical signal to air valve |
| | Multiple position | No positive way to control |
| Weight estimate (lb) | | Basic cowl 186.0<br>Nose dome 17.0<br>Radial vanes and actuation and control 110.0<br>Anti-icing system 66.0<br>Total inlet 379.0<br>Engine penalty 34.0<br>Total 413.0 |
| Smoothness | | Depression in vane cross section at cruise |
| Bird strike | | Can be handled structurally |
| Anti-icing system | | Can be accomplished with fixed plumbing |
| Performance concerns | Leakage | Not as big a problem as (1), (2), and (3) |
| | Angle-of-attack sensitivity | Same as (1) |
| | Pressure recovery | Same as (1) |
| | Distortion | Same as (1) |
| | Diffusion angle | Same as (1) |
| | Vane airfoil | Cruise T/C = 0.073; approach T/C = 0.185 |
| | Flow passage Mach no. mismatch | Same as (1) |
| | Cruise flow restrictions | Less restriction than (1), (2), and (3) |
| Acoustic potential | | Acoustic material on vanes would have less area and be less effective than (1), (2), and (3) |

*FIGURE 16.—Continued*

| Design Consideration | | Translating Radial Vane and Centerbody (5) |
|---|---|---|
| | | 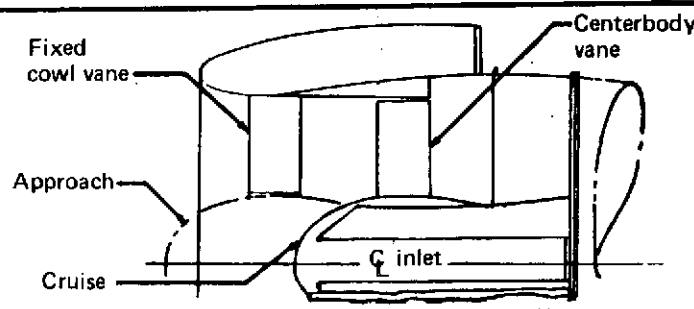 See figure A-5, volume II |
| Basic design | Lines | Good area progression; L/D = 1.07 |
| | Structure | Conventional skin and frame outer cowl with centerbody supported by IGVs or struts |
| | Mechanism | Actuator-driven centerbody translating on slide blocks and tracks |
| | Seals | None required |
| | Range of application | Same limitations as (2) |
| Actuation | Power source | Same as (1) |
| | Type of actuation | Same as (1) |
| | Load and stroke | Load ≈ 3500 lb; stroke = 20.0 in. |
| | Synchronization | None required (single actuator) |
| | Failsafe potential | Plug venting or locking devices required to counteract adverse pressure loads |
| Control | Two position | |
| | Multiple position | Same as (1) |
| Weight estimate (lb) | | Basic cowl 140.0<br>Translating centerbody 38.0<br>IGV modification or centerbody 34.0<br>Support struts centerbody support structure 69.0<br>Vanes 88.0<br>Actuation and control 20.0<br>Anti-icing system 75.0<br>Total inlet 464.0<br>Engine penalty 32.0<br>Total 496.0 |
| Smoothness | | No surface roughness anticipated |
| Bird strike | | Can be handled structurally |
| Anti-icing system | | Outer cowl leading edge comparable to existing inlets; telescopic routing to centerbody and vane leading edges required |
| Performance concerns | Leakage | Not a problem |
| | Angle-of-attack sensitivity | Centerbody extension at approach could create adverse flow conditions |
| | Pressure recovery | Same as (1) |
| | Distortion | Same as (1) |
| | Diffusion angle | Same as (1) |
| | Vane airfoil | Maximum T/C = 0.09 |
| | Flow passage Mach no. mismatch | Diffusion angles differ on sides of flow passages at approach |
| | Cruise flow restrictions | Stowed vanes disrupt diffusion |
| Acoustic potential | | Same as (1) plus centerbody lining is also possible |

*FIGURE 16.—Continued*

| Design Consideration | | Translating Ring (6) |
|---|---|---|
| | | 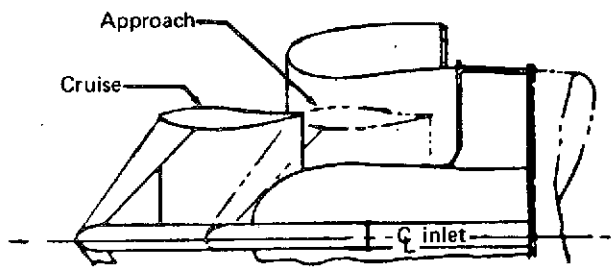 See figure A-7, volume II |
| Basic design | Lines | Achievement of good area progression is complicated by shape and position of ring; $L/D_{cowl}$ = 0.75, $L/D_{ring}$ = 1.14 |
| | Structure | Conventional skin and frame outer cowl with centerbody and ring supported by IGVs or struts |
| | Mechanism | Actuator-driven centerbody translating on slide block and tracks |
| | Seals | None required |
| | Range of application | Larger area changes can be achieved by increased ring size and cowl length |
| Actuation | Power source | Same as (1) |
| | Type of actuation | Same as (1) |
| | Load and stroke | Load ≈ 2000 lb; stroke = 21.3 in. |
| | Synchronization | Same as (5) |
| | Failsafe potential | Will probably stay in last position called for if actuator fails |
| Control | Two-position | |
| | Multiple position | Same as (1) |
| Weight estimate (lb) | | Basic cowl 91.0<br>Translating ring 50.0<br>Fixed centerbody 66.0<br>Ring support 33.0<br>IGV modification or struts 34.0<br>Actuation and control 20.0<br>Anti-icing system 75.0<br>Total inlet 369.0<br>Engine penalty 30.0<br>Total 399.0 |
| Smoothness | | No major surface roughness anticipated |
| Bird strike | | Can be handled structurally |
| Anti-icing system | | Outer cowl comparable to existing inlets; telescopic routing to translating centerbody and ring required |
| Performance concerns | Leakage | Not a problem |
| | Angle-of-attack sensitivity | Could be a major problem |
| | Pressure recovery | Same as (1) |
| | Distortion | Circumferential wake (radial distortion) |
| | Diffusion angle | 5.5° |
| | Vane airfoil | NACA 64-415 |
| | Flow passage Mach no. mismatch | Positioning ring to match exit Mach numbers from flow passages at both cruise and approach will be a problem |
| | Cruise flow restrictions | Ring and support struts in freestream |
| Acoustic potential | | Has potential for choking plus acoustic material on ring, cowl, and centerbody |

*FIGURE 16.—Continued*

| Design Consideration | | Translating Ring and Centerbody (7) |
|---|---|---|
| | | 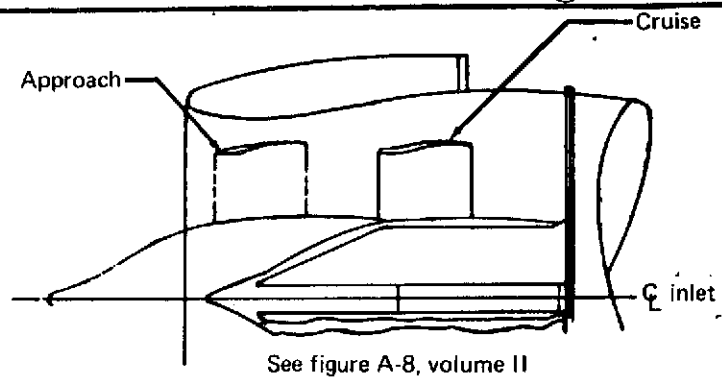 See figure A-8, volume II |
| Basic design | Lines | Same as (6) except L/D = 0.95 |
| | Structure | Conventional skin and frame outer cowl with centerbody supported by IGVs or struts |
| | Mechanism | Same as (6) |
| | Seals | None required |
| | Range of application | Larger area changes possible by increasing cowl length and translation |
| Actuation | Power source | Same as (1) and (6) |
| | Type of actuation | Same as (1) and (6) |
| | Load and stroke | Load ≈ 3500 lb; stroke = 21.8 in. |
| | Synchronization | Same as (5) |
| | Failsafe potential | Same as (6) |
| Control | Two position | |
| | Multiple position | Same as (1) |
| Weight estimate (lb) | | Basic cowl 126.0<br>Translating centerbody 55.0<br>IGV modification or support struts 34.0<br>Centerbody support structure 70.0<br>Actuation and control 22.0<br>Anti-icing system 65.0<br>Total inlet 387.0<br>Engine penalty 20.0<br>Total 407.0 |
| Smoothness | | Same as (6) |
| Bird strike | | Same as (6) |
| Anti-icing system | | Same as (6) |
| Performance concerns | Leakage | Not a problem |
| | Angle-of-attack sensitivity | Less cause for concern than (6) |
| | Pressure recovery | Same as (1) |
| | Distortion | Same as (6) |
| | Diffusion angle | 9.5° |
| | Vane airfoil | T/C = 0.08 |
| | Flow passage Mach no. mismatch | Similar problem but to a lesser degree than (6) |
| | Cruise flow restrictions | Ring and support struts in diffuser |
| Acoustic potential | | Same as (6) |

*FIGURE 16.—Continued*

| Design Consideration | | Variable Inlet Guide Vanes (8) |
|---|---|---|
| | | 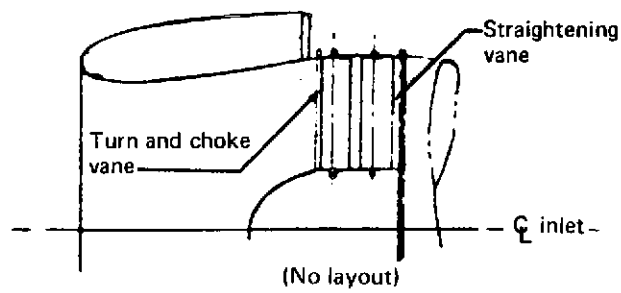 (No layout) |
| Basic design | Lines | Comparable to current inlets; L/D = 0.94 |
| | Structure | Conventional skin and frame outer cowl with engine case and shaft extended for vane support |
| | Mechanism | Actuator-driven unison ring that rotates around engine driving links that rotate vanes |
| | Seals | 72 rotary seals required as configured |
| | Range of application | A Mach 0.80 throat requires close to limit vane turning of 40° |
| Actuation | Power source | Same as (1) |
| | Type of actuation | Same as (1) |
| | Load and stroke | Load ≈ 1500 lb; stroke = 2.04 in. |
| | Synchronization | Same as (5) |
| | Failsafe potential | Vane pivot points should be forward of center of pressure for vanes to trail in failsafe position (see detail I on LO-INSP-014) |
| Control | Two position | |
| | Multiple position | Same as (1) |
| Weight estimate (lb) | | Basic cowl 111.0<br>Engine case extension 49.0<br>IGVs 230.0<br>Vane support hub 19.0<br>Shaft extension and spinner 15.0<br>Actuation and control 54.0<br>Anti-icing system 56.0<br>Total inlet 535.0<br>Engine penalty 12.0<br>Total 547.0 |
| Smoothness | | Surface imperfections will occur at vane ends due to rotation within curved surfaces |
| Bird strike | | Bird strike with vanes at 40°rotation could be difficult to handle |
| Anti-icing system | | Outer cowl comparable to existing inlets; vane leading edge requires multiple complex routing |
| Performance concerns | Leakage | Not a problem |
| | Angle-of-attack sensitivity | Comparable to current inlets |
| | Pressure recovery | Unknown |
| | Distortion | Same as (1) |
| | Diffusion angle | 7.7° |
| | Vane airfoil | T/C = 0.087 |
| | Flow passage Mach no. mismatch | Not a problem from an area standpoint |
| | Cruise flow restrictions | IGVs in diffuser |
| Acoustic potential | | Same as (1) |

*FIGURE 16.—Concluded*

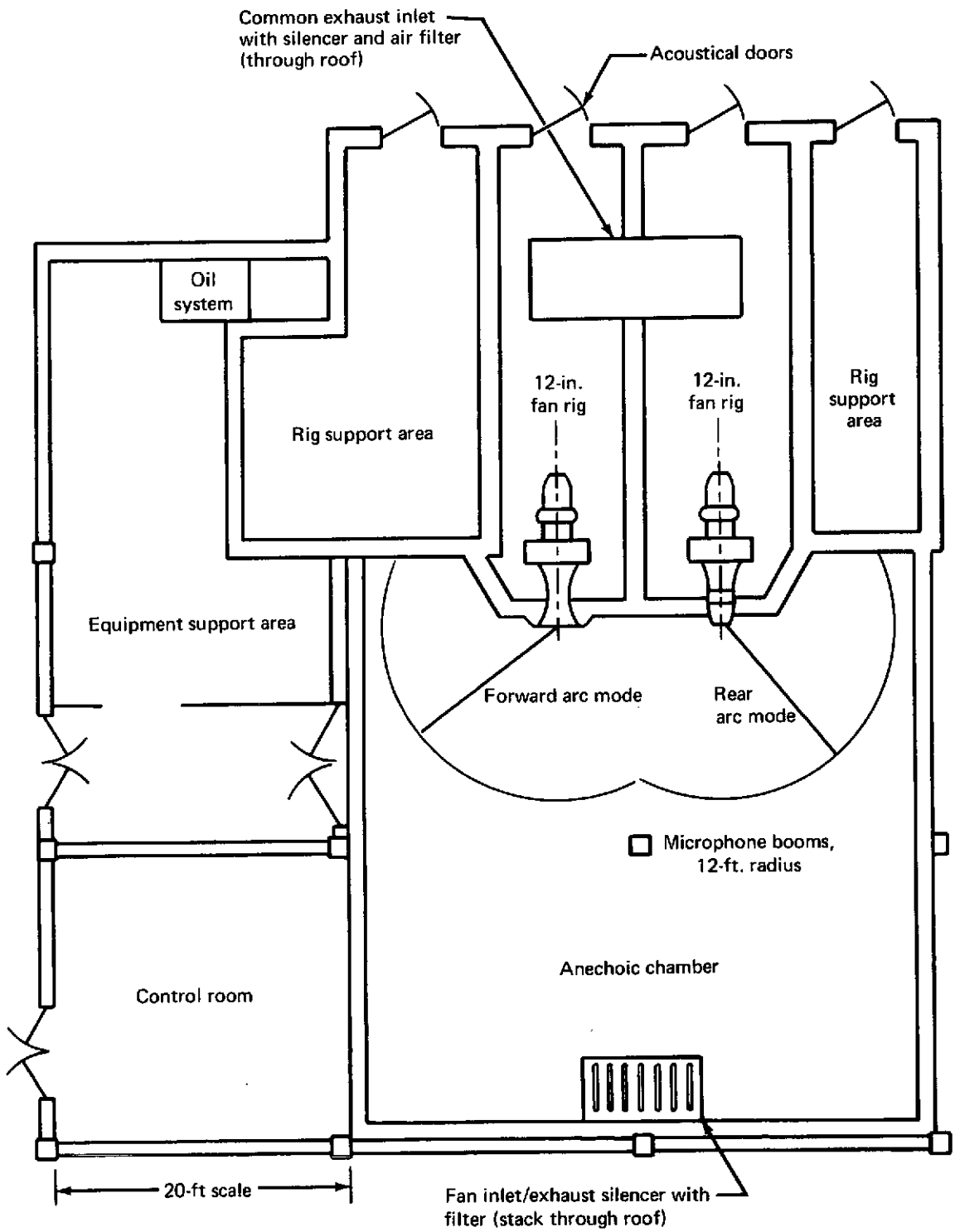


*FIGURE 17.–ACOUSTIC TEST FACILITY–12.-IN. FAN*

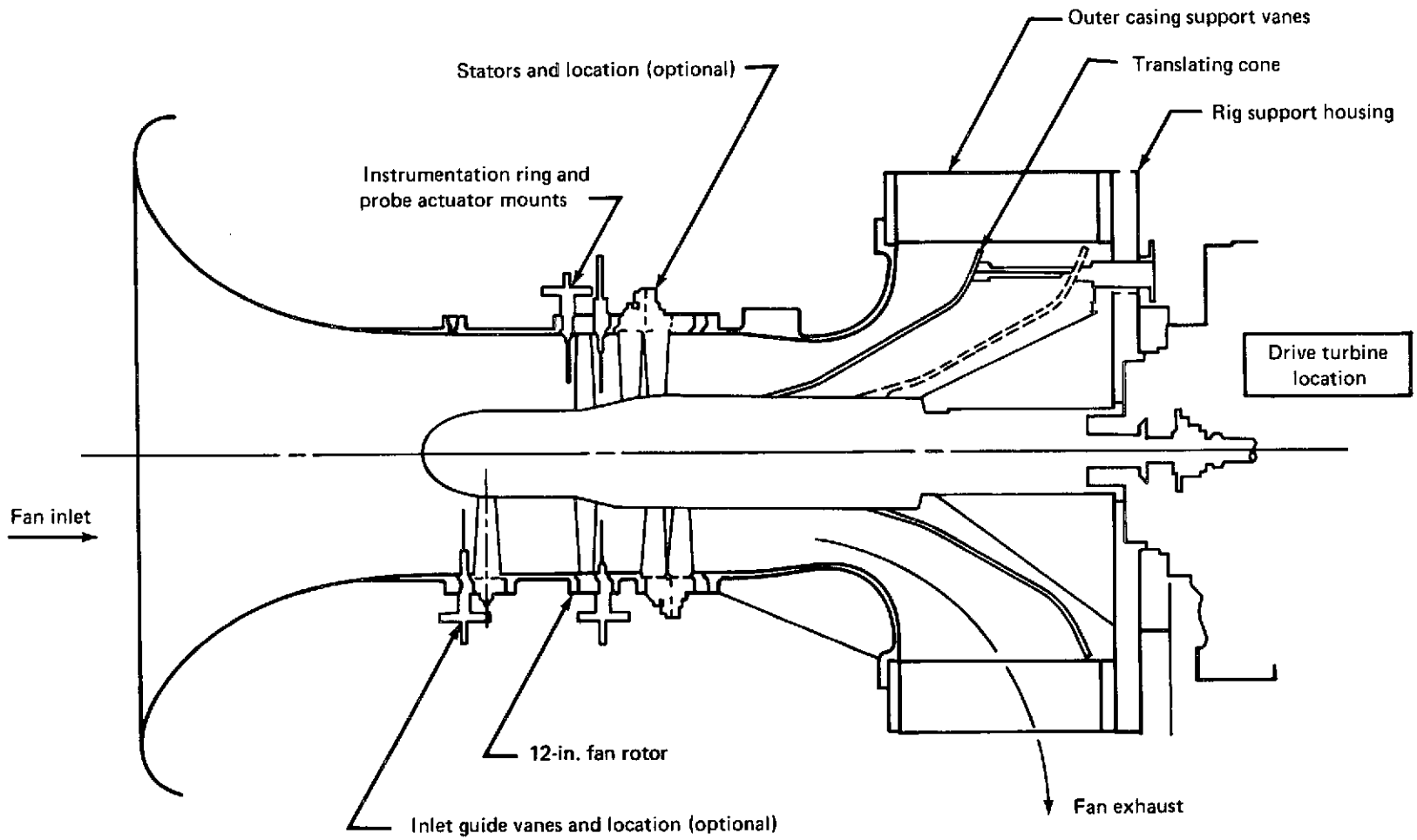


*FIGURE 18.–FORWARD ARC NOISE MODE–12-IN. FAN*

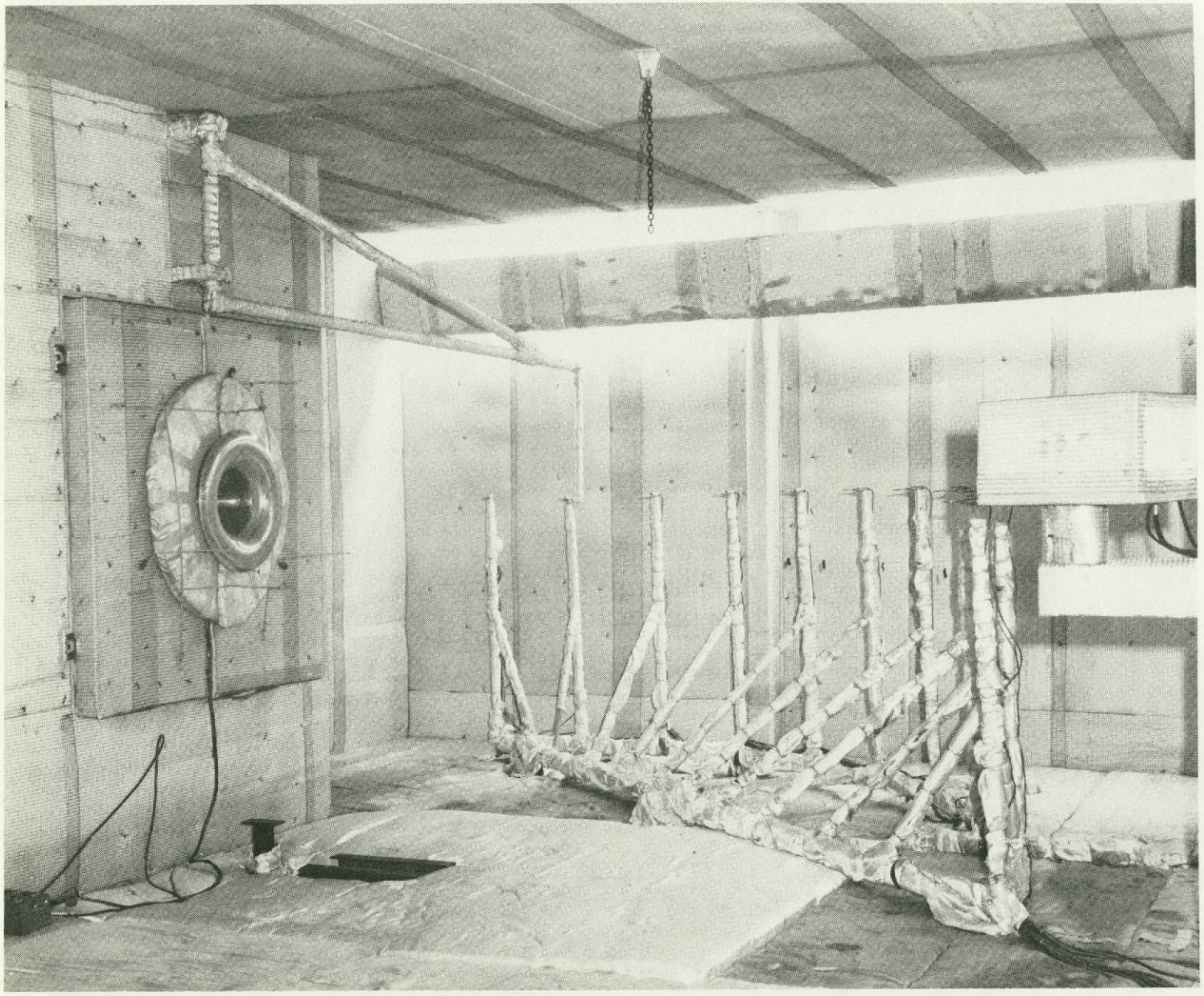

*FIGURE 19.—ANECHOIC ROOM WITH MODEL AND BELLMOUTH INSTALLED*

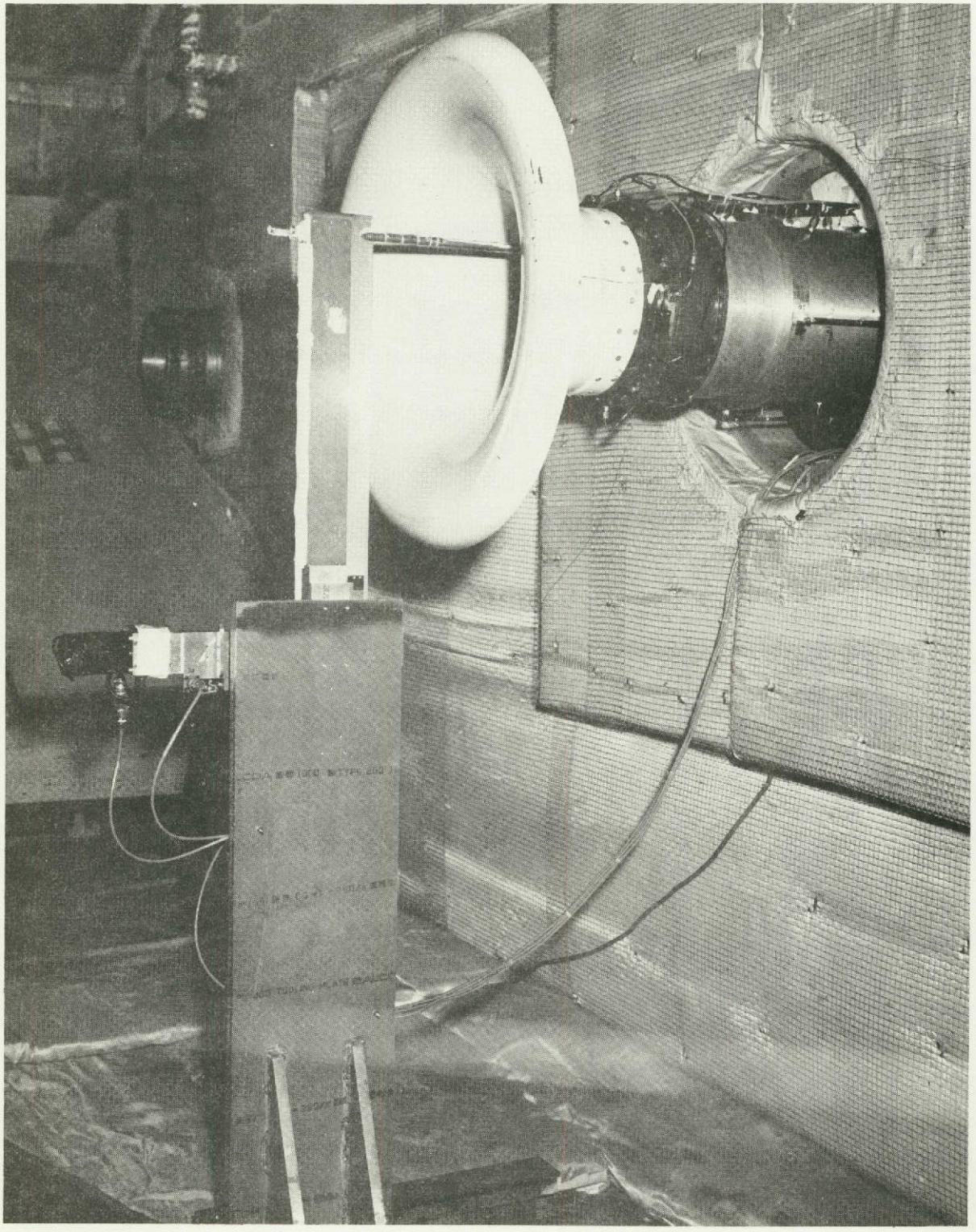

*FIGURE 20.—STINGER PROBE INSTALLATION*

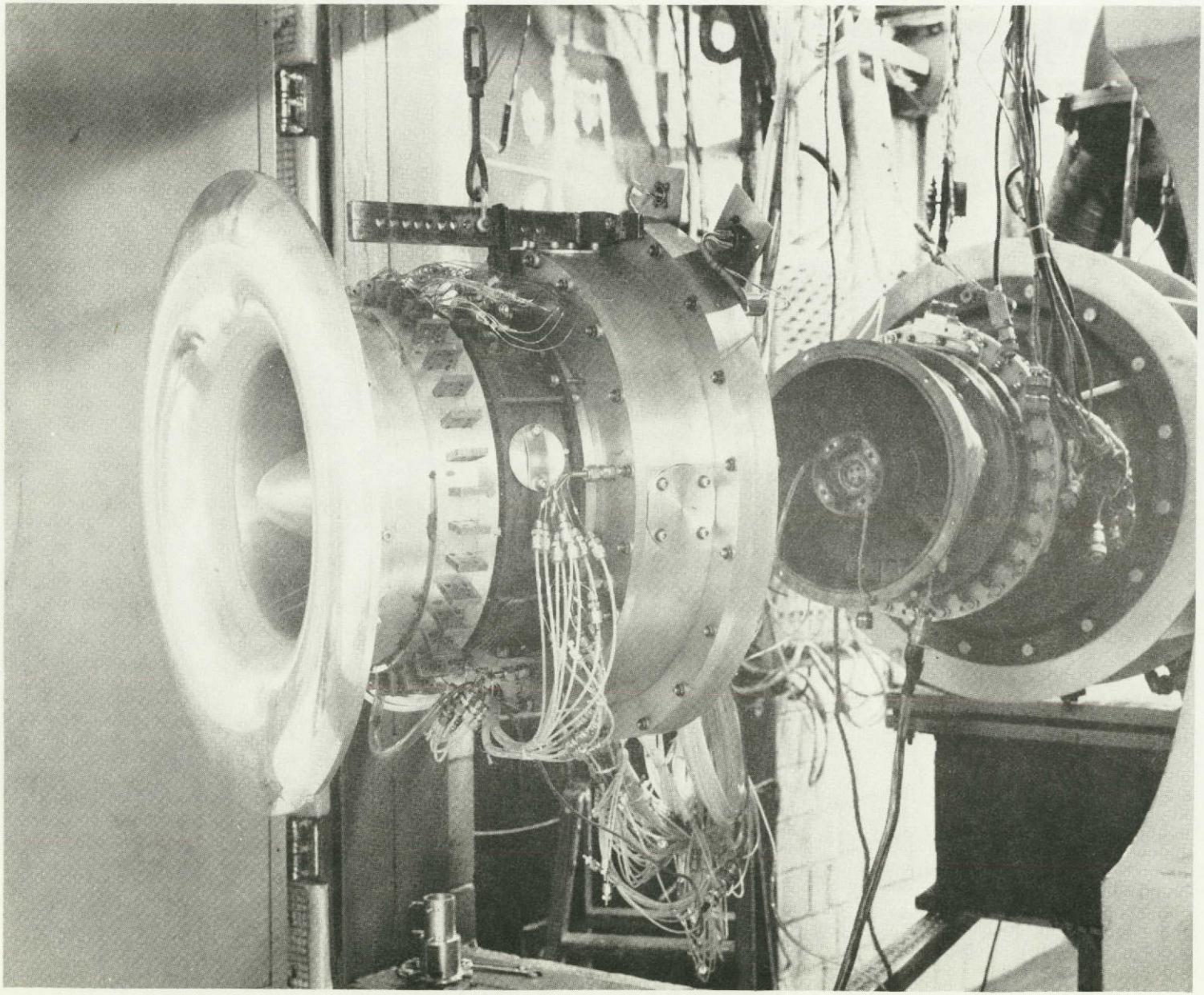

*FIGURE 21.–TEST APPARATUS*

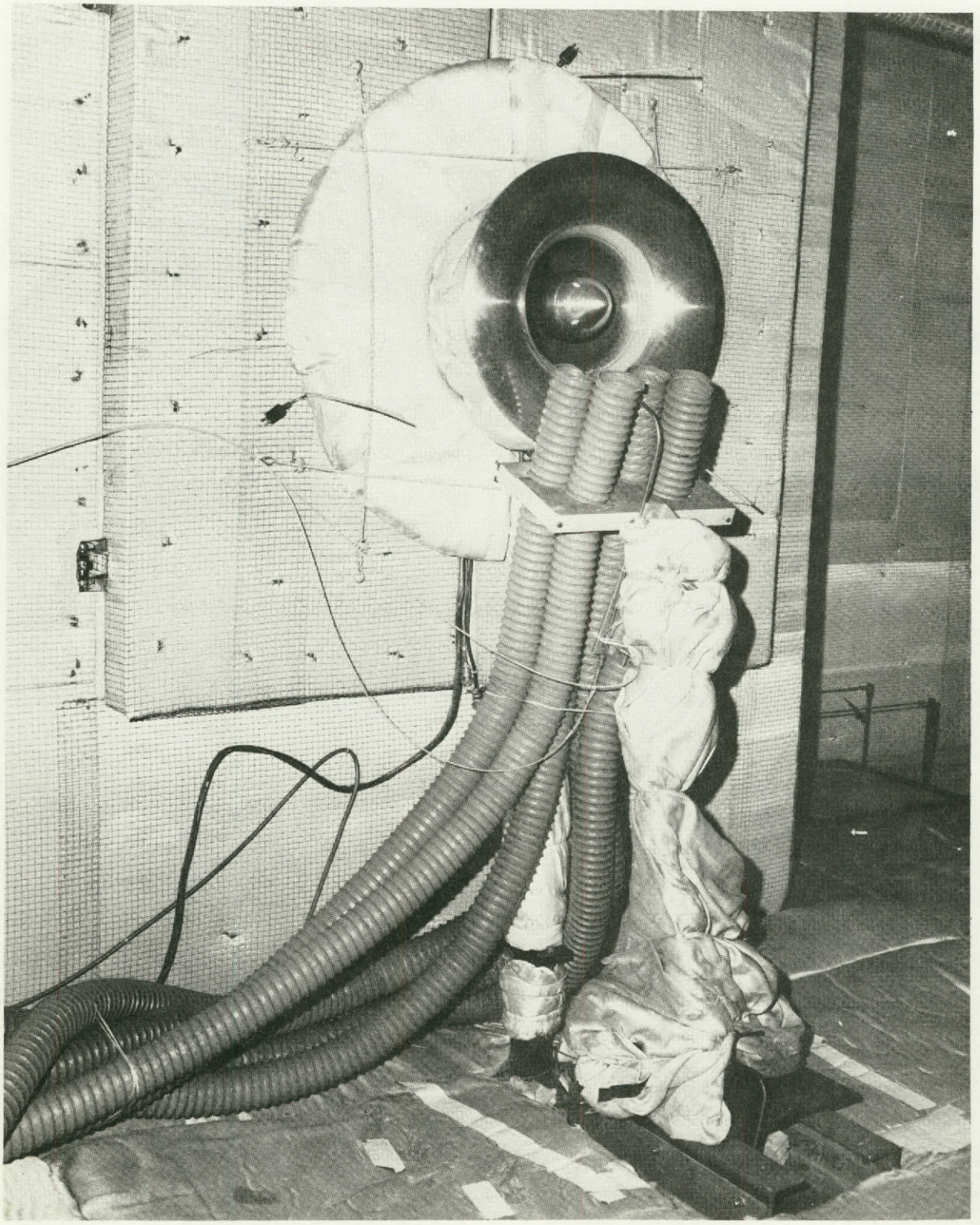

*FIGURE 22.—CROSSWIND BLOWING RIG*

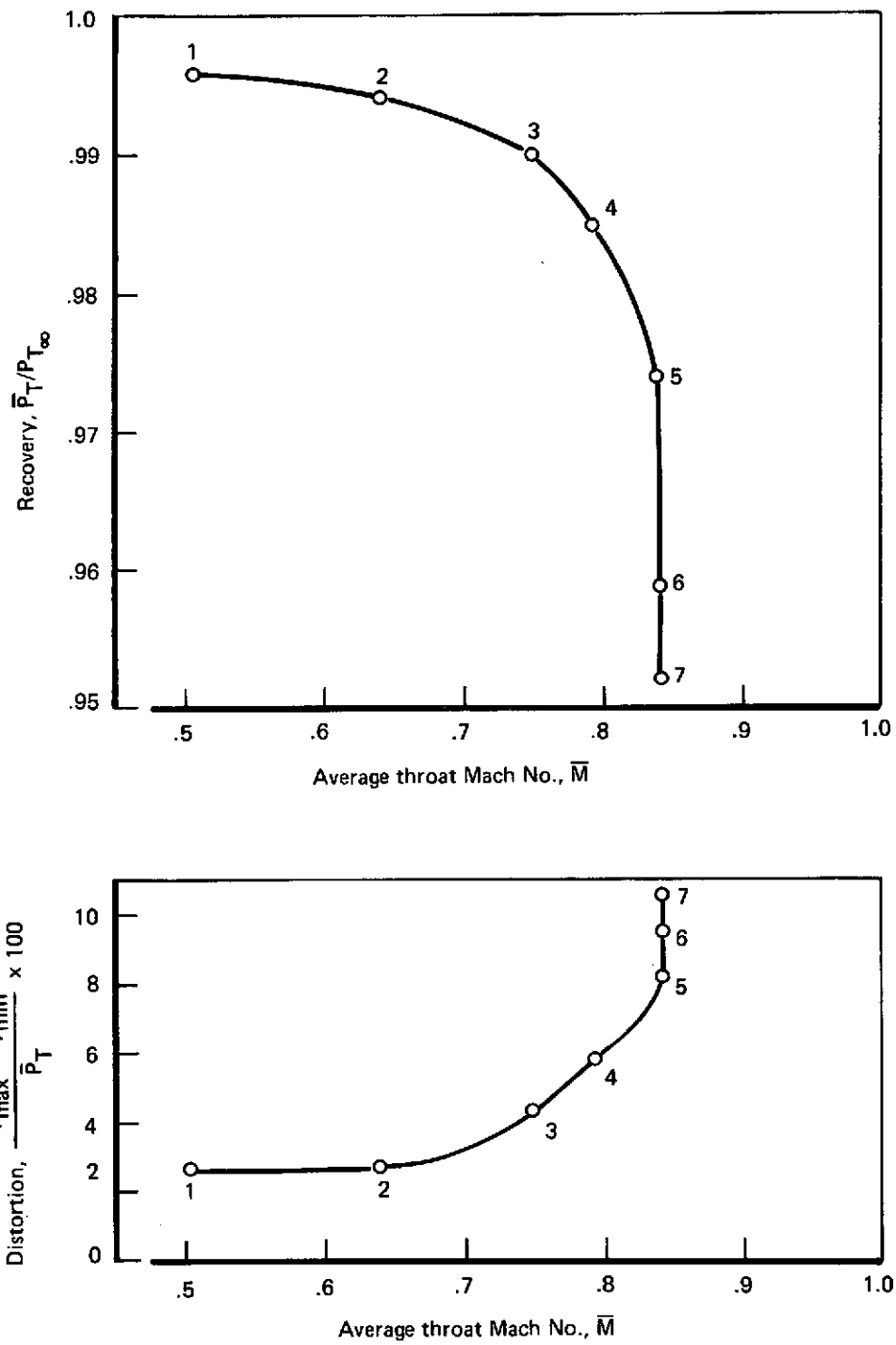


*FIGURE 23.–RECOVERY AND DISTORTION VS THROAT MACH NUMBER–RUN 2, MODEL 1*

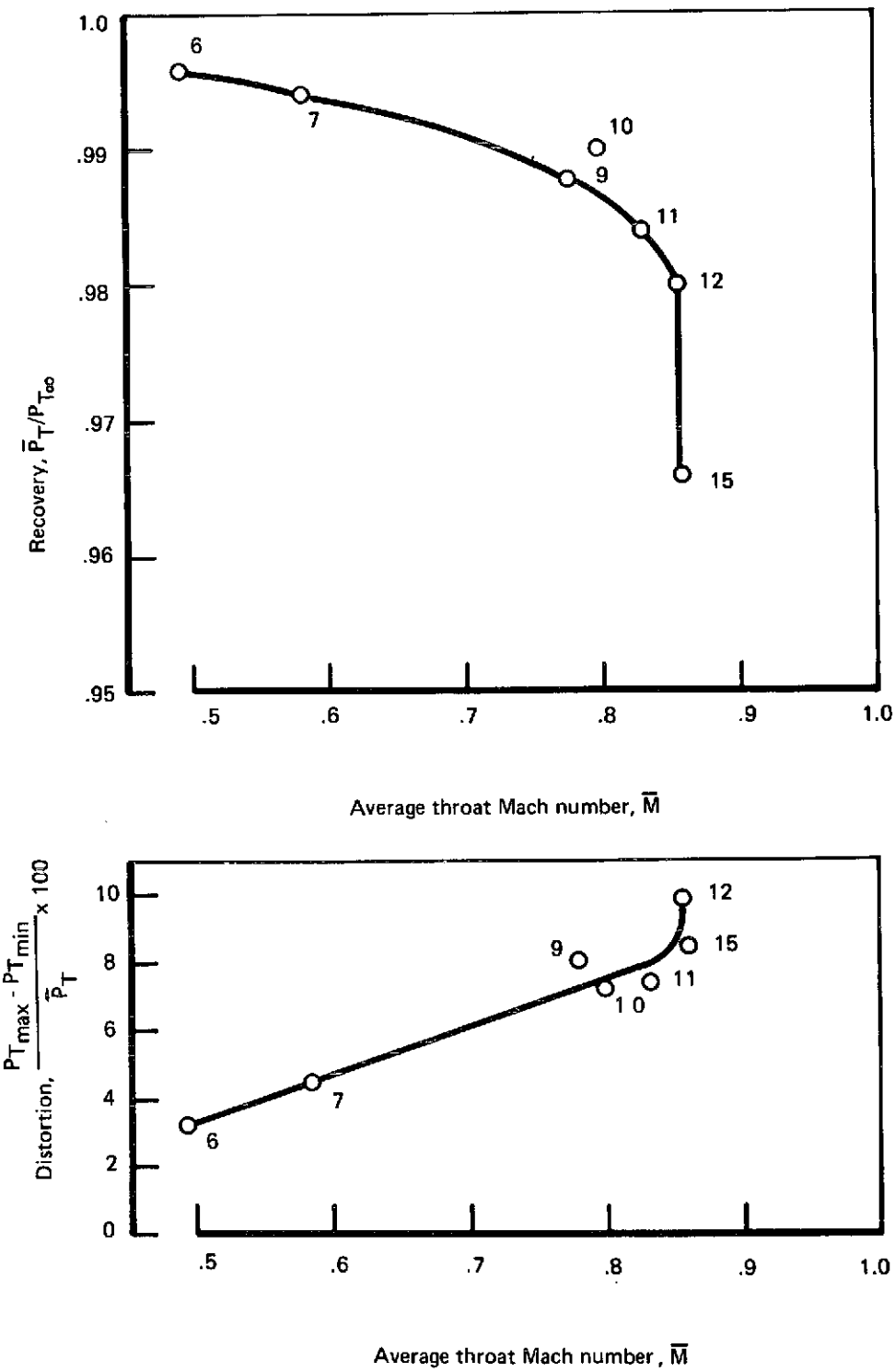


*FIGURE 24.–RECOVERY AND DISTORTION VS THROAT MACH NUMBER–RUN 4, MODEL 3*

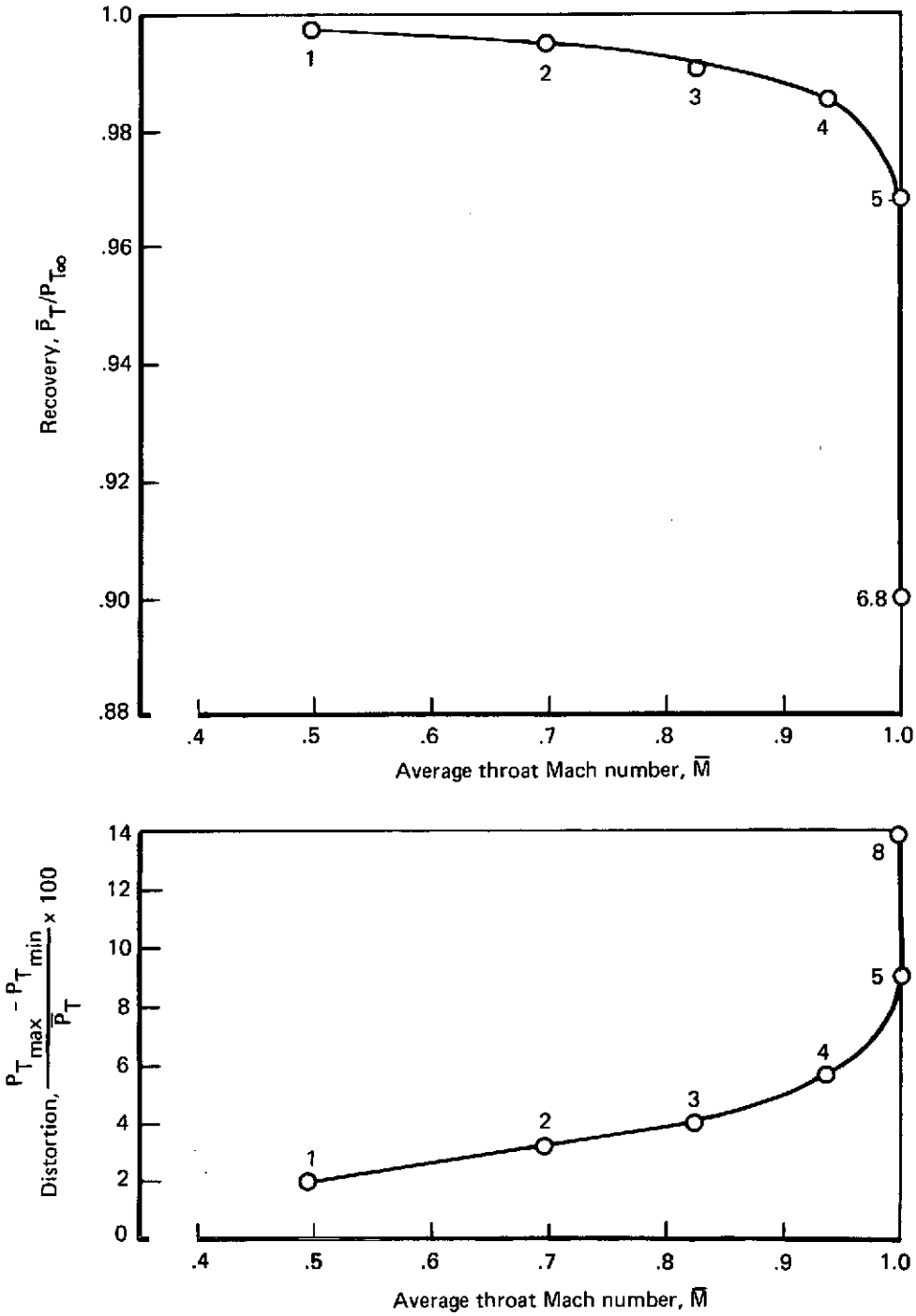


*FIGURE 25.–RECOVERY AND DISTORTION VS THROAT MACH NUMBER–RUN 6, MODEL 4*

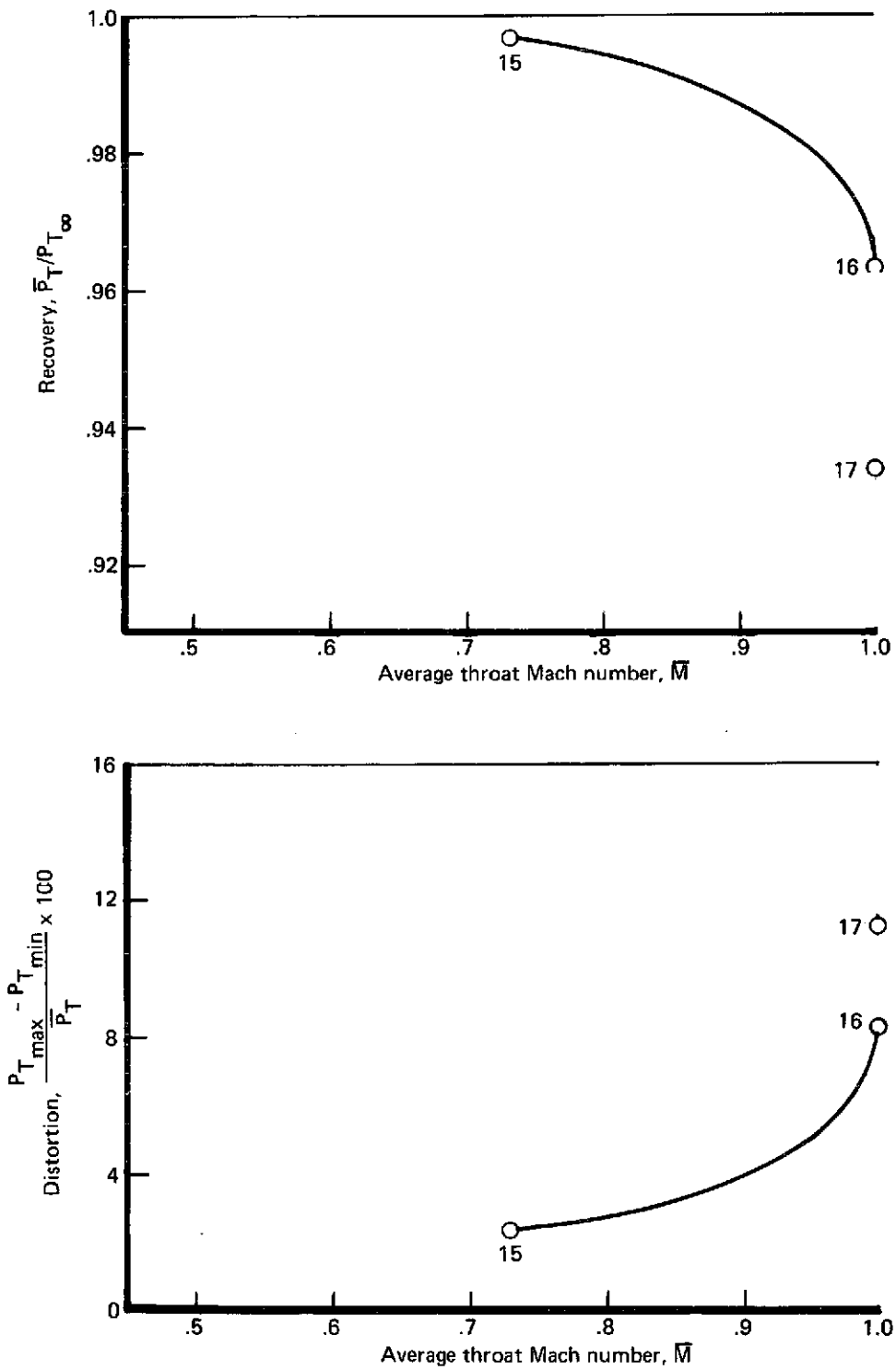


*FIGURE 26.–RECOVERY AND DISTORTION VS THROAT MACH NUMBER–RUN 11, MODEL 4*

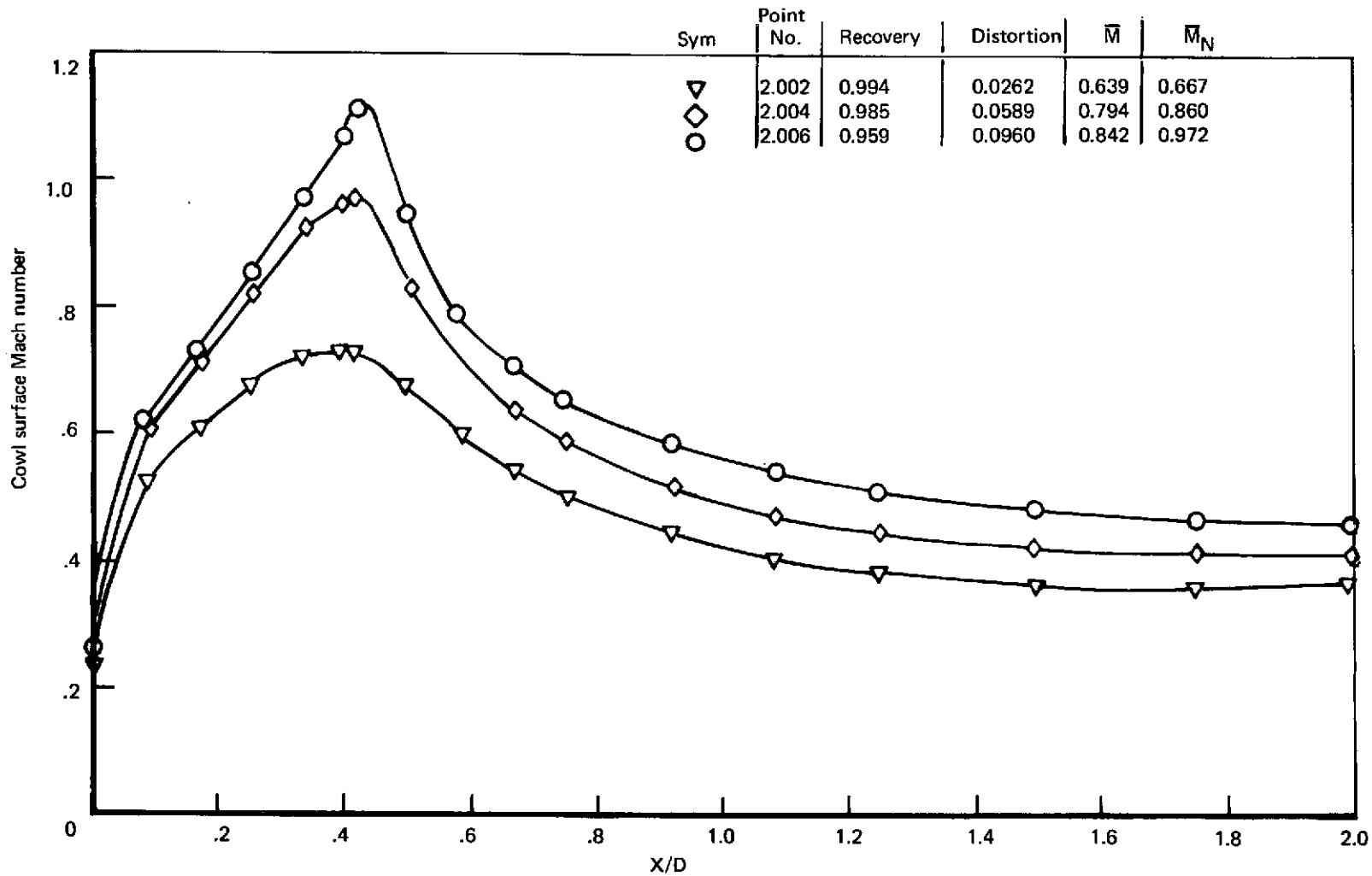


*FIGURE 27.–COWL SURFACE MACH NUMBER DISTRIBUTION–RUN 2, MODEL 1*

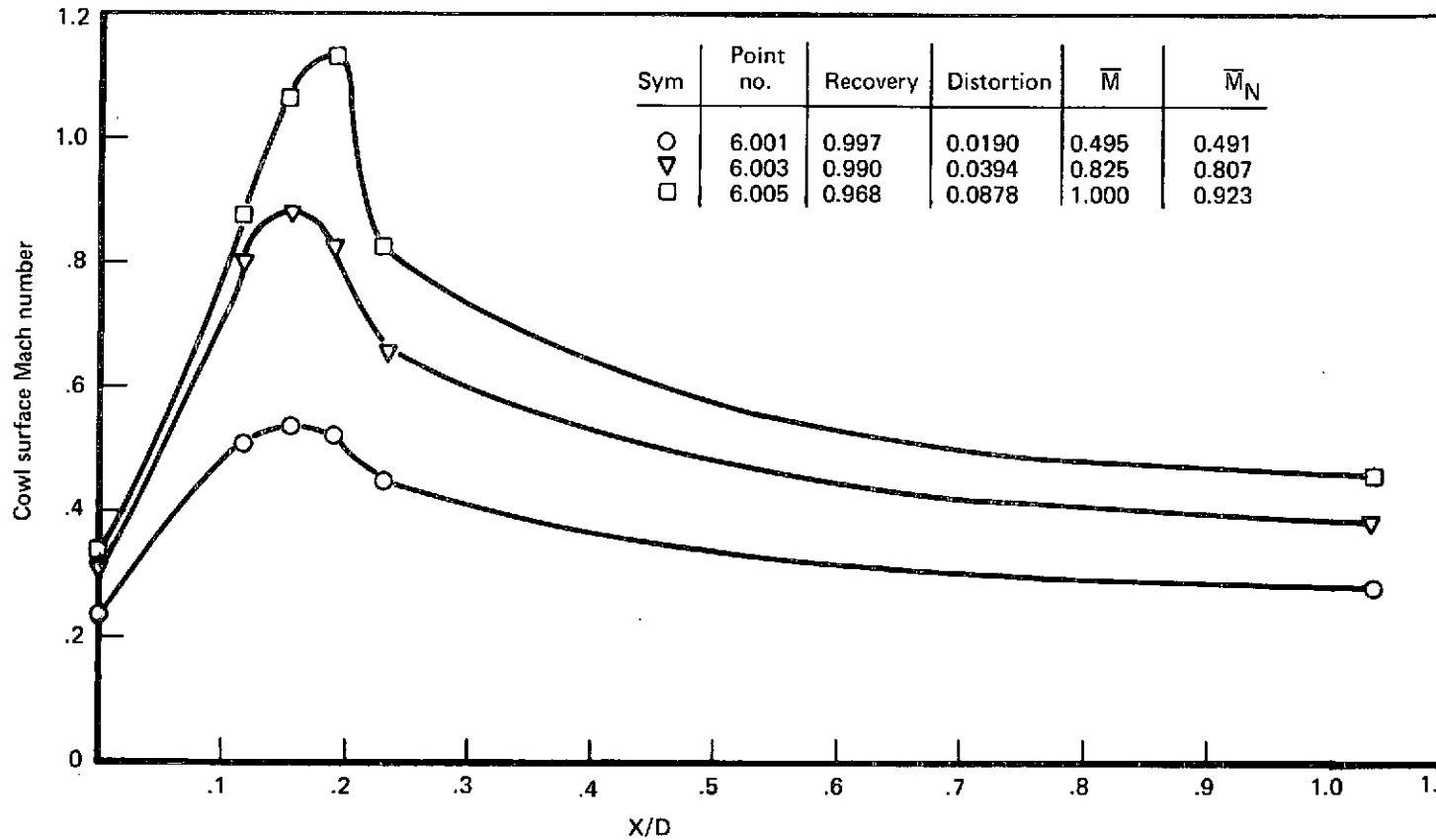


*FIGURE 28.—COWL SURFACE MACH NUMBER DISTRIBUTION— RUN 6, MODEL 4*

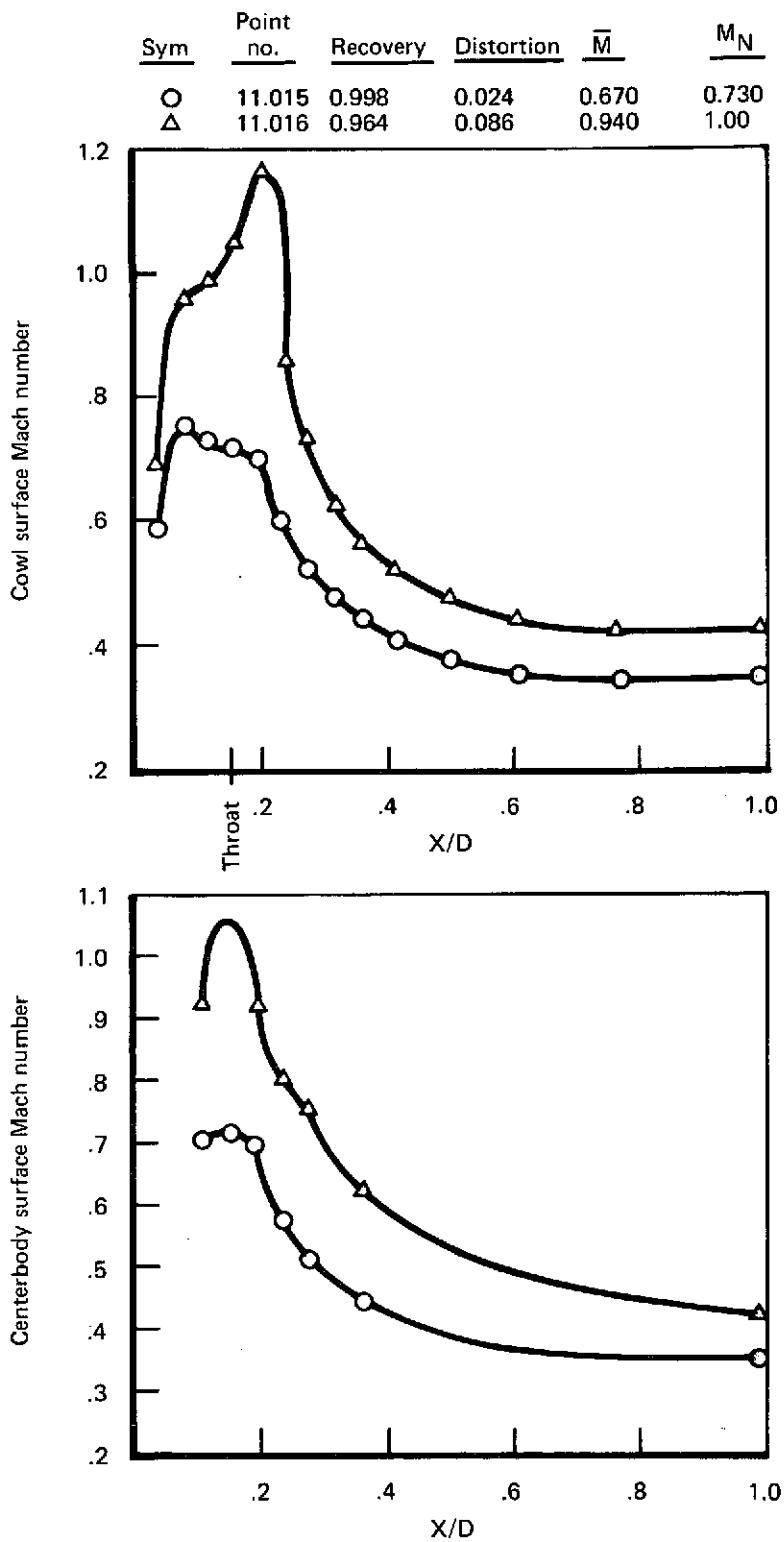


*FIGURE 29.–MODEL SURFACE MACH NUMBER DISTRIBUTION–RUN 11, MODEL 4*

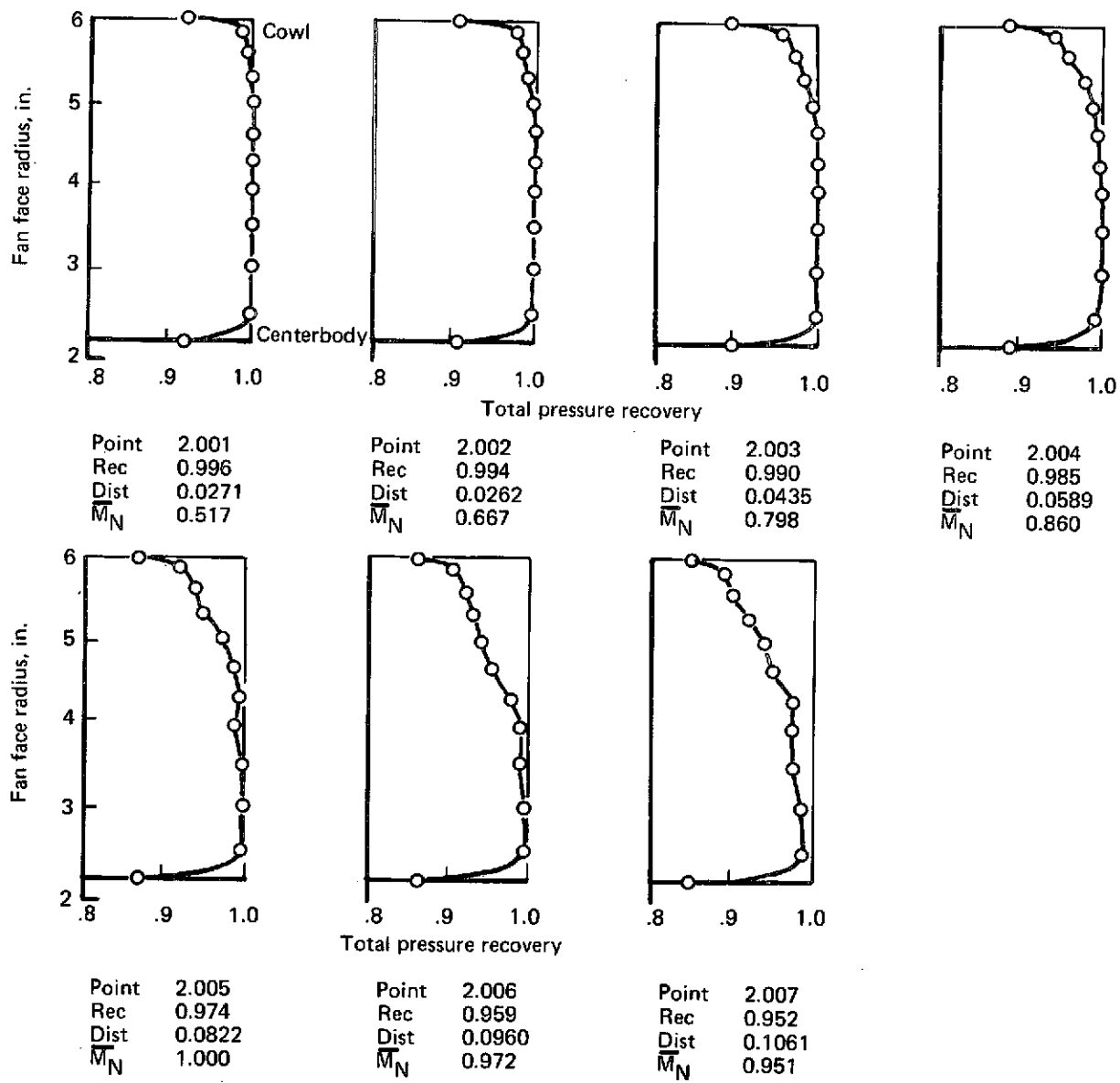


*FIGURE 30.–RECOVERY PROFILES–RUN 2, MODEL 1*

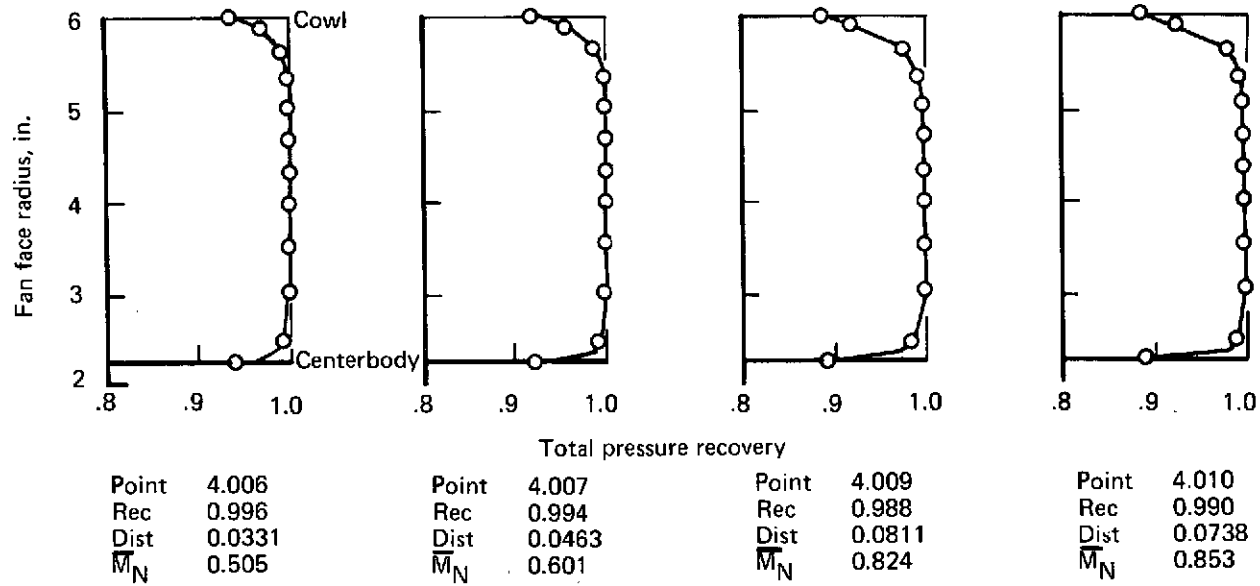


| Point | 4.006 |
|---|---|
| Rec | 0.996 |
| Dist | 0.0331 |
| $\overline{M}_N$ | 0.505 |

| Point | 4.007 |
|---|---|
| Rec | 0.994 |
| Dist | 0.0463 |
| $\overline{M}_N$ | 0.601 |

| Point | 4.009 |
|---|---|
| Rec | 0.988 |
| Dist | 0.0811 |
| $\overline{M}_N$ | 0.824 |

| Point | 4.010 |
|---|---|
| Rec | 0.990 |
| Dist | 0.0738 |
| $\overline{M}_N$ | 0.853 |

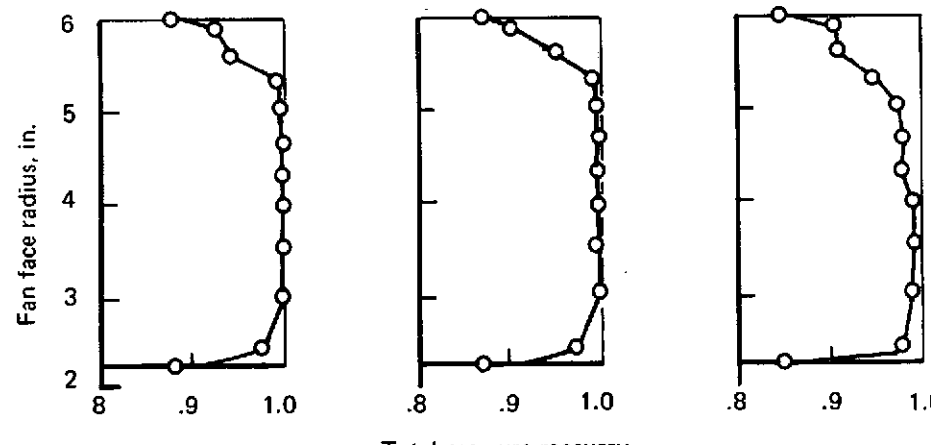


| Point | 4.011 |
|---|---|
| Rec | 0.984 |
| Dist | 0.0752 |
| $\overline{M}_N$ | 0.905 |

| Point | 4.012 |
|---|---|
| Rec | 0.980 |
| Dist | 0.0990 |
| $\overline{M}_N$ | 1.000 |

| Point | 4.015 |
|---|---|
| Rec | 0.966 |
| Dist | 0.0858 |
| $\overline{M}_N$ | 0.893 |

*FIGURE 31.—RECOVERY PROFILES—RUN 4, MODEL 3*

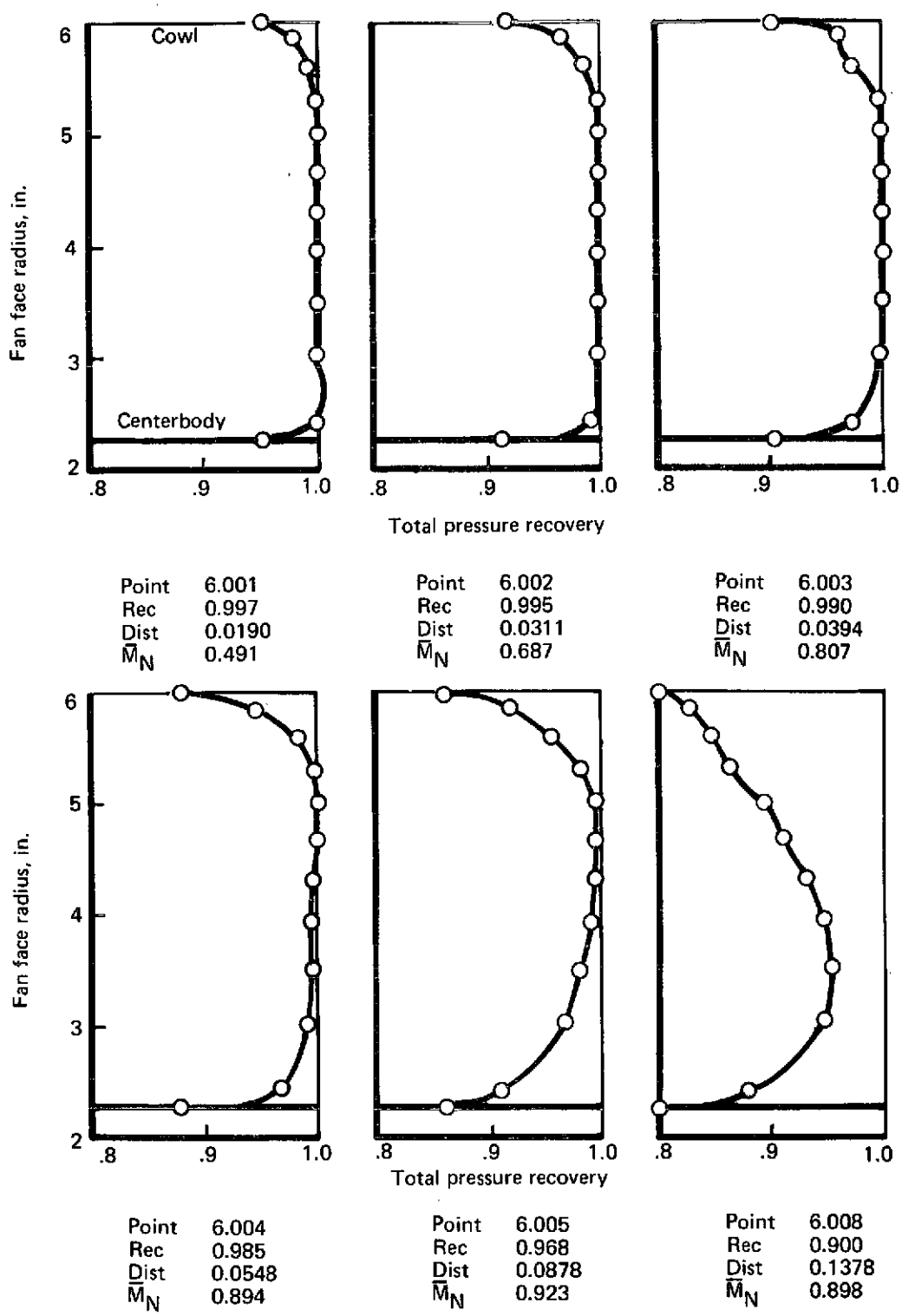


*FIGURE 32.–RECOVERY PROFILES–RUN 6, MODEL 4*

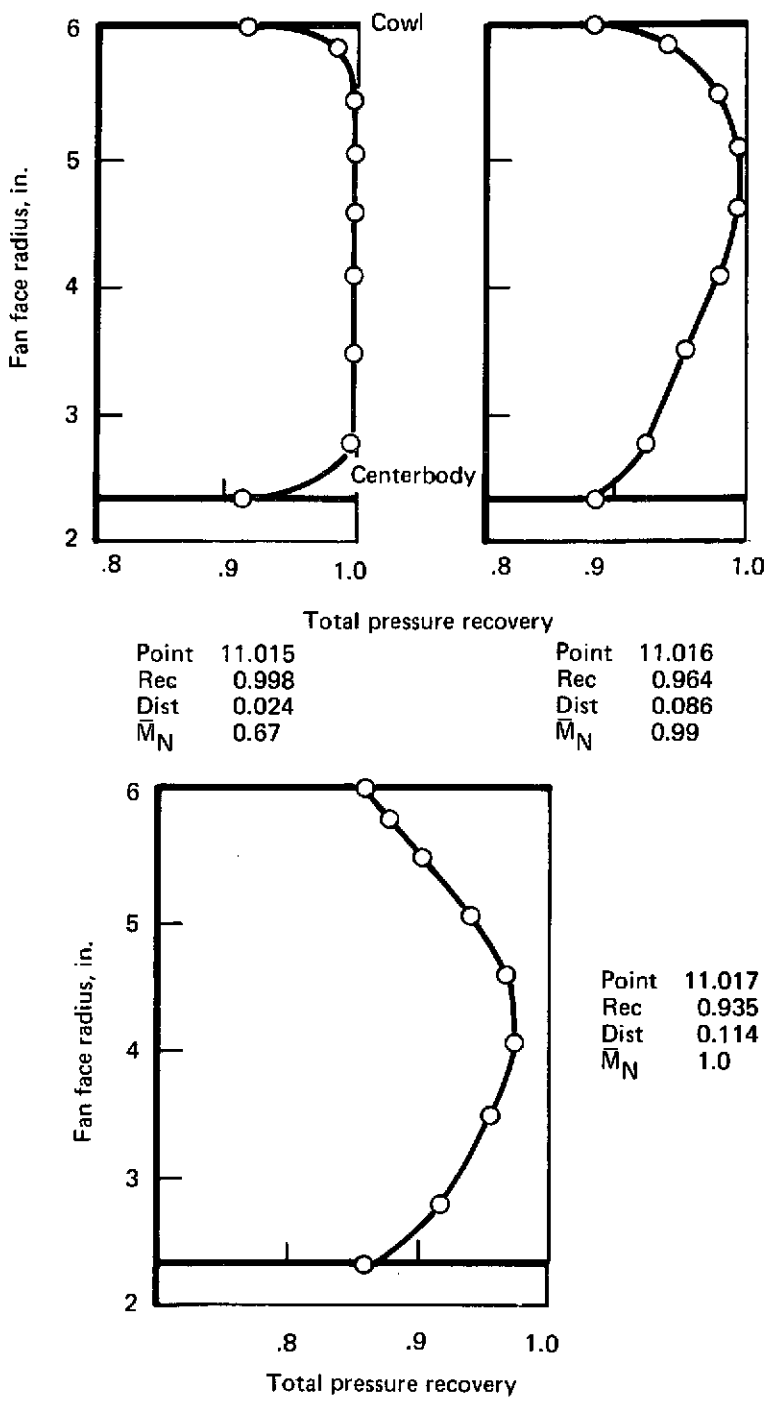


*FIGURE 33.–RECOVERY PROFILES–RUN 11, MODEL 4*

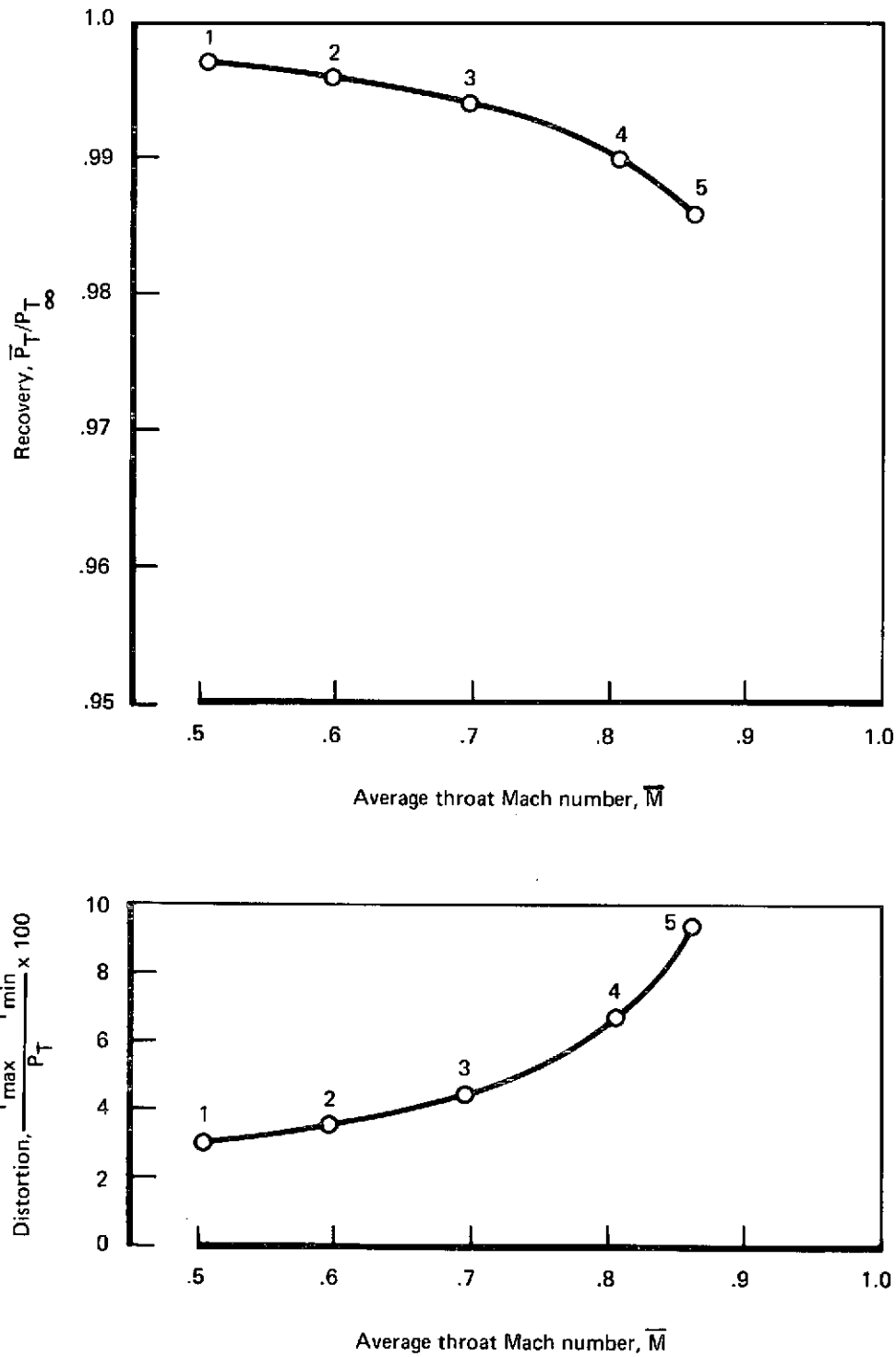


*FIGURE 34.—RECOVERY AND DISTORTION VS THROAT MACH NUMBER—RUN 3, MODEL 2*

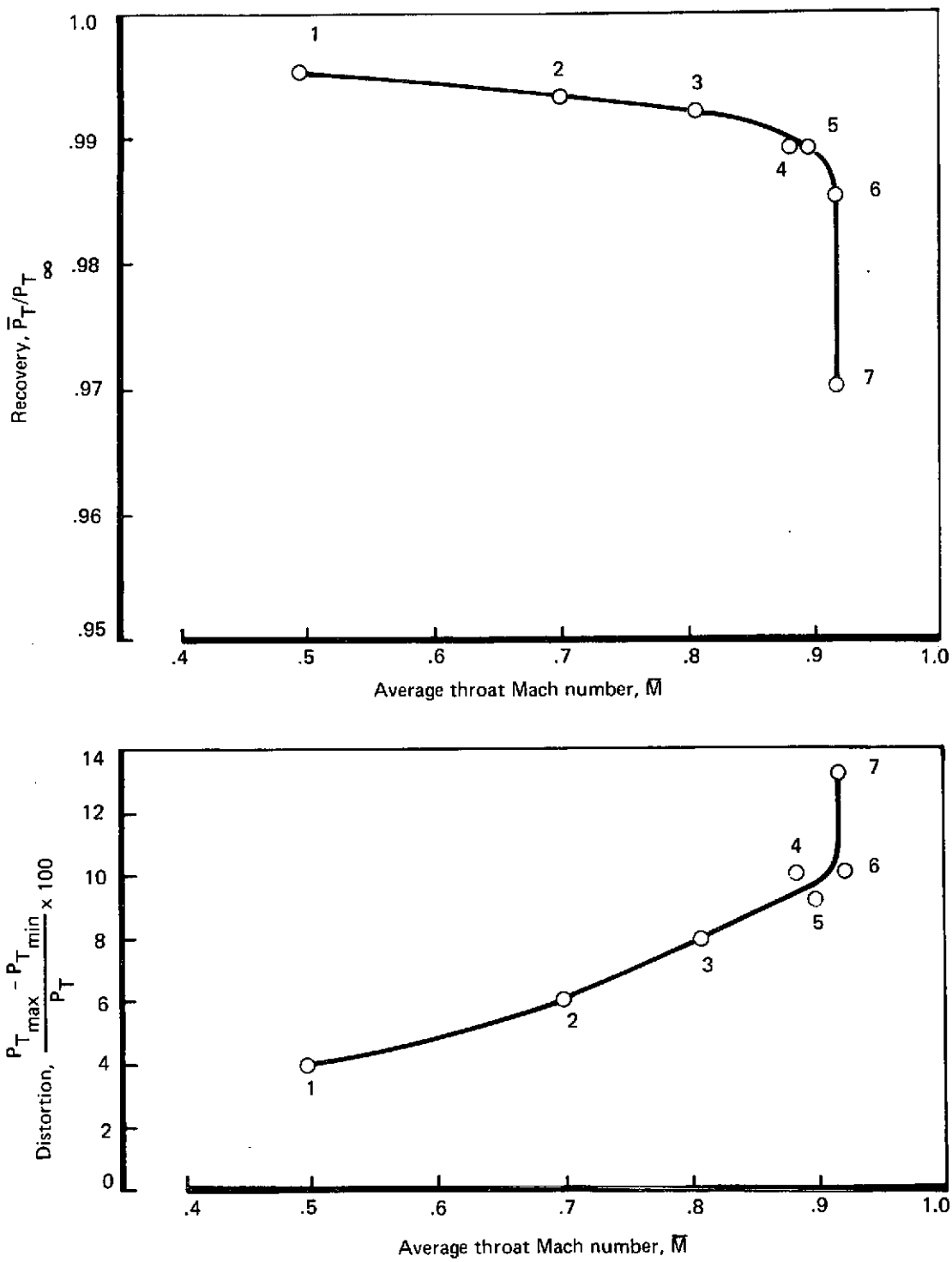


*FIGURE 35.—RECOVERY AND DISTORTION VS THROAT MACH NUMBER—RUN 5, MODEL 3*

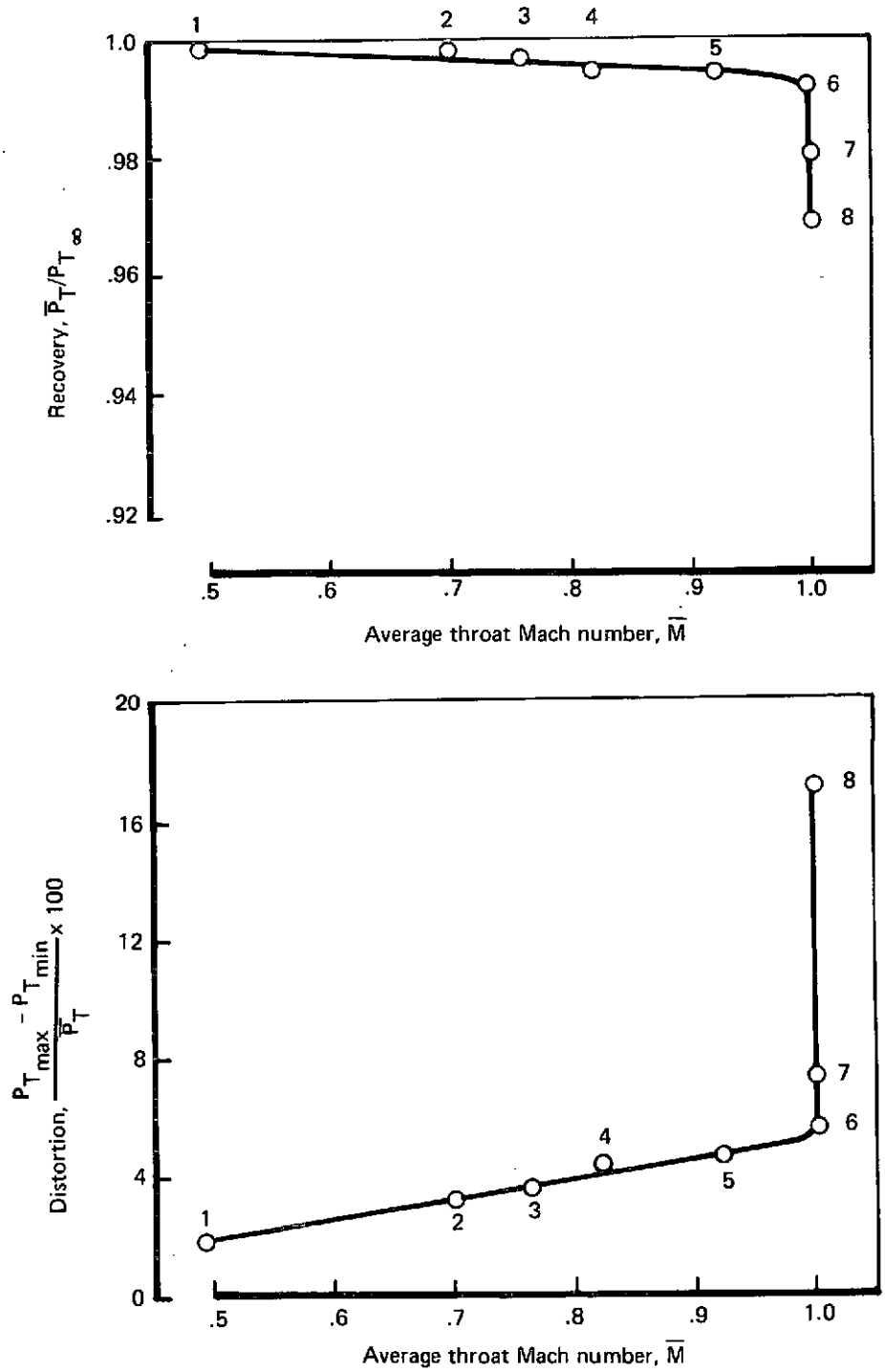


*FIGURE 36.–RECOVERY AND DISTORTION VS THROAT MACH NUMBER–RUN 12, MODEL 4*

| Symbol | Run no. | Rec. | Dist. | $\bar{M}_T$ | $M_T$ |
|---|---|---|---|---|---|
| ○ | 12.001 | 0.993 | 0.019 | 0.465 | 0.490 |
| △ | 12.003 | 0.996 | 0.036 | 0.690 | 0.760 |
| □ | 12.006 | 0.991 | 0.056 | 0.810 | 1.00 |

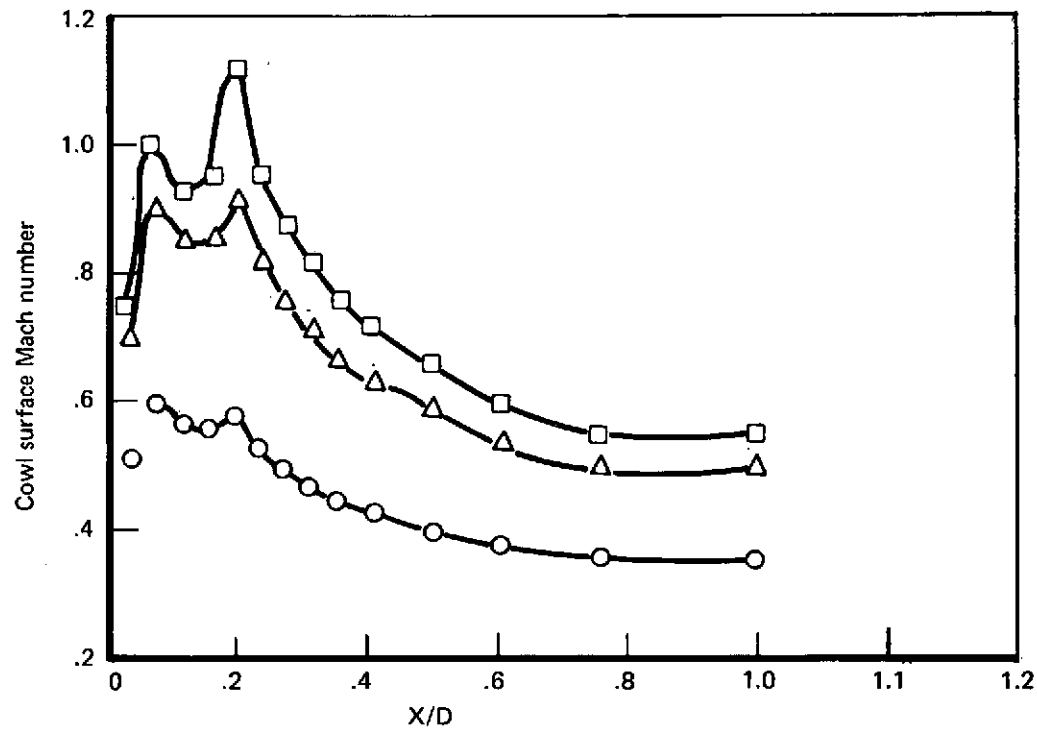


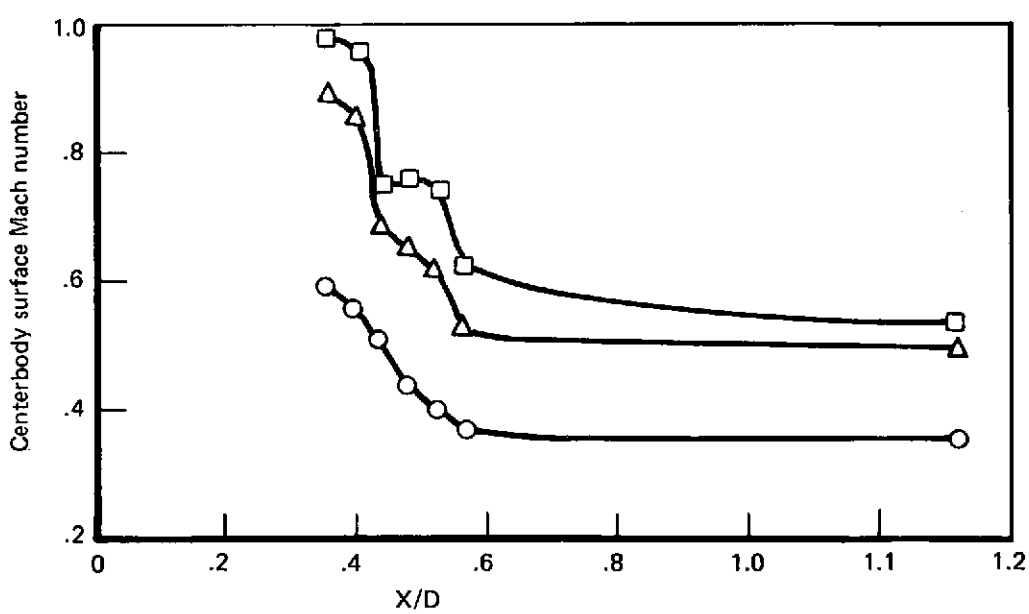


*FIGURE 37.—MODEL SURFACE MACH NUMBER DISTRIBUTION—RUN 12, MODEL 4*

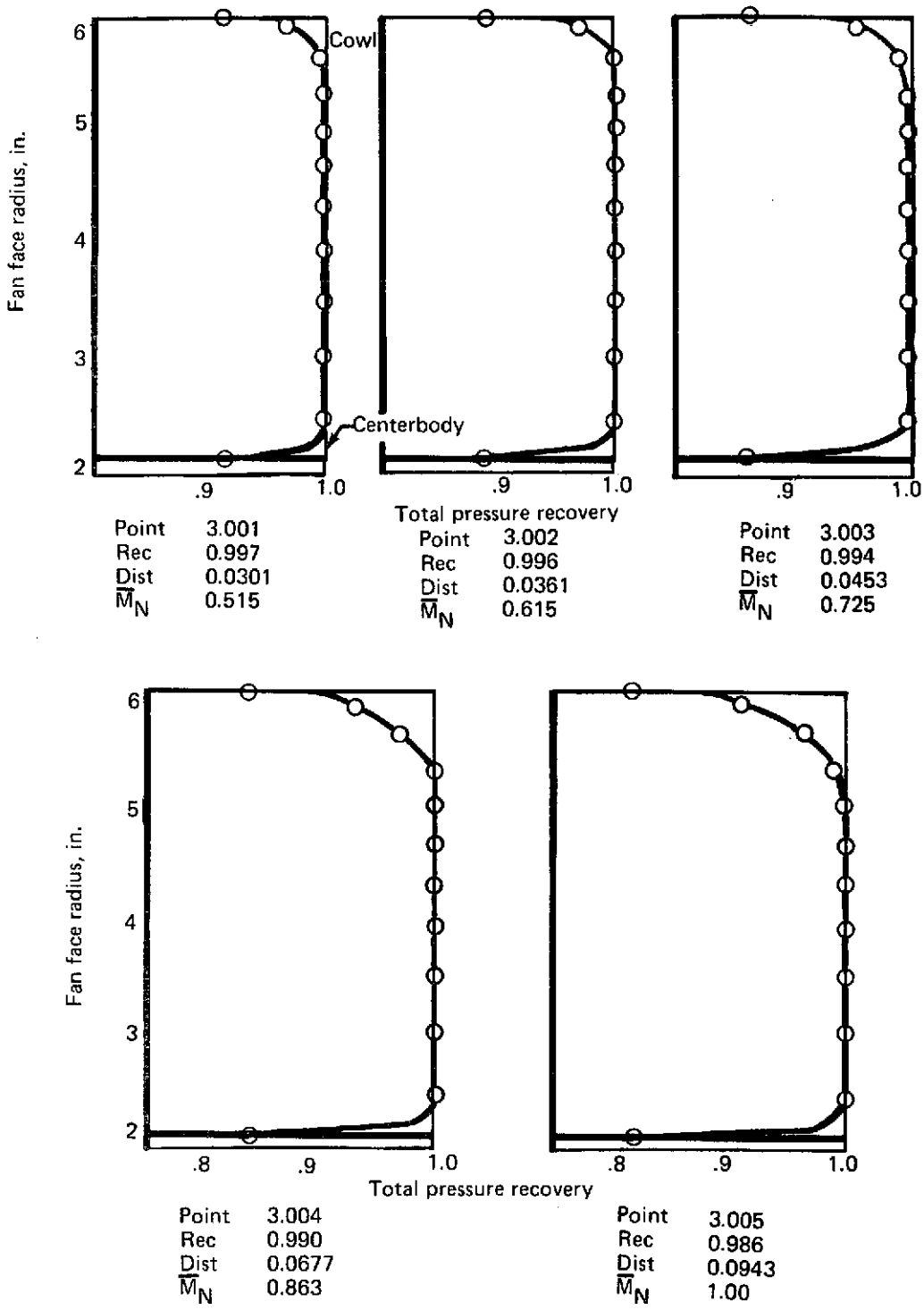


*FIGURE 38.–RECOVERY PROFILES–RUN 3, MODEL 2*

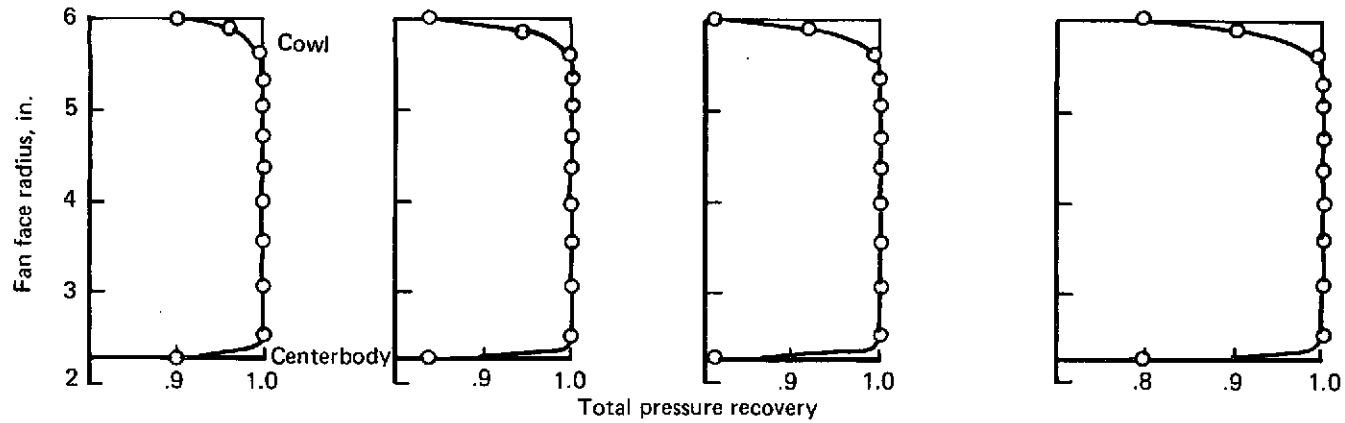


| Point | 5.001 |
|---|---|
| Rec | 0.995 |
| Dist | 0.0382 |
| $\overline{M}_N$ | 0.498 |

| Point | 5.002 |
|---|---|
| Rec | 0.993 |
| Dist | 0.0595 |
| $\overline{M}_N$ | 0.707 |

| Point | 5.003 |
|---|---|
| Rec | 0.992 |
| Dist | 0.0787 |
| $\overline{M}_N$ | 0.821 |

| Point | 5.004 |
|---|---|
| Rec | 0.989 |
| Dist | 0.0992 |
| $\overline{M}_N$ | 0.911 |

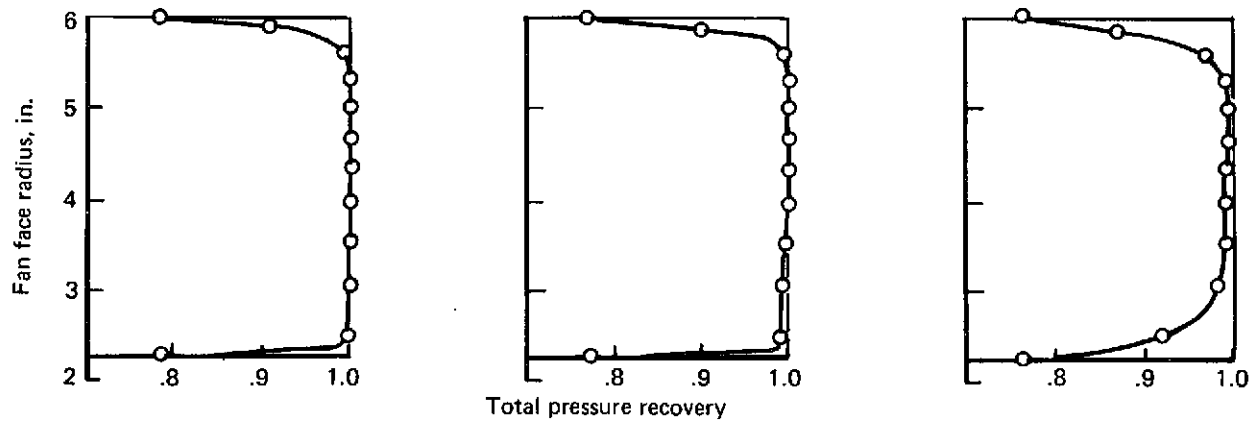


| Point | 5.005 |
|---|---|
| Rec | 0.989 |
| Dist | 0.0912 |
| $\overline{M}_N$ | 0.937 |

| Point | 5.006 |
|---|---|
| Rec | 0.985 |
| Dist | 0.1005 |
| $\overline{M}_N$ | 1.00 |

| Point | 5.007 |
|---|---|
| Rec | 0.970 |
| Dist | 0.1312 |
| $\overline{M}_N$ | 1.00 |

*FIGURE 39.—RECOVERY PROFILES—RUN 5, MODEL 3*

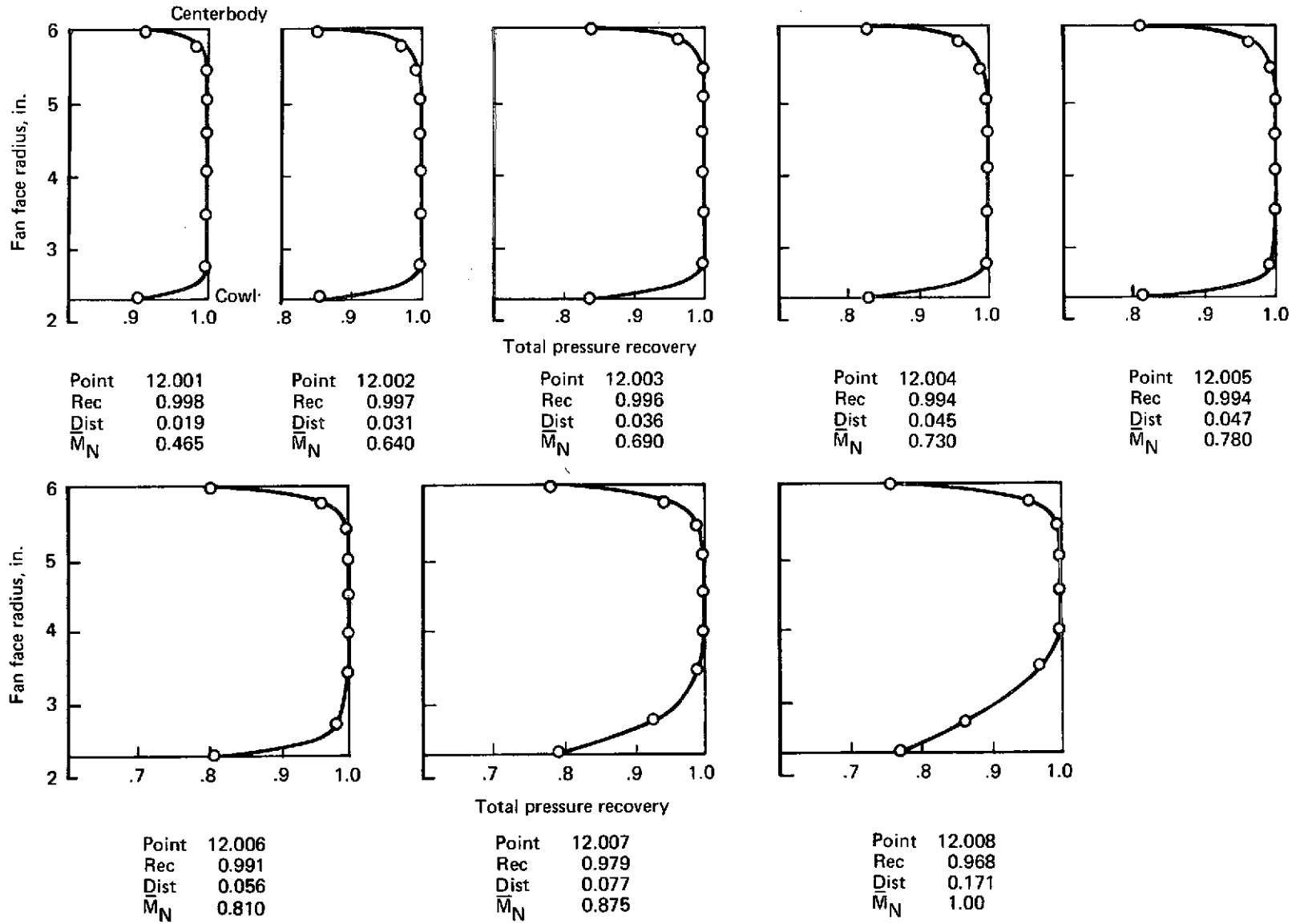


*FIGURE 40.–RECOVERY PROFILES–RUN 12, MODEL 4*

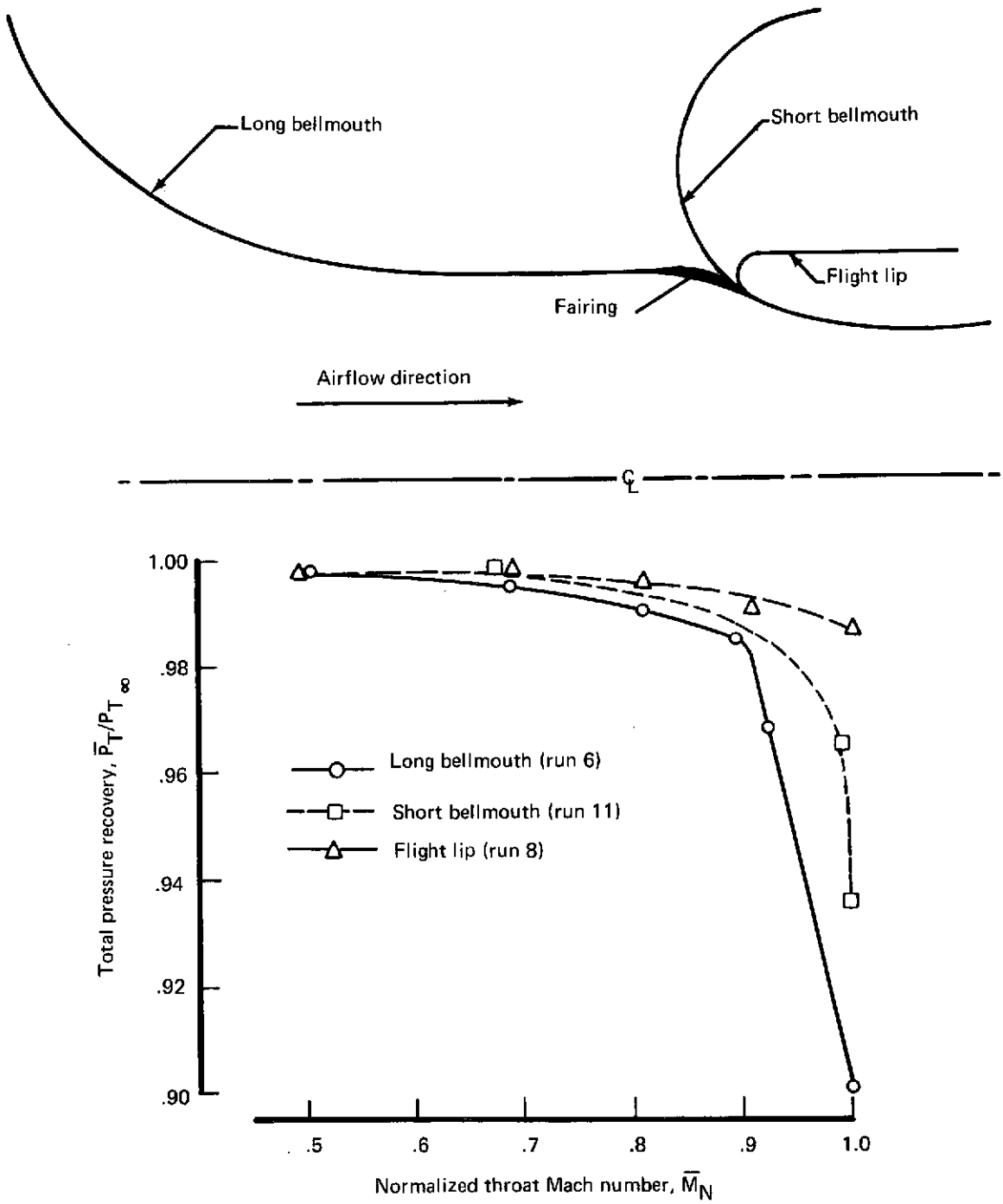


*FIGURE 41.—INLET RECOVERY COMPARISON BETWEEN TWO TYPES OF BELLMOUTH AND FLIGHT LIP*

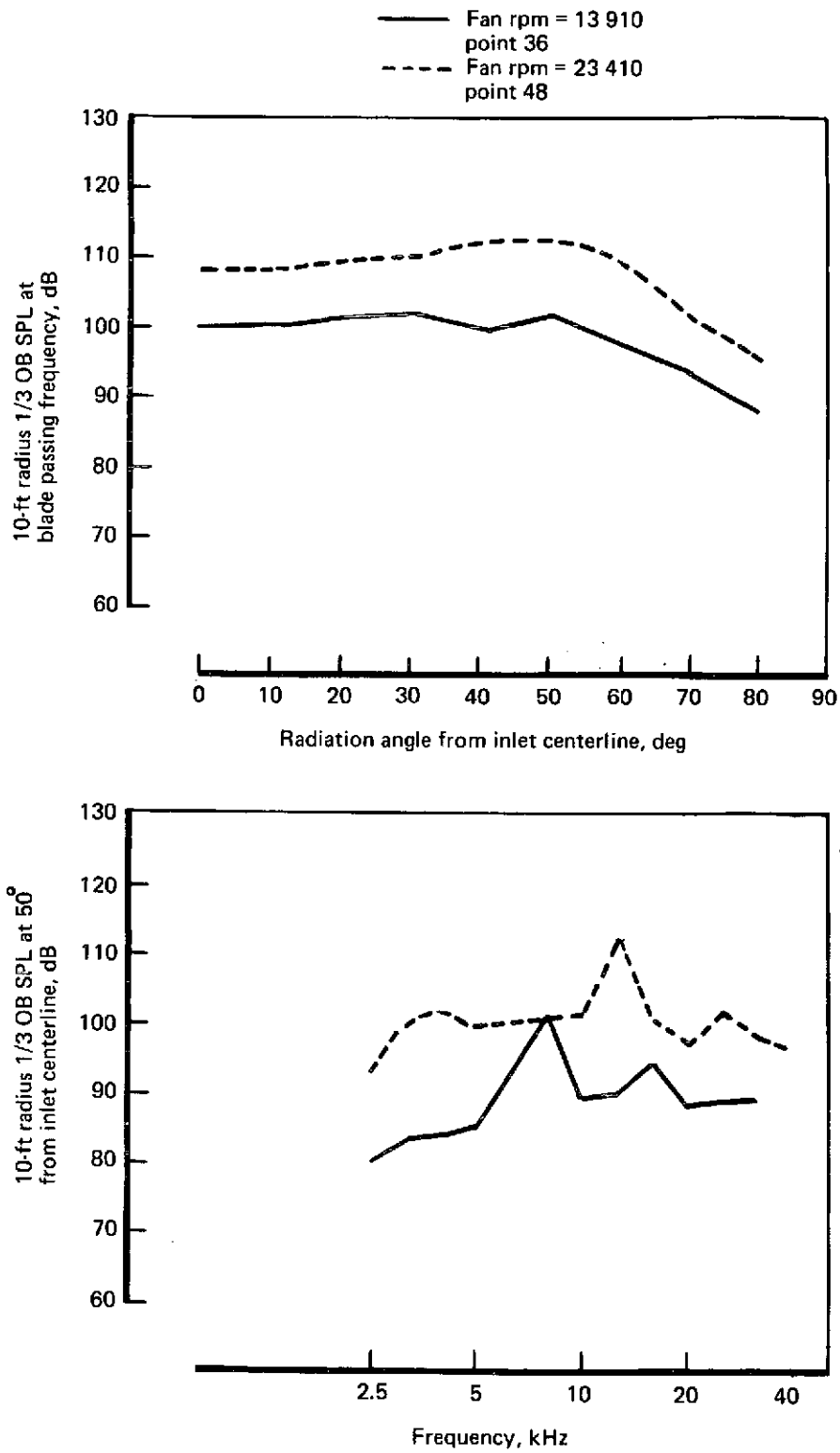


*FIGURE 42.–SPL DIRECTIVITY AND SPECTRUM (APPROACH), MODEL DATA–RUN 1, MODEL 0*

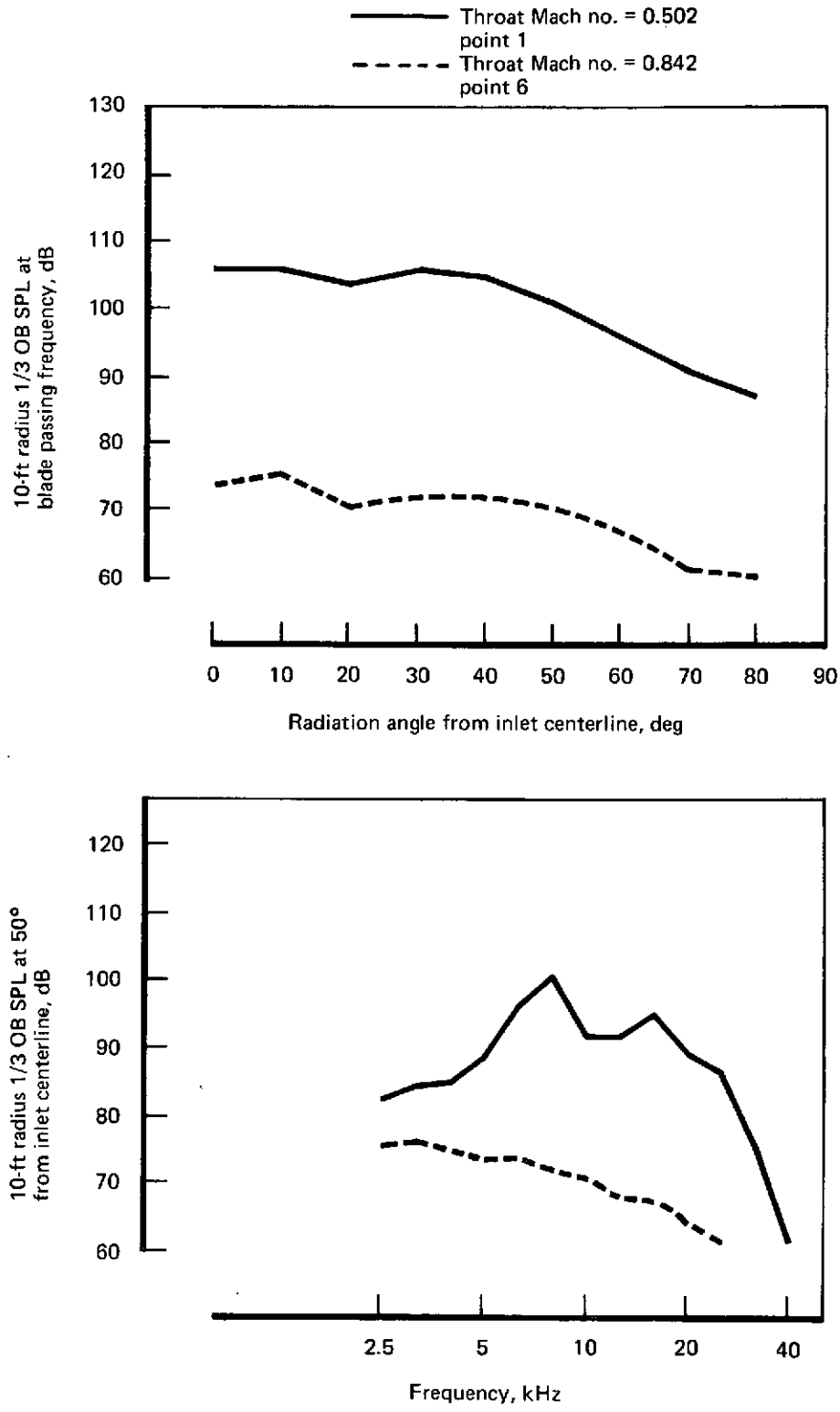


*FIGURE 43.–SPL DIRECTIVITY AND SPECTRUM (APPROACH), MODEL DATA–RUN 2, MODEL 1*

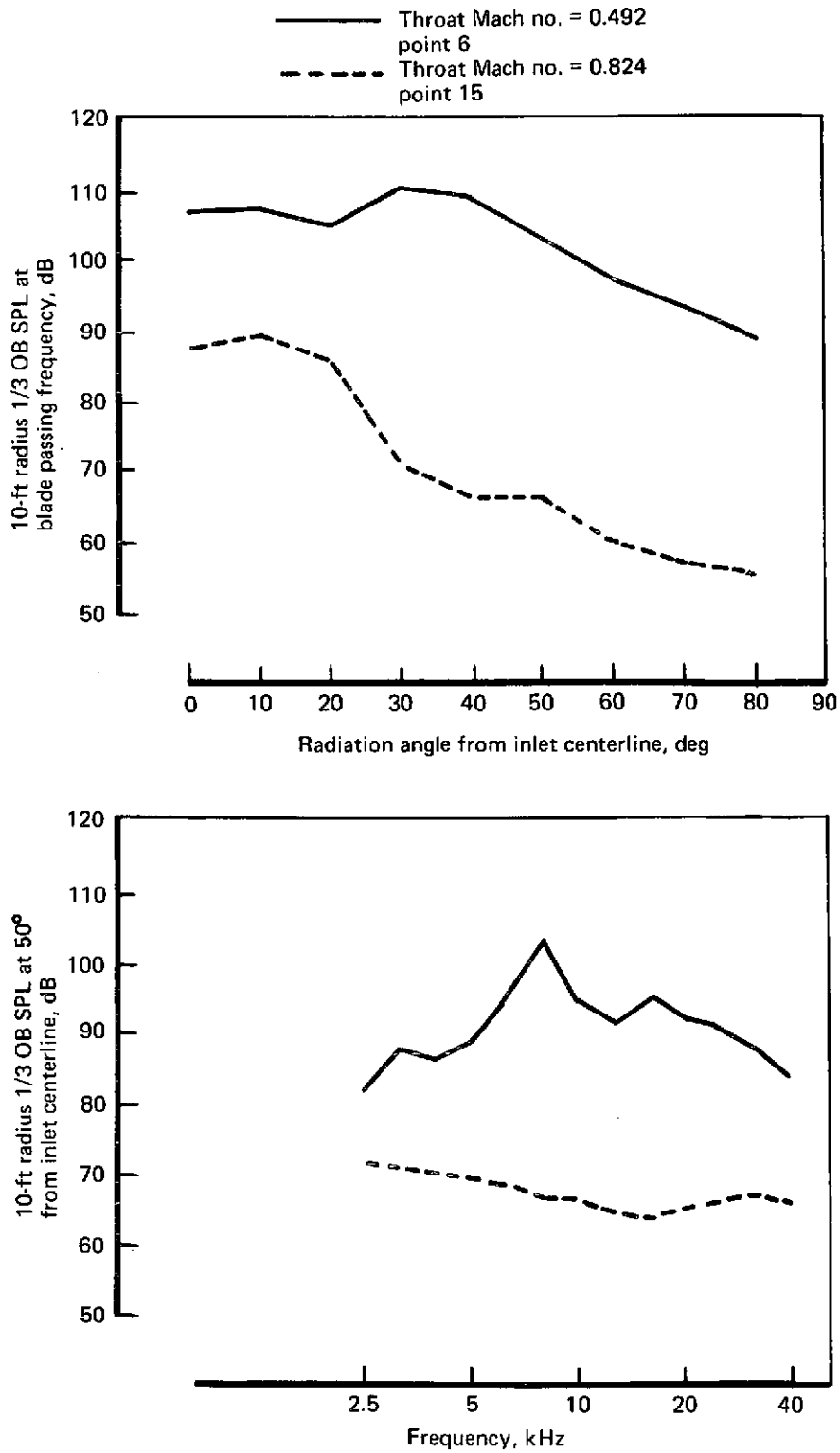


*FIGURE 44.–SPL DIRECTIVITY AND SPECTRUM (APPROACH), MODEL DATA–RUN 4, MODEL 3*

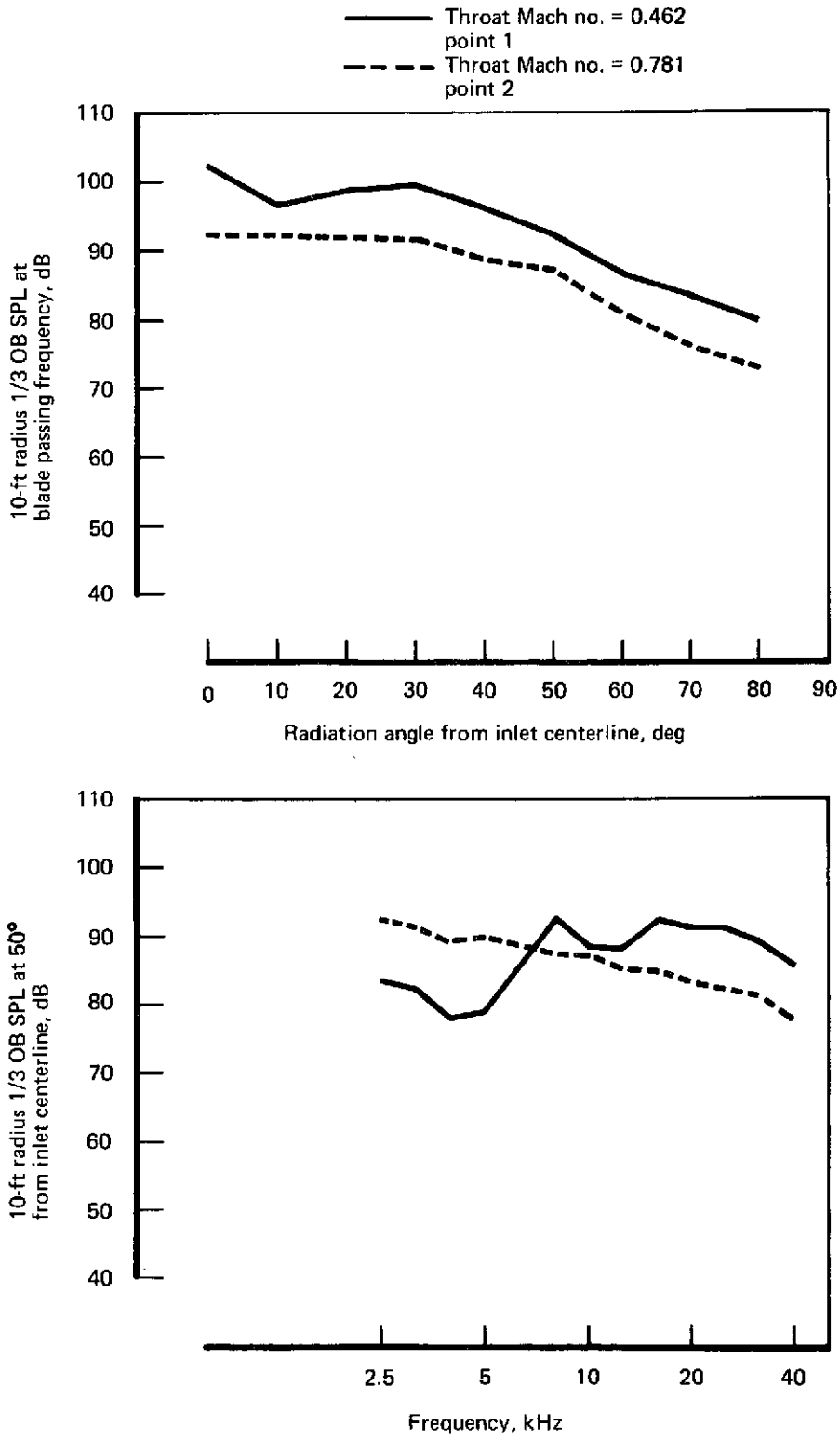


*FIGURE 45.—SPL DIRECTIVITY AND SPECTRUM (APPROACH), MODEL DATA—RUN 101, MODEL 3A*

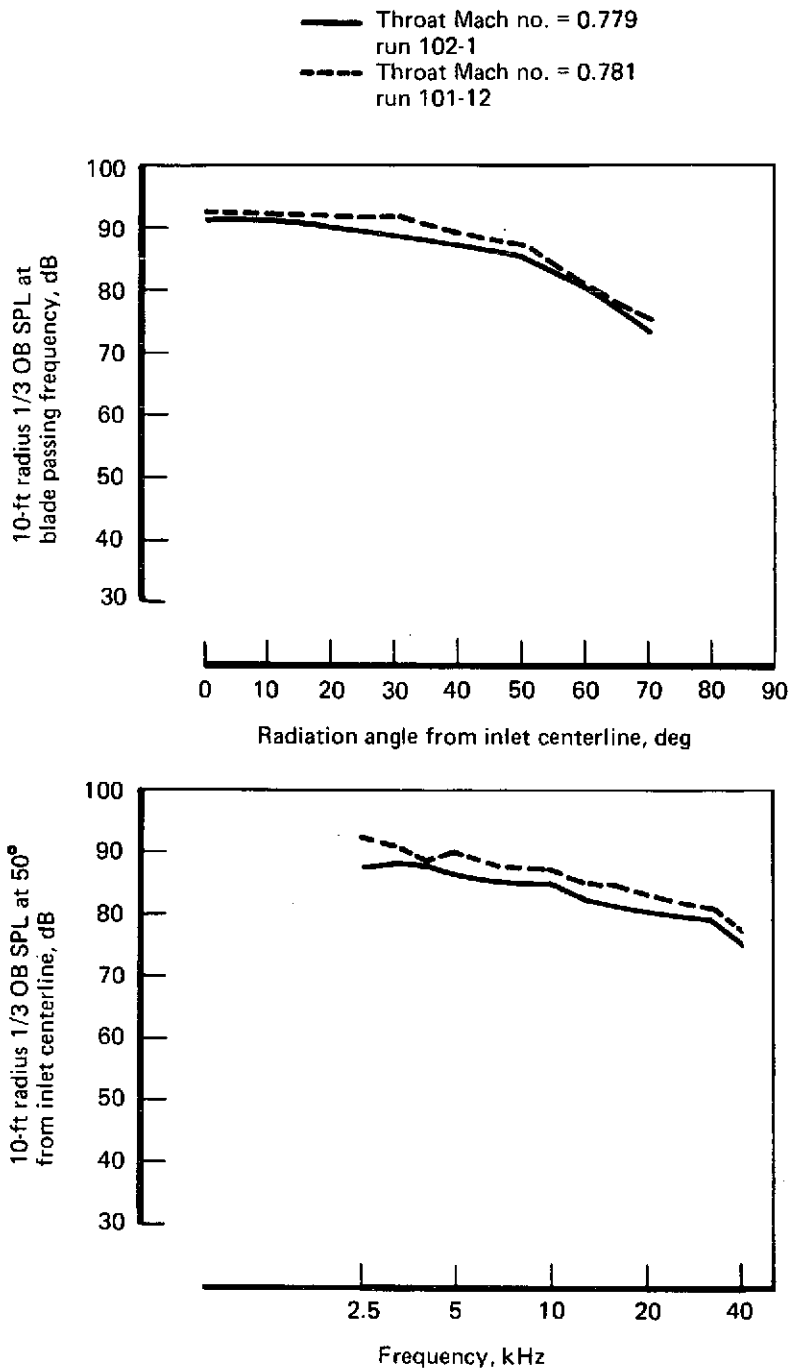


*FIGURE 46.–SPL DIRECTIVITY AND SPECTRUM (APPROACH), MODEL DATA–RUN 102, MODEL 3B*

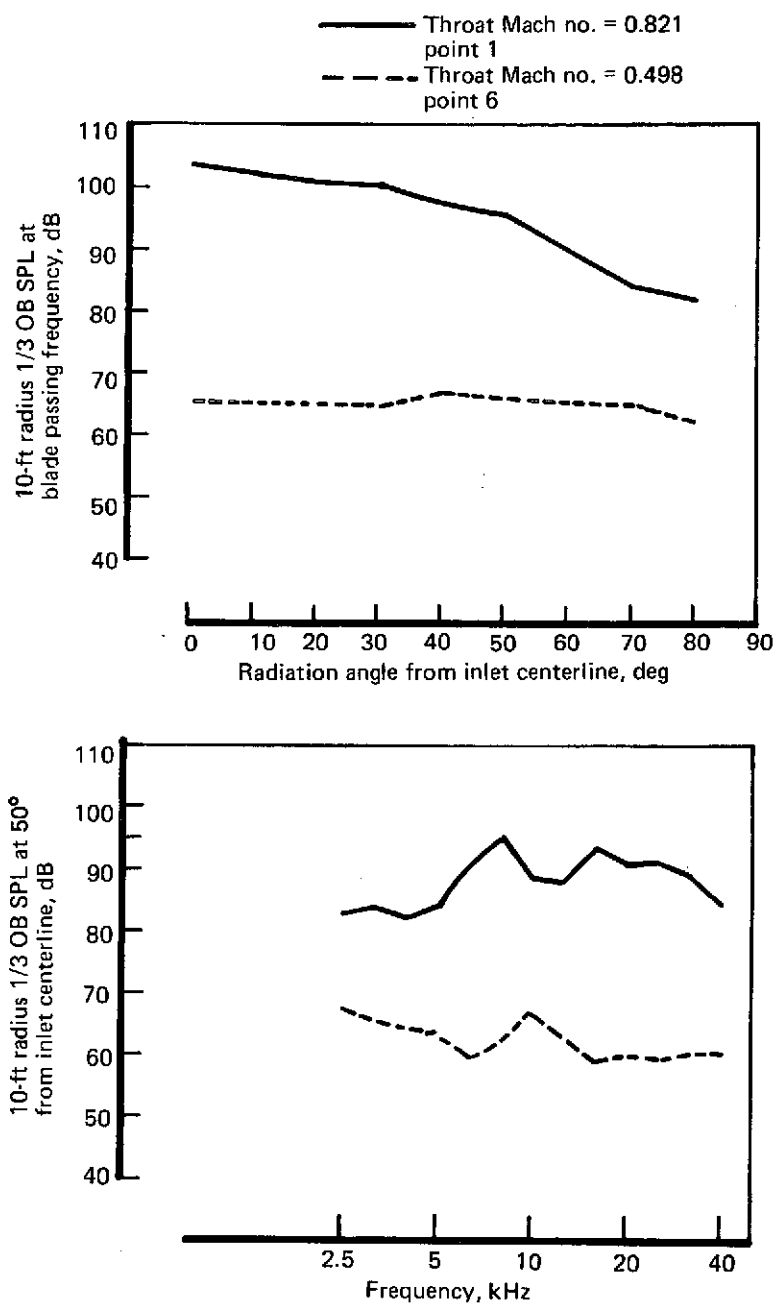


*FIGURE 47.—SPL DIRECTIVITY AND SPECTRUM (APPROACH), MODEL DATA—RUN 10, MODEL 3C*

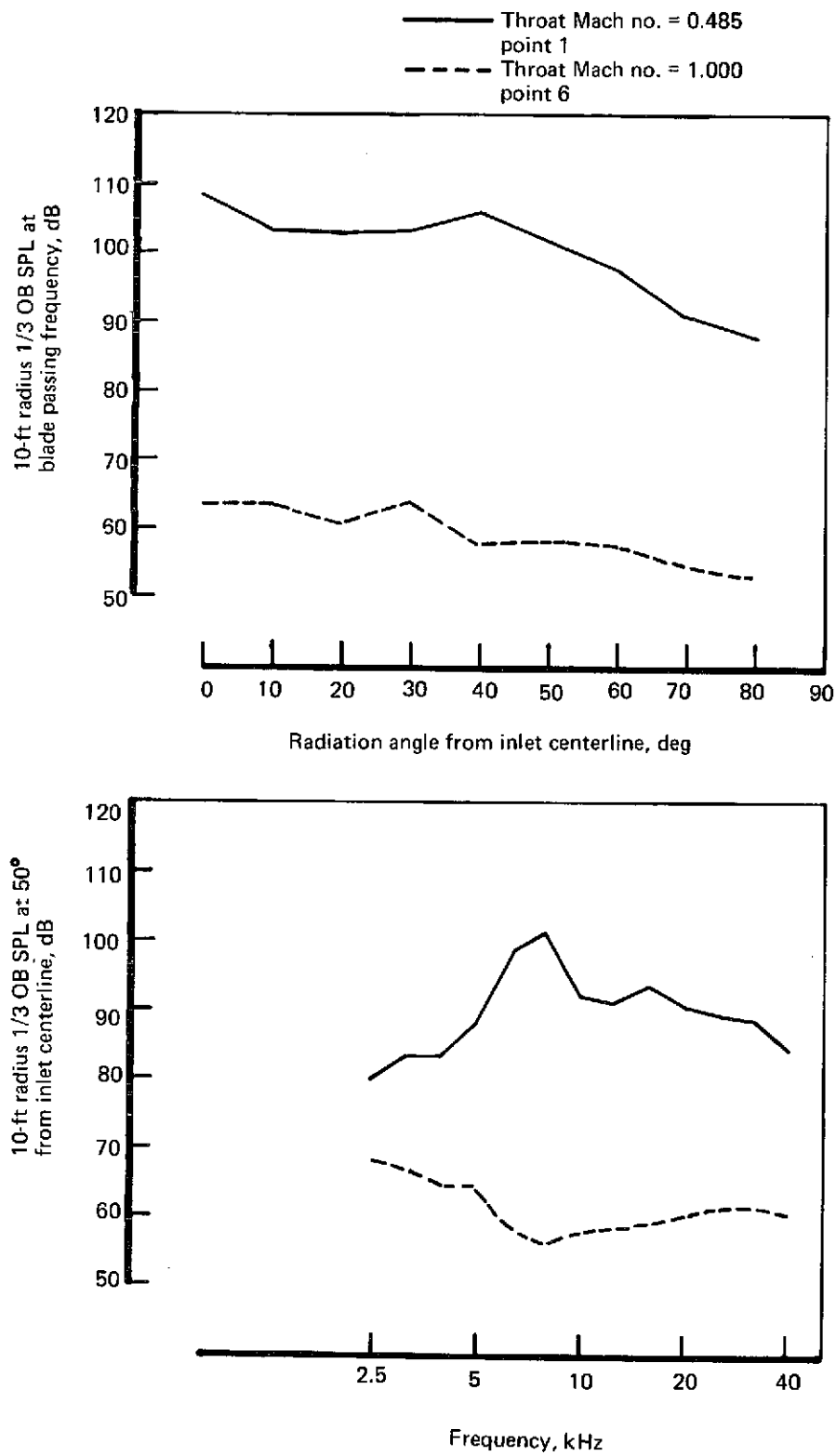


*FIGURE 48.—SPL DIRECTIVITY AND SPECTRUM (APPROACH), MODEL DATA—RUN 6, MODEL 4*

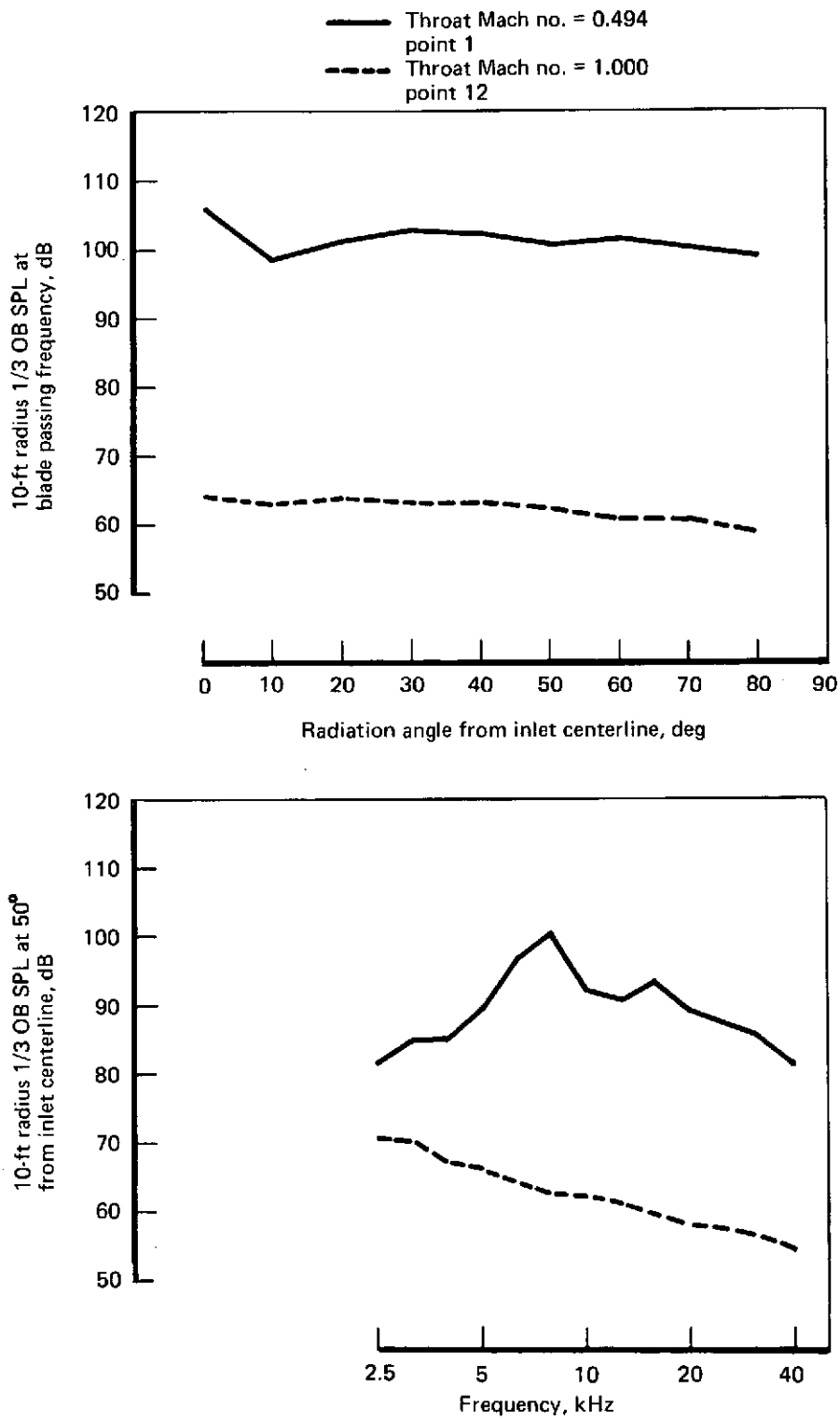


*FIGURE 49.–SPL DIRECTIVITY AND SPECTRUM (APPROACH), MODEL DATA–RUN 8, MODEL 4*

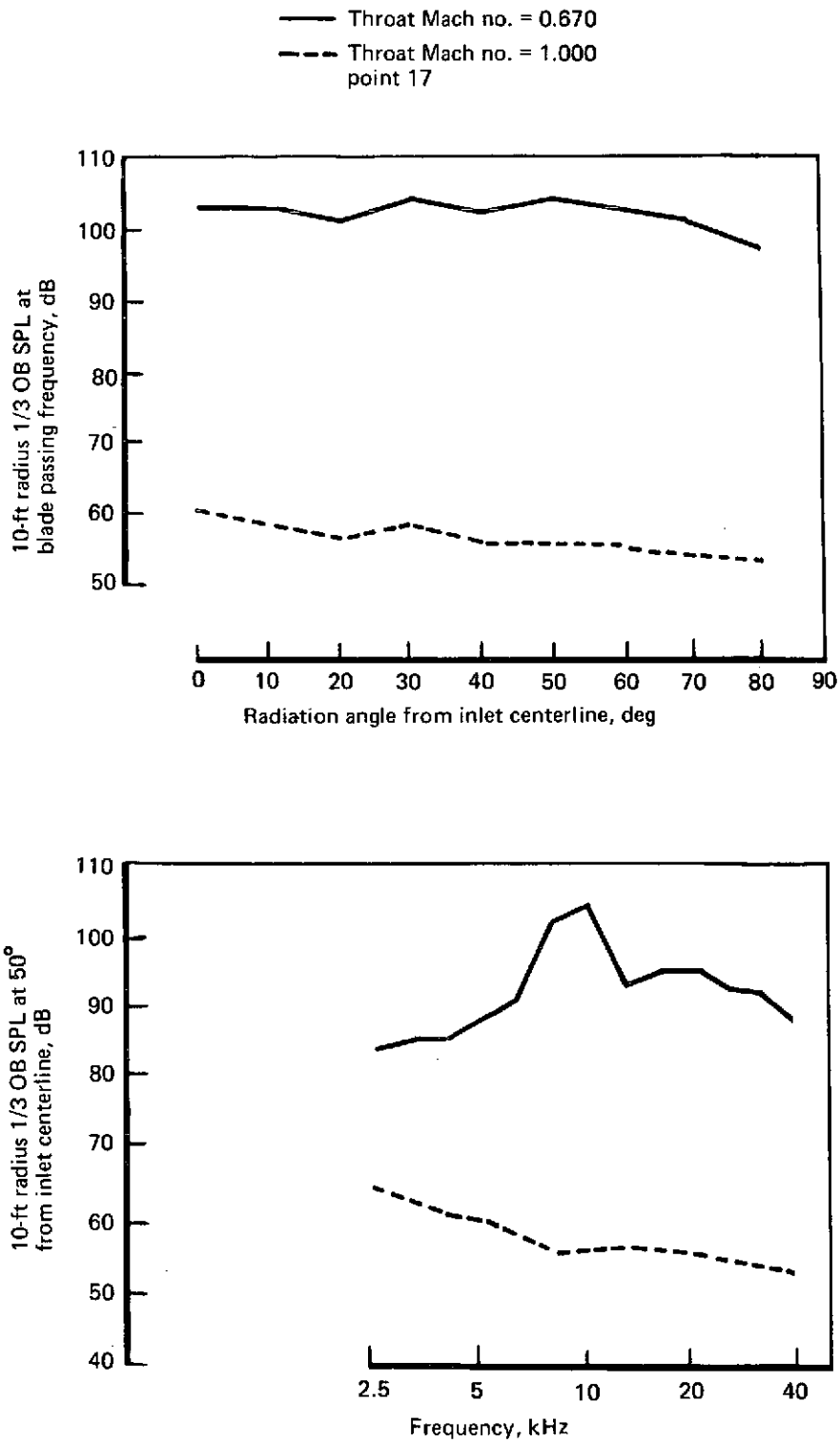


*FIGURE 50.–SPL DIRECTIVITY AND SPECTRUM (APPROACH), MODEL DATA–RUN 11, MODEL 4*

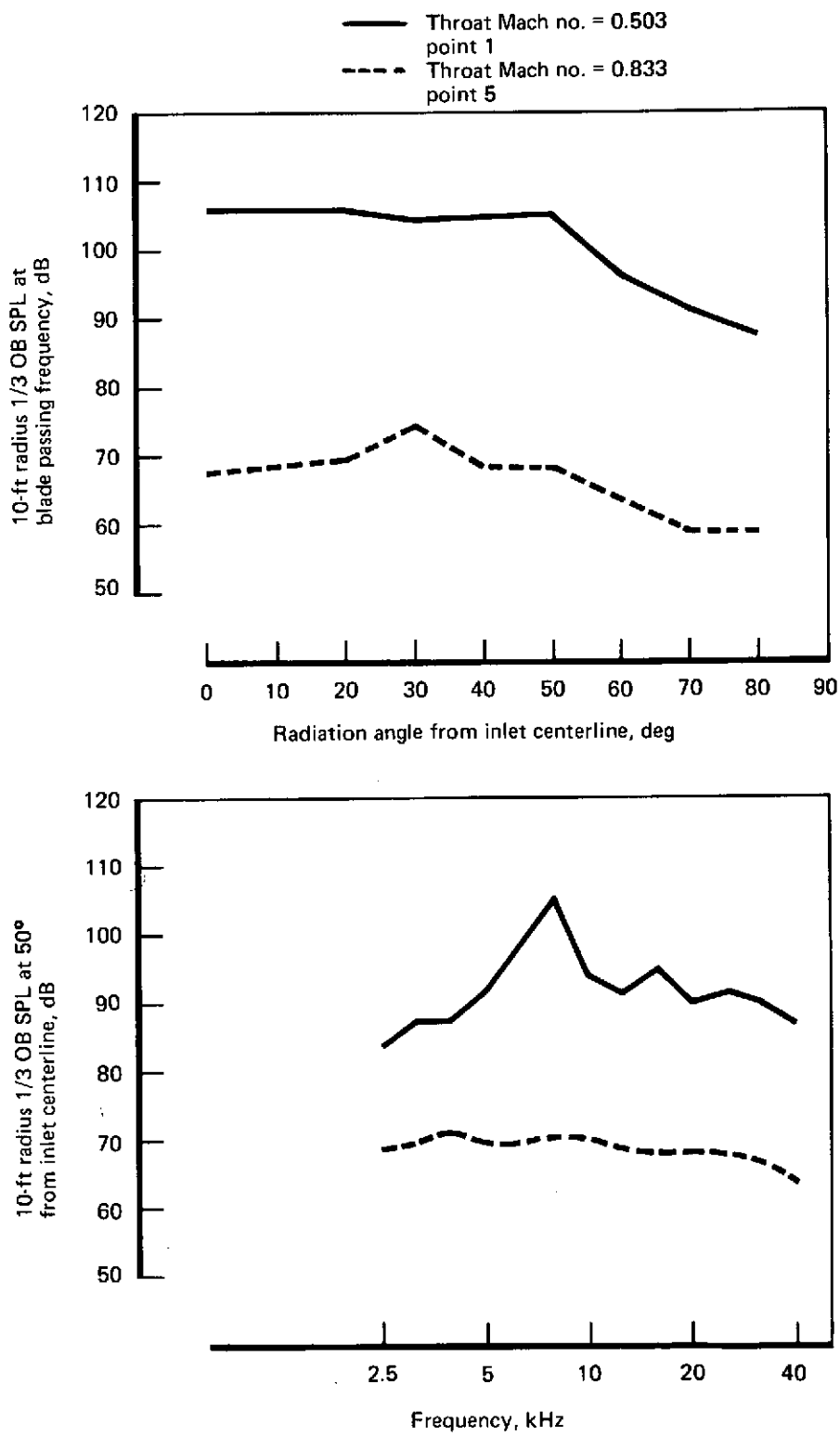


*FIGURE 51.—SPL DIRECTIVITY AND SPECTRUM (APPROACH), MODEL DATA—RUN 7, MODEL 5A*

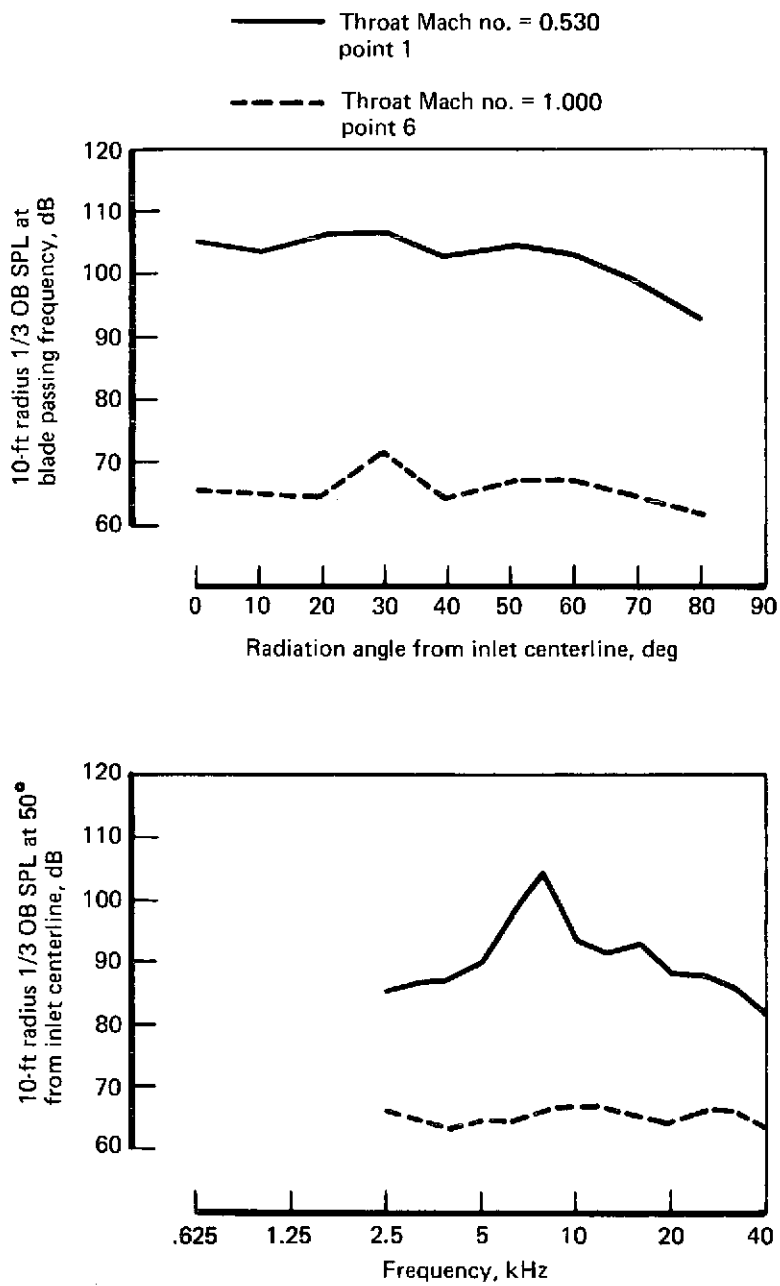


*FIGURE 52.—SPL DIRECTIVITY AND SPECTRUM (APPROACH), MODEL DATA—RUN 13, MODEL 5B*

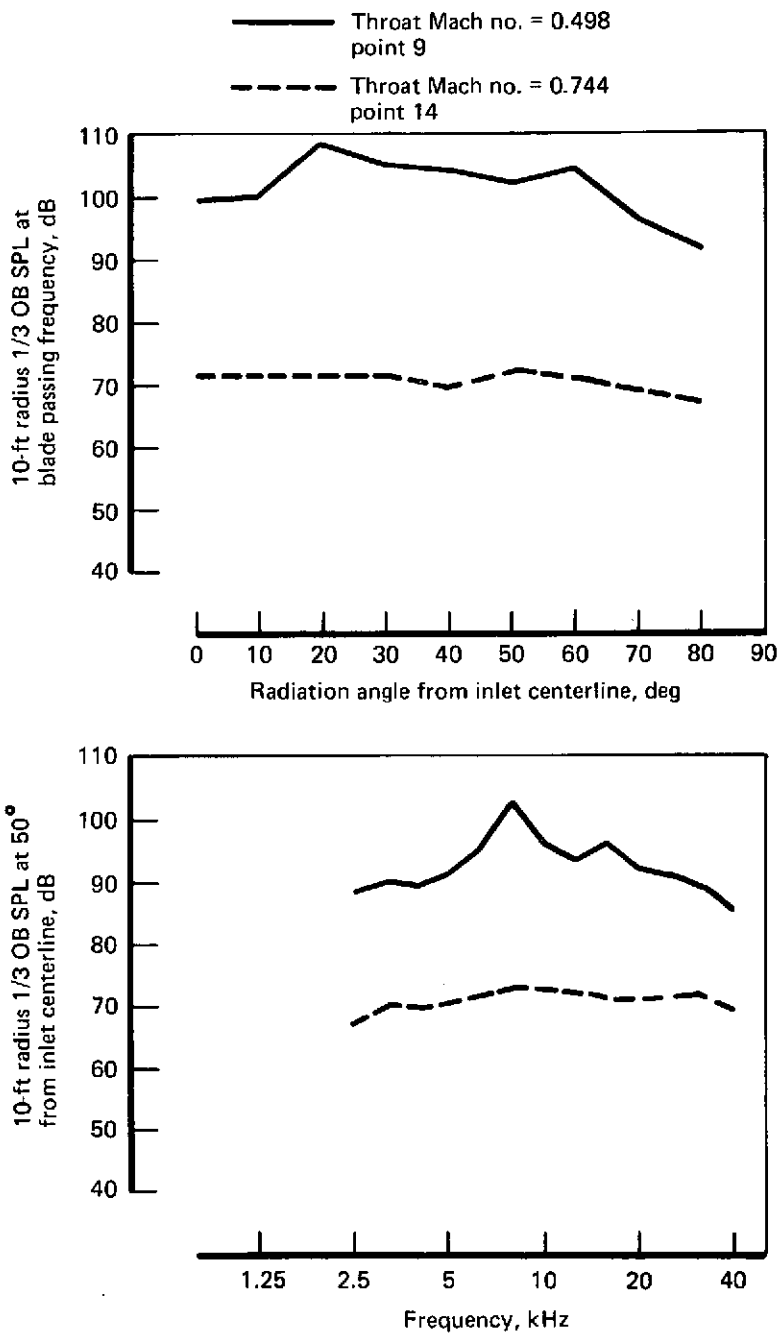


*FIGURE 53.–SPL DIRECTIVITY AND SPECTRUM (APPROACH), MODEL DATA–RUN 9, MODEL 6*

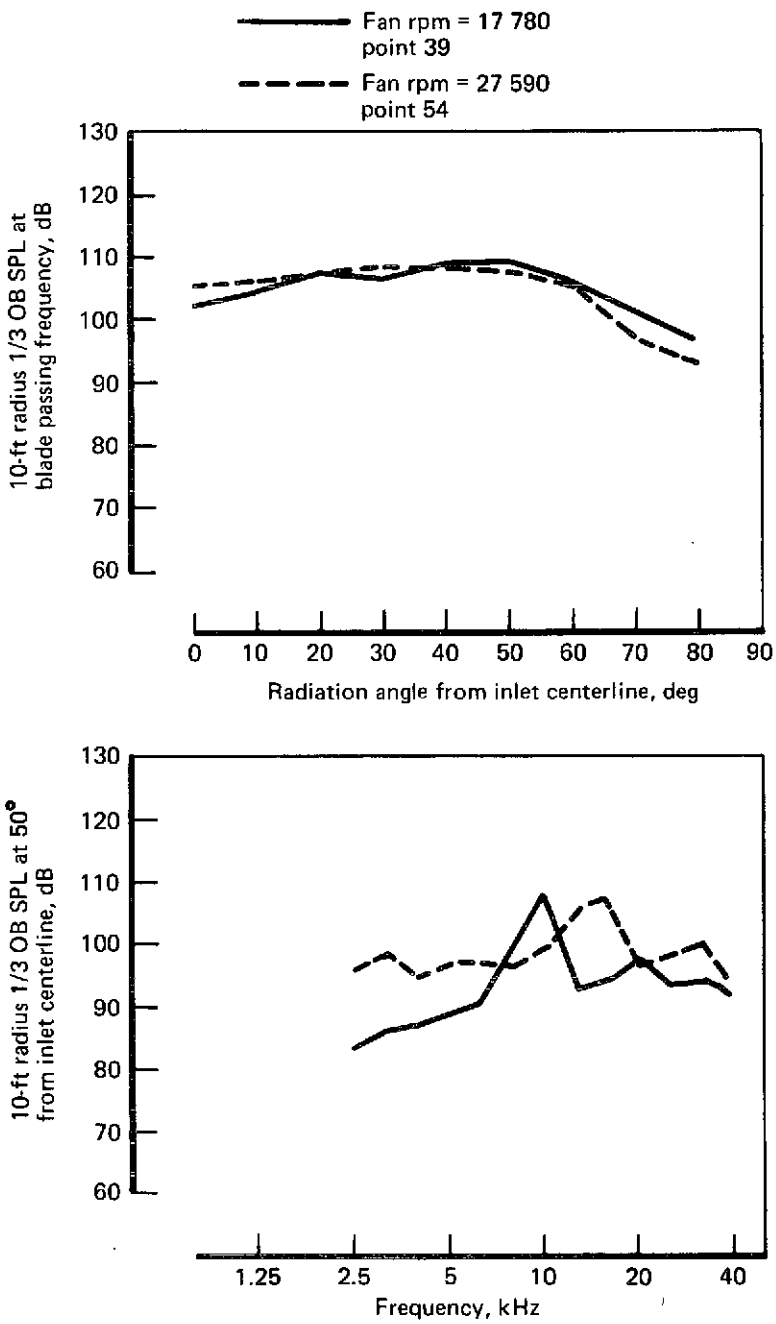


*FIGURE 54.–SPL DIRECTIVITY AND SPECTRUM (TAKEOFF), MODEL DATA–RUN 1, MODEL 0*

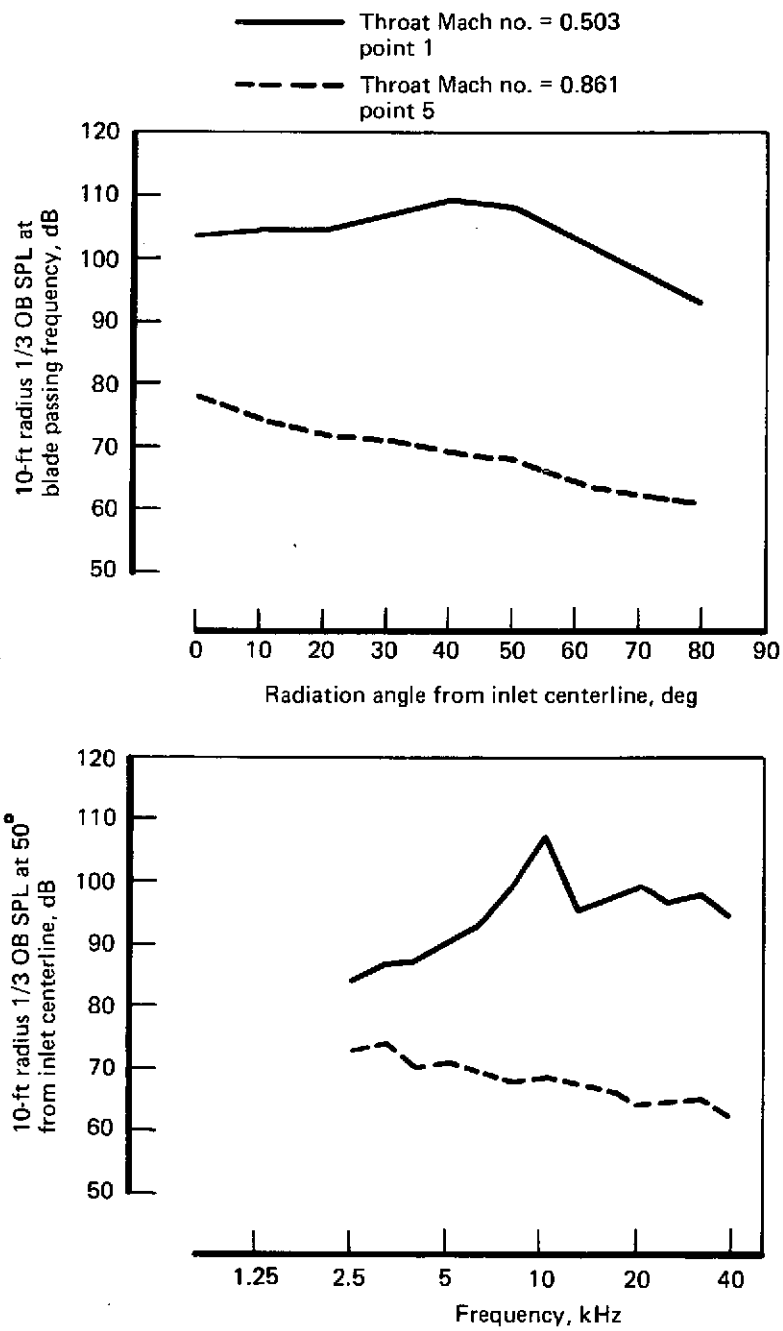


*FIGURE 55.–SPL DIRECTIVITY AND SPECTRUM (TAKEOFF), MODEL DATA–RUN 3, MODEL 2*

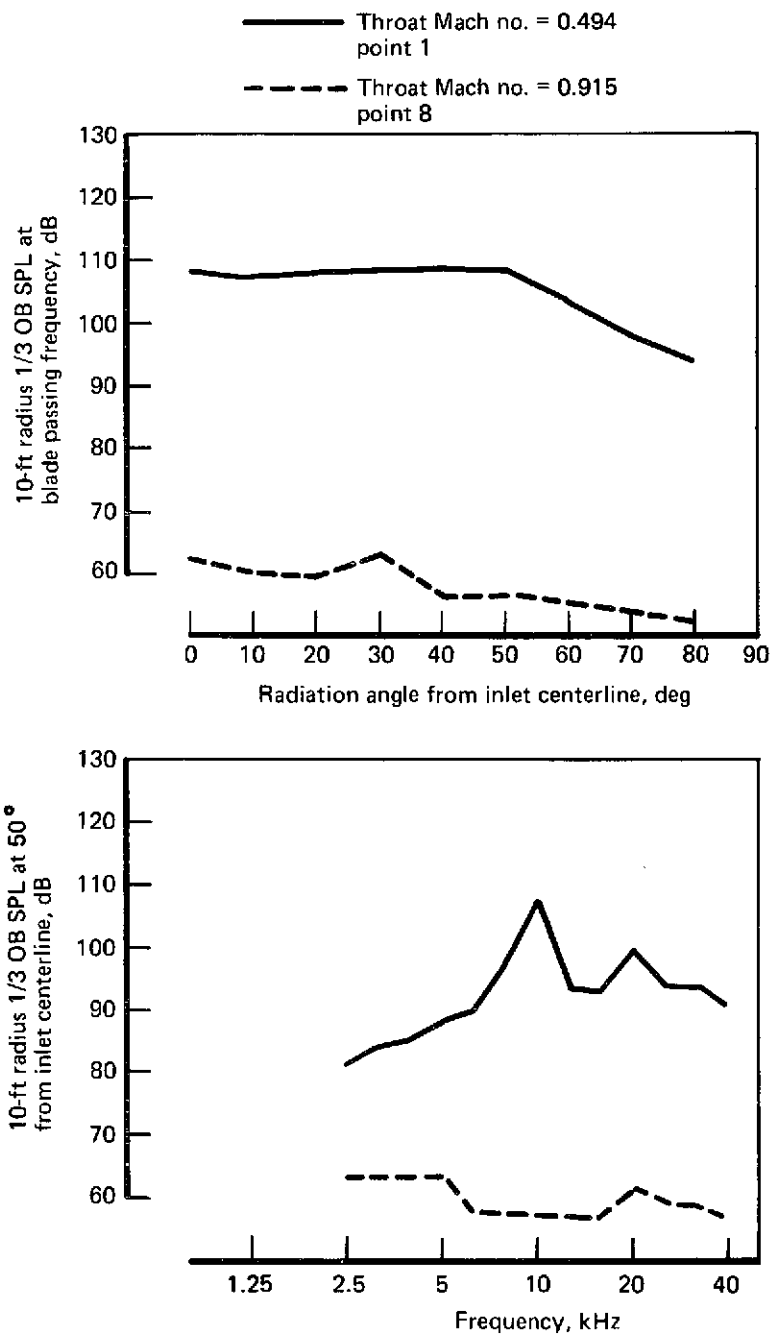


*FIGURE 56.–SPL DIRECTIVITY AND SPECTRUM (TAKEOFF), MODEL DATA–RUN 5, MODEL 3*

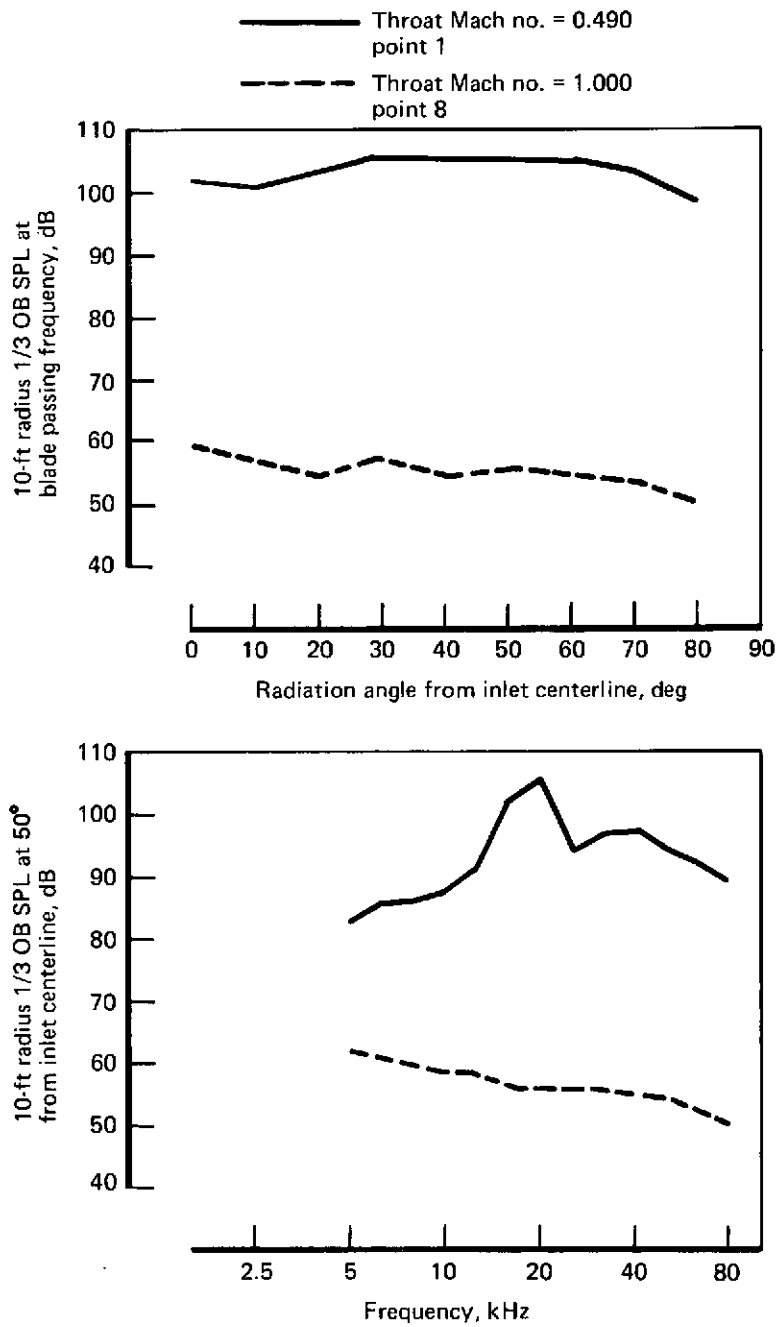


*FIGURE 57.–SPL DIRECTIVITY AND SPECTRUM (TAKEOFF), MODEL DATA–RUN 12, MODEL 4*

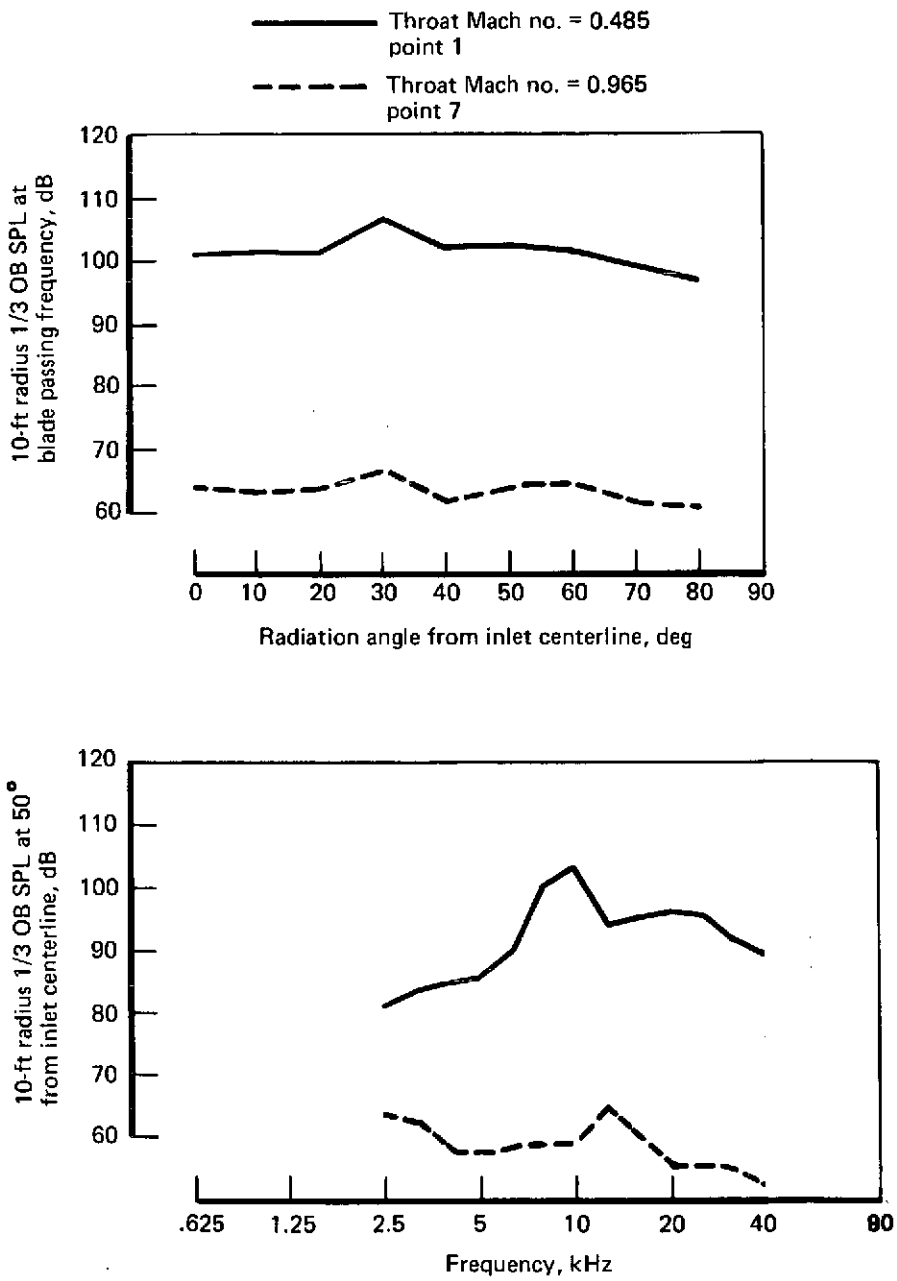


*FIGURE 58.–SPL DIRECTIVITY AND SPECTRUM (TAKEOFF), MODEL DATA–RUN 14, MODEL 5B*

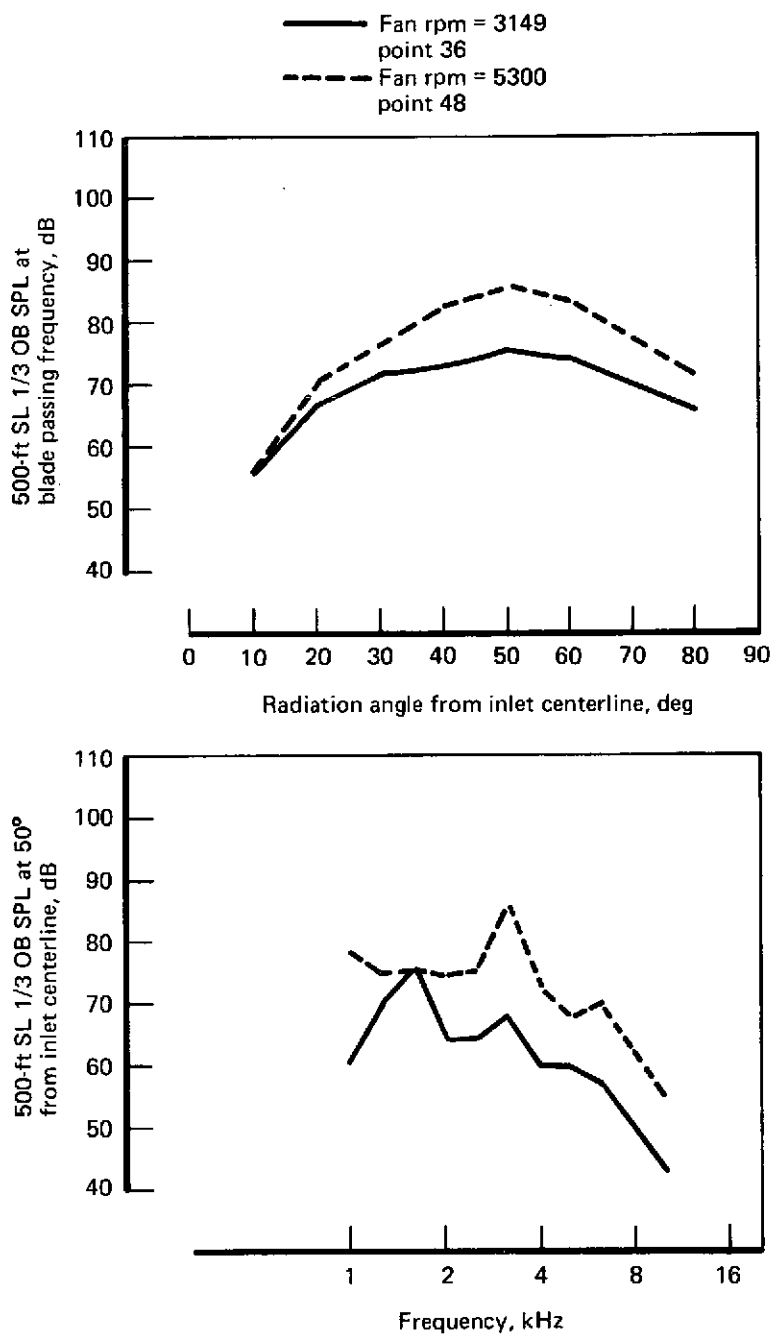


*FIGURE 59.–SPL DIRECTIVITY AND SPECTRUM (APPROACH), SCALED-UP DATA–RUN 1, MODEL 0*

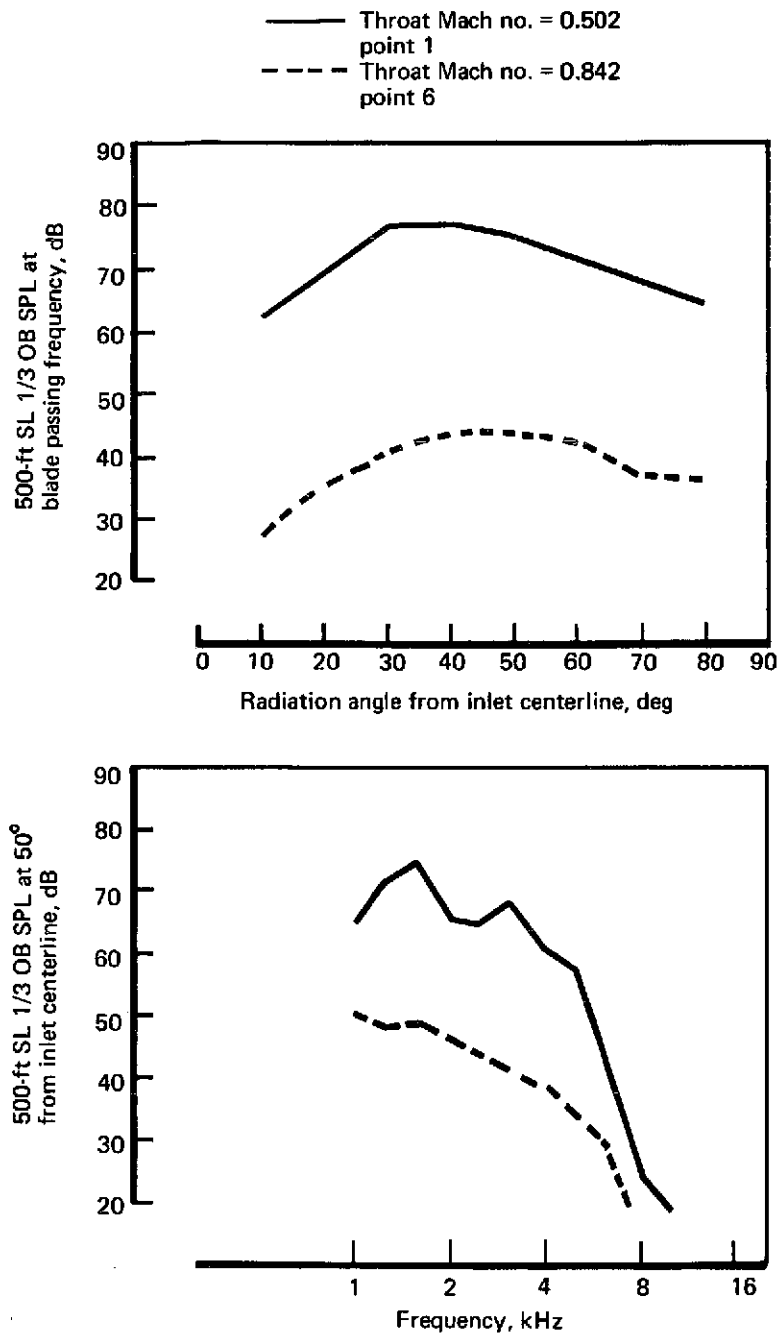


*FIGURE 60.—SPL DIRECTIVITY AND SPECTRUM (APPROACH), SCALED-UP DATA—RUN 2, MODEL 1*

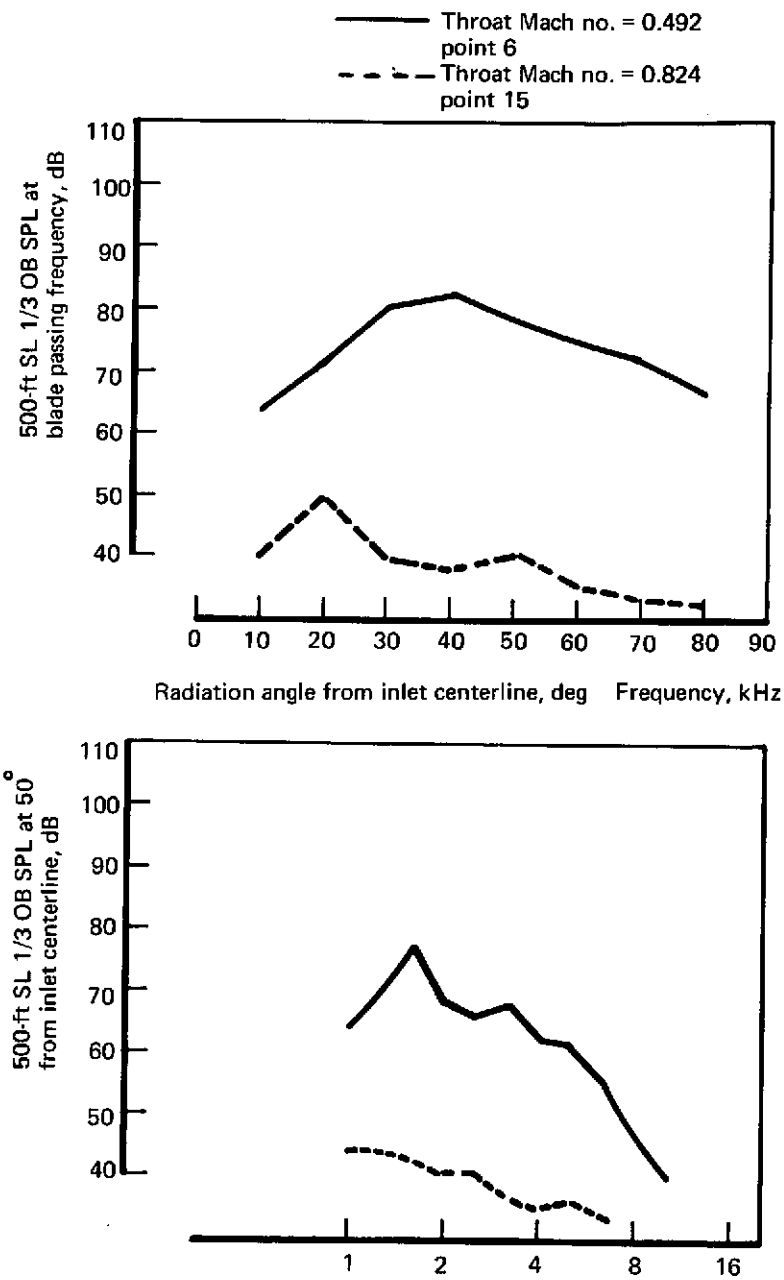


*FIGURE 61.—SPL DIRECTIVITY AND SPECTRUM (APPROACH), SCALED-UP DATA—RUN 4, MODEL 3*

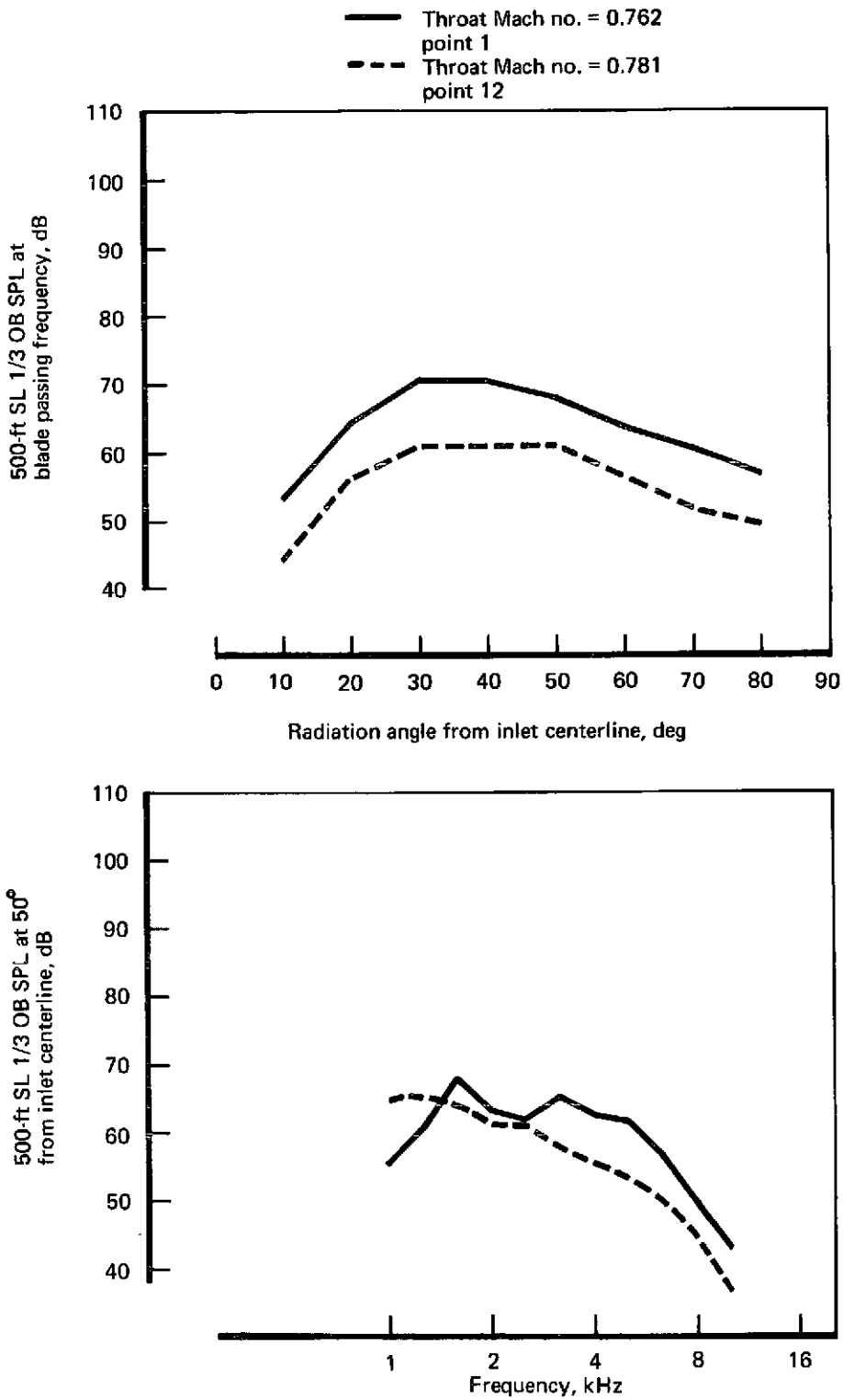


*FIGURE 62.–SPL DIRECTIVITY AND SPECTRUM (APPROACH), SCALED-UP DATA–RUN 101, MODEL 3A*

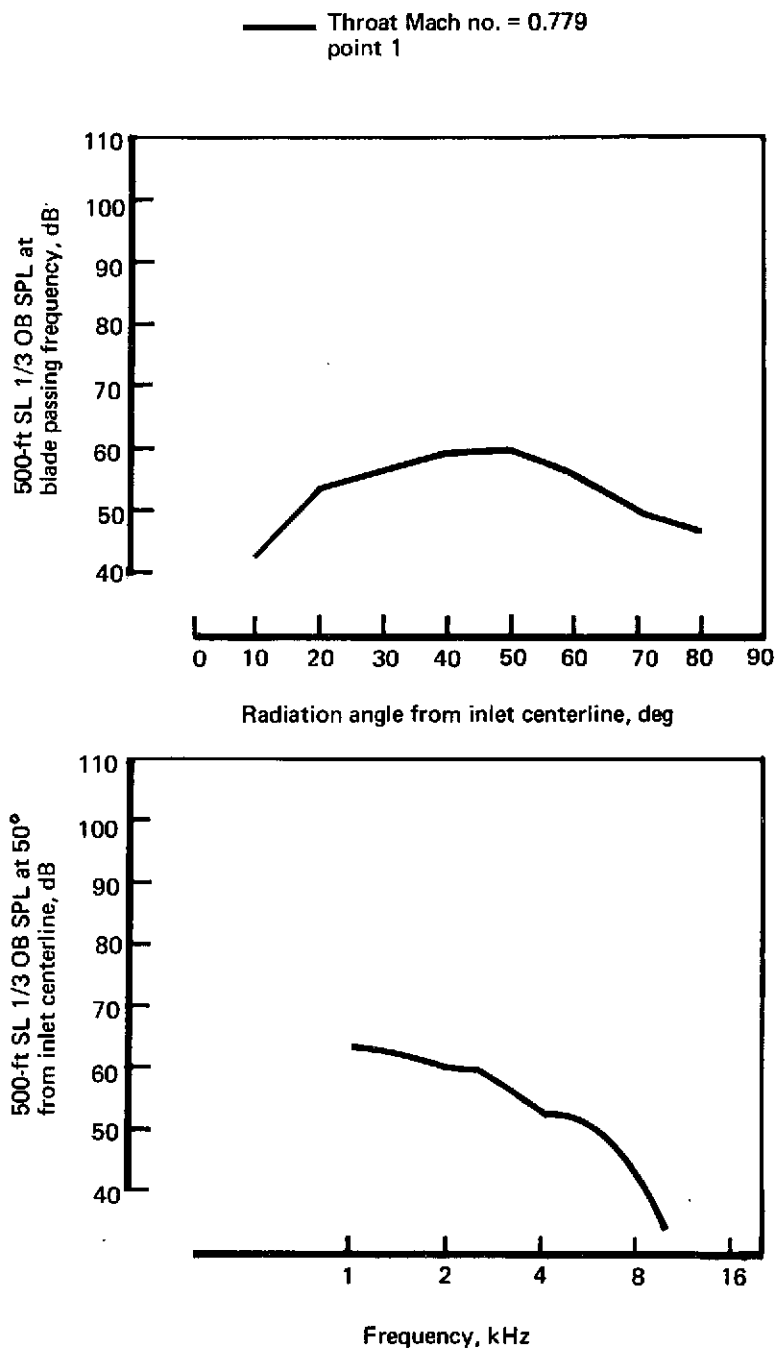


*FIGURE 63.–SPL DIRECTIVITY AND SPECTRUM (APPROACH), SCALED-UP DATA–RUN 102, MODEL 3B*

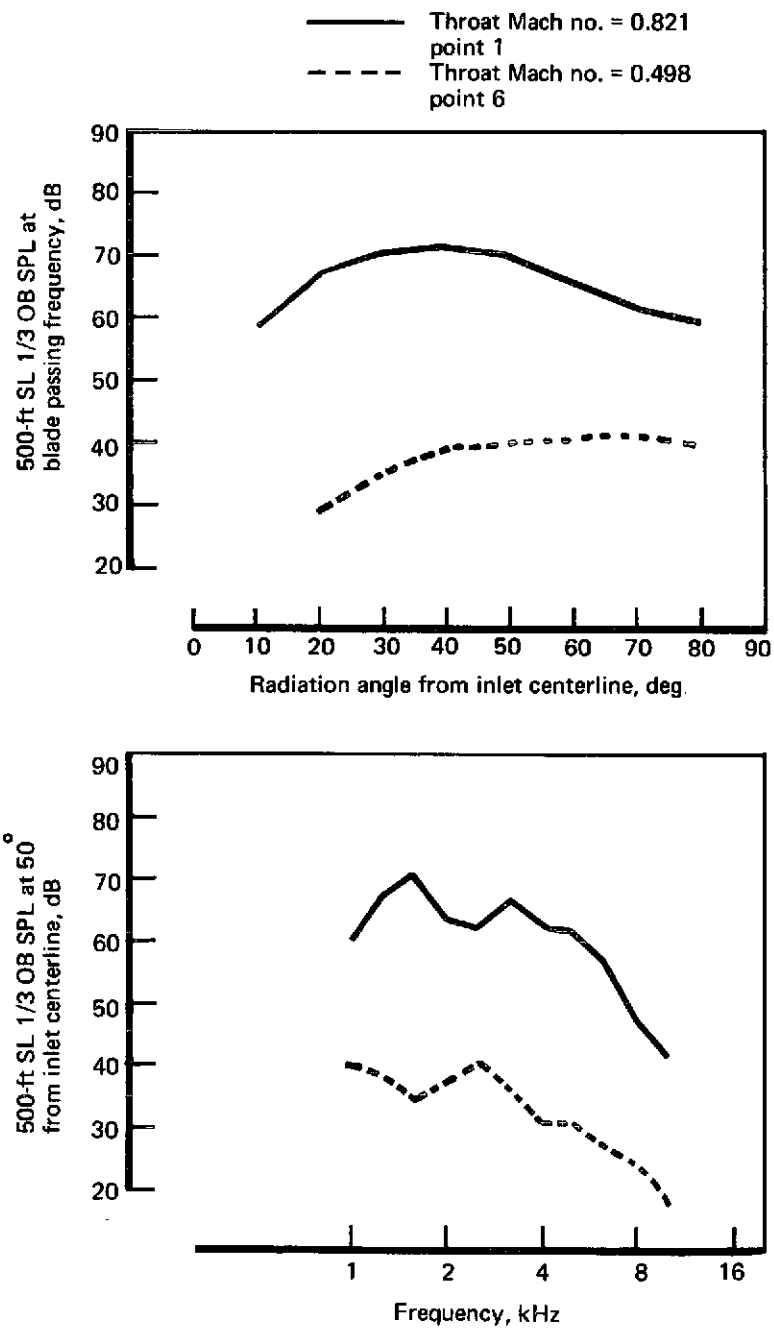


*FIGURE 64.—SPL DIRECTIVITY AND SPECTRUM (APPROACH), SCALED-UP DATA— RUN 10, MODEL 3C*

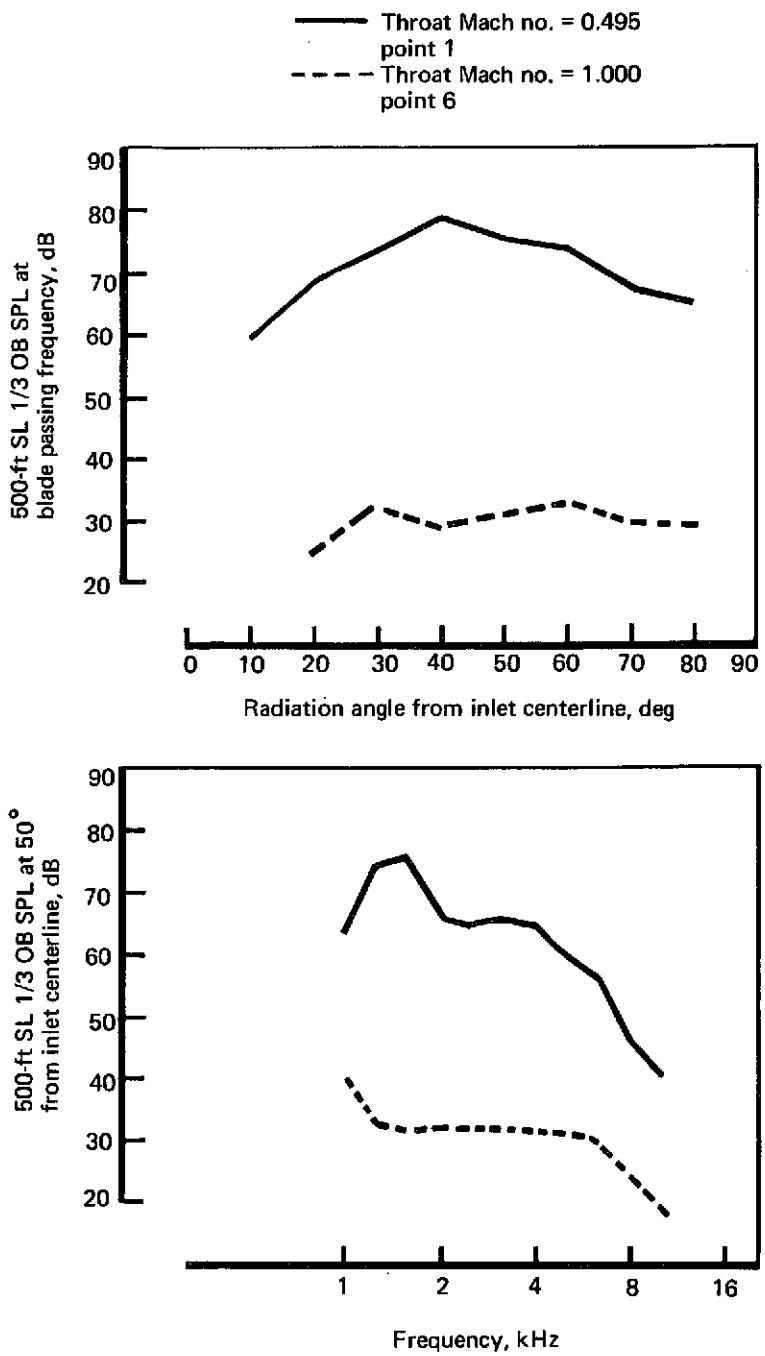


*FIGURE 65.—SPL DIRECTIVITY AND SPECTRUM (APPROACH), SCALED-UP DATA—RUN 6, MODEL 4*

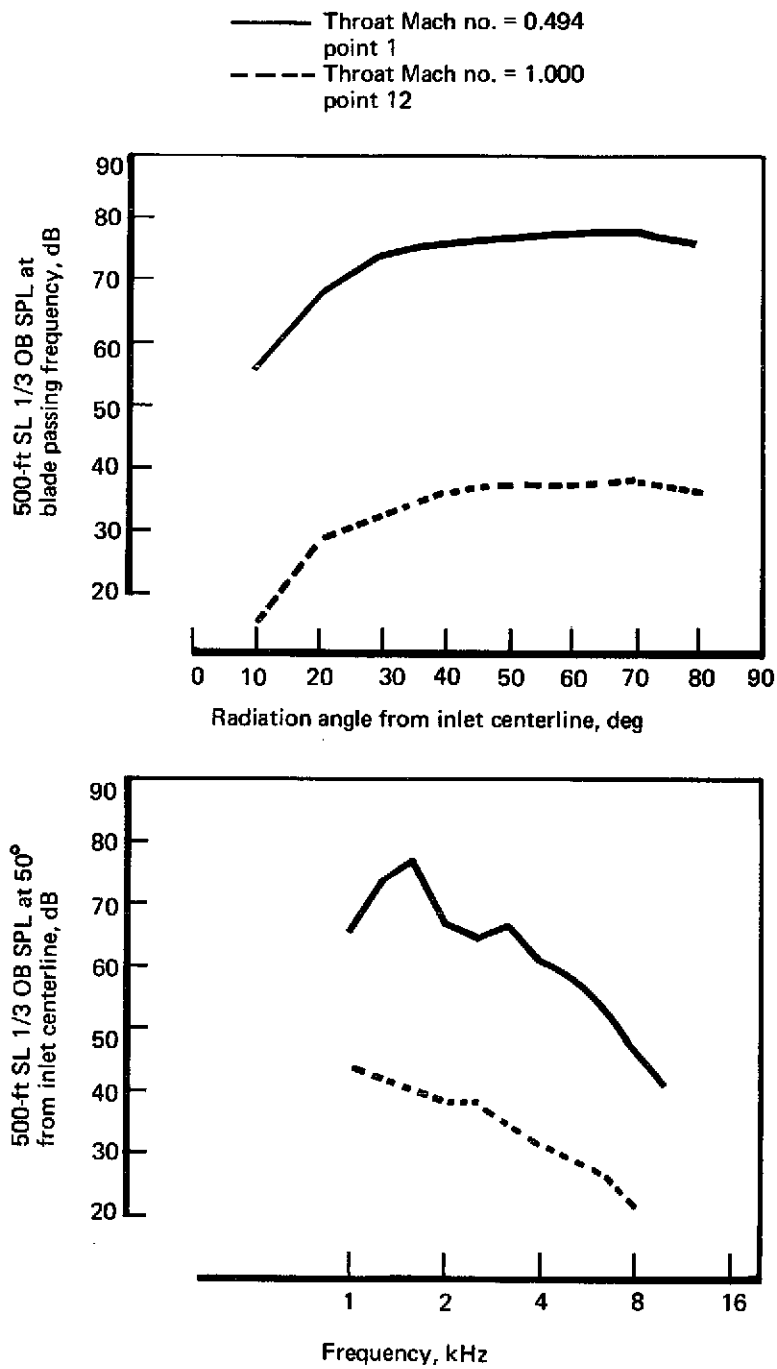


*FIGURE 66.—SPL DIRECTIVITY AND SPECTRUM (APPROACH), SCALED-UP DATA—RUN 8, MODEL 4*

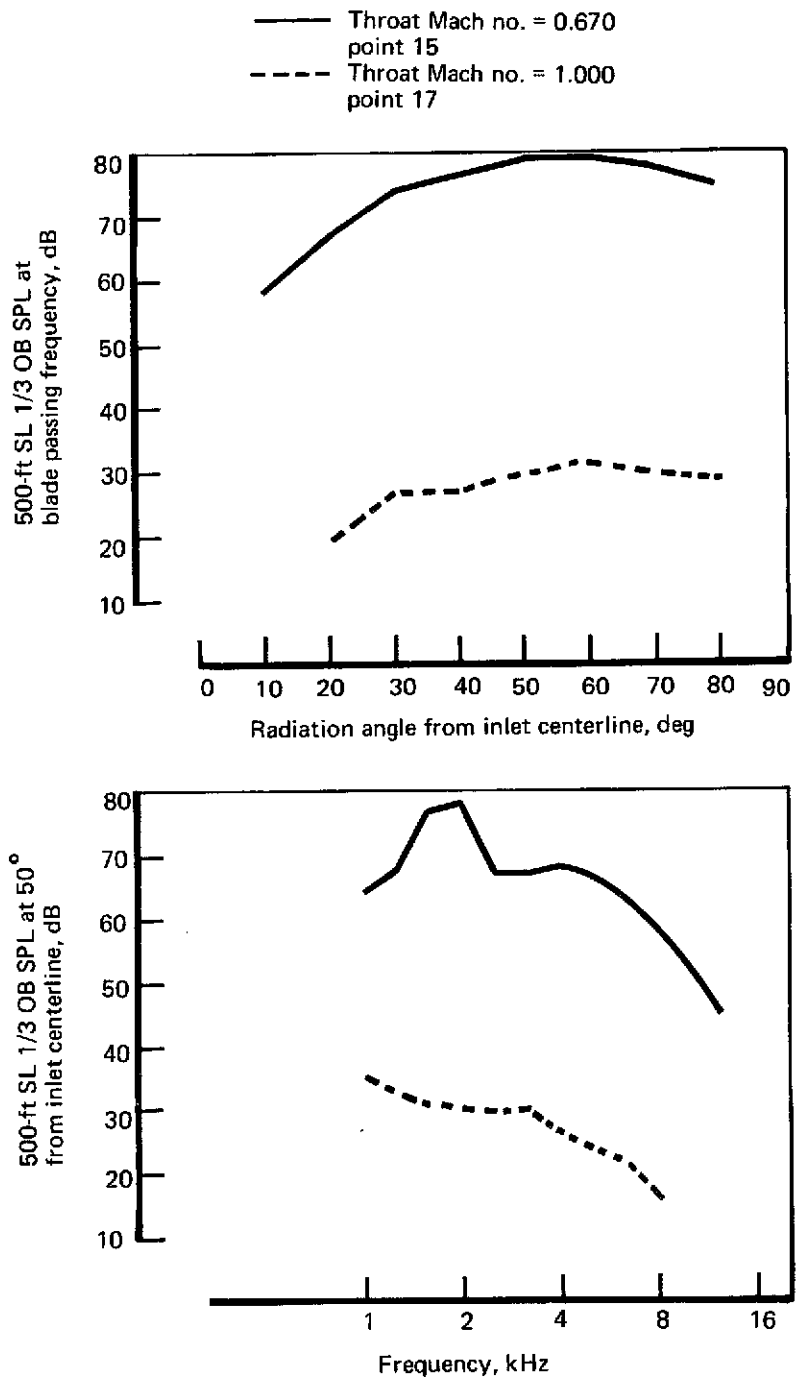


*FIGURE 67.–SPL DIRECTIVITY AND SPECTRUM (APPROACH), SCALED-UP DATA–RUN 11, MODEL 4*

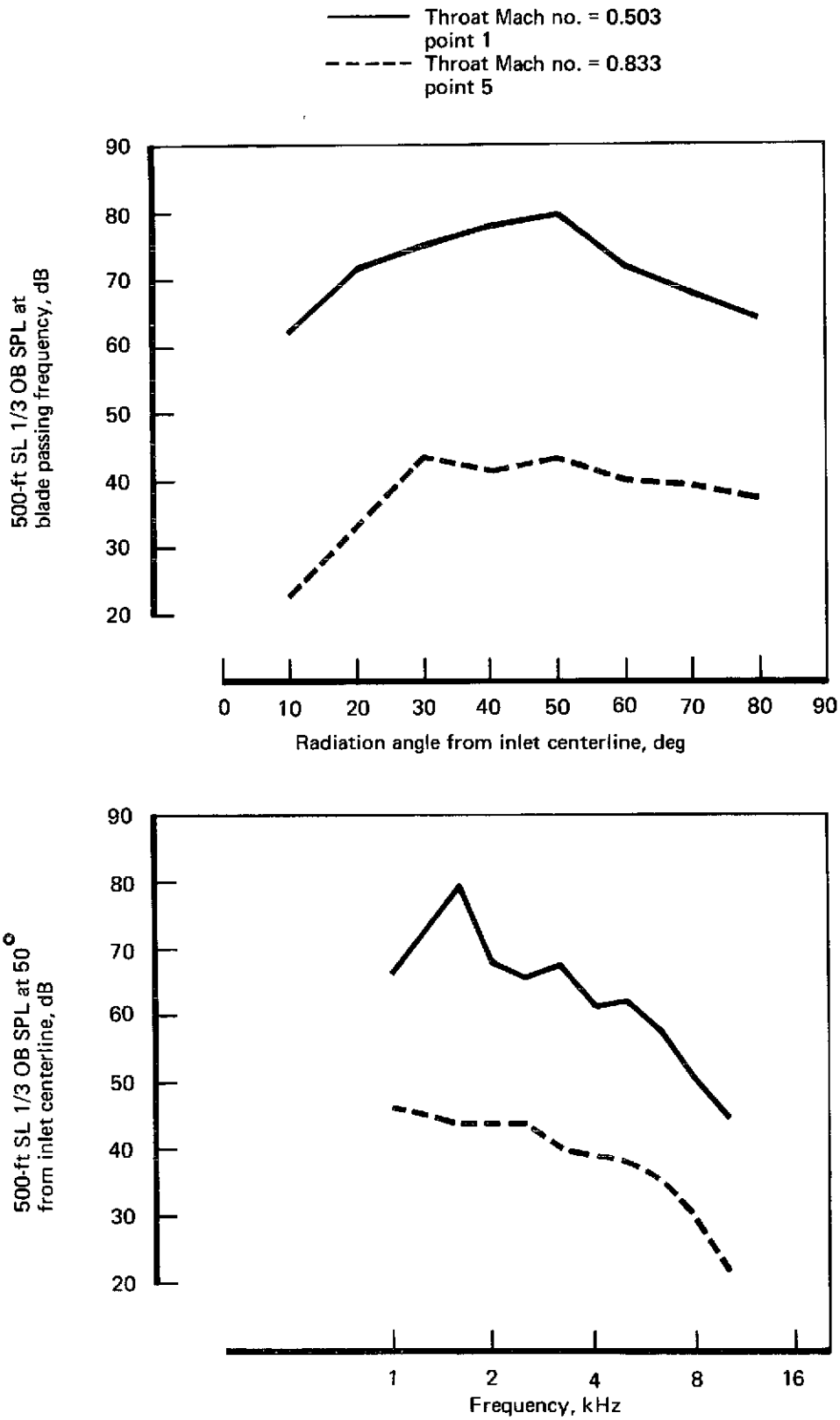


*FIGURE 68.–SPL DIRECTIVITY AND SPECTRUM (APPROACH), SCALED-UP DATA–RUN 7, MODEL 5A*

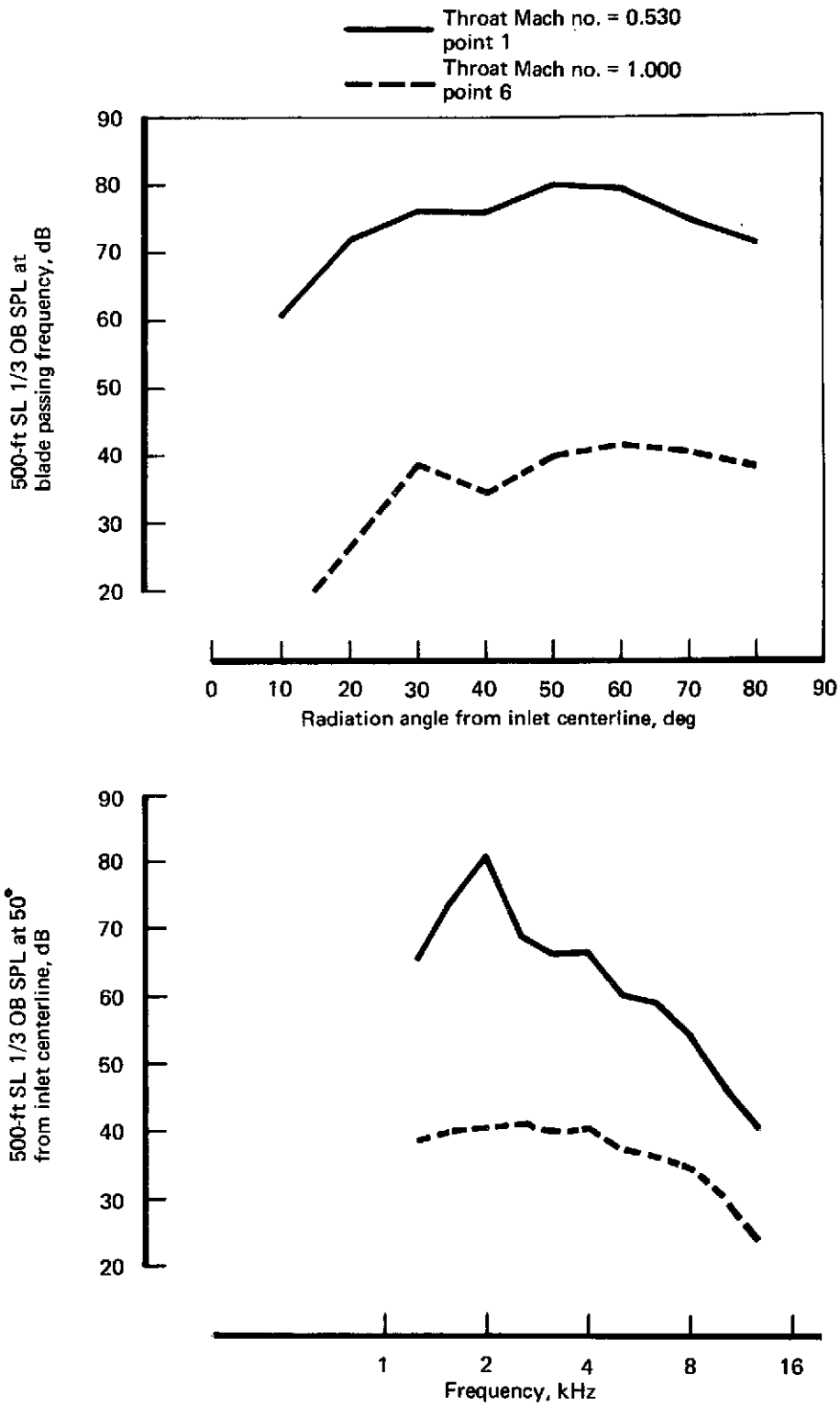


*FIGURE 69.—SPL DIRECTIVITY AND SPECTRUM (APPROACH), SCALED-UP DATA—RUN 13, MODEL 5B*

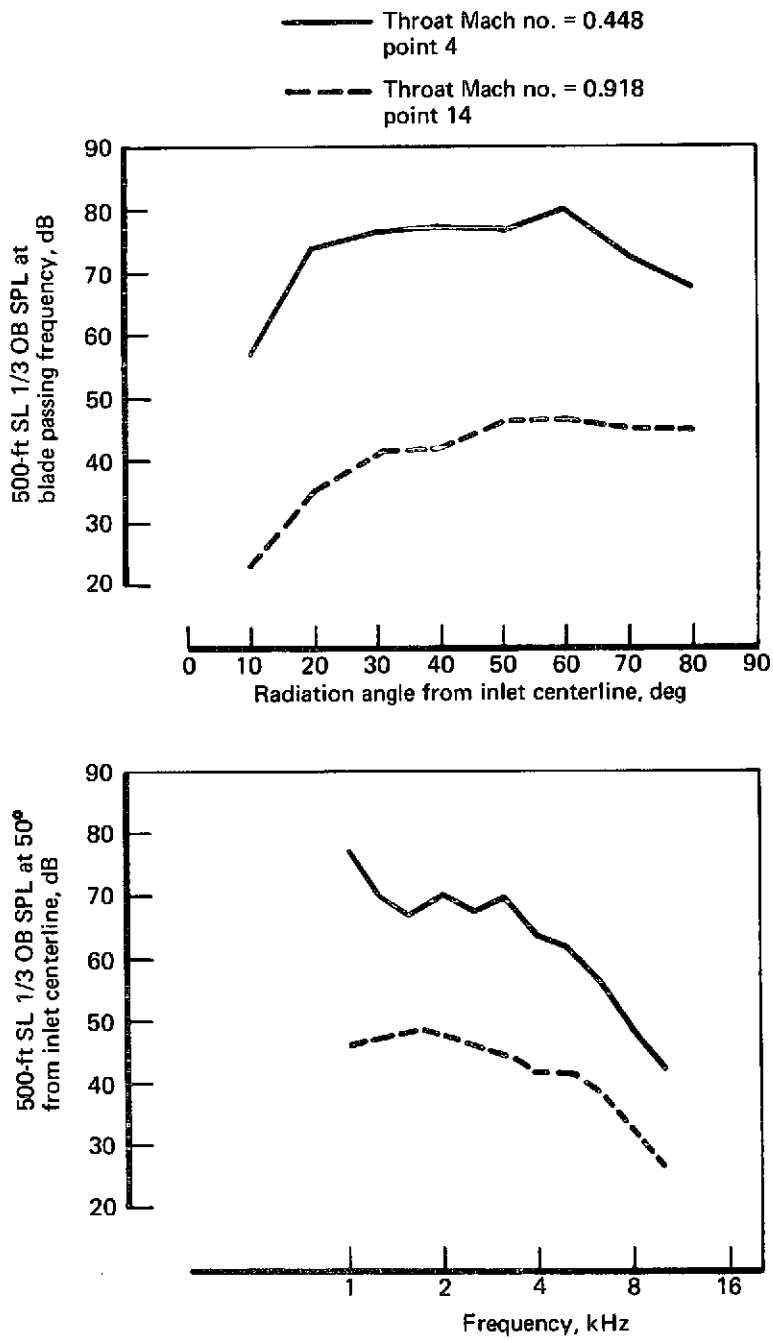


*FIGURE 70.–SPL DIRECTIVITY AND SPECTRUM (APPROACH), SCALED-UP DATA–RUN 9, MODEL 6*

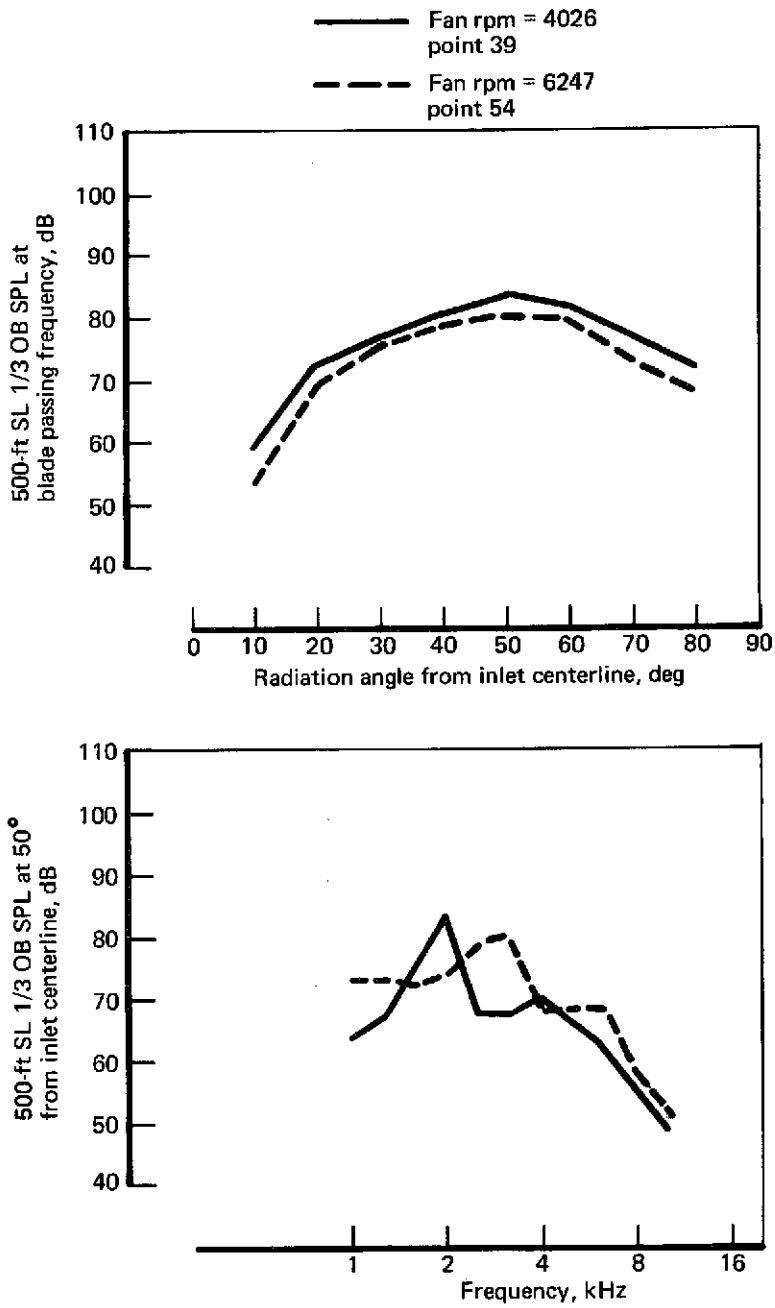


*FIGURE 71.—SPL DIRECTIVITY AND SPECTRUM (TAKEOFF), SCALED-UP DATA—RUN 1, MODEL 0*

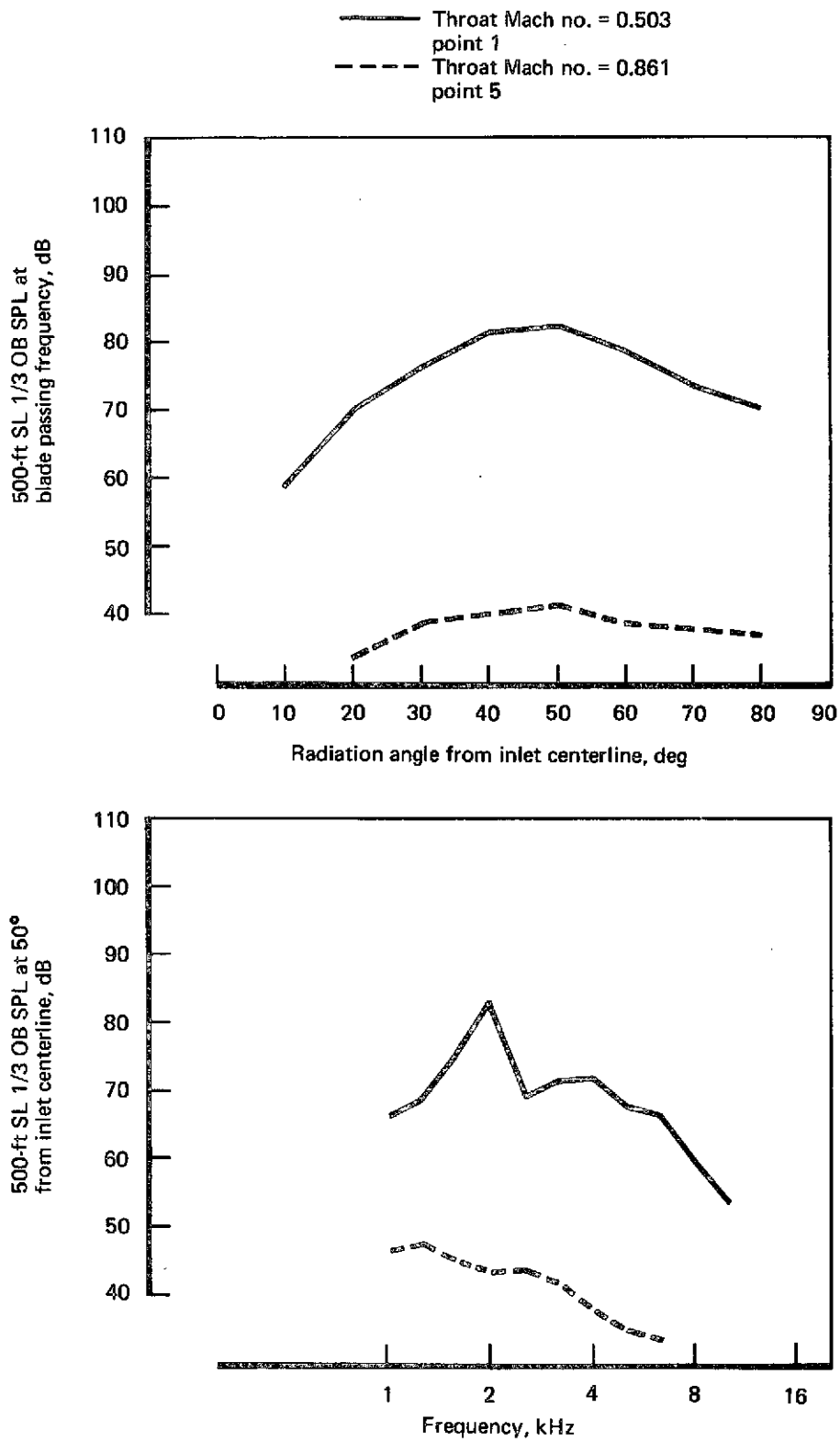


*FIGURE 72.–SPL DIRECTIVITY AND SPECTRUM (TAKEOFF), SCALED-UP DATA–RUN 3, MODEL 2*

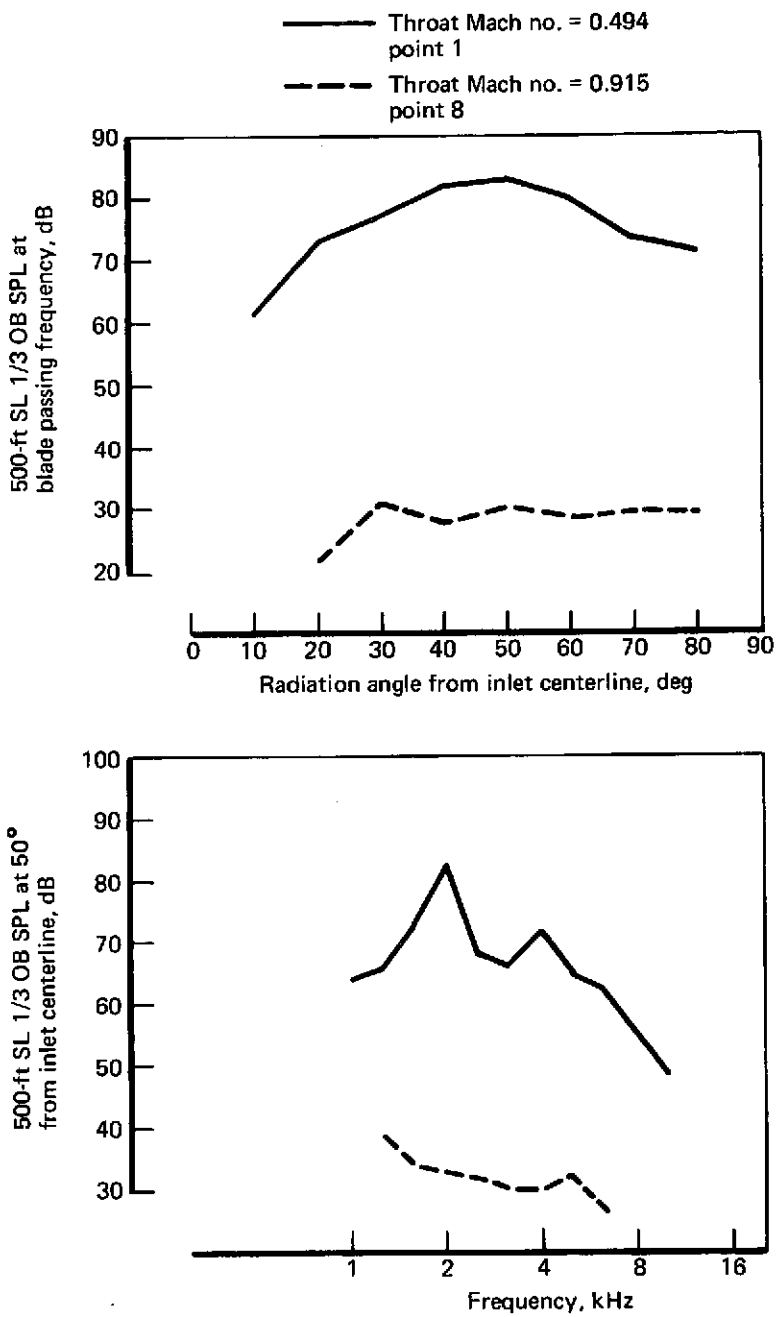


*FIGURE 73.–SPL DIRECTIVITY AND SPECTRUM (TAKEOFF), SCALED-UP DATA–RUN 5, MODEL 3*

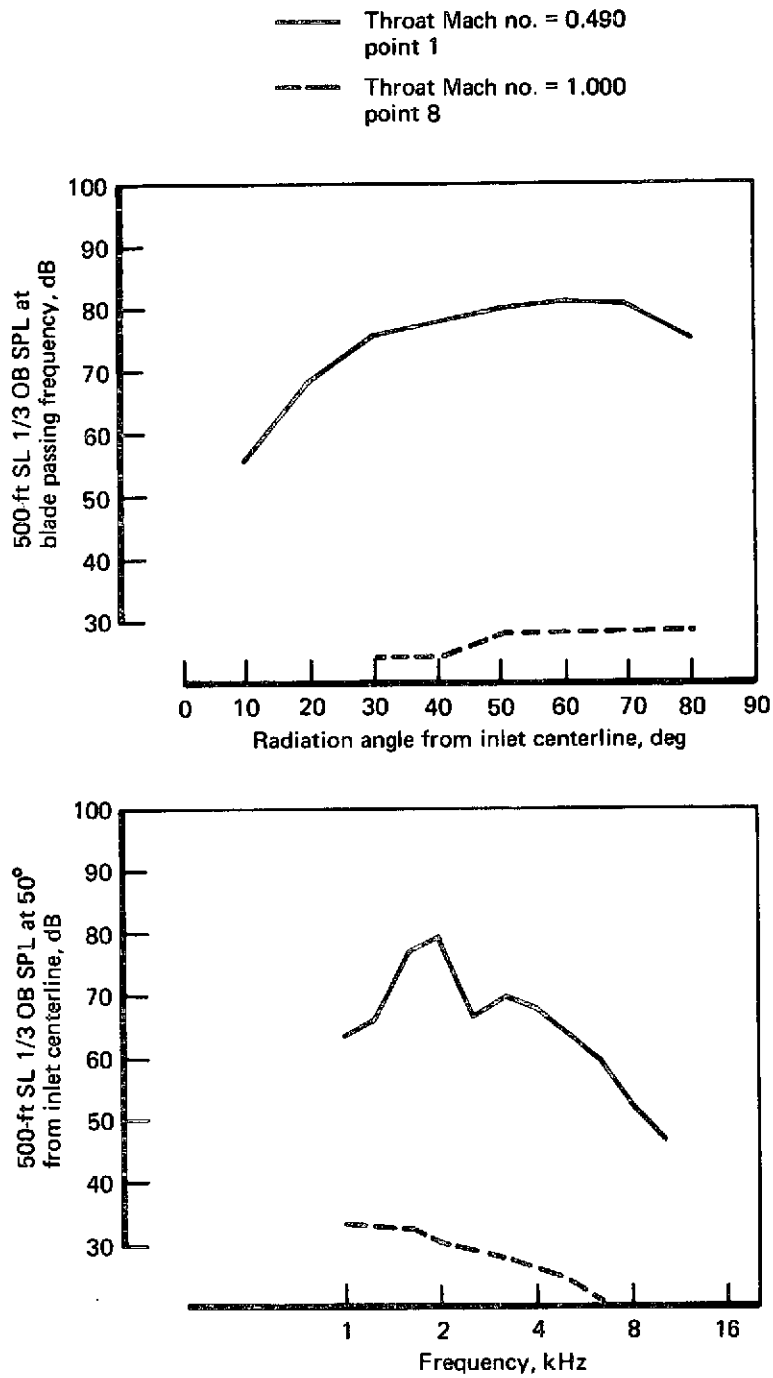


*FIGURE 74.–SPL DIRECTIVITY AND SPECTRUM (TAKEOFF), SCALED-UP DATA–RUN 12, MODEL 4*

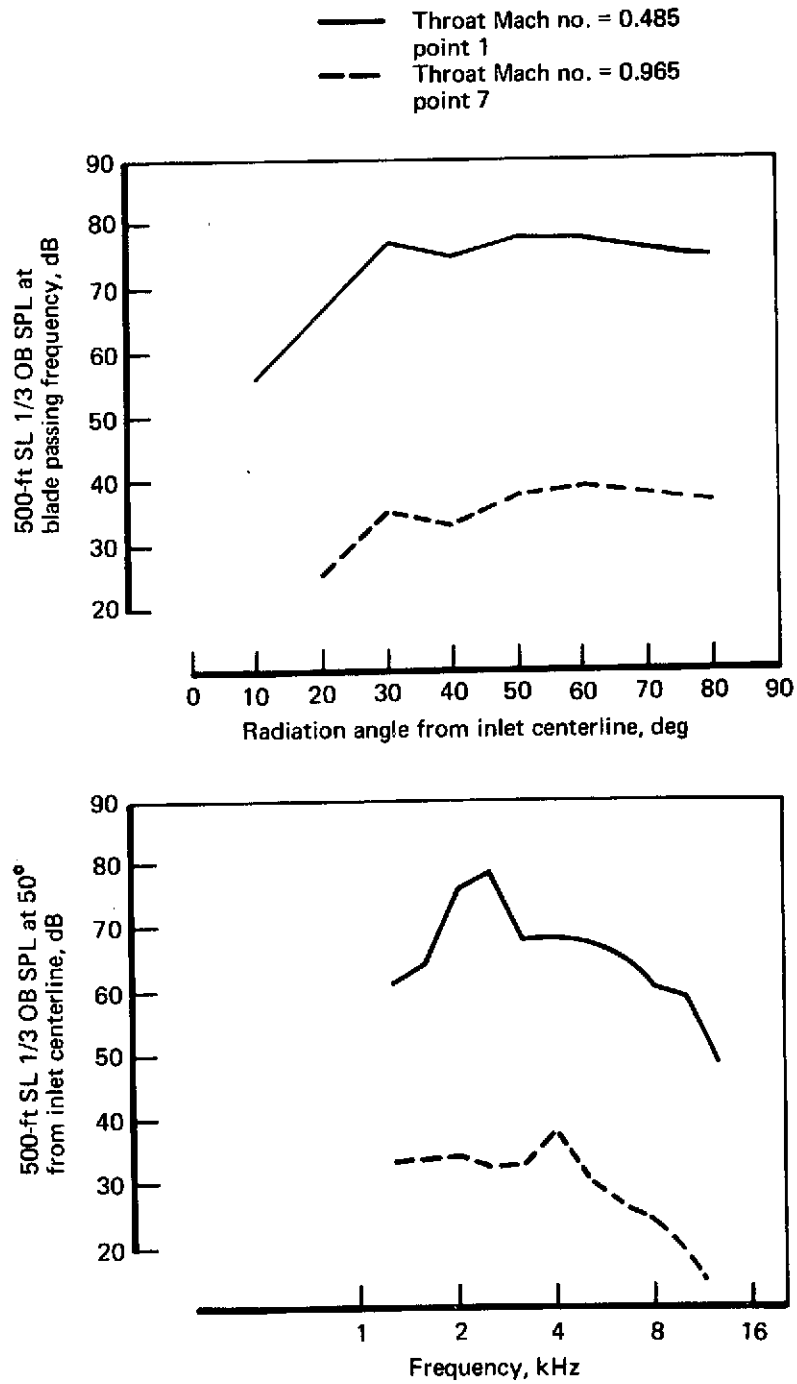


*FIGURE 75.—SPL DIRECTIVITY AND SPECTRUM (TAKEOFF), SCALED-UP DATA—RUN 14, MODEL 5B*

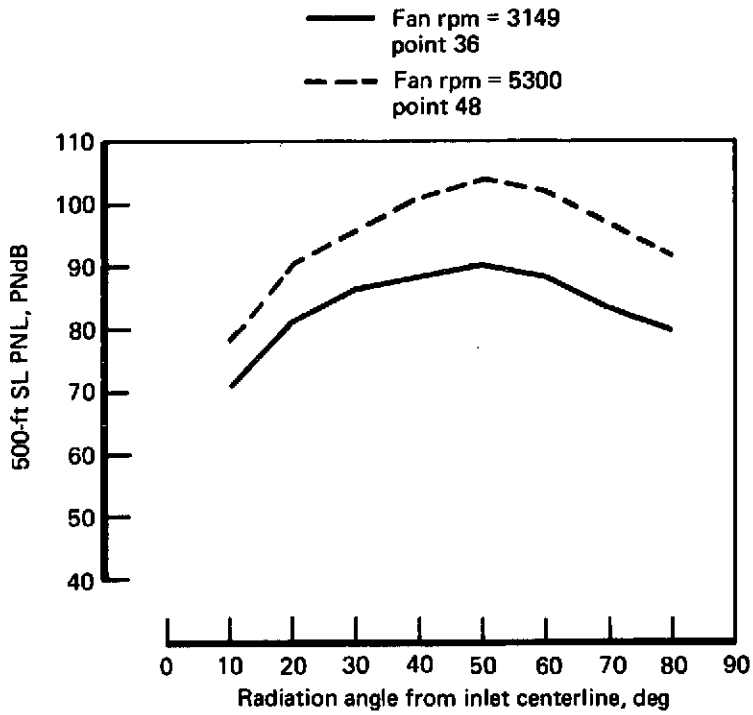


*FIGURE 76.—PNL DIRECTIVITY (APPROACH), SCALED-UP DATA—RUN 1, MODEL 0*

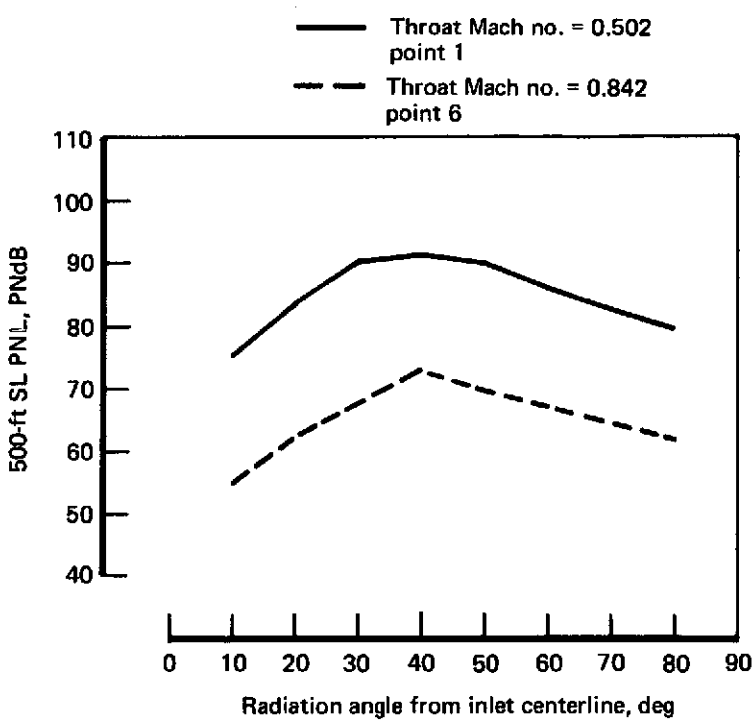


*FIGURE 77.—PNL DIRECTIVITY (APPROACH), SCALED-UP DATA—RUN 2, MODEL 1*

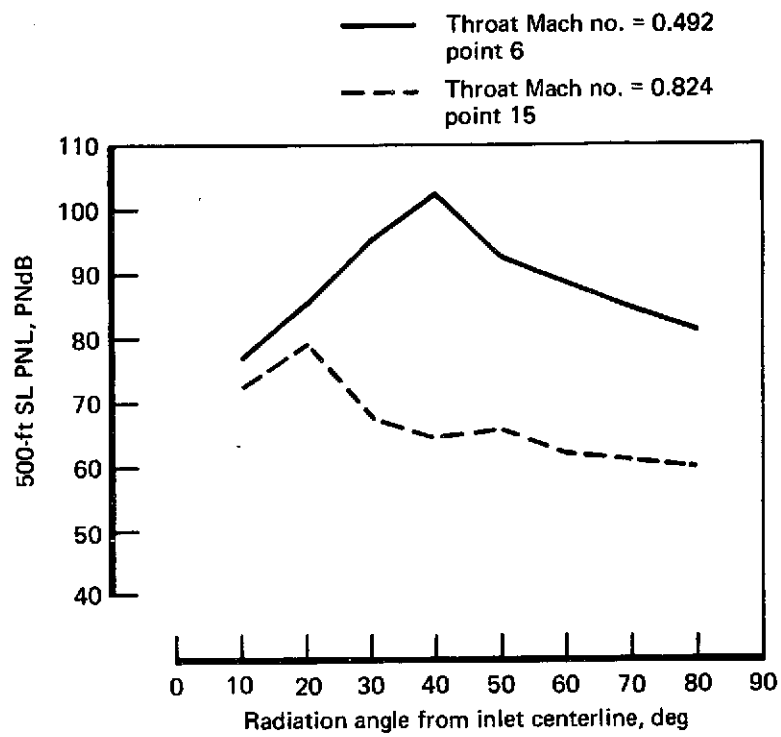


*FIGURE 78.—PNL DIRECTIVITY (APPROACH), SCALED-UP DATA—RUN 4, MODEL 3*

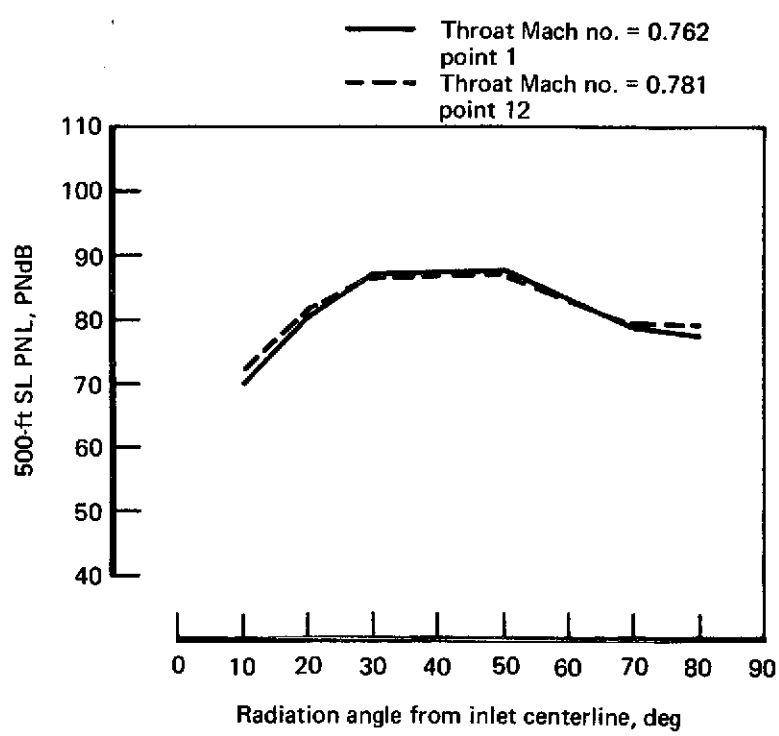


*FIGURE 79.—PNL DIRECTIVITY (APPROACH), SCALED-UP DATA—RUN 101, MODEL 3A*

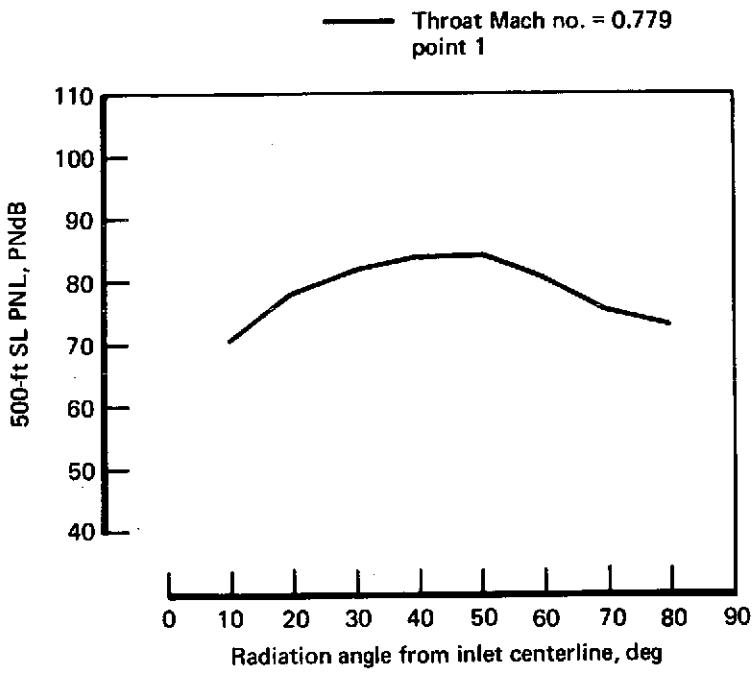


*FIGURE 80.–PNL DIRECTIVITY (APPROACH, SCALED-UP DATA–RUN 102, MODEL 3B*

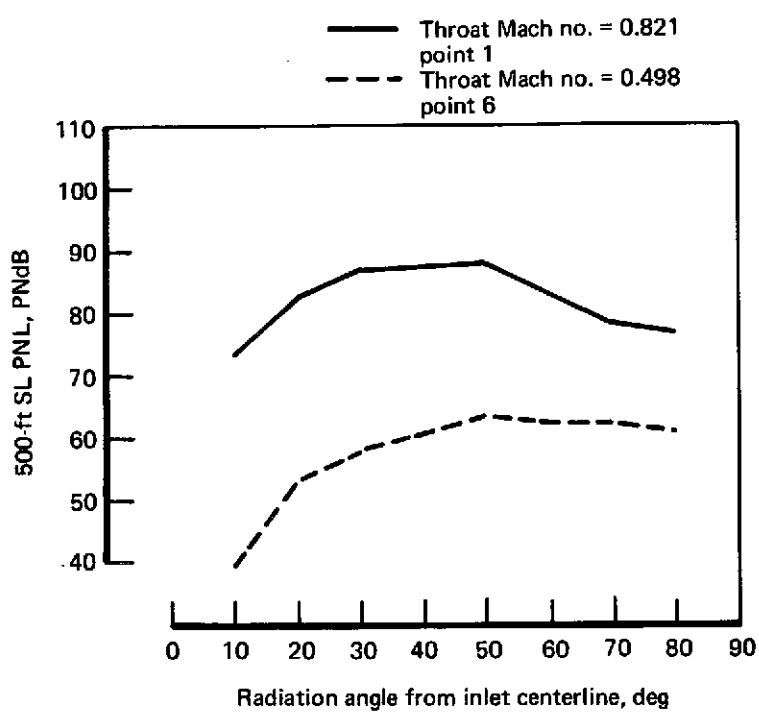


*FIGURE 81.–PNL DIRECTIVITY (APPROACH), SCALED-UP DATA–RUN 10, MODEL 3C*

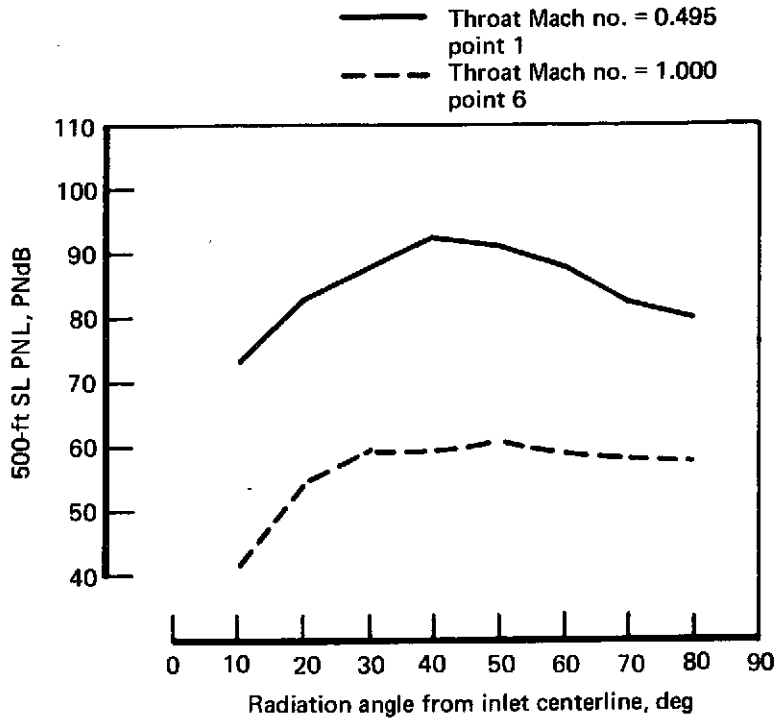


*FIGURE 82.–PNL DIRECTIVITY (APPROACH), SCALED-UP DATA–RUN 6, MODEL 4*

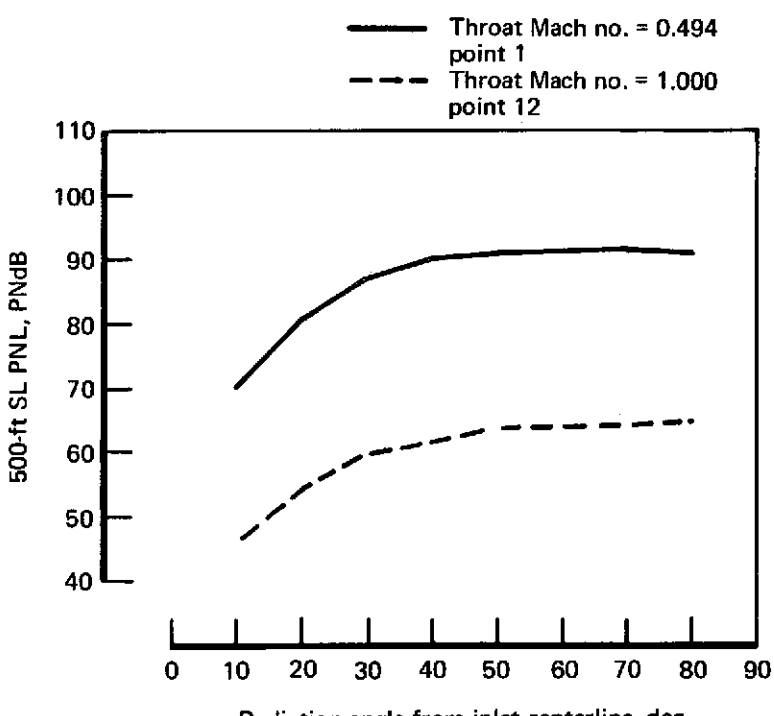


*FIGURE 83.–PNL DIRECTIVITY (APPROACH), SCALED-UP DATA–RUN 8, MODEL 4*

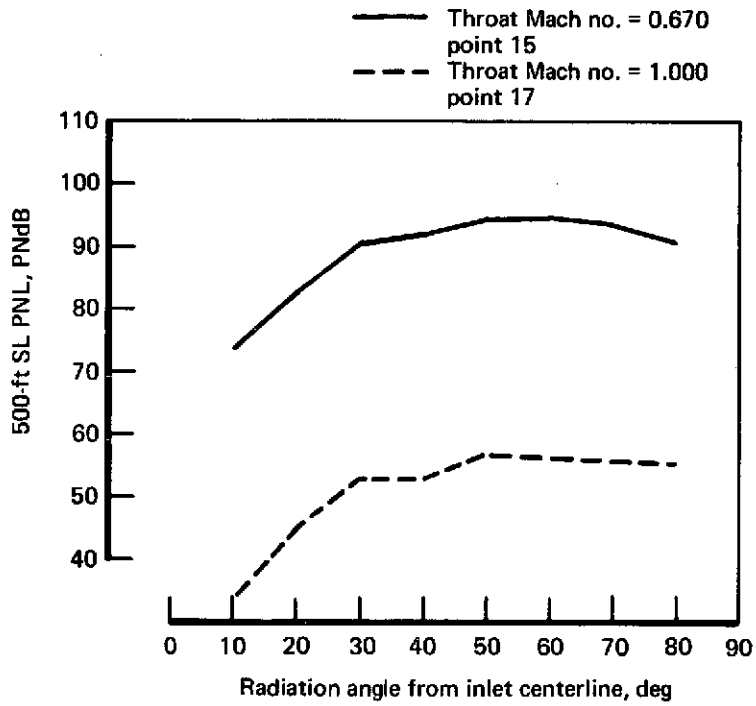


*FIGURE 84.–PNL DIRECTIVITY (APPROACH), SCALED-UP DATA–RUN 11, MODEL 4*

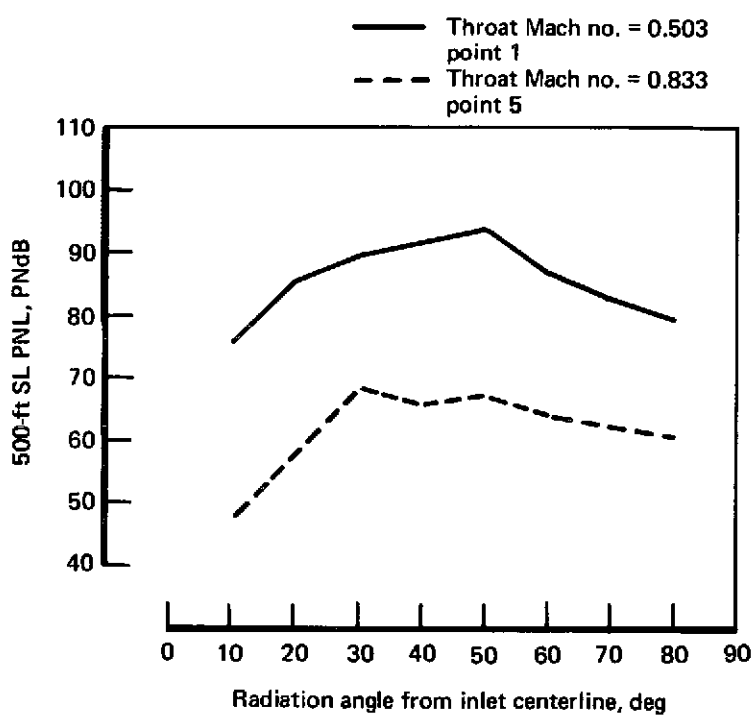


*FIGURE 85.–PNL DIRECTIVITY (APPROACH), SCALED-UP DATA–RUN 7, MODEL 5*

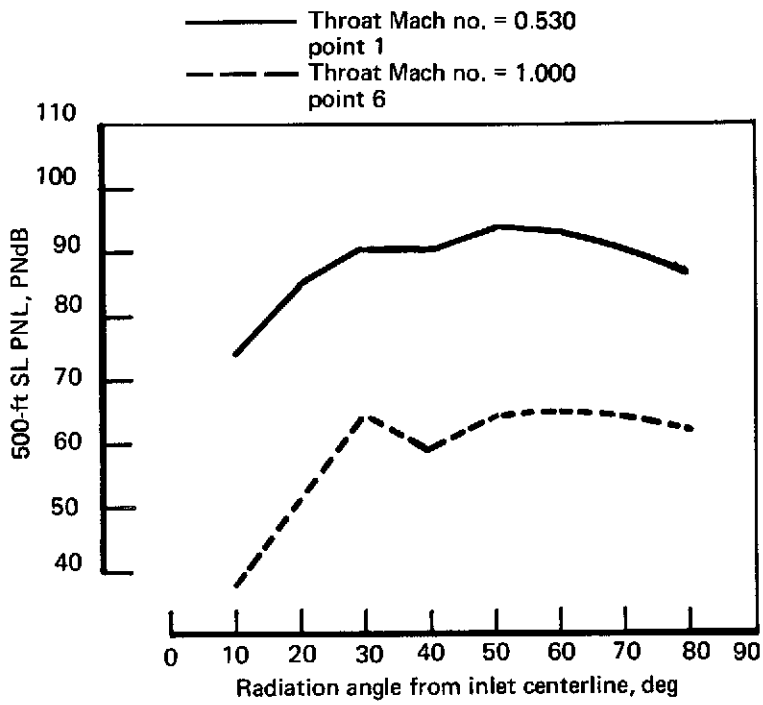


*FIGURE 86.–PNL DIRECTIVITY (APPROACH), SCALED-UP DATA–RUN 13, MODEL 5B*

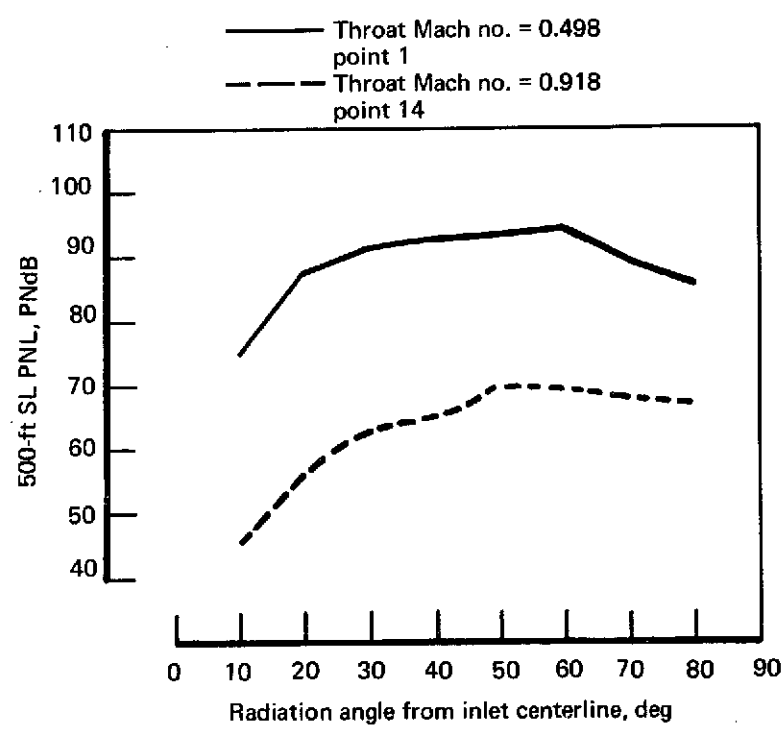


*FIGURE 87.–PNL DIRECTIVITY (APPROACH, SCALED-UP DATA–RUN 9, MODEL 6*

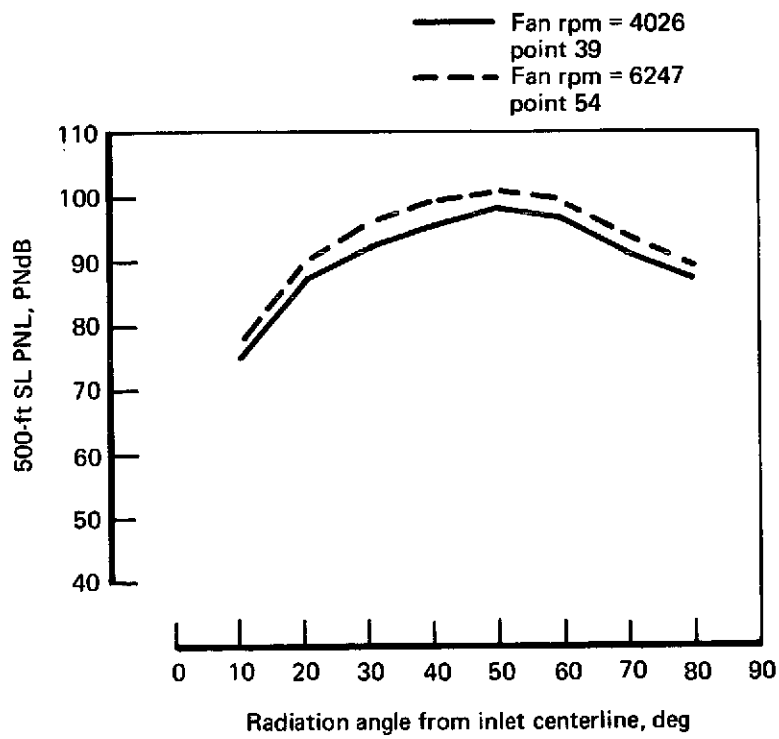


*FIGURE 88.–PNL DIRECTIVITY (TAKEOFF), SCALED-UP DATA–RUN 1, MODEL 0*

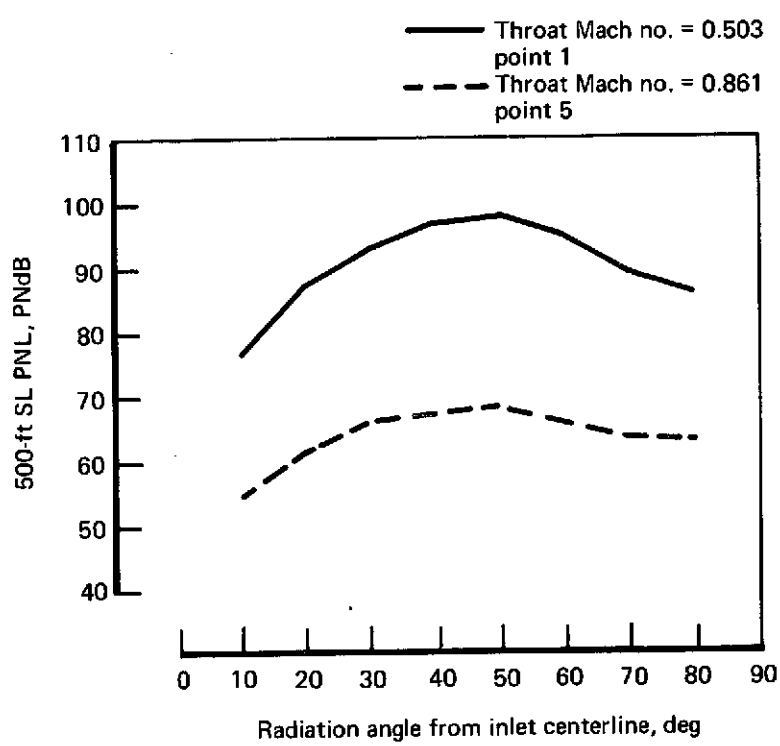


*FIGURE 89.–PNL DIRECTIVITY (TAKEOFF), SCALED-UP DATA–RUN 3, MODEL 2*

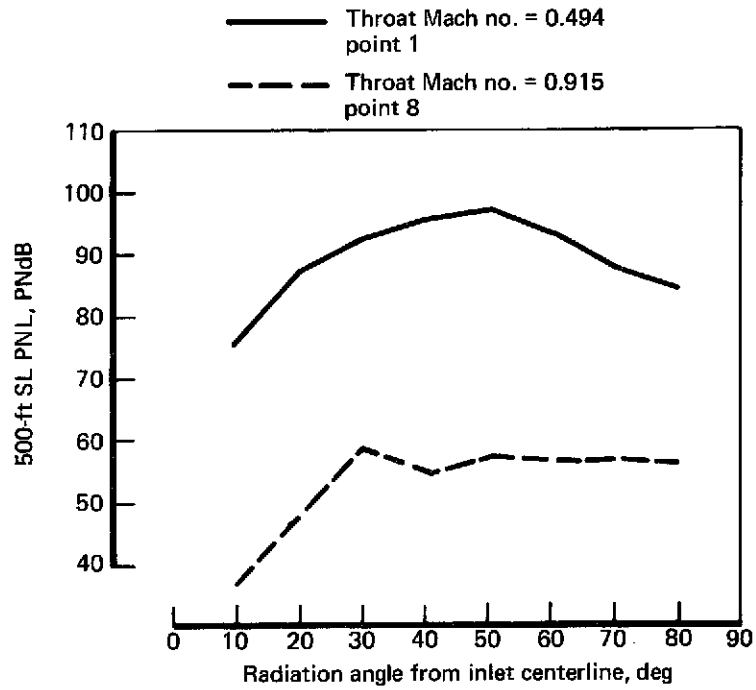


*FIGURE 90.–PNL DIRECTIVITY (TAKEOFF), SCALED-UP DATA–RUN 5, MODEL 3*

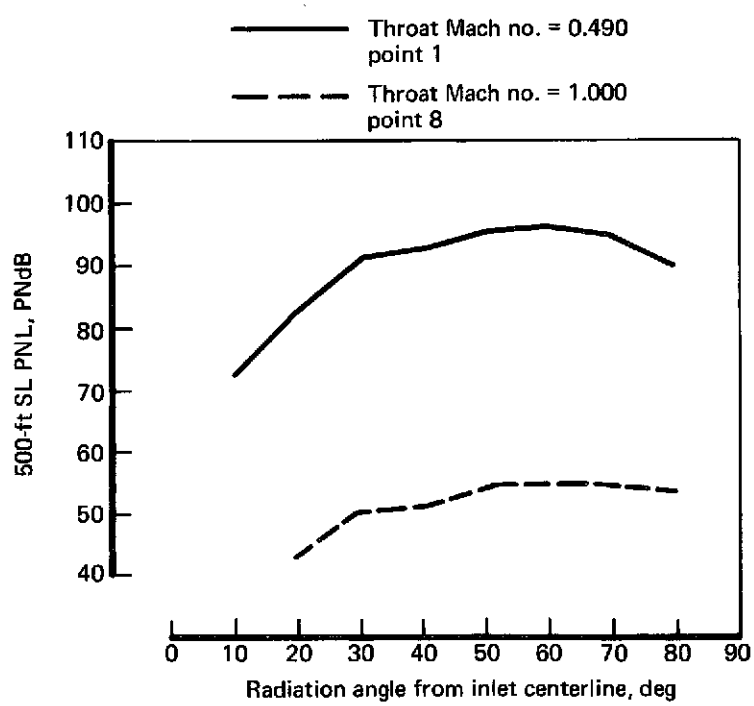


*FIGURE 91.–PNL DIRECTIVITY (TAKEOFF), SCALED-UP DATA–RUN 12, MODEL 4*

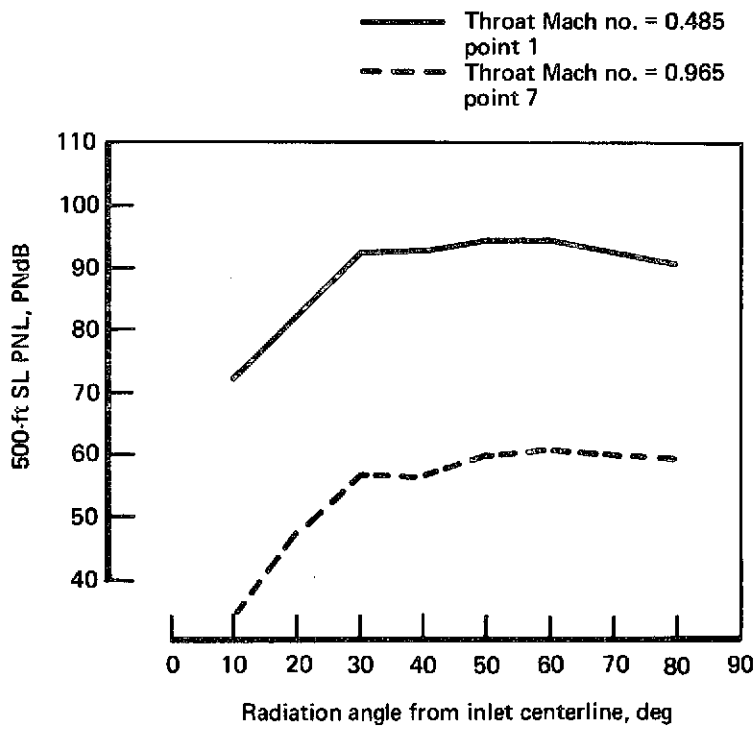


*FIGURE 92.—PNL DIRECTIVITY (TAKEOFF), SCALED-UP DATA—RUN 14, MODEL 5B*

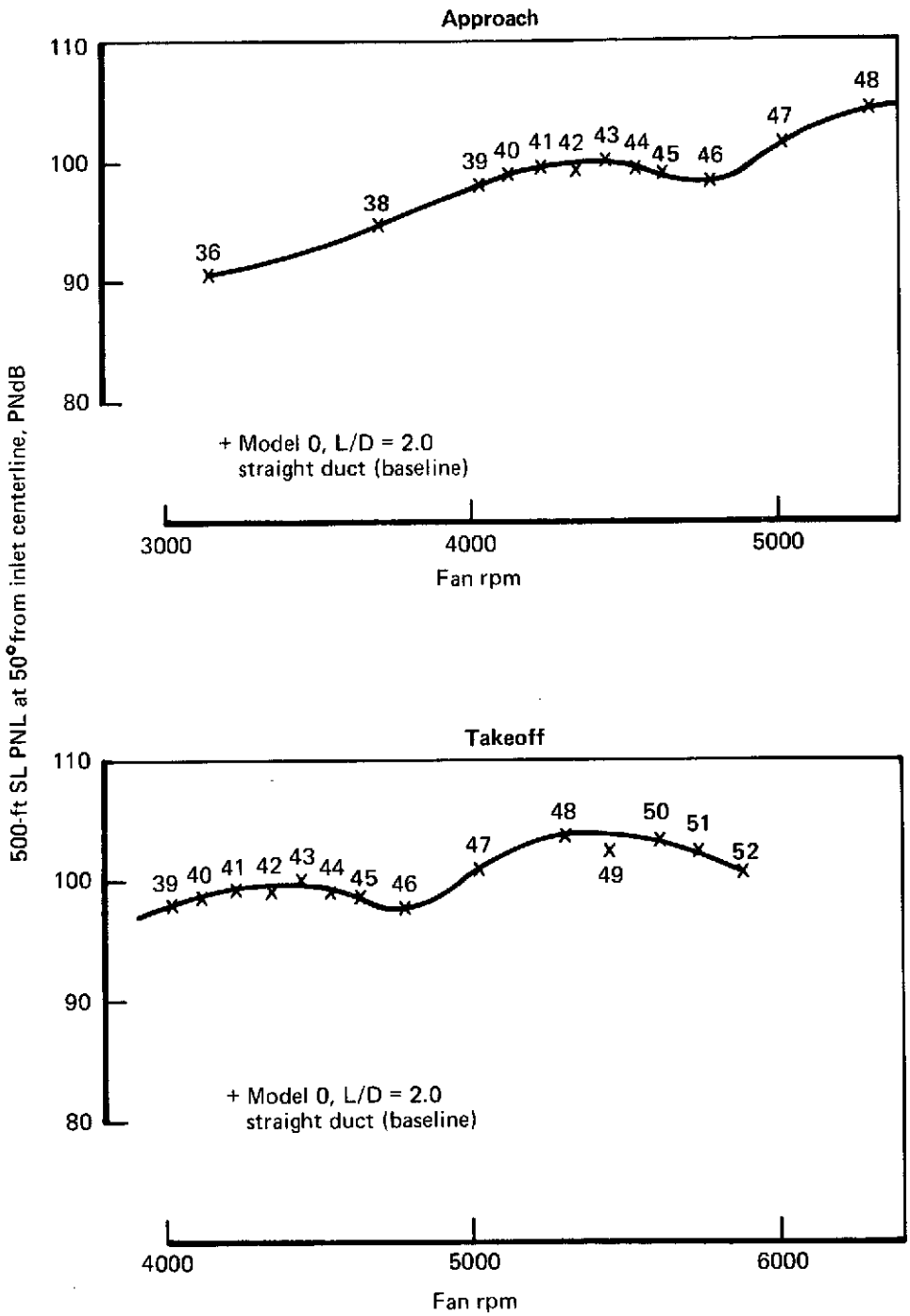


*FIGURE 93.–PNL VS FAN RPM (APPROACH AND TAKEOFF), SCALED-UP DATA–RUN 1, MODEL 0*

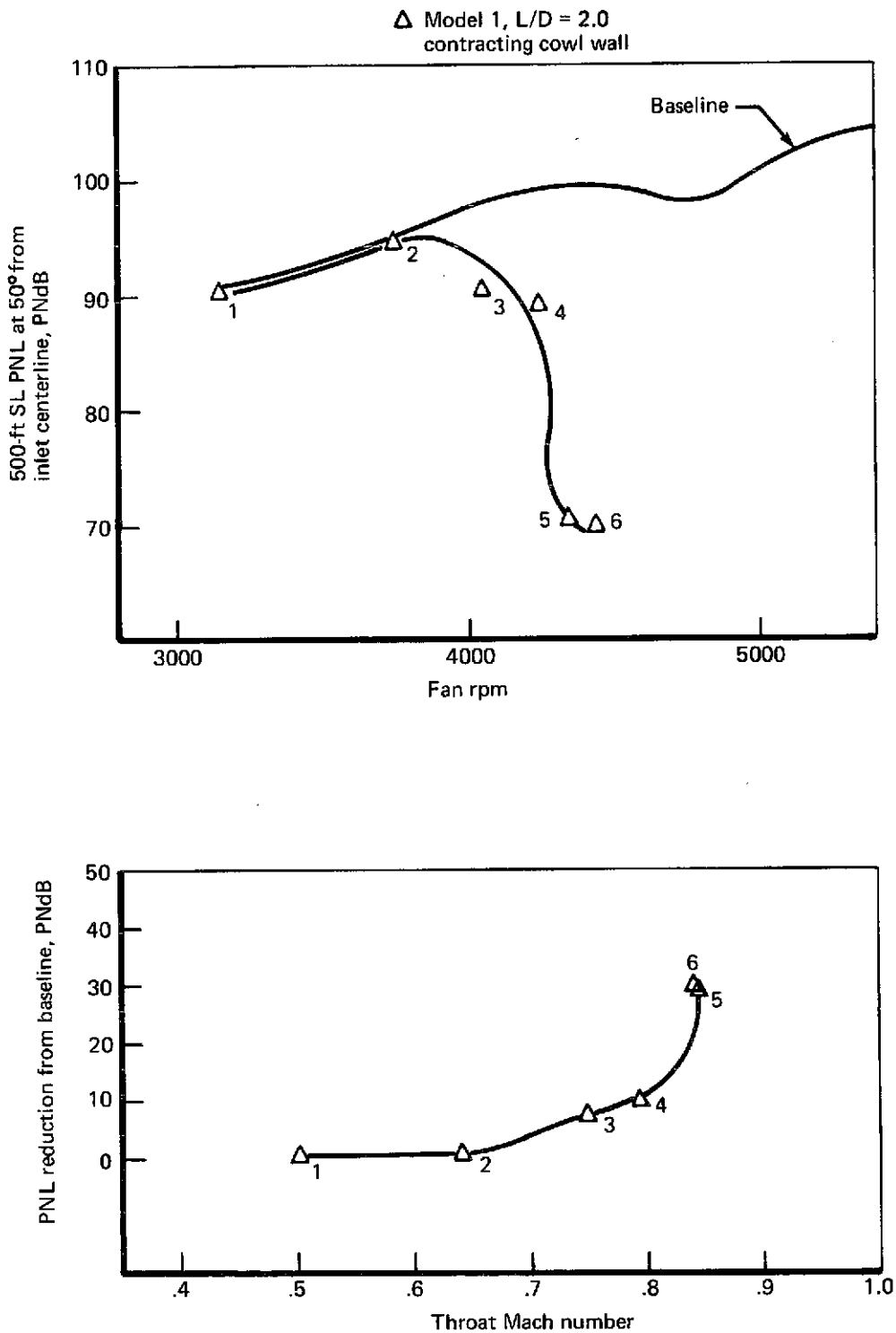


*FIGURE 94.—PNL VS FAN RPM AND PNL REDUCTION VS THROAT MACH NUMBER (APPROACH), SCALED-UP DATA—RUN 2, MODEL 1*

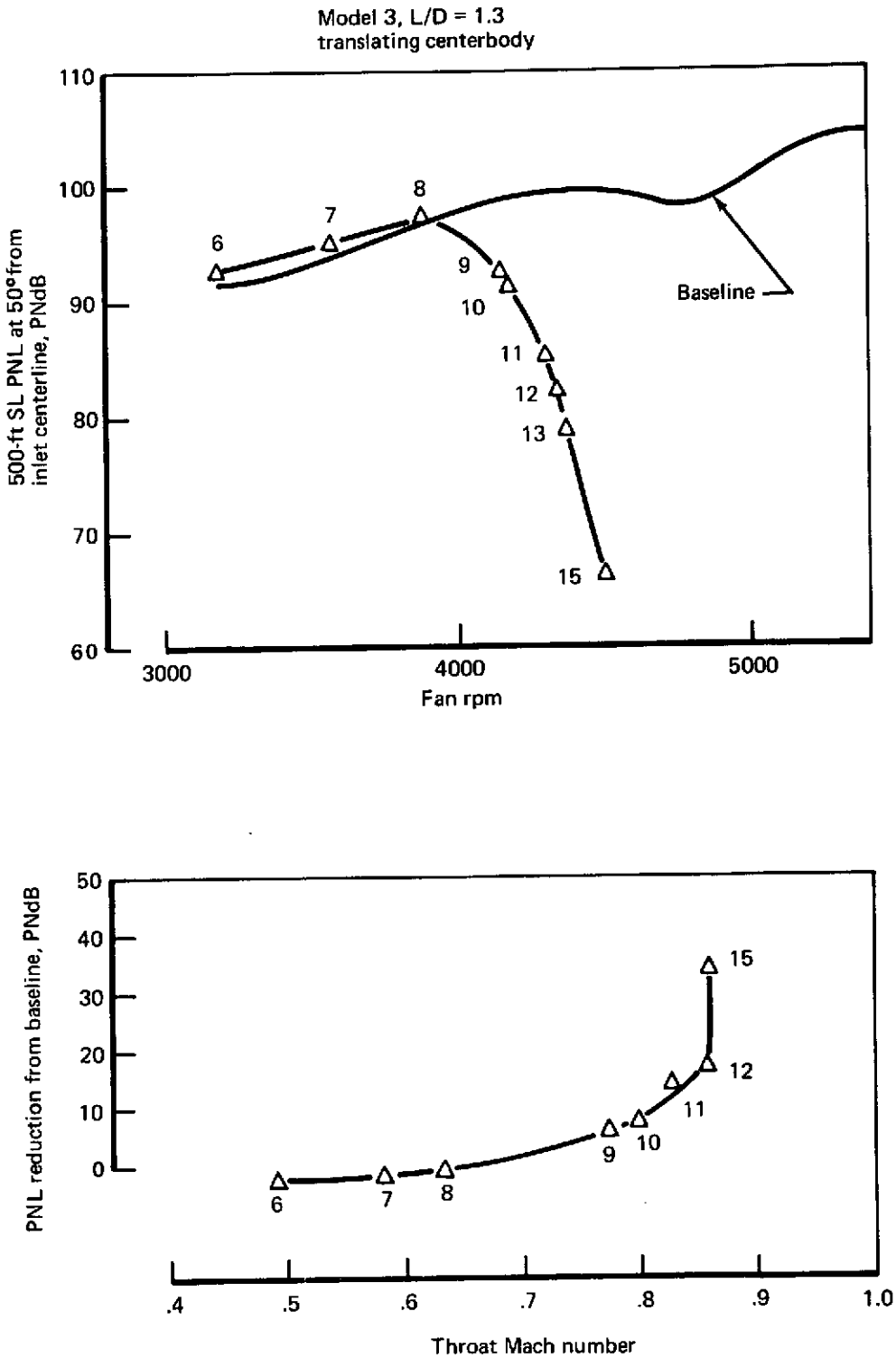


*FIGURE 95.—PNL VS FAN RPM AND PNL REDUCTION VS THROAT MACH NUMBER (APPROACH), SCALED-UP DATA—RUN 4, MODEL 3*

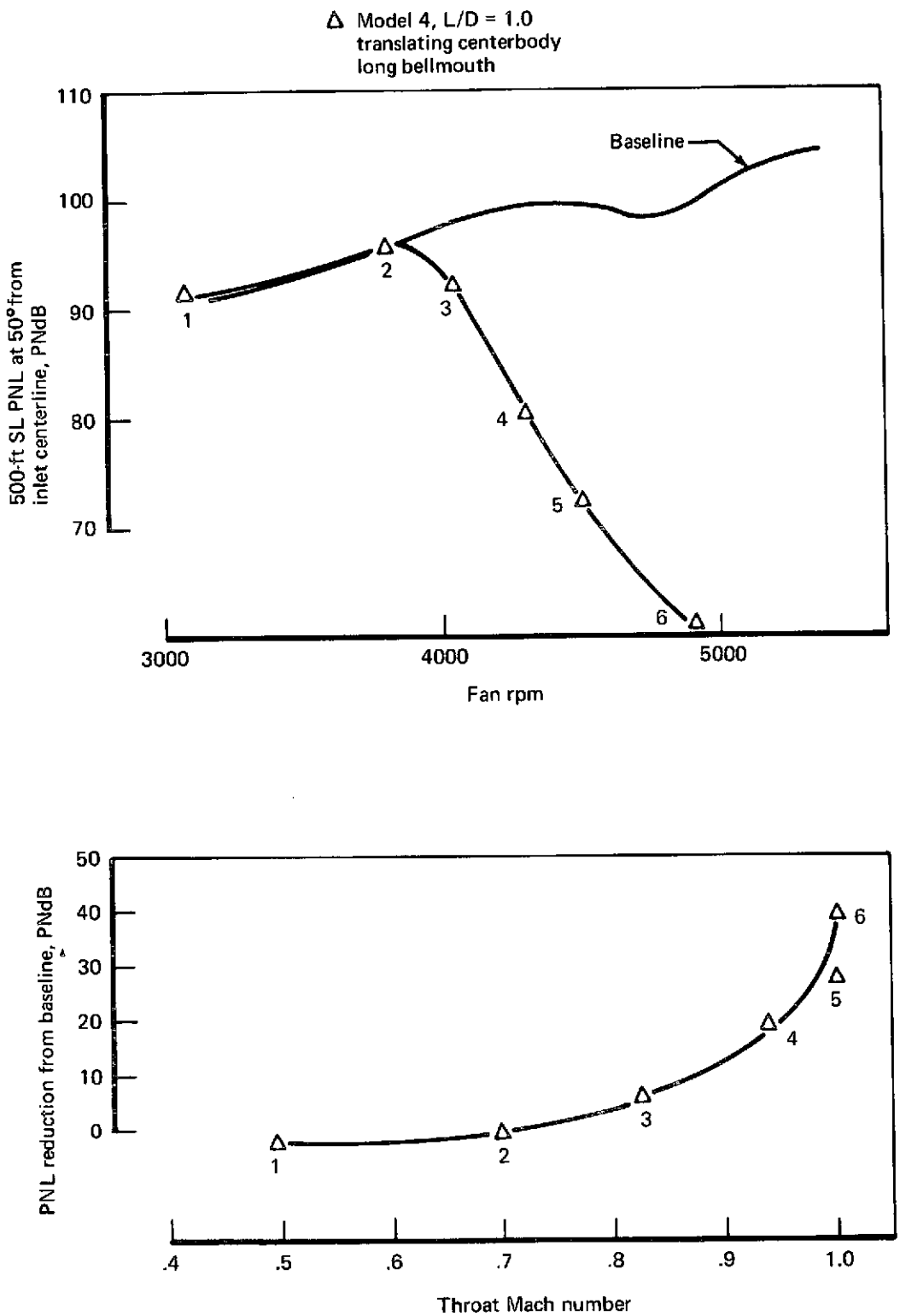


*FIGURE 96.—PNL VS FAN RPM AND PNL REDUCTION VS THROAT MACH NUMBER (APPROACH), SCALED-UP DATA—RUN 6, MODEL 4*

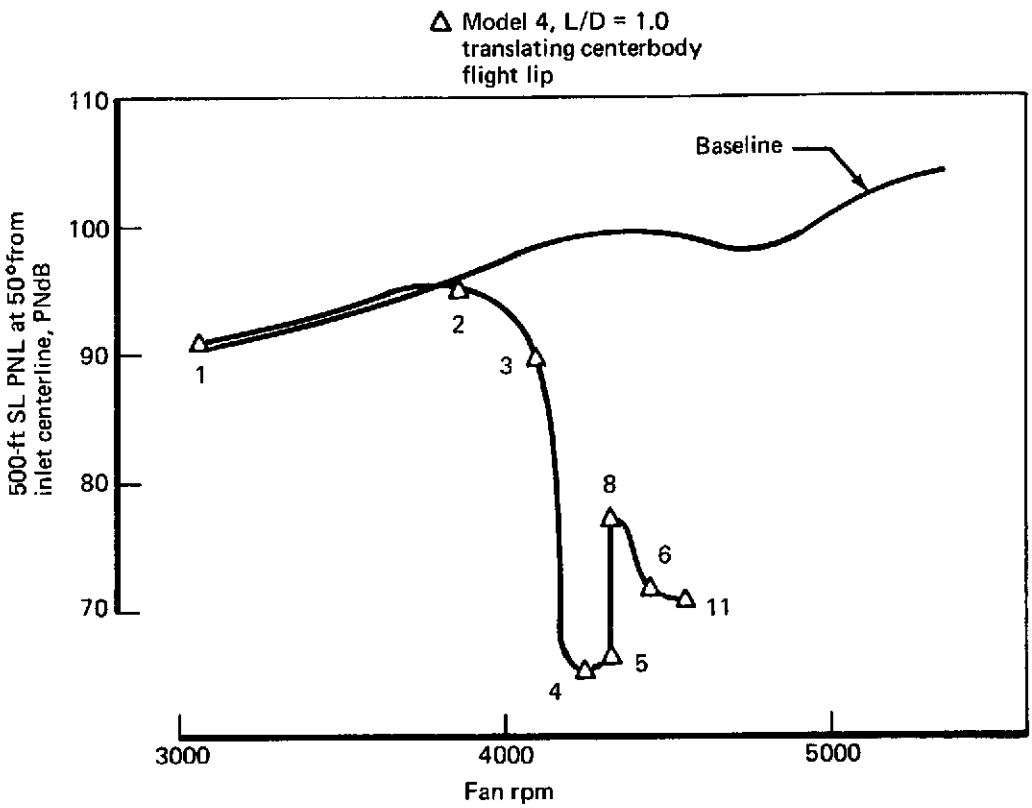


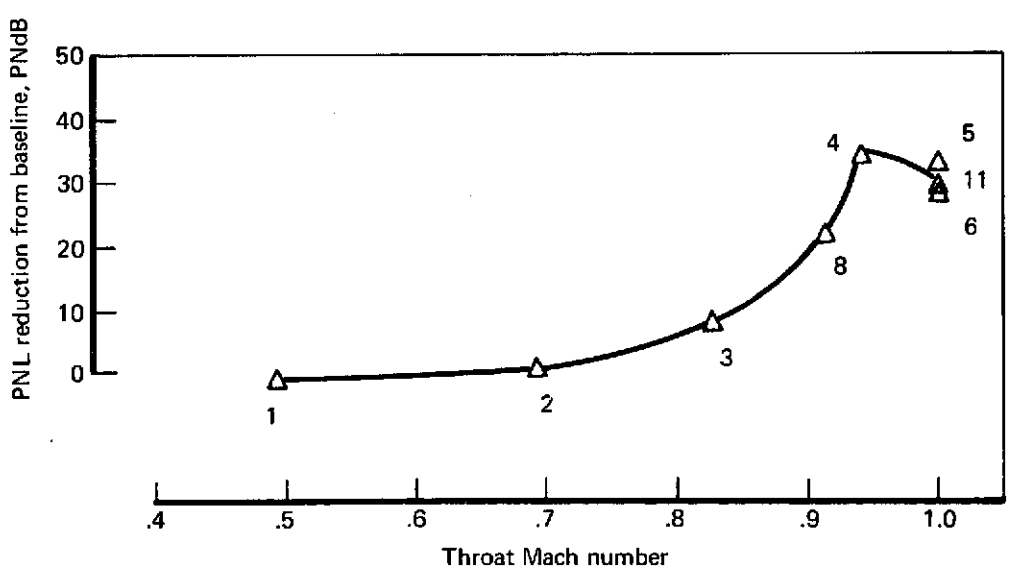


*FIGURE 97.–PNL VS FAN RPM AND PNL REDUCTION VS THROAT MACH NUMBER(APPROACH), SCALED-UP DATA–RUN 8, MODEL 4*

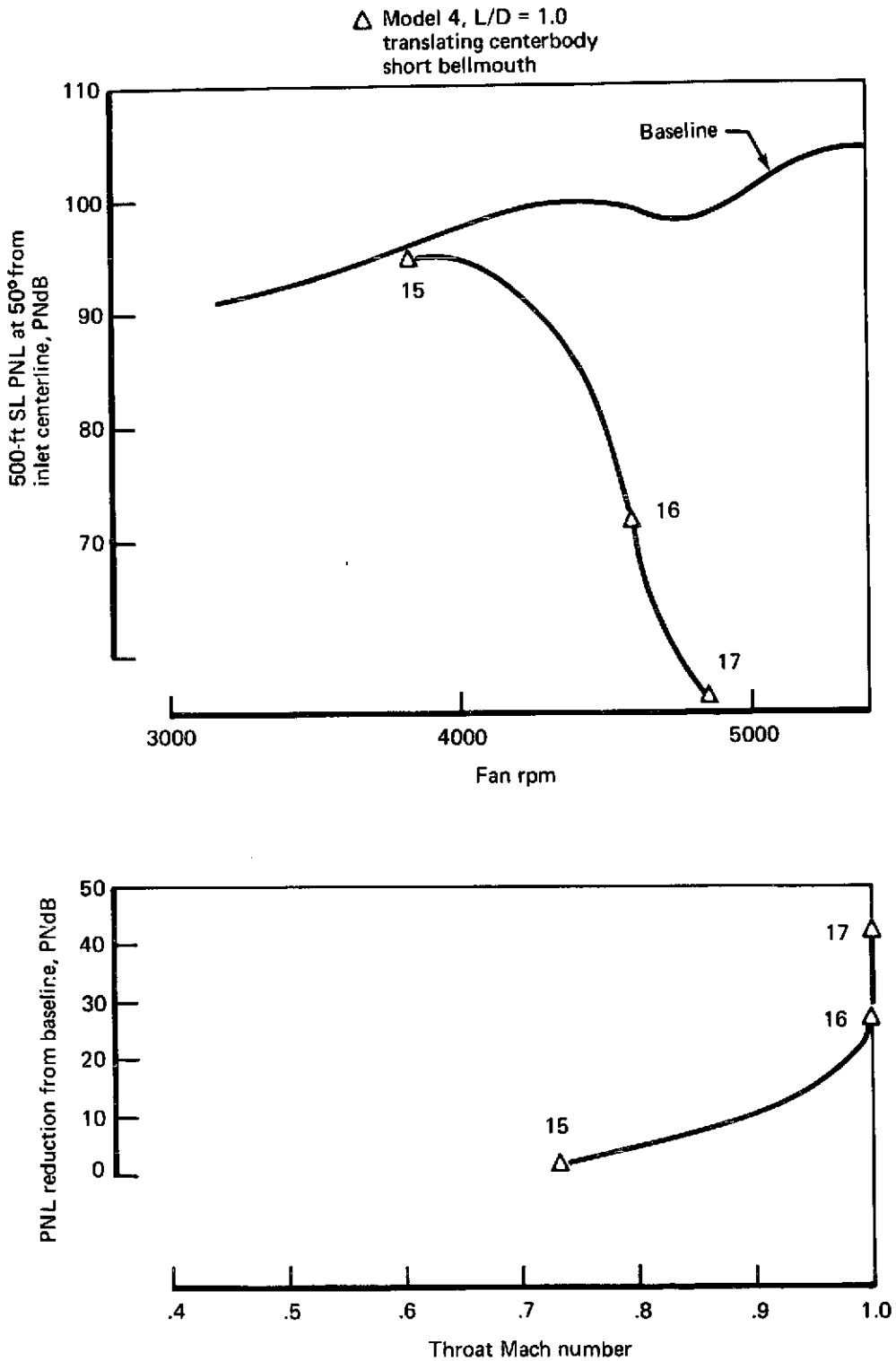


*FIGURE 98.–PNL VS FAN RPM AND PNL REDUCTION VS THROAT MACH NUMBER (APPROACH), SCALED-UP DATA–RUN 11, MODEL 4*

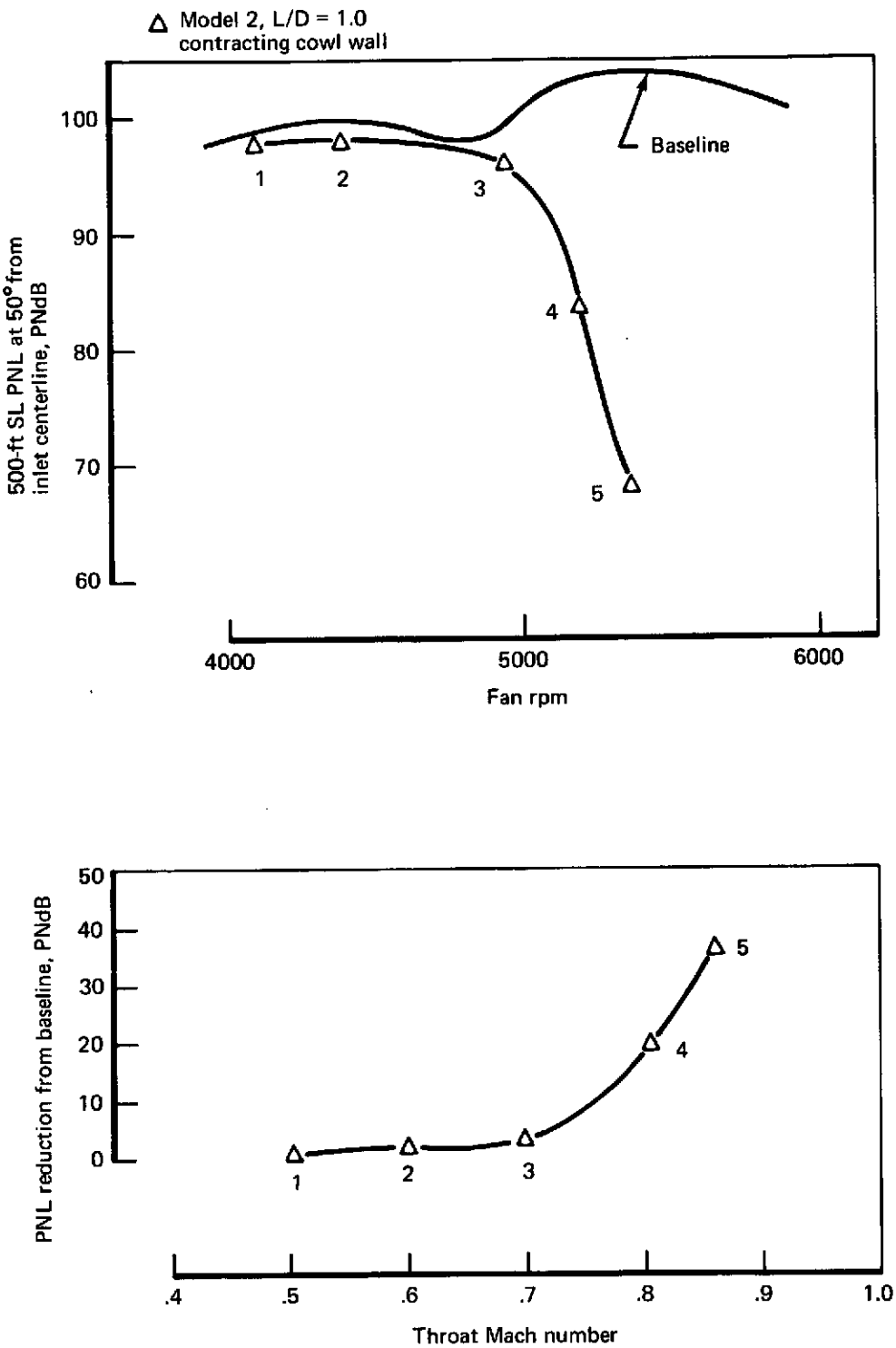


*FIGURE 99.—PNL VS FAN RPM AND PNL REDUCTION VS THROAT MACH NUMBER (TAKEOFF), SCALED-UP DATA—RUN 3, MODEL 2*

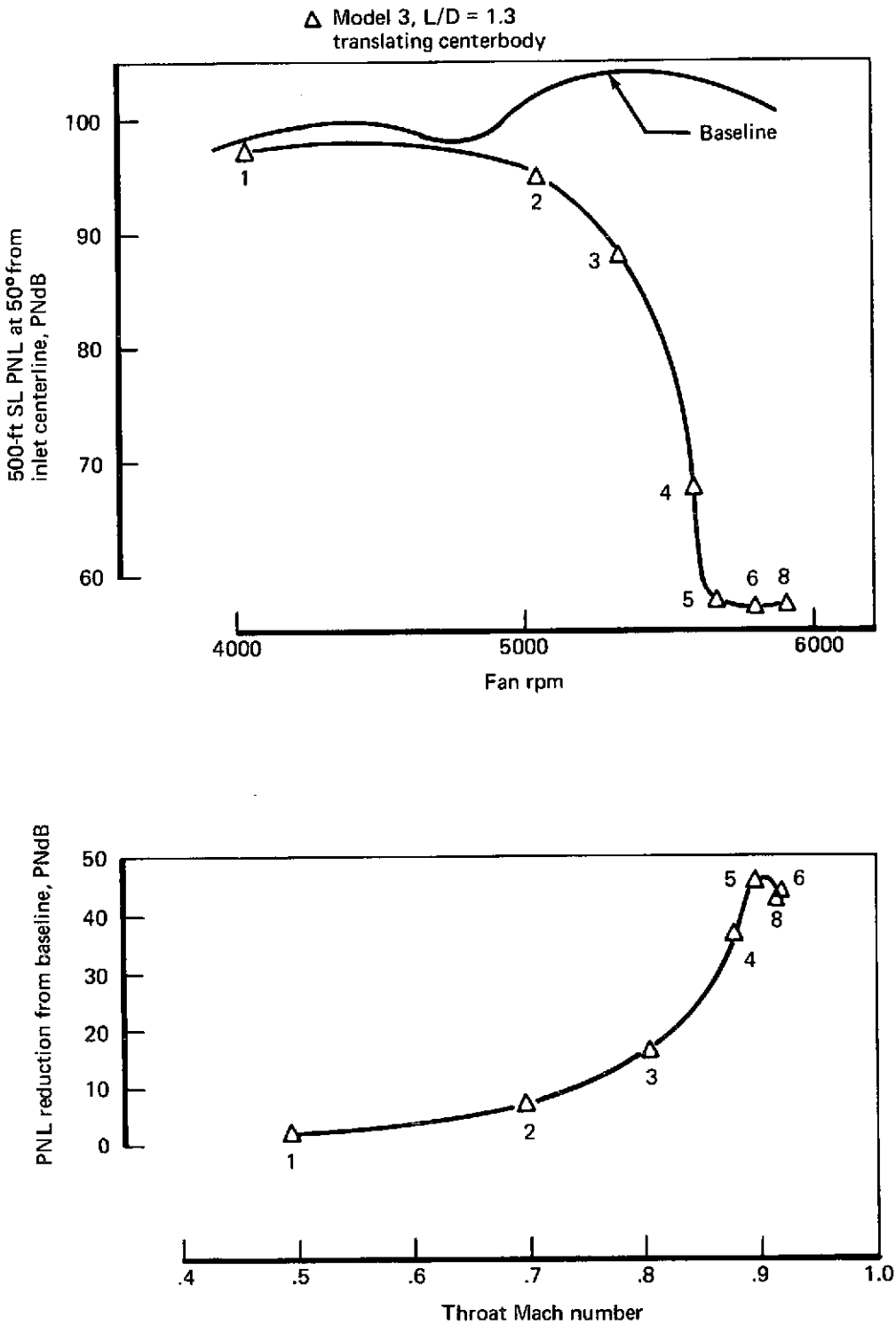


*FIGURE 100.–PNL VS FAN RPM AND PNL REDUCTION VS THROAT MACH NUMBER (TAKEOFF), SCALED-UP DATA–RUN 5, MODEL 3*

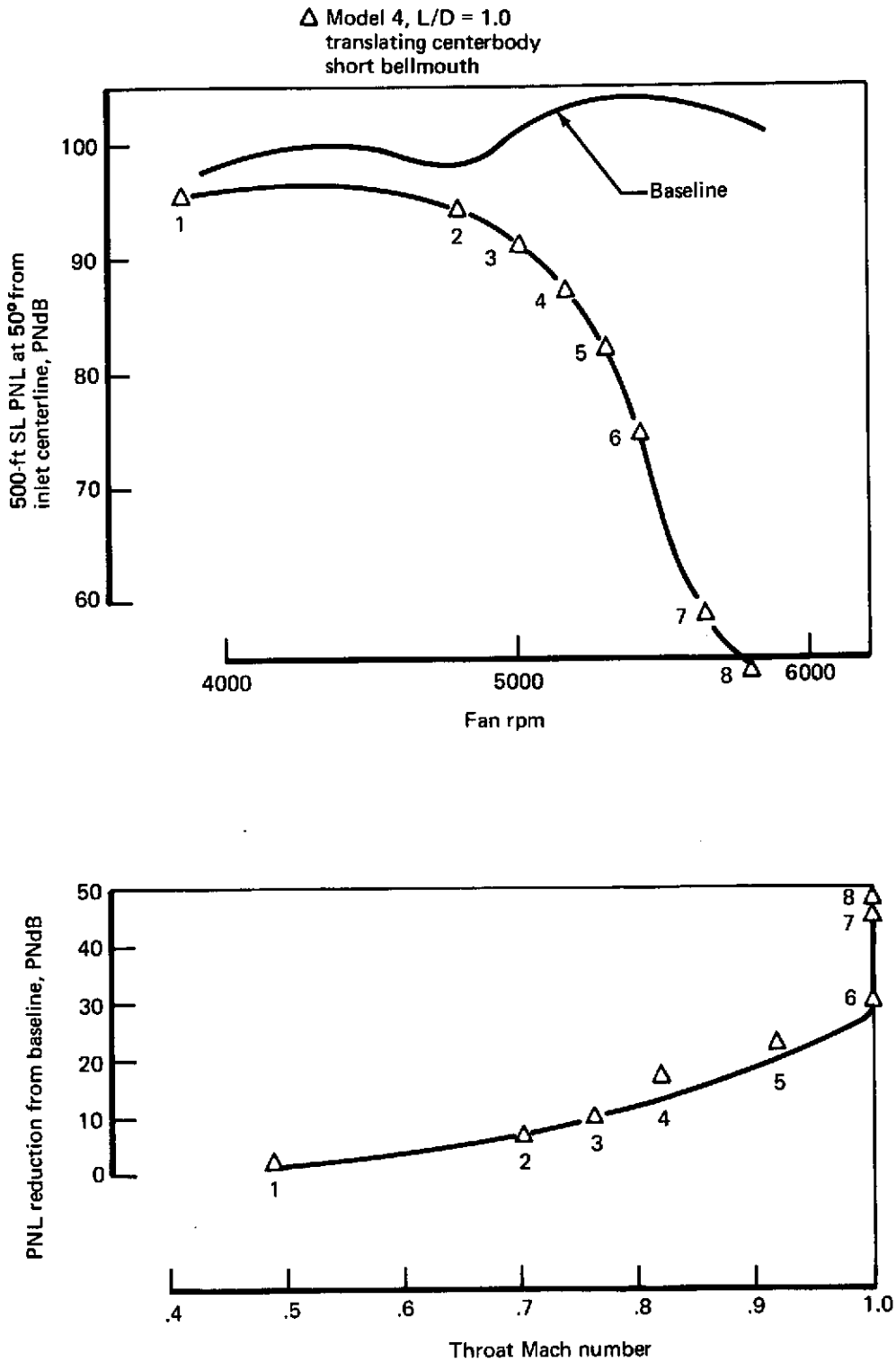


*FIGURE 101.—PNL VS FAN RPM AND PNL REDUCTION VS THROAT MACH NUMBER (TAKEOFF), SCALED-UP DATA—RUN 12, MODEL 4*

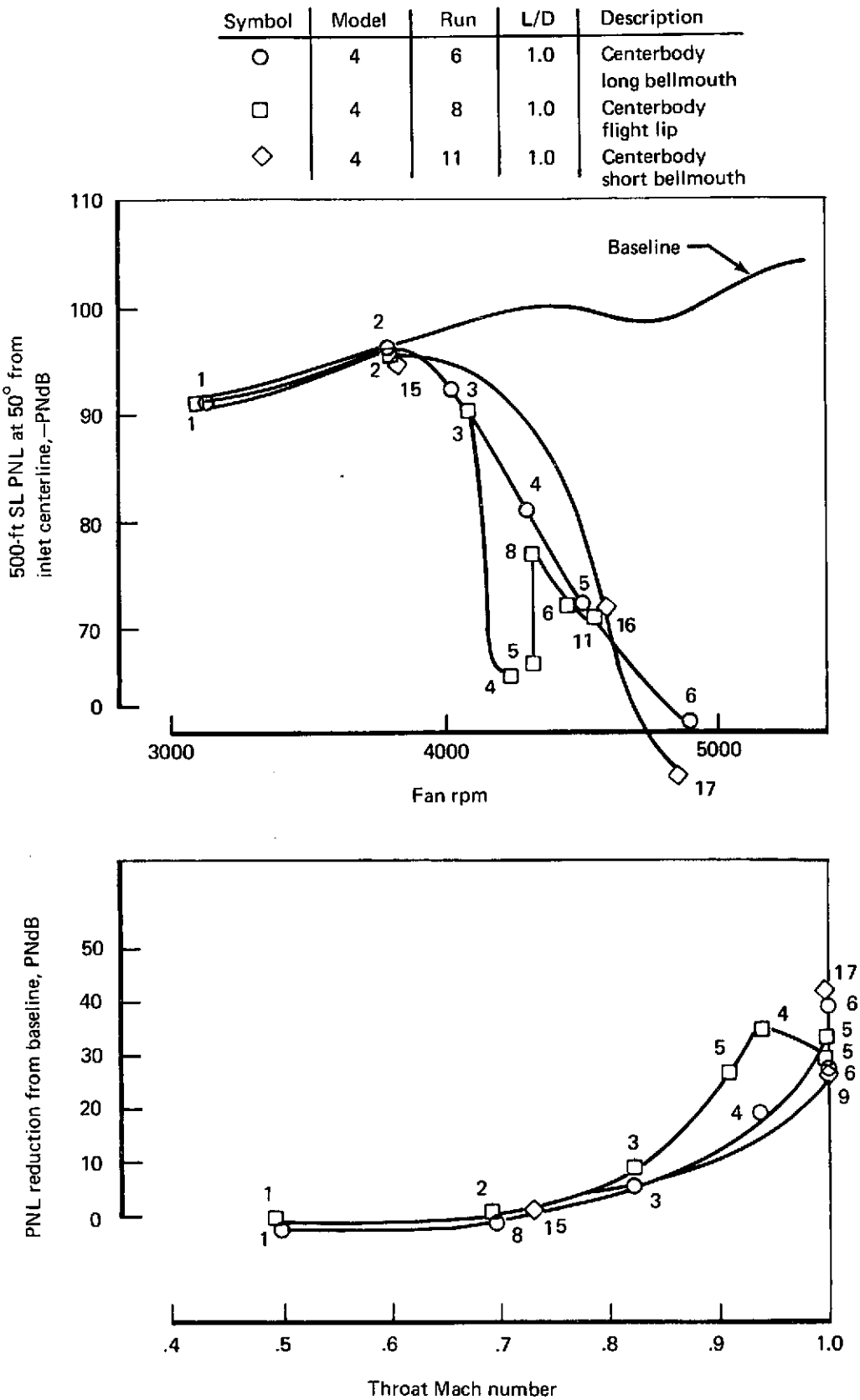


*FIGURE 102.—BELLMOUTH NOISE PERFORMANCE, SINGLE-PASSAGE INLETS—MODEL 4*

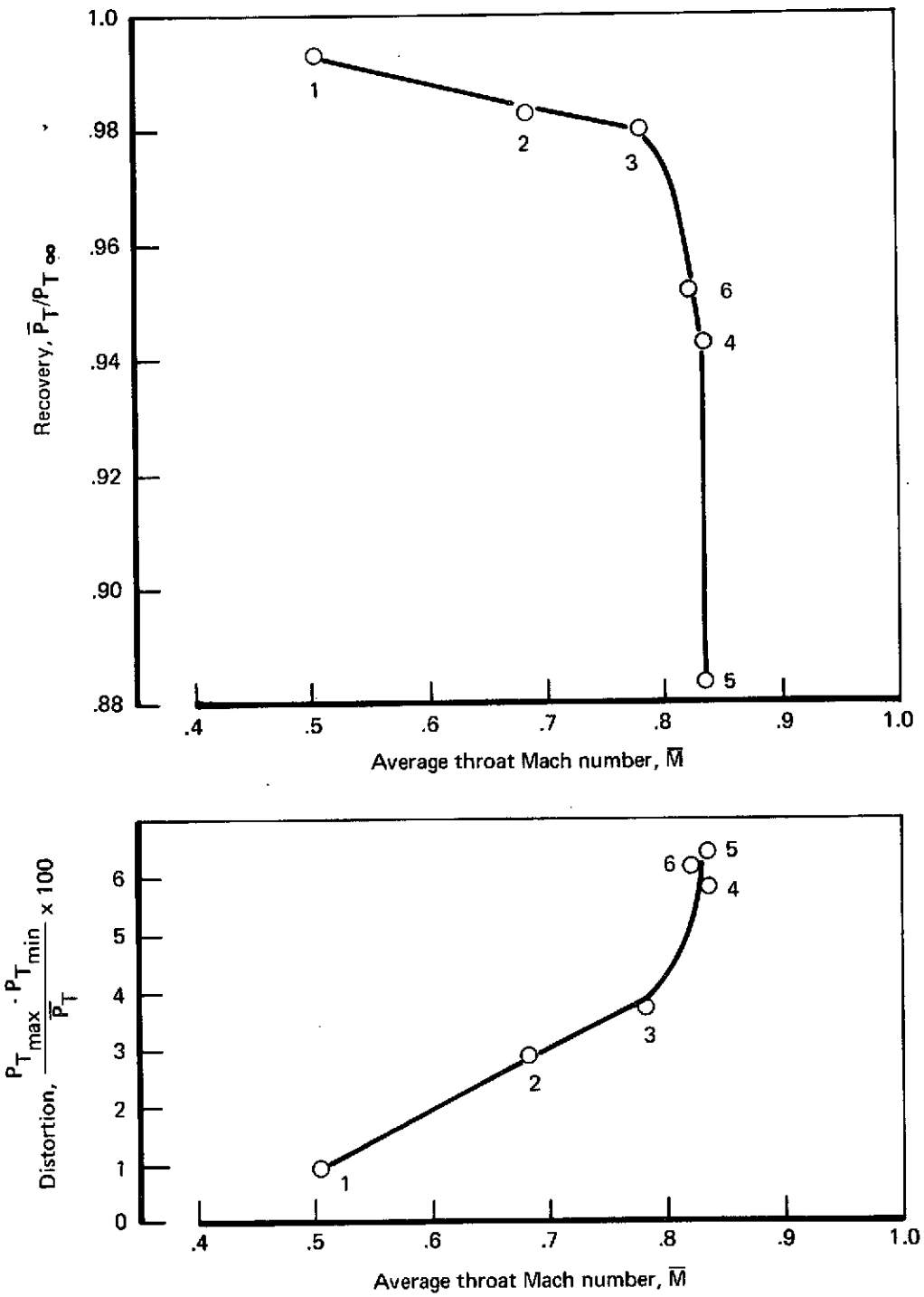


*FIGURE 103.—RECOVERY AND DISTORTION VS THROAT MACH NUMBER—RUN 7, MODEL 5A*

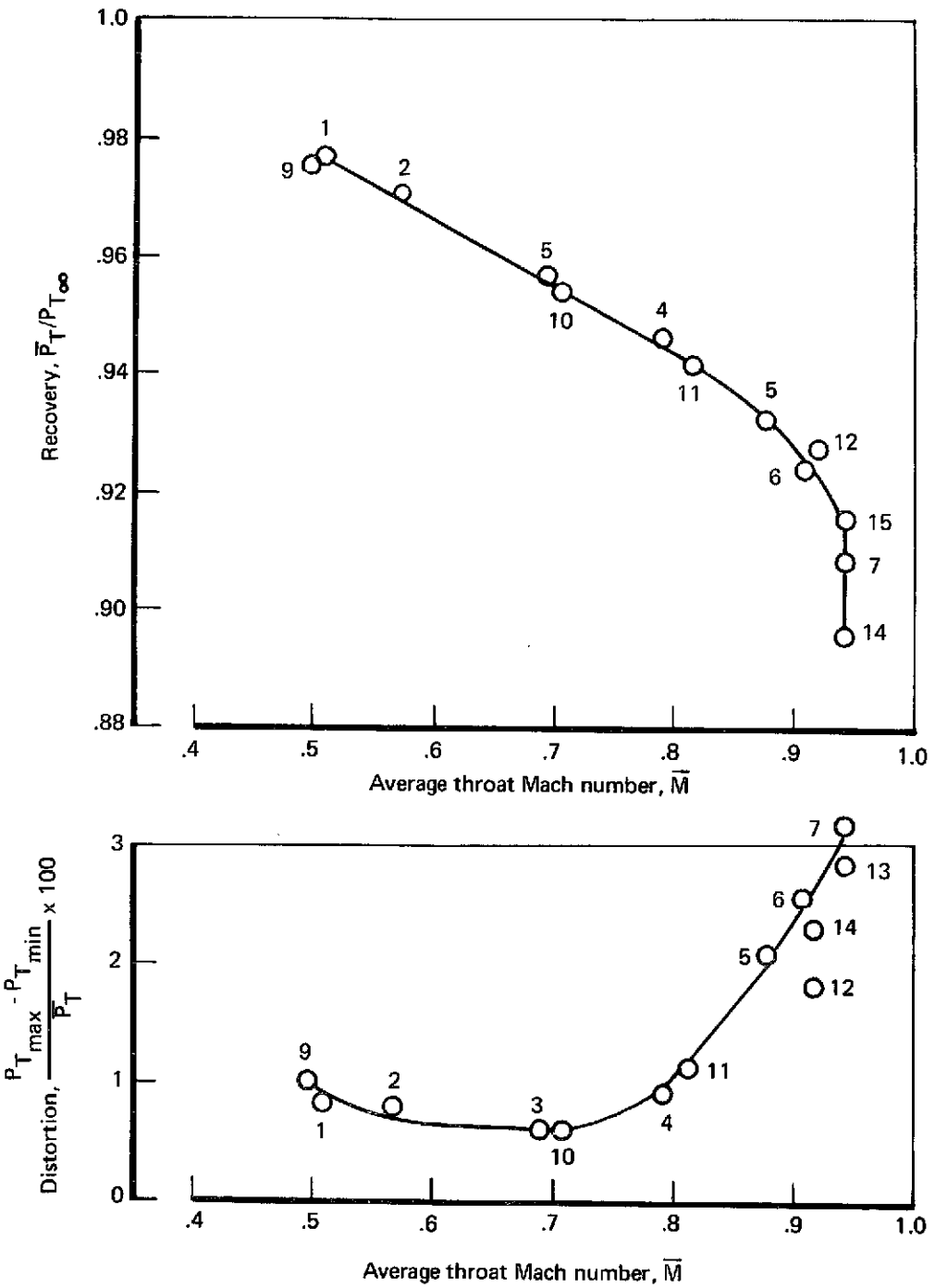


*FIGURE 104.—RECOVERY AND DISTORTION VS THROAT MACH NUMBER—RUN 9, MODEL 6*

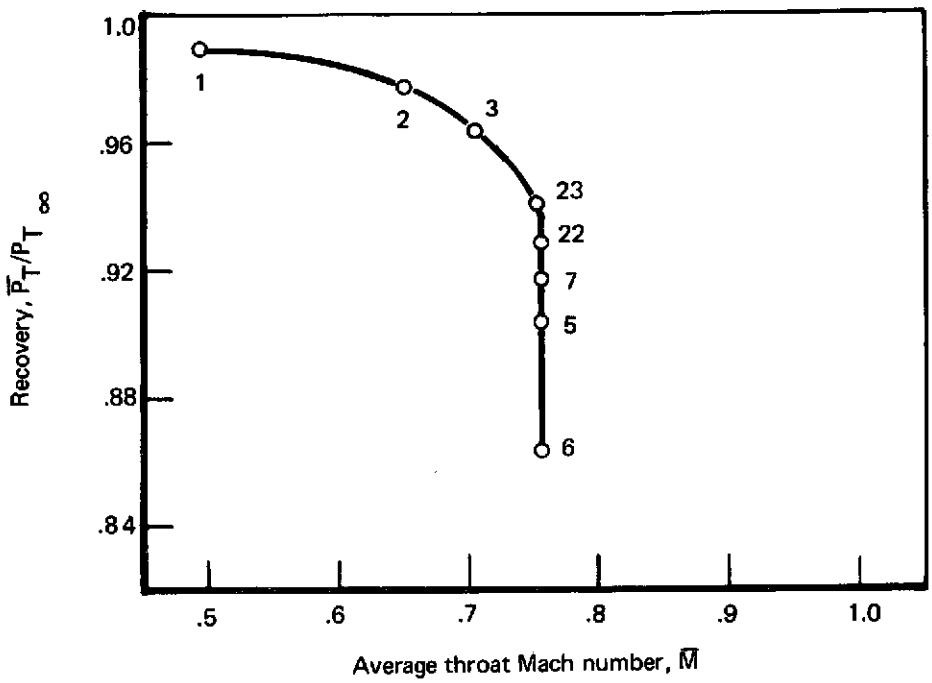


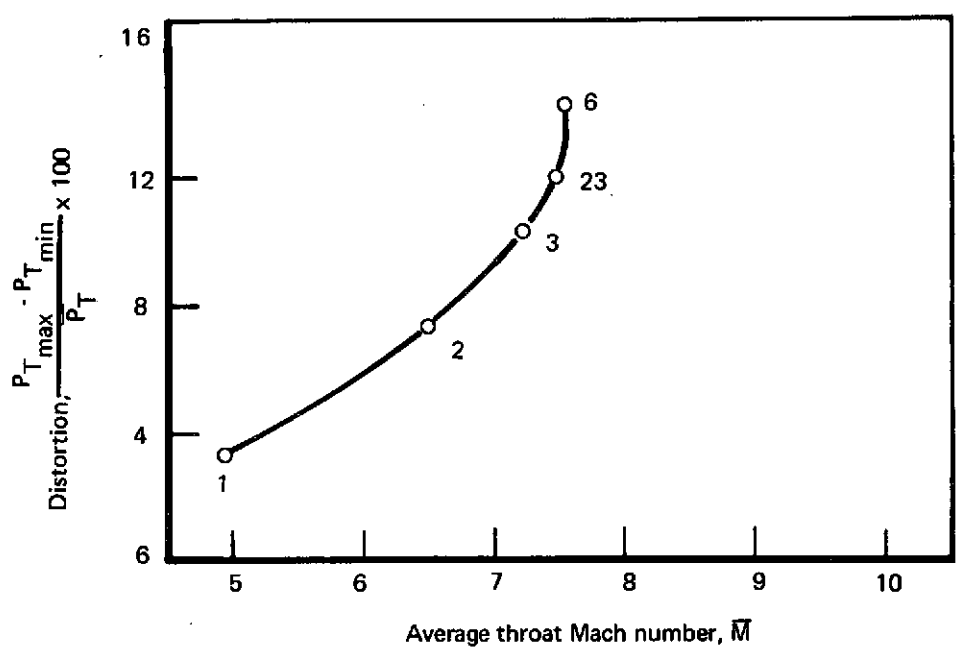


*FIGURE 105.–RECOVERY AND DISTORTION VS THROAT MACH NUMBER–RUN 13, MODEL 5B*

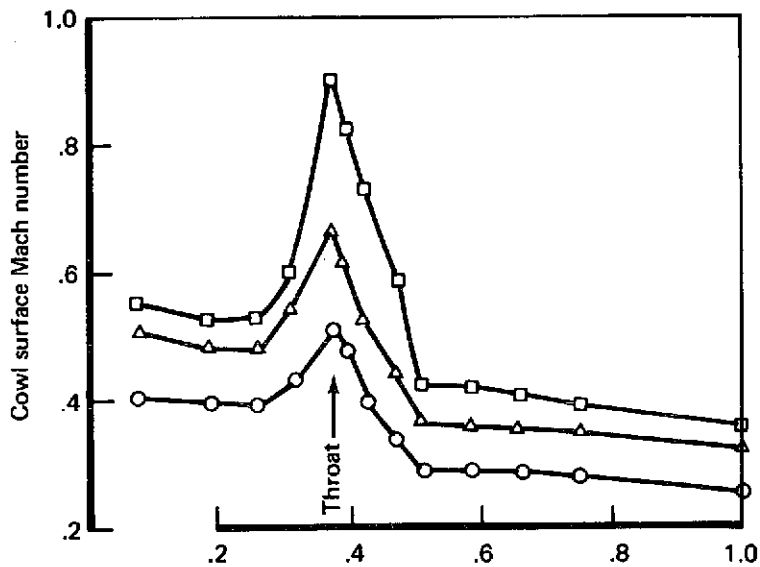


| Sym | Point no. | Rec | Dist | $\overline{M}_T$ | $M_T$ |
|---|---|---|---|---|---|
| ○ | 13.001 | 0.989 | 0.0344 | 0.530 | 0.490 |
| △ | 13.002 | 0.978 | 0.0725 | 0.735 | 0.650 |
| □ | 13.022 | 0.929 | 0.1313 | 1.00 | 0.755 |

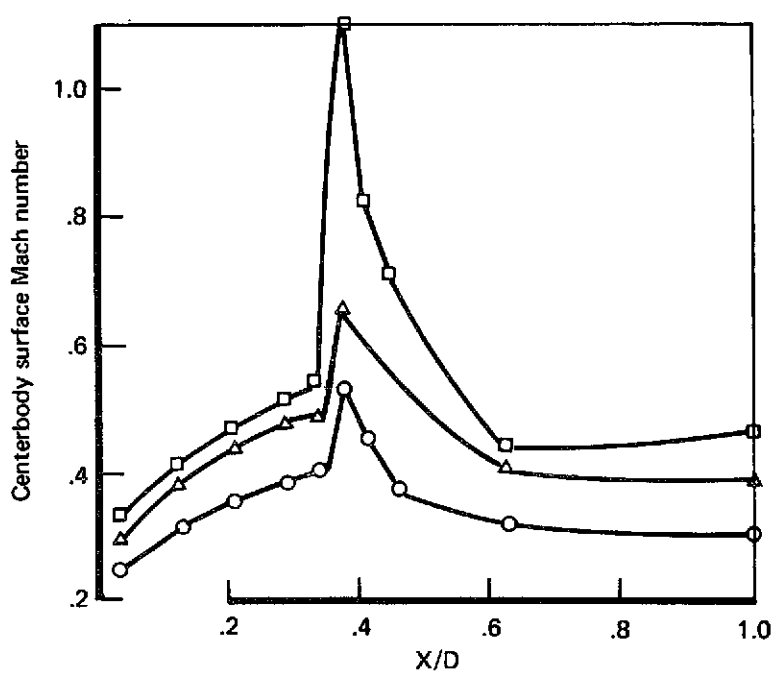


*FIGURE 106.—MODEL SURFACE MACH NUMBER DISTRIBUTION—RUN 13, MODEL 5B*

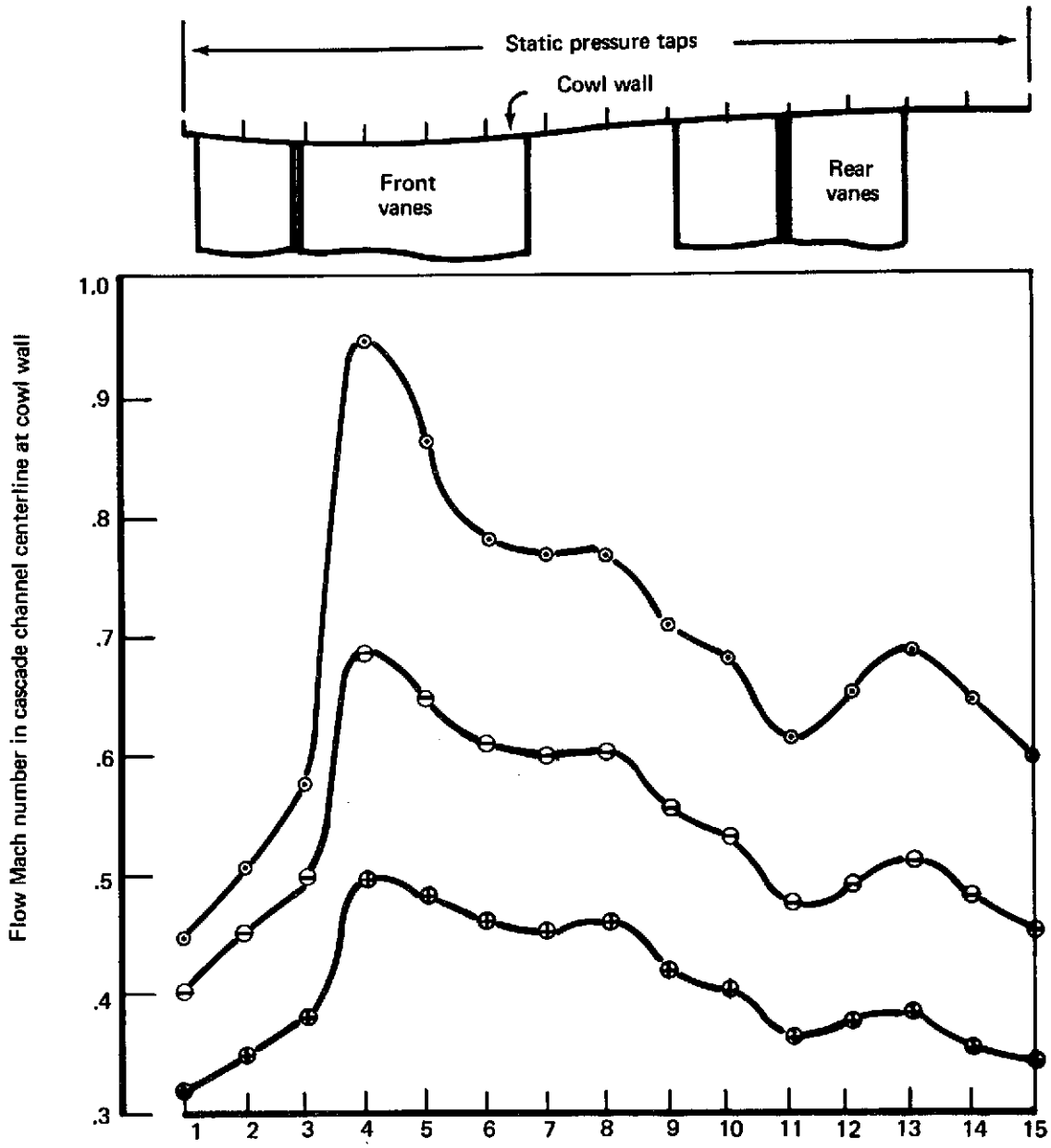


| Sym | Condition | $\overline{M}_T$ |
|---|---|---|
| ⊖ | 9.003 | 0.691 |
| ⊕ | 9.009 | 0.498 |
| ⊙ | 9.013 | 0.942 |

*FIGURE 107.—DOUBLE-ARTICULATED VANE INLET CASCADE CHANNEL FLOW—RUN 9, MODEL 6*

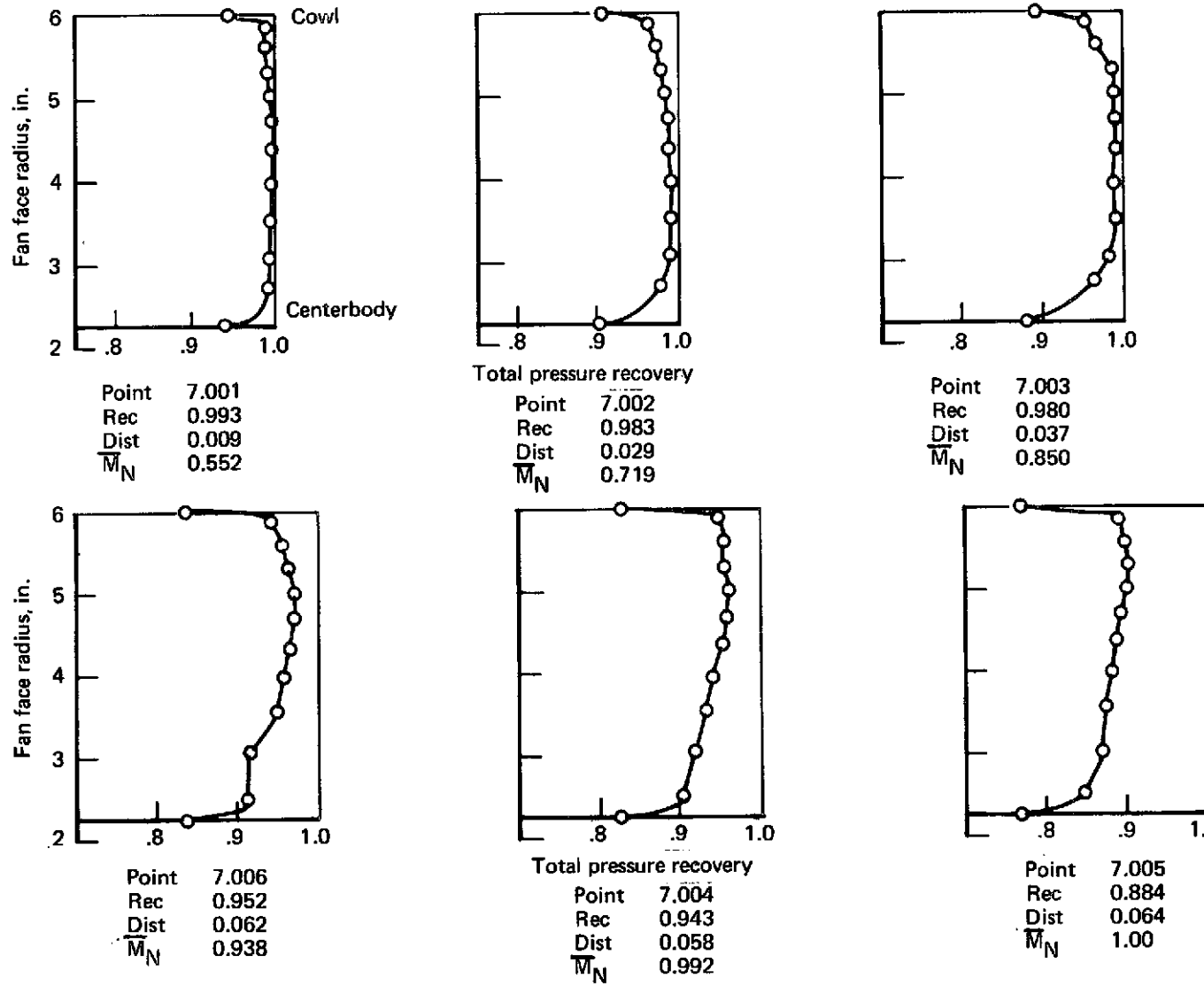


*FIGURE 108.–RECOVERY PROFILES–RUN 7, MODEL 5A*

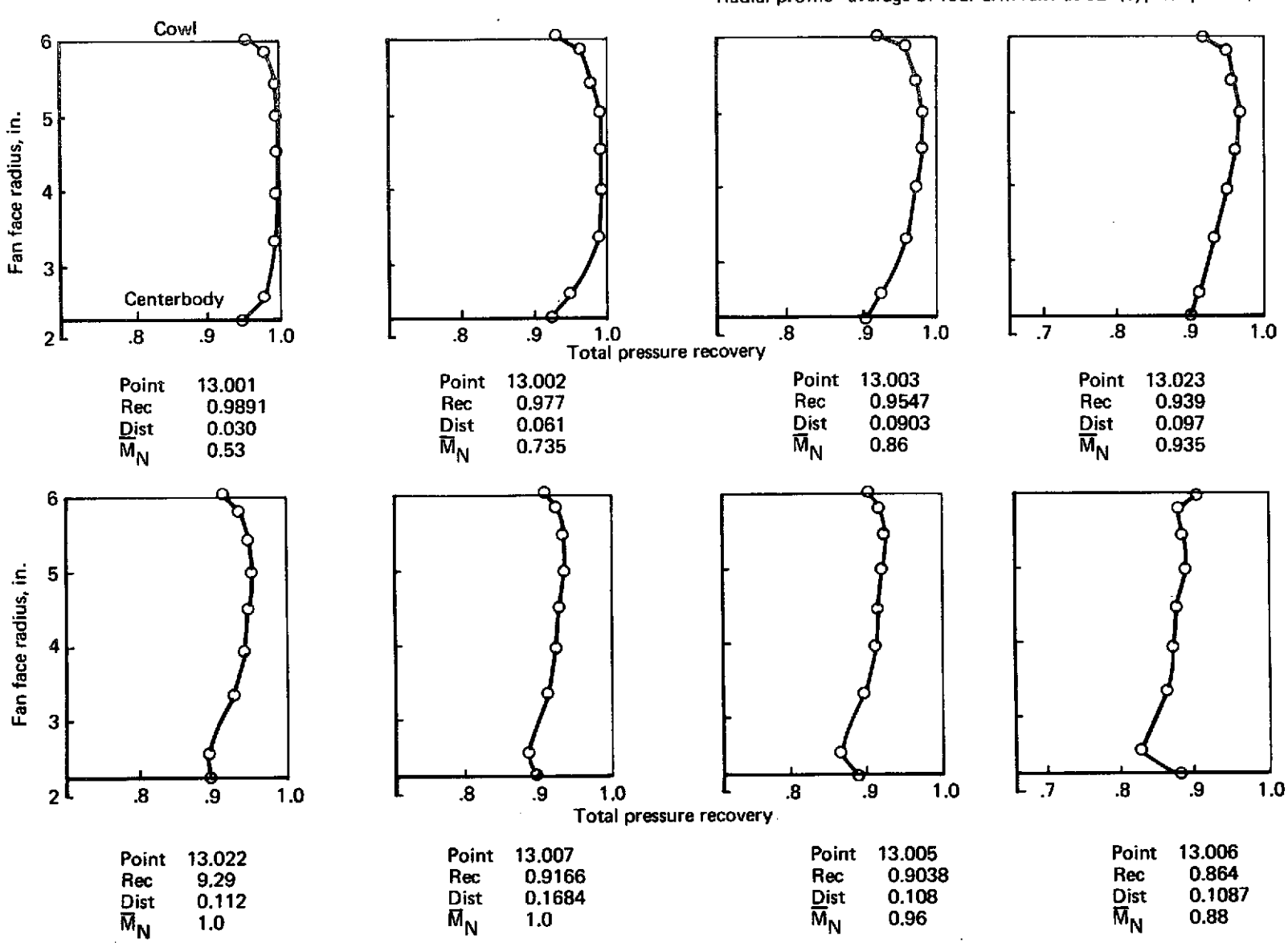


*FIGURE 109.—RECOVERY PROFILES—RUN 13, MODEL 5B*

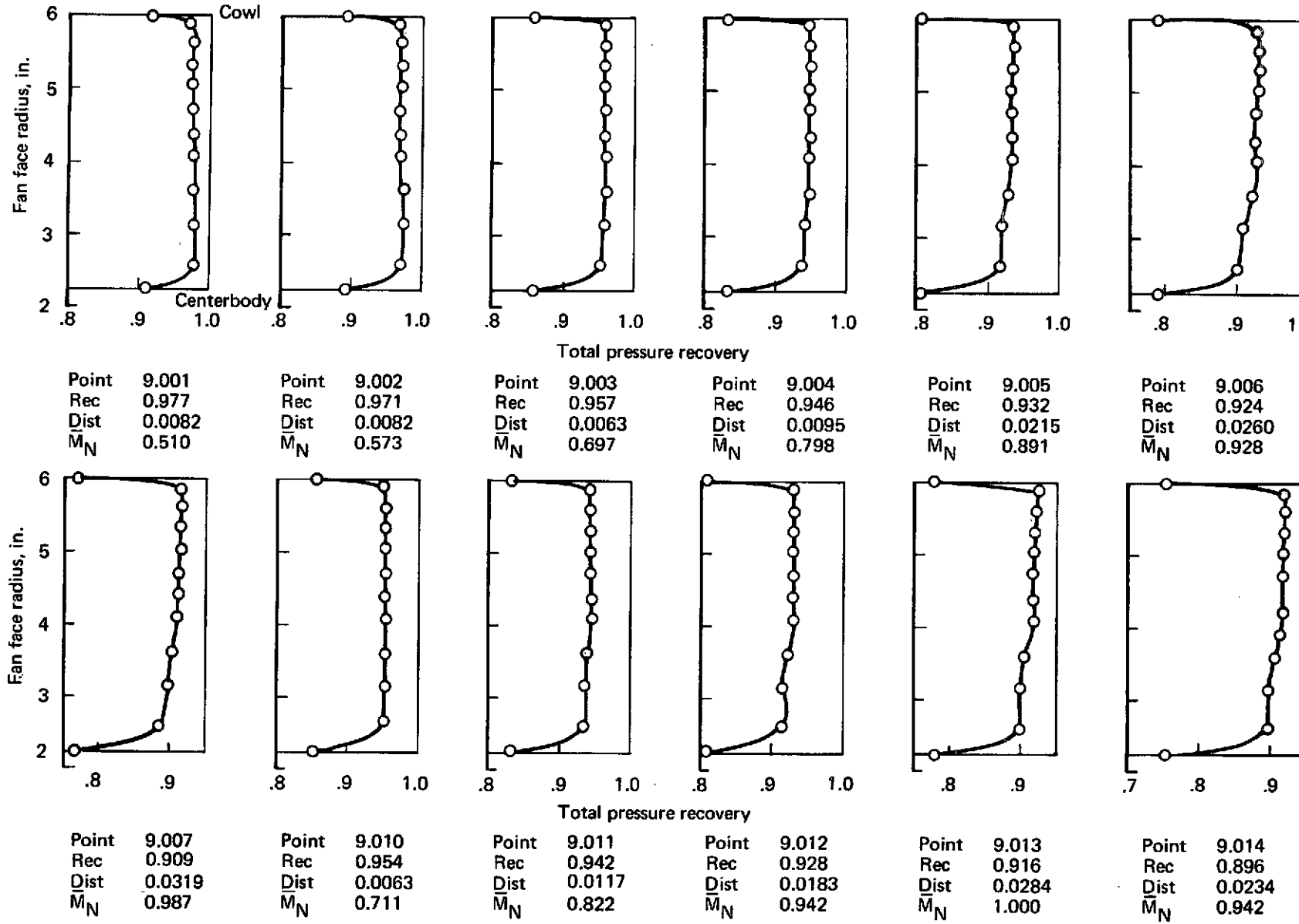


*FIGURE 110.–RECOVERY PROFILES–RUN 9, MODEL 6*

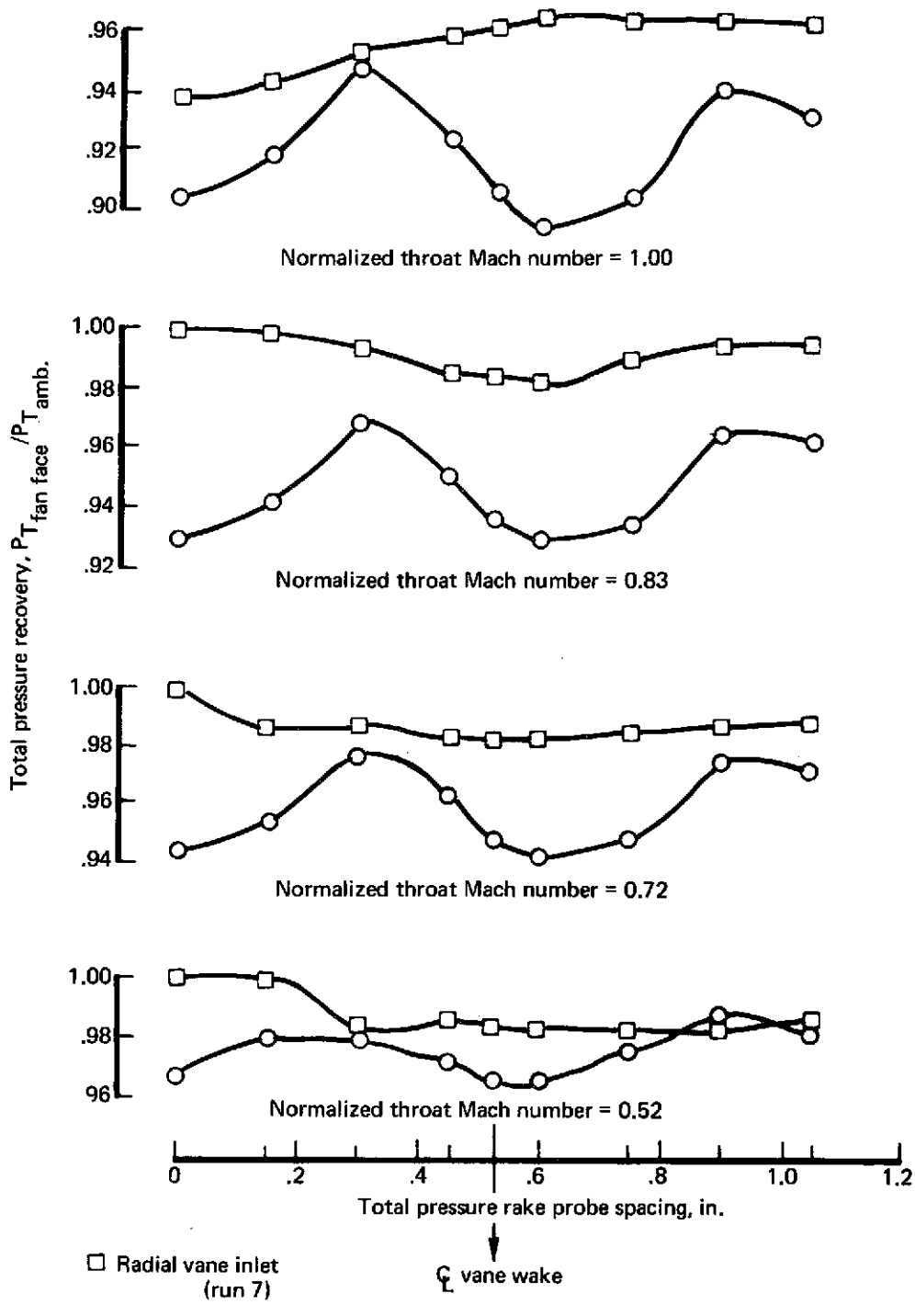


Note: Each profile is for the radius with greatest distortion for the given condition

*FIGURE 111.–MULTIPASSAGE INLETS–VANE WAKE TOTAL PRESSURE PROFILES*

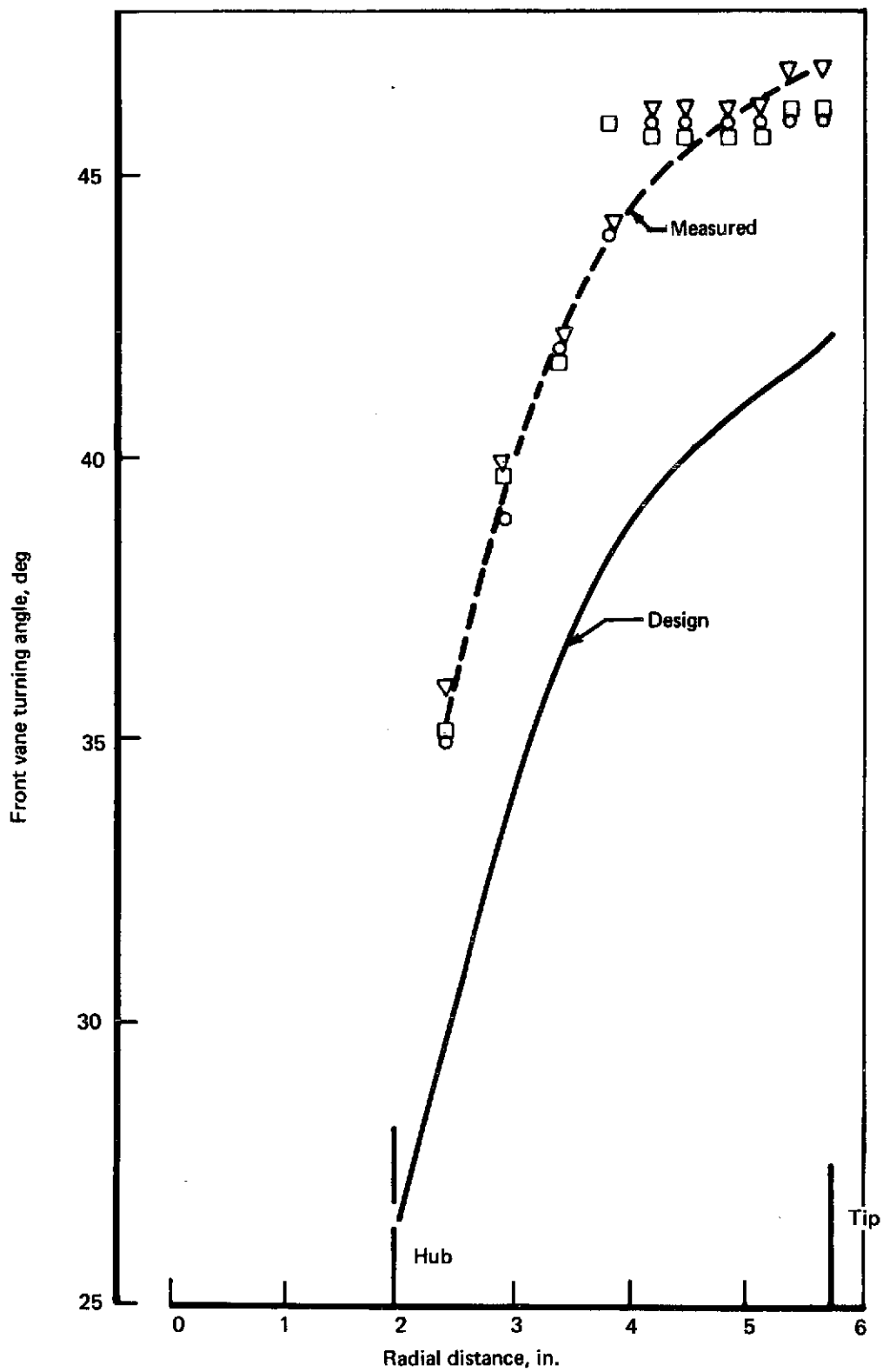


*FIGURE 112.–DOUBLE-ARTICULATED VANE INLET–FRONT VANE TURNING ANGLE DISTRIBUTION*

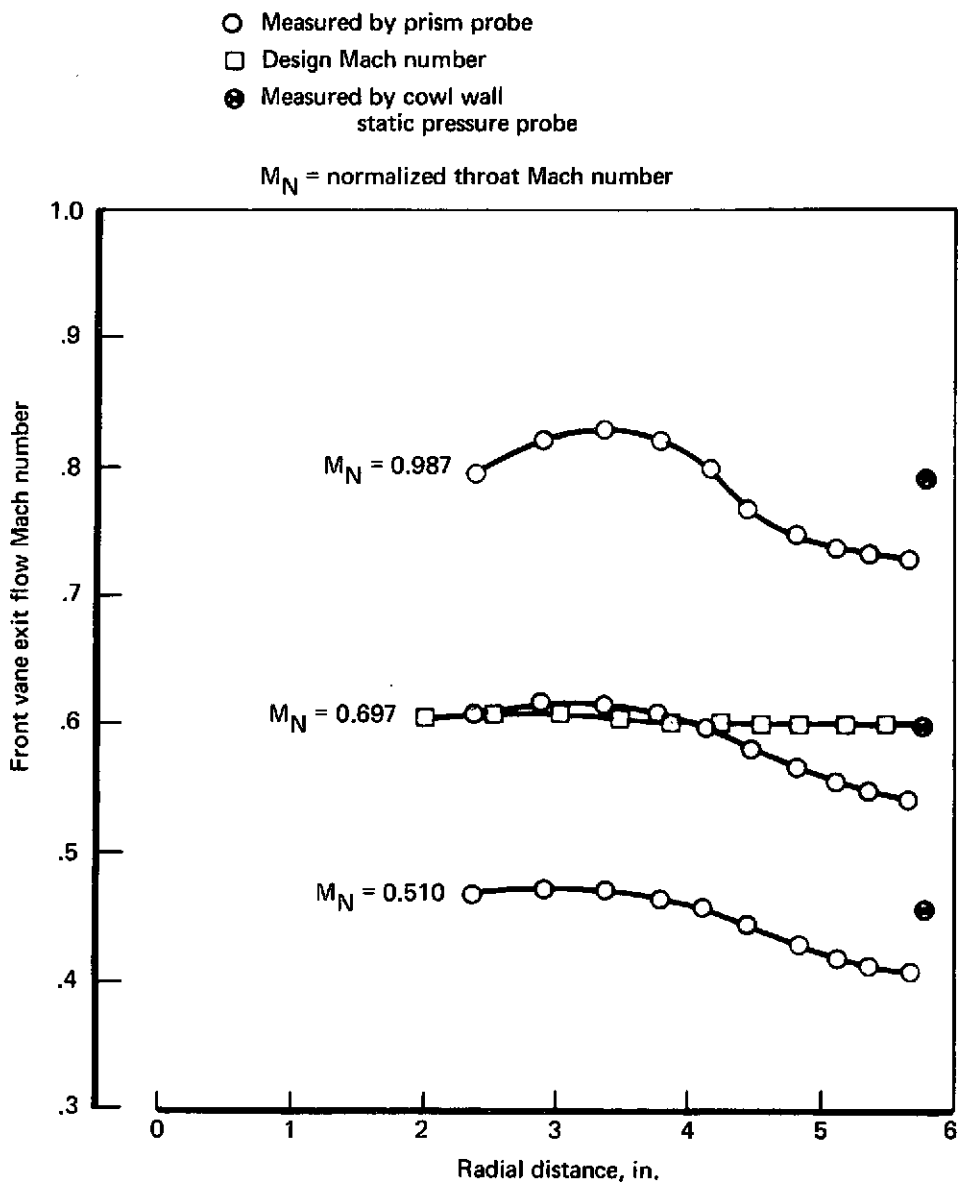


*FIGURE 113.–DOUBLE-ARTICULATED VANE INLET–FRONT VANE EXIT FLOW MACH NUMBER DISTRIBUTION*

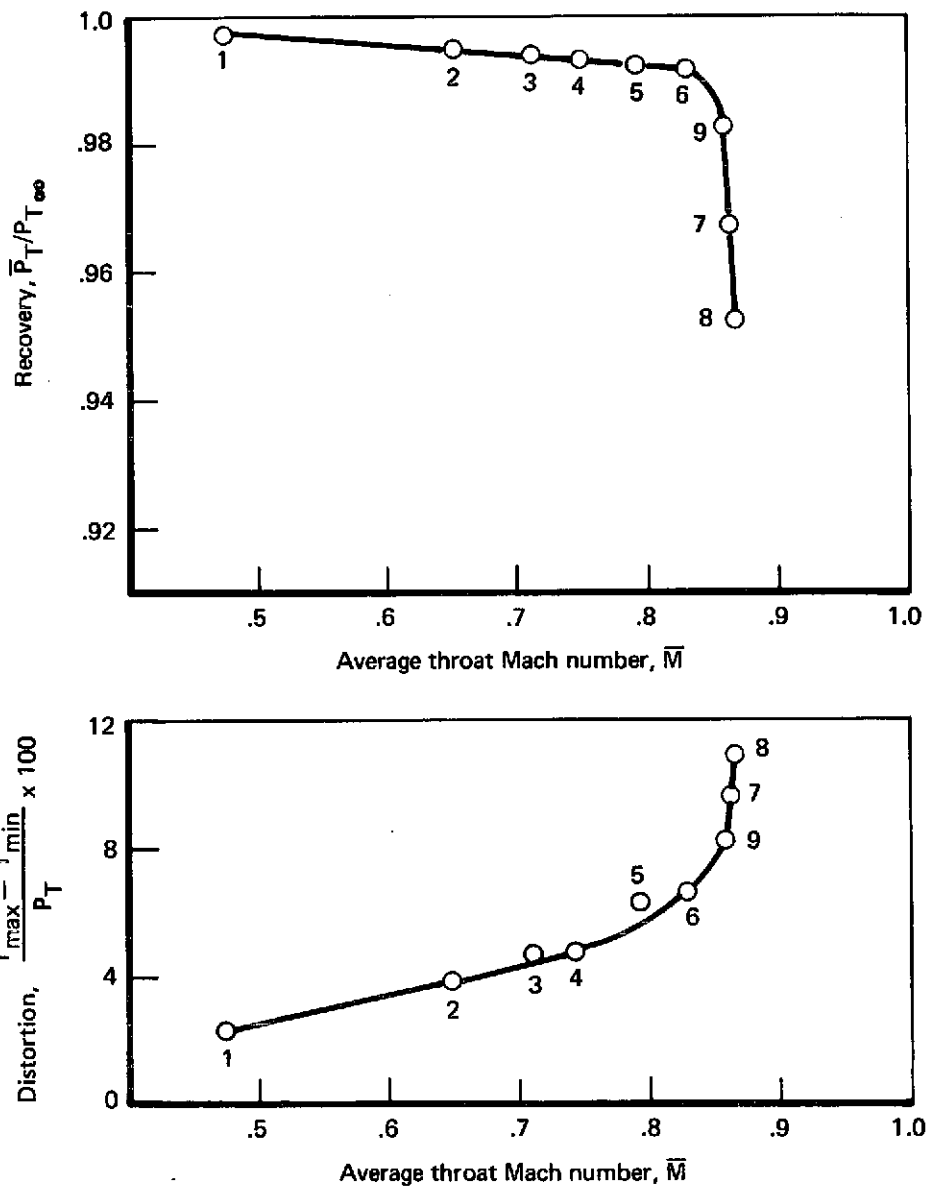


*FIGURE 114.–RECOVERY AND DISTORTION VS THROAT MACH NUMBER–RUN 14, MODEL 5B*

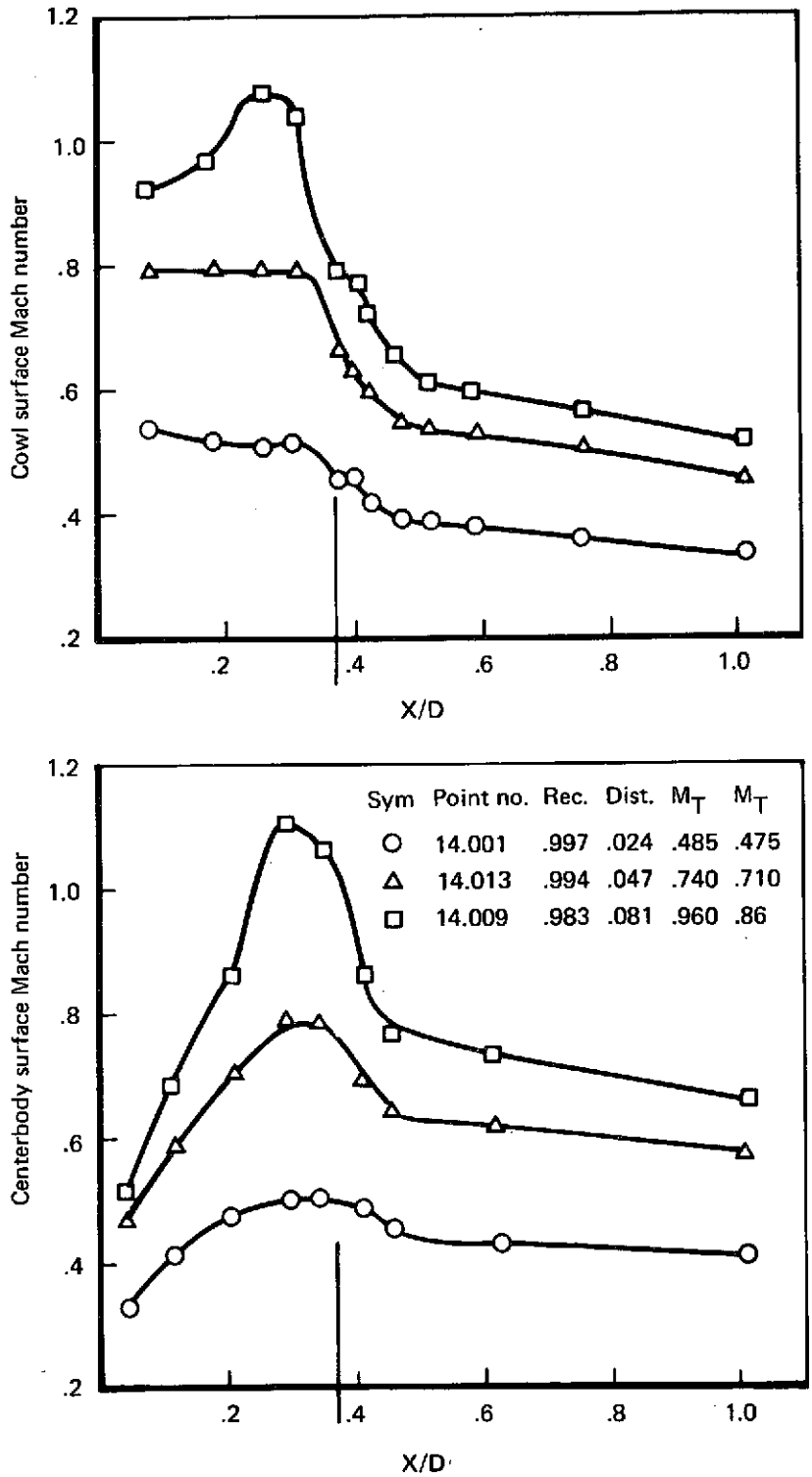


*FIGURE 115.–MODEL SURFACE MACH NUMBER DISTRIBUTION–RUN 14, MODEL 5B*

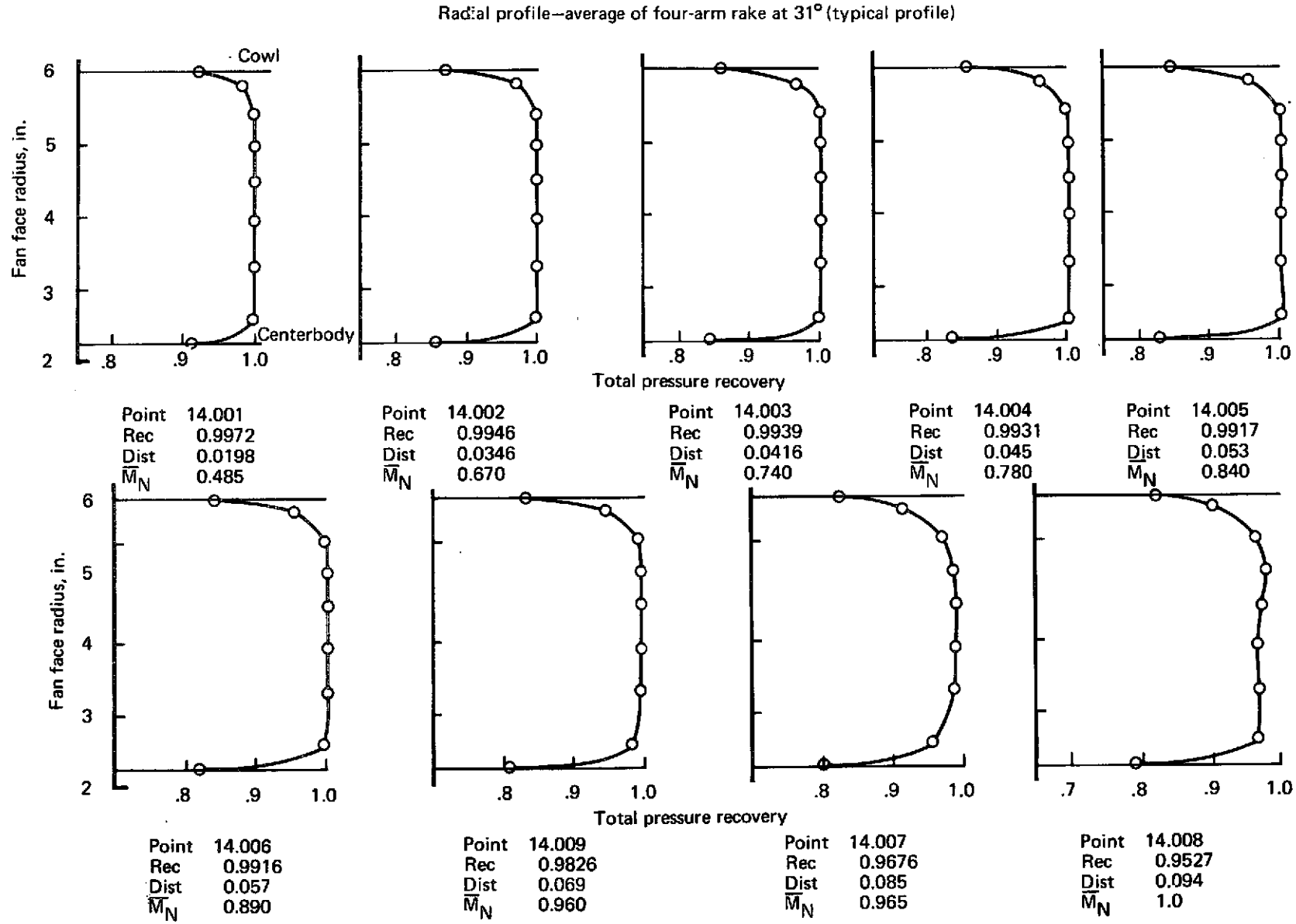


*FIGURE 116.—RECOVERY PROFILES—RUN 14, MODEL 5B*

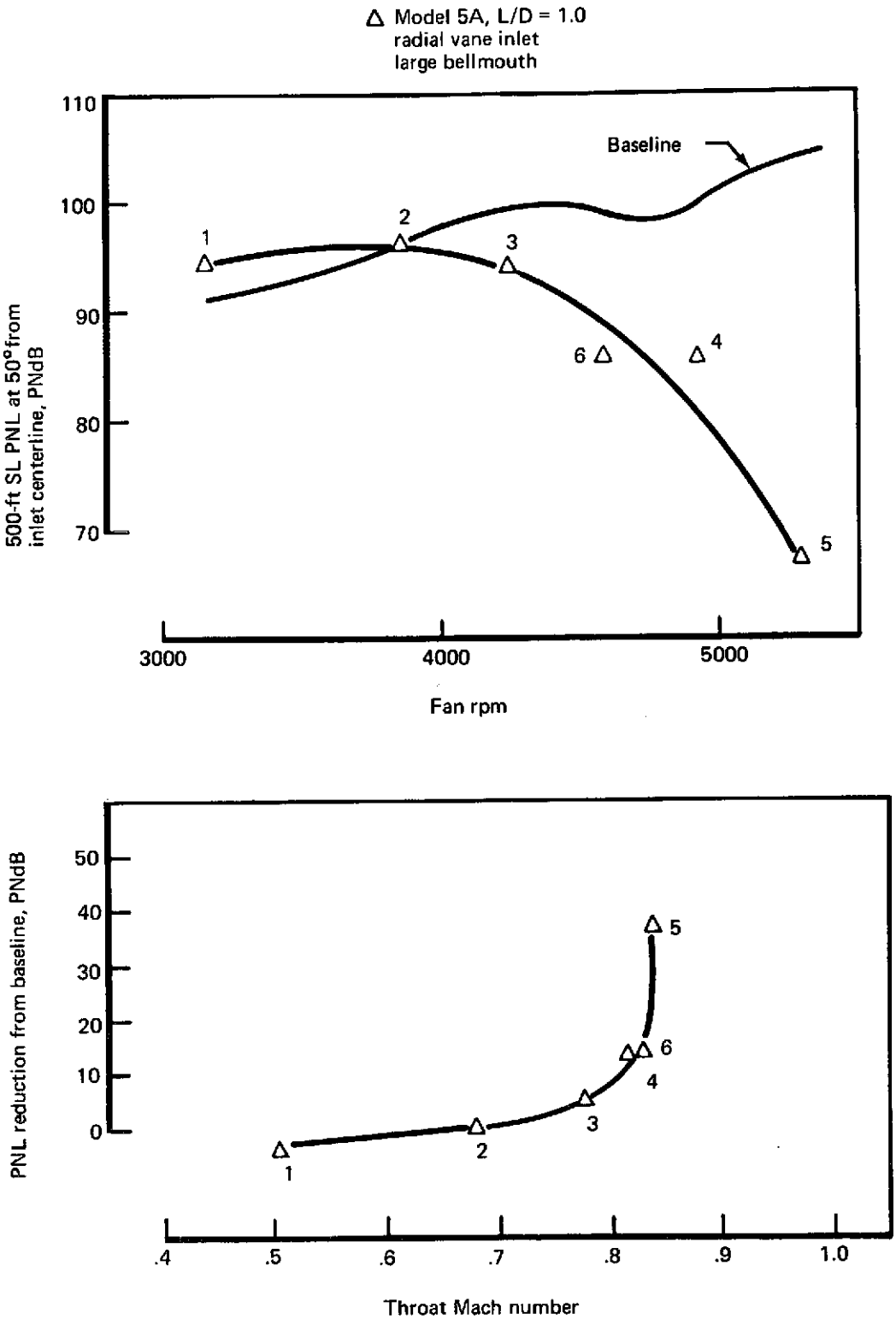


*FIGURE 117.–PNL VS FAN RPM AND PNL REDUCTION VS THROAT MACH NUMBER (APPROACH), SCALED-UP DATA–RUN 7, MODEL 5A*

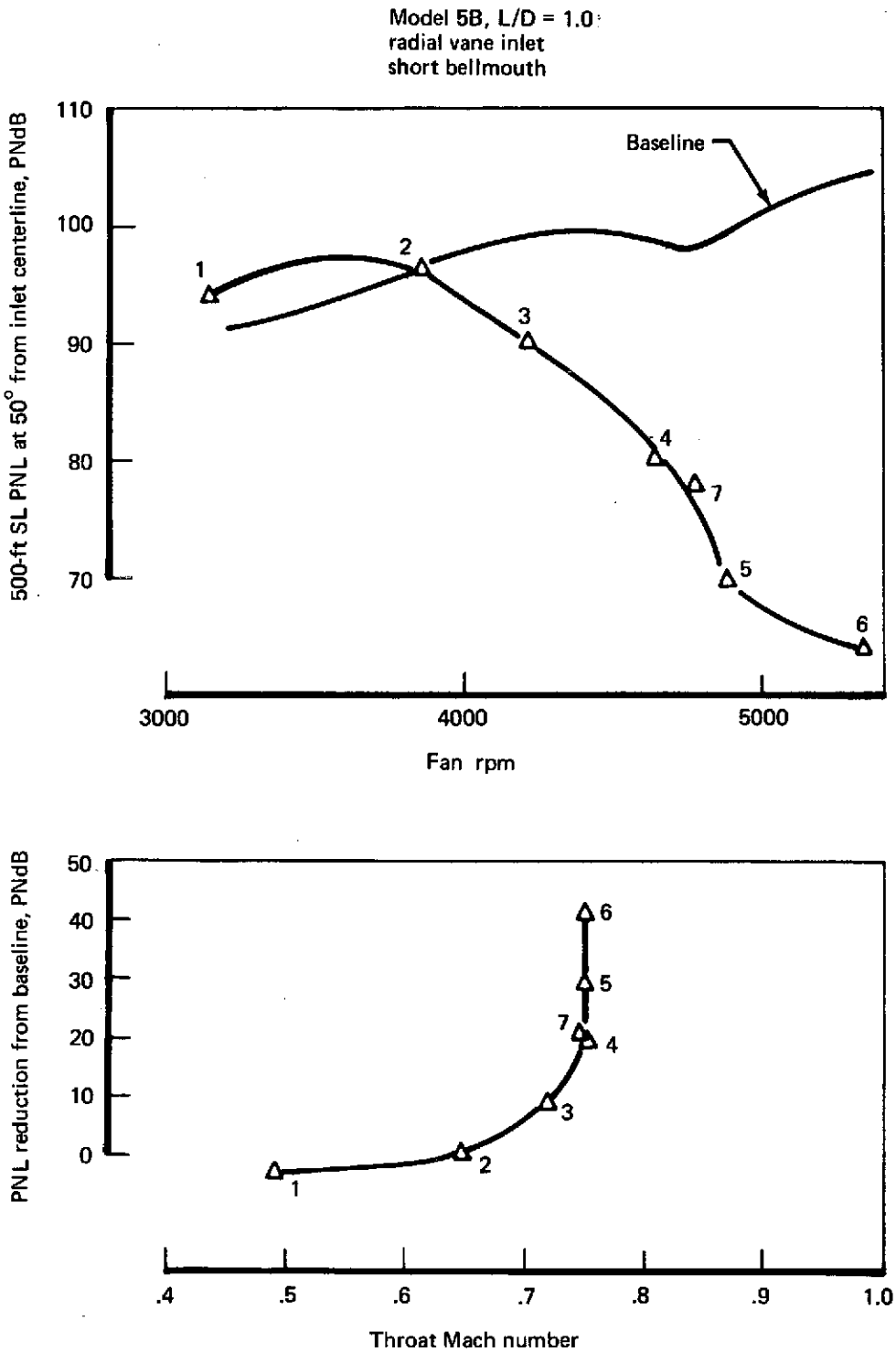


*FIGURE 118.–PNL VS FAN RPM AND PNL REDUCTION VS THROAT MACH NUMBER (APPROACH), SCALED-UP DATA–RUN 13, MODEL 5B*

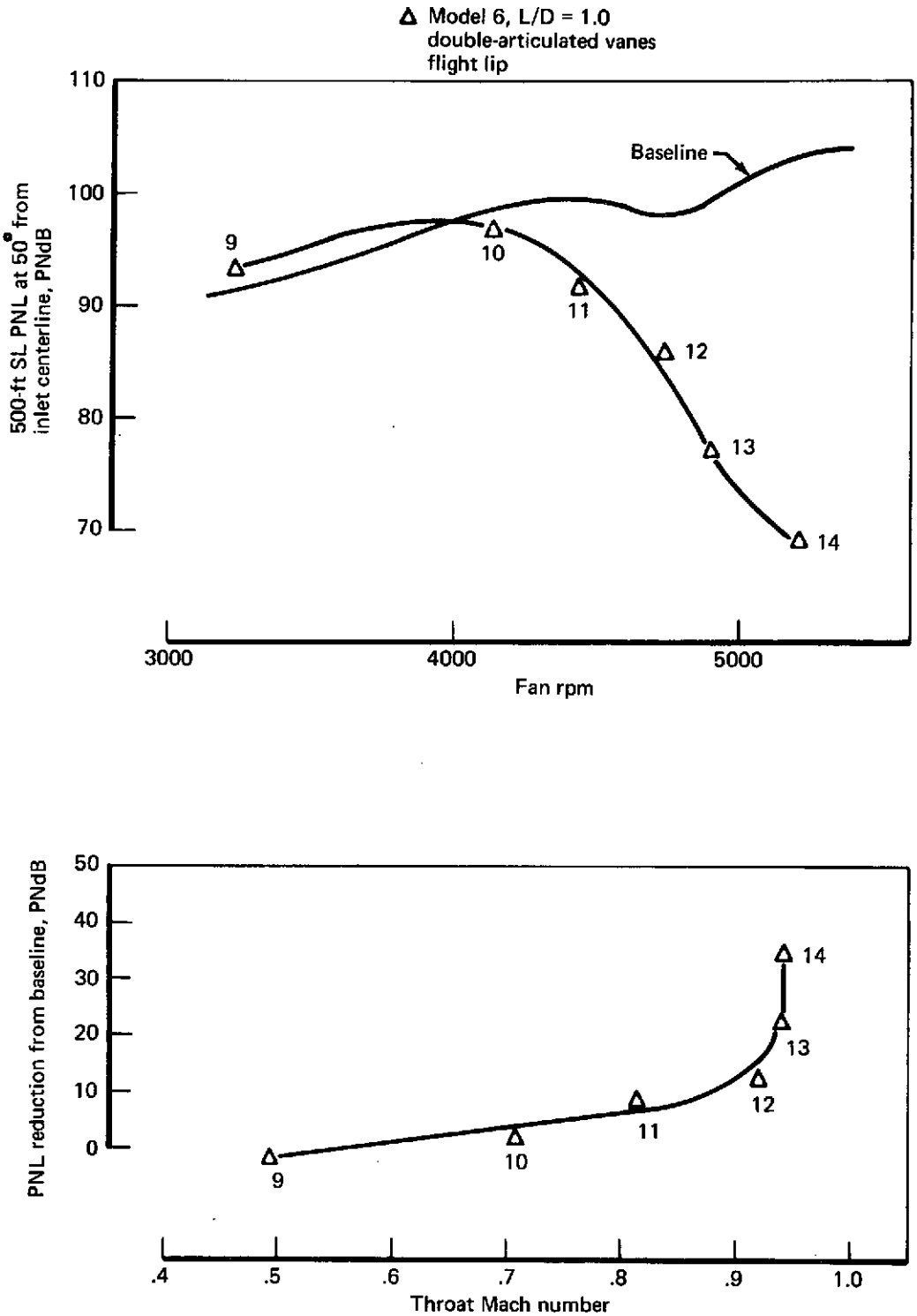


*FIGURE 119.—PNL VS FAN RPM AND PNL REDUCTION VS THROAT MACH NUMBER (APPROACH), SCALED-UP DATA—RUN 9, MODEL 6*

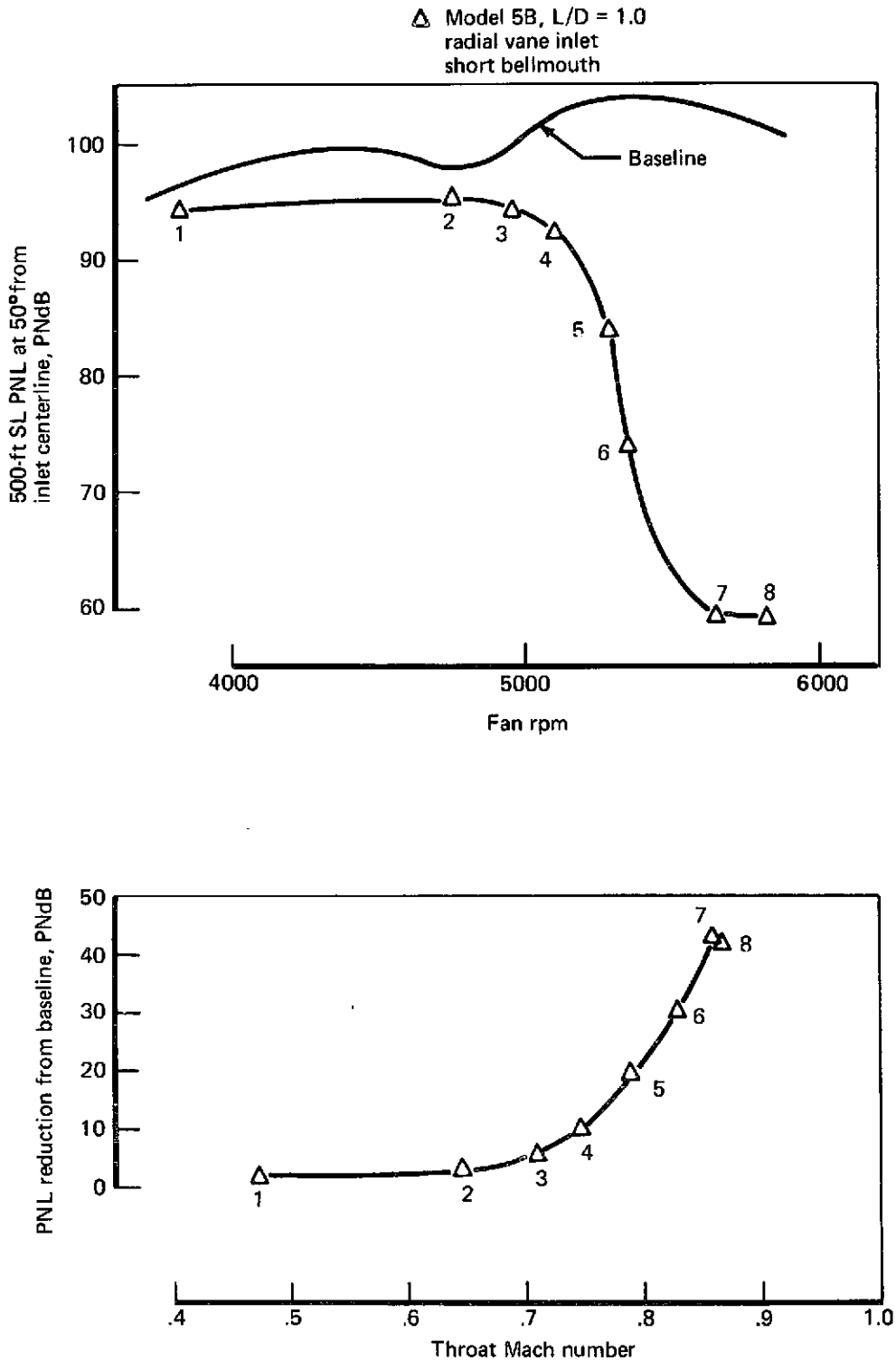


*FIGURE 120.—PNL VS FAN RPM AND PNL REDUCTION VS THROAT MACH NUMBER (TAKEOFF), SCALED-UP DATA—RUN 14, MODEL 5B*

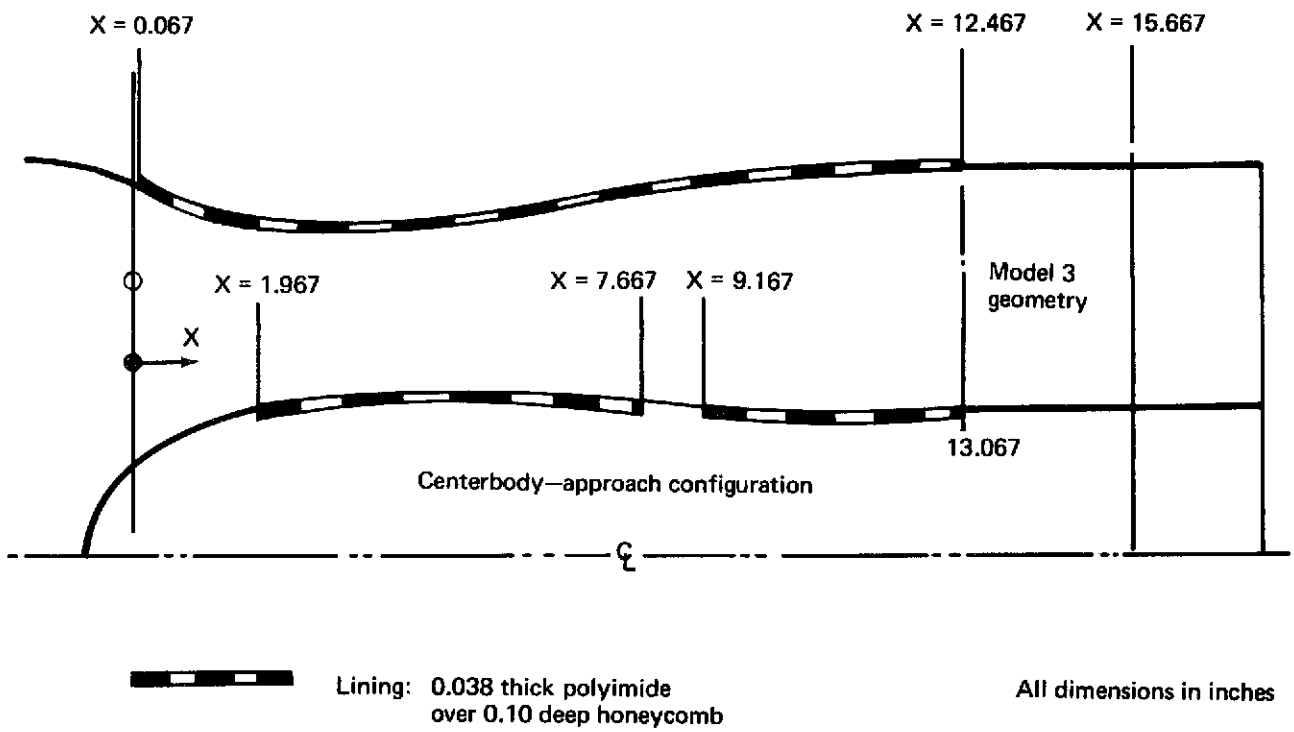


*FIGURE 121.—ACOUSTIC LINING DETAILS—MODEL 3A, L/D = 1.3*

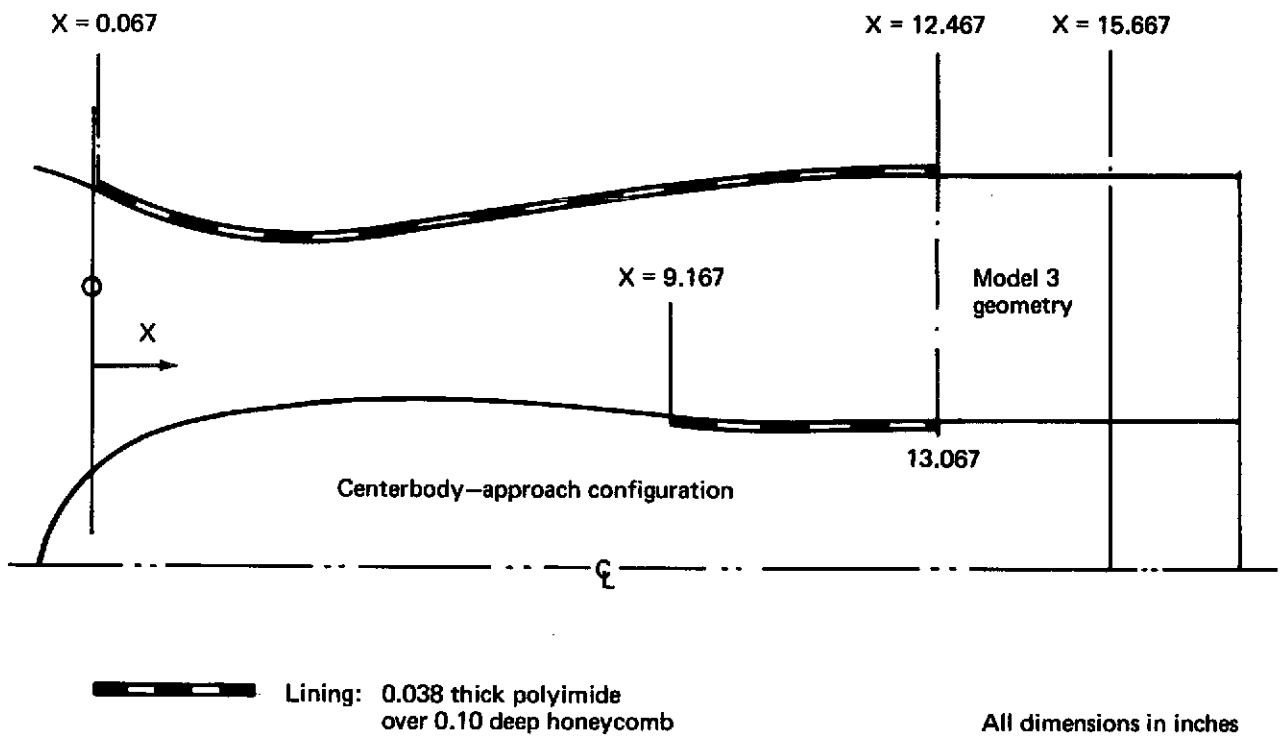


*FIGURE 122.—ACOUSTIC LINING DETAILS—MODEL 3B, L/D = 1.3*

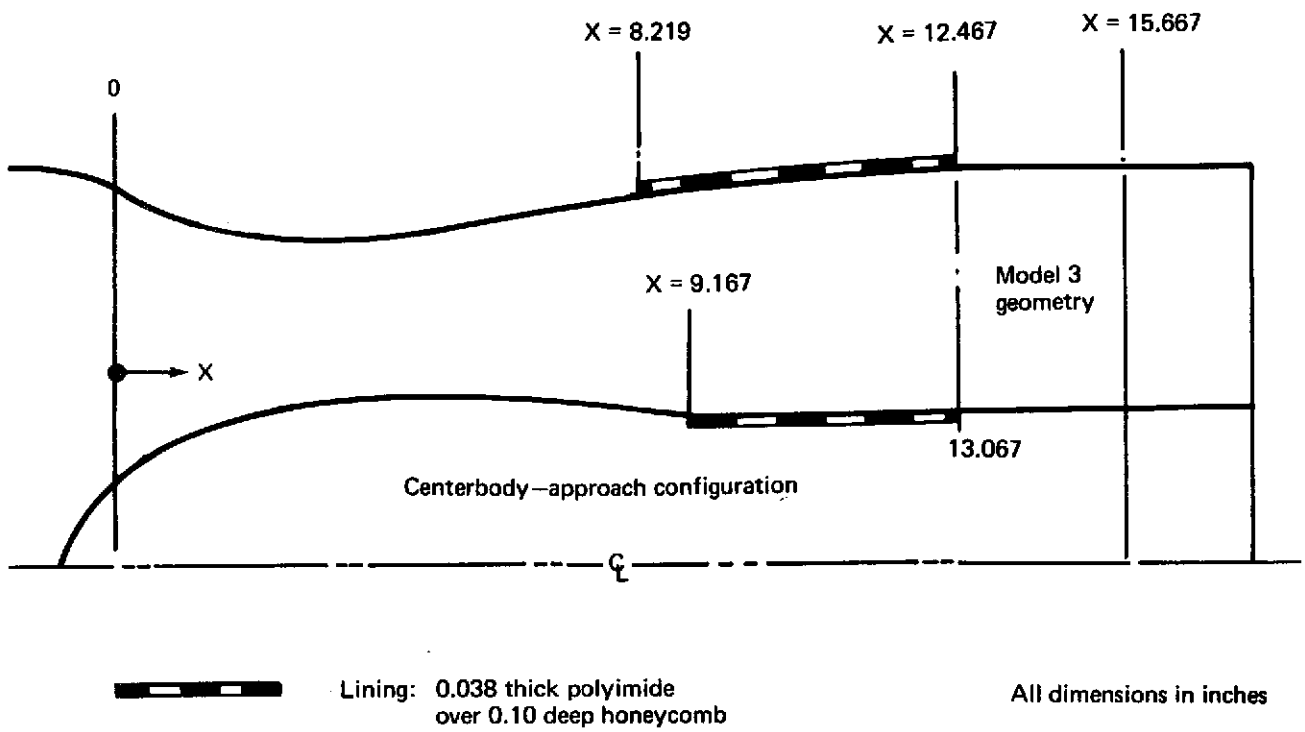


*FIGURE 123.—ACOUSTIC LINING DETAILS—MODEL 3C, L/D = 1.3*

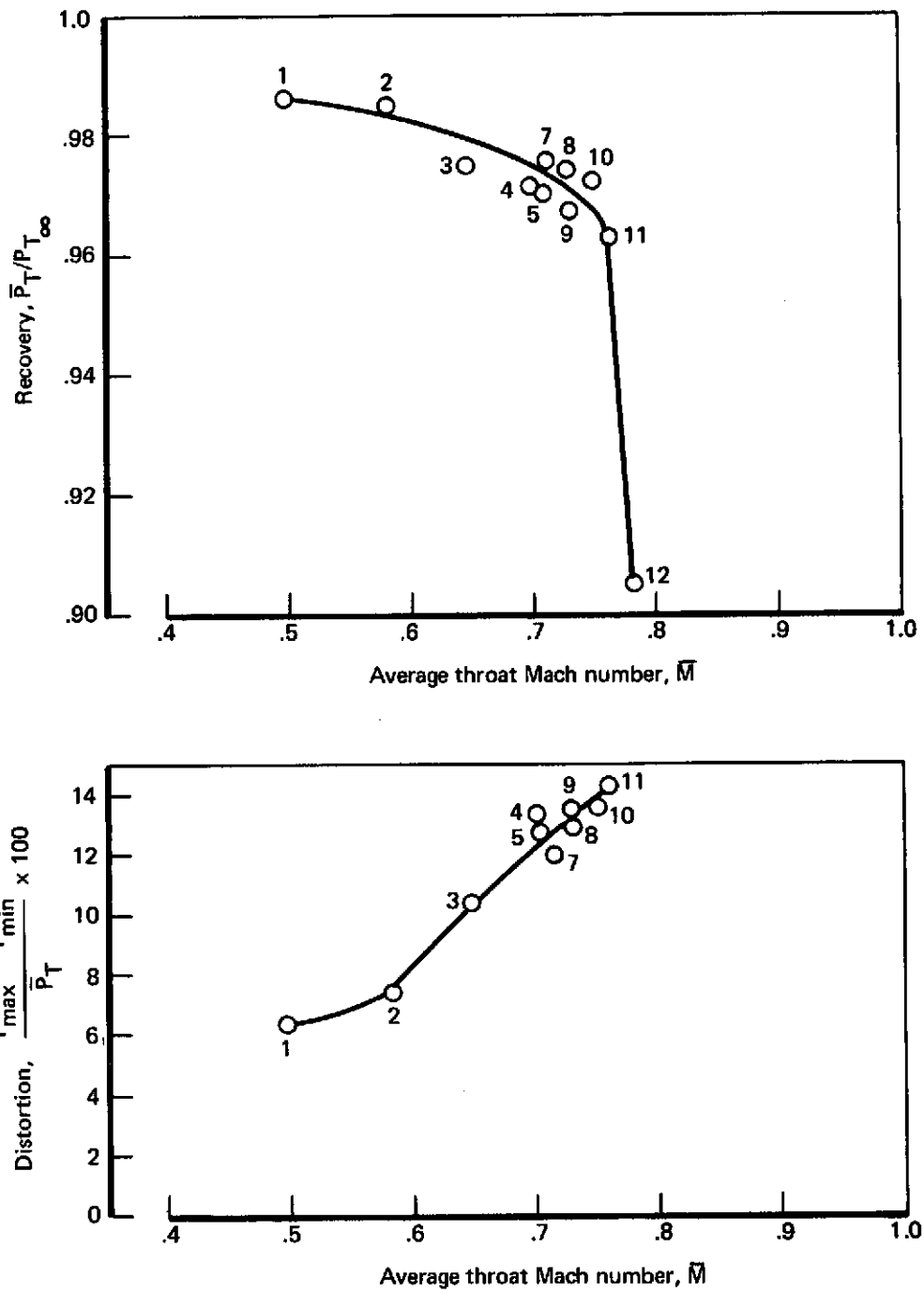


*FIGURE 124.—RECOVERY AND DISTORTION VS THROAT MACH NUMBER—RUN 101, MODEL 3A*

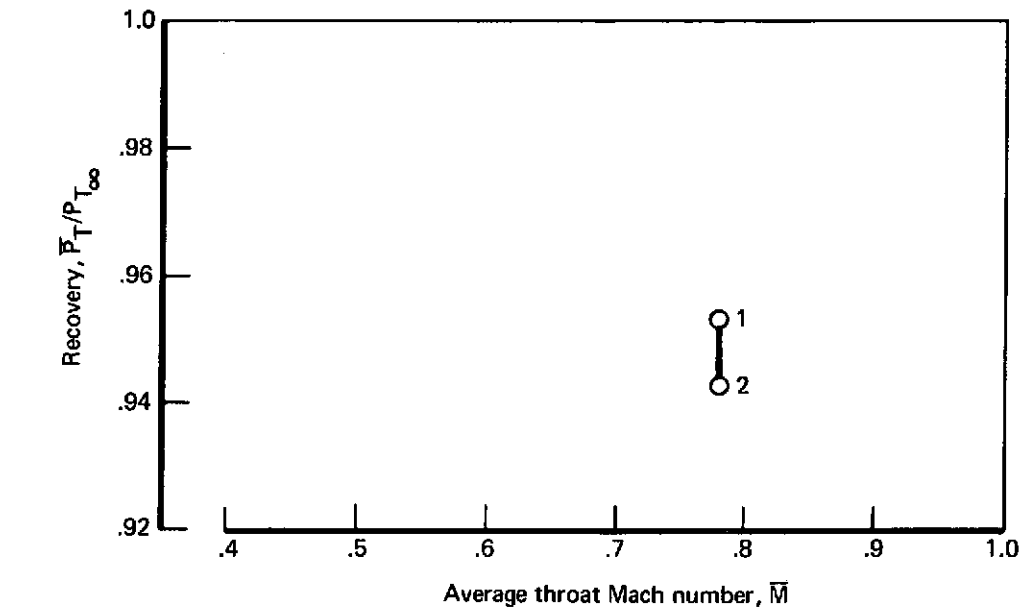


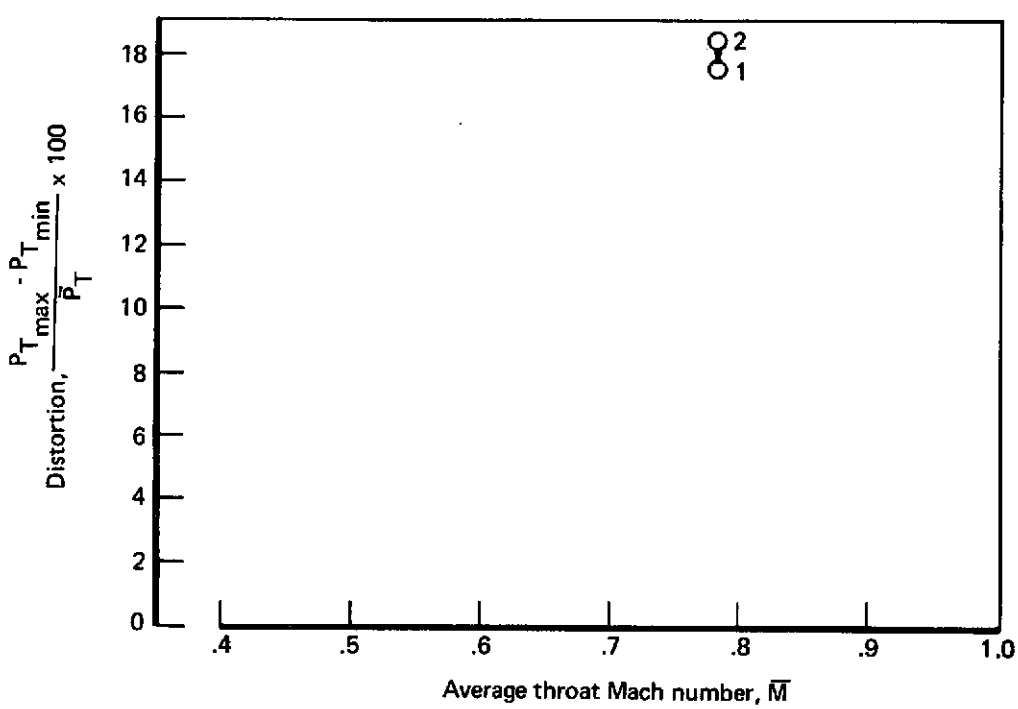


*FIGURE 125.–RECOVERY AND DISTORTION VS THROAT MACH NUMBER–RUN 102, MODEL 3B*

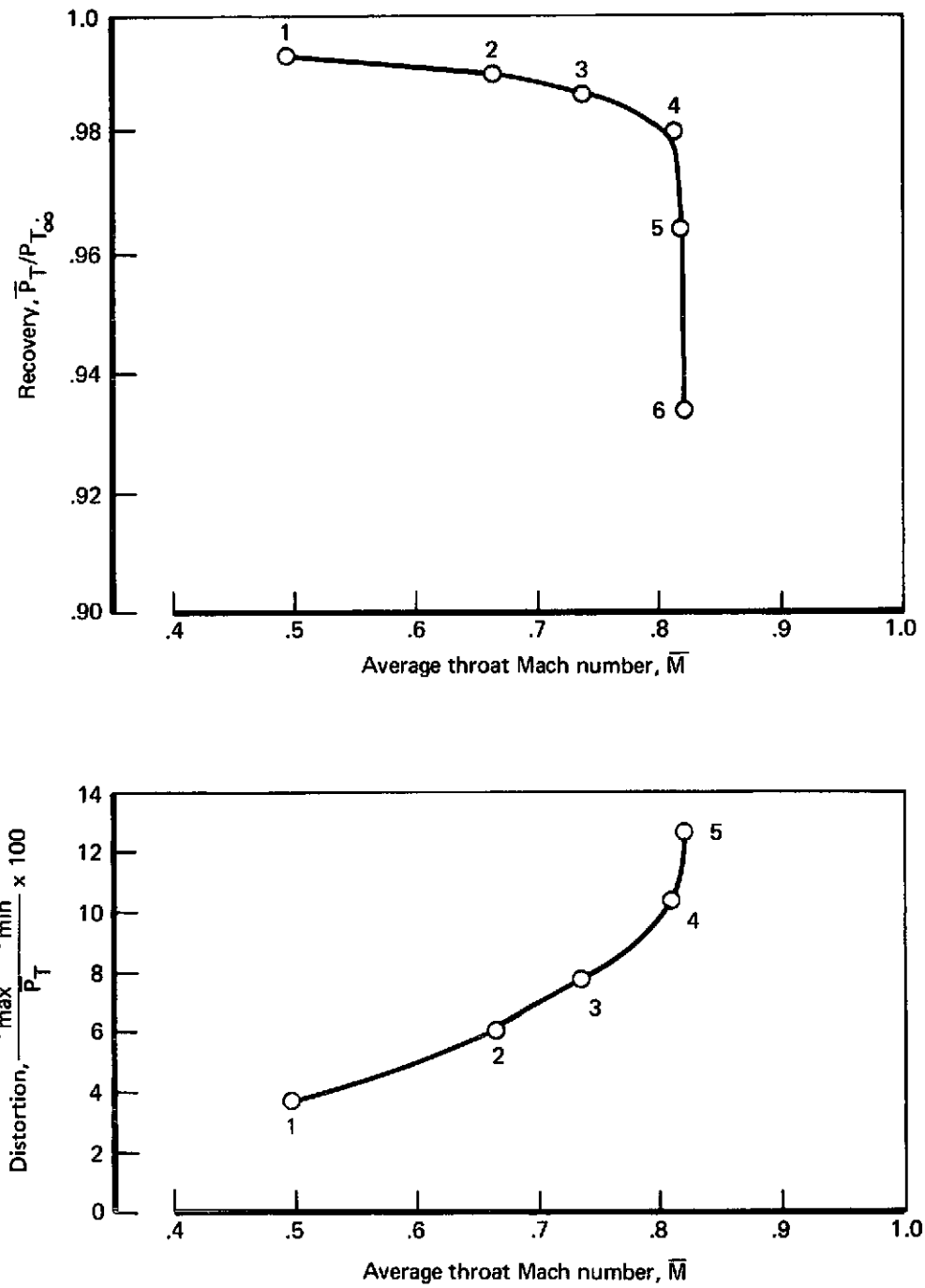


*FIGURE 126.–RECOVERY AND DISTORTION VS THROAT MACH NUMBER–RUN 10, MODEL 3C*

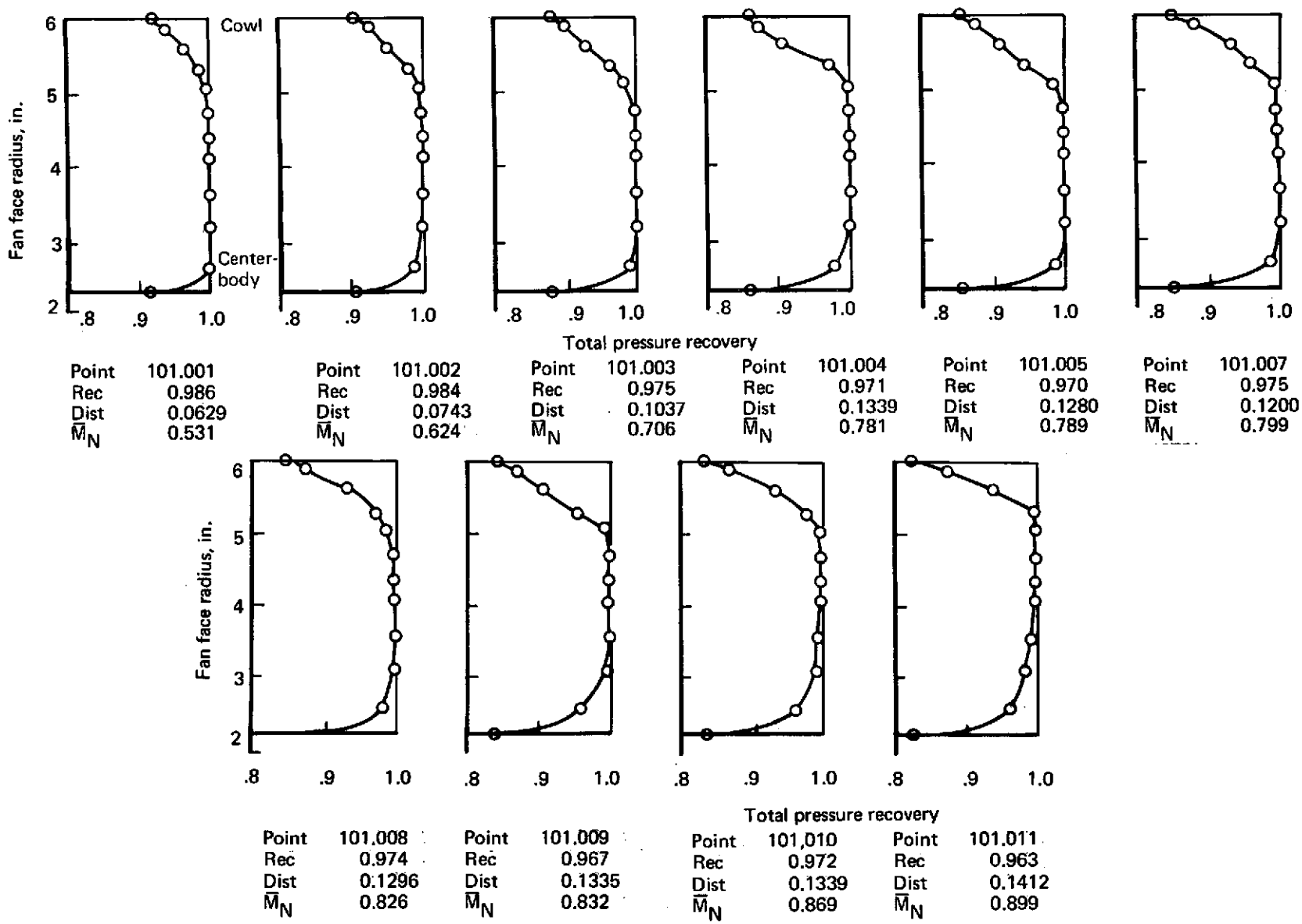


*FIGURE 127.–RECOVERY PROFILES–RUN 101, MODEL 3A*

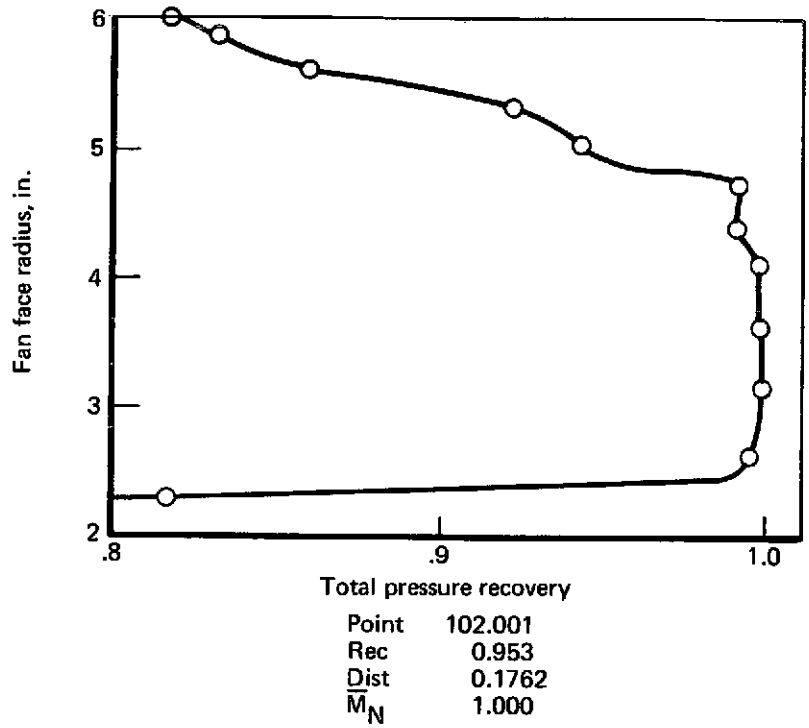


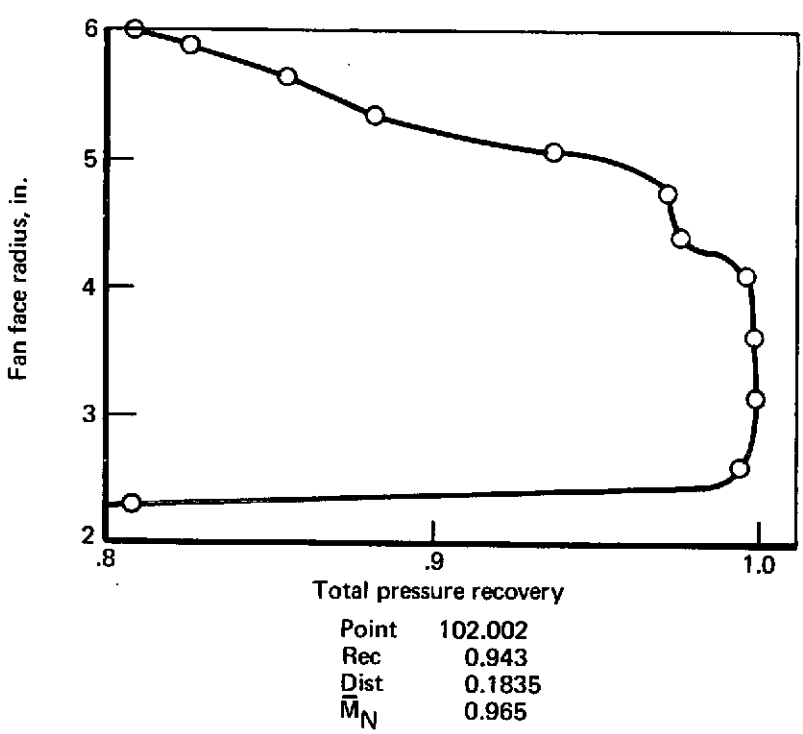


*FIGURE 128.–RECOVERY PROFILES–RUN 102, MODEL 3B*

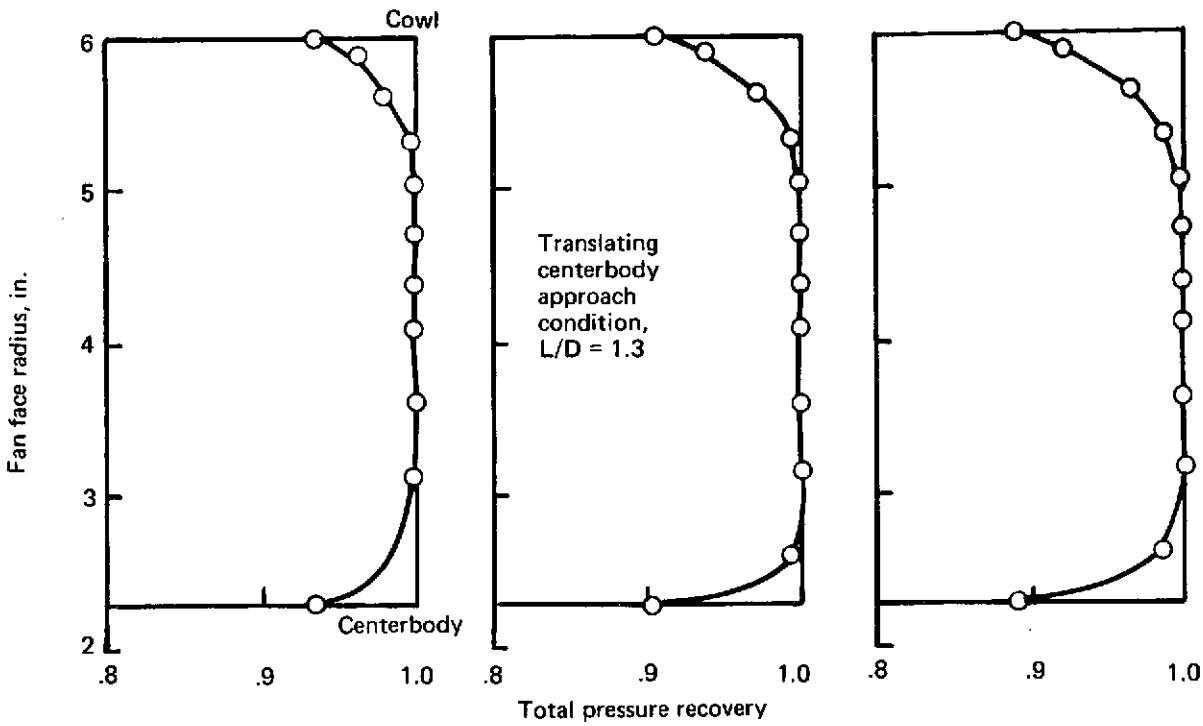


| Point | 10.001 | Point | 10.002 | Point | 10.003 |
|---|---|---|---|---|---|
| Rec | 0.993 | Rec | 0.990 | Rec | 0.986 |
| Dist | 0.0373 | Dist | 0.0617 | Dist | 0.0781 |
| $\bar{M}_N$ | 0.520 | $\bar{M}_N$ | 0.705 | $\bar{M}_N$ | 0.795 |

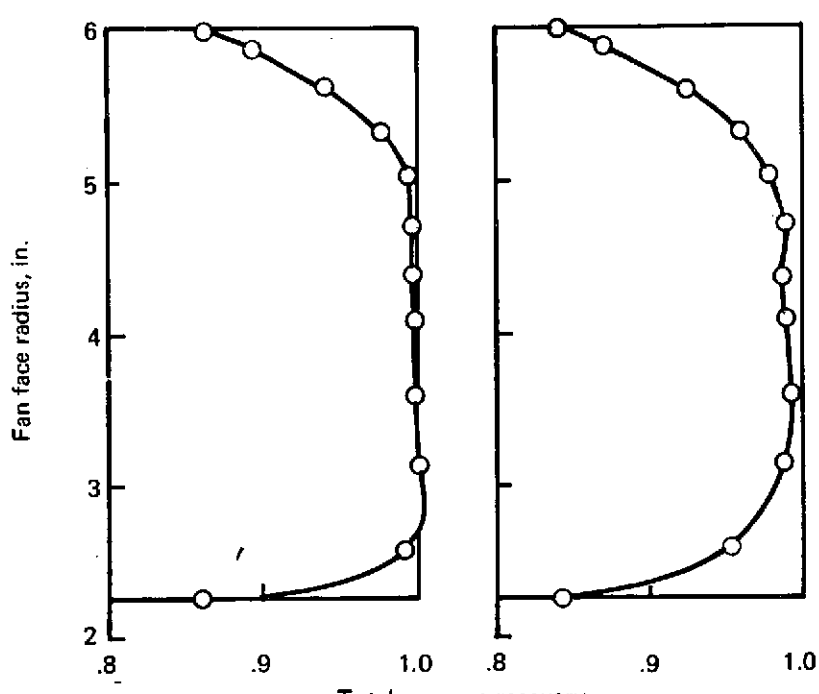


| Point | 10.004 | Point | 10.005 |
|---|---|---|---|
| Rec | 0.980 | Rec | 0.964 |
| Dist | 0.1040 | Dist | 0.1278 |
| $\bar{M}_N$ | 0.938 | $\bar{M}_N$ | 0.976 |

*FIGURE 129.–RECOVERY PROFILES–RUN 10, MODEL 3C*

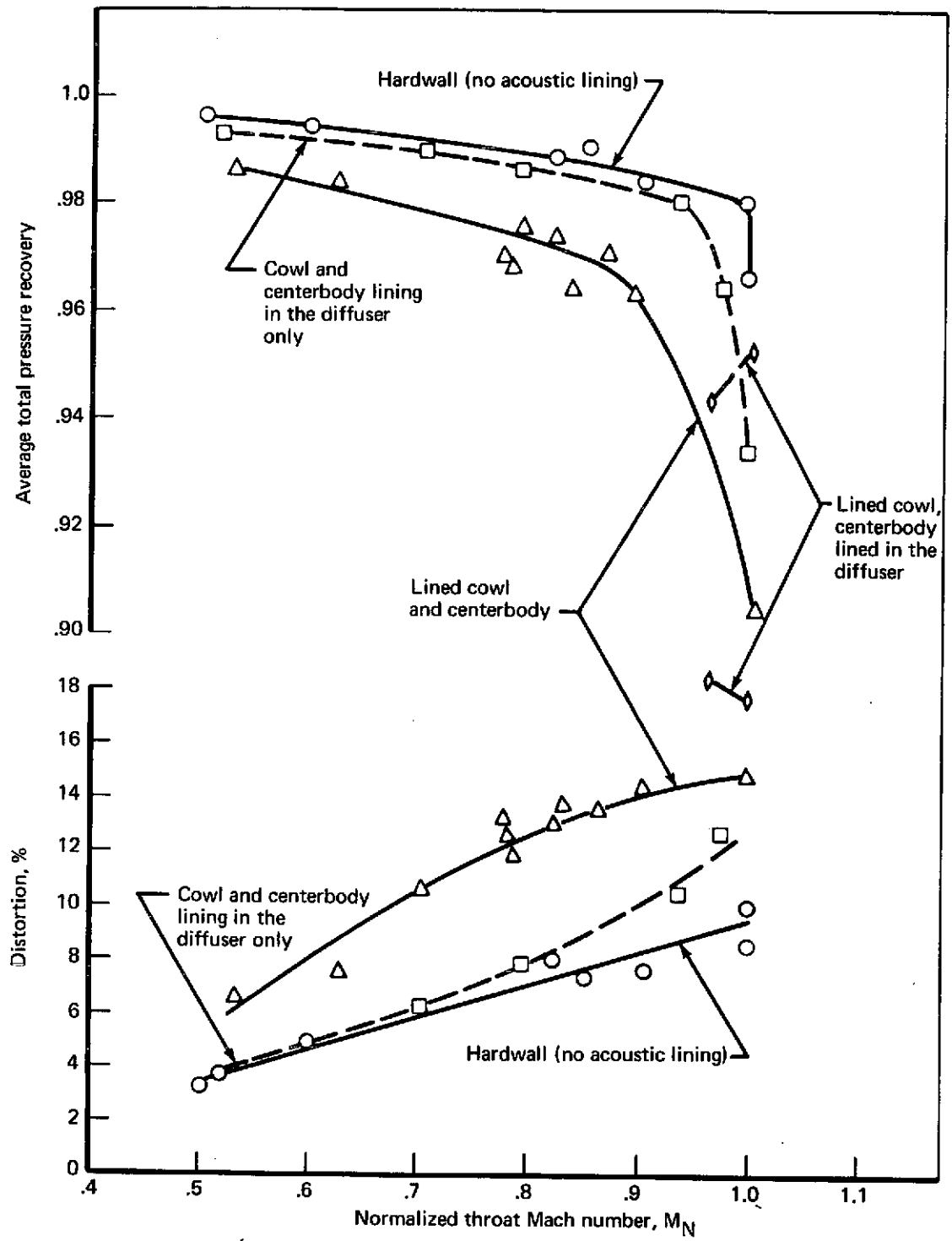


*FIGURE 130.—RECOVERY AND DISTORTION COMPARISON VS THROAT MACH NUMBER— RUNS 4, 101, 102, and 10; MODELS 3, 3A, 3B, AND 3C*

| Symbol | Run no. | Rec | Dist | $M_N$ | Lining configuration |
|---|---|---|---|---|---|
| ——— | 4.011 | 0.984 | 0.0752 | 0.905 | No lining |
| — — — | 101.011 | 0.963 | 0.1412 | 0.899 | Lined cowl and centerbody |
| - - - - | 102.001 | 0.953 | 0.1762 | 1.000 | Lined cowl, centerbody lining in the diffuser only |
| ..... | 10.004 | 0.980 | 0.1040 | 0.938 | Cowl and centerbody lining in diffuser only |

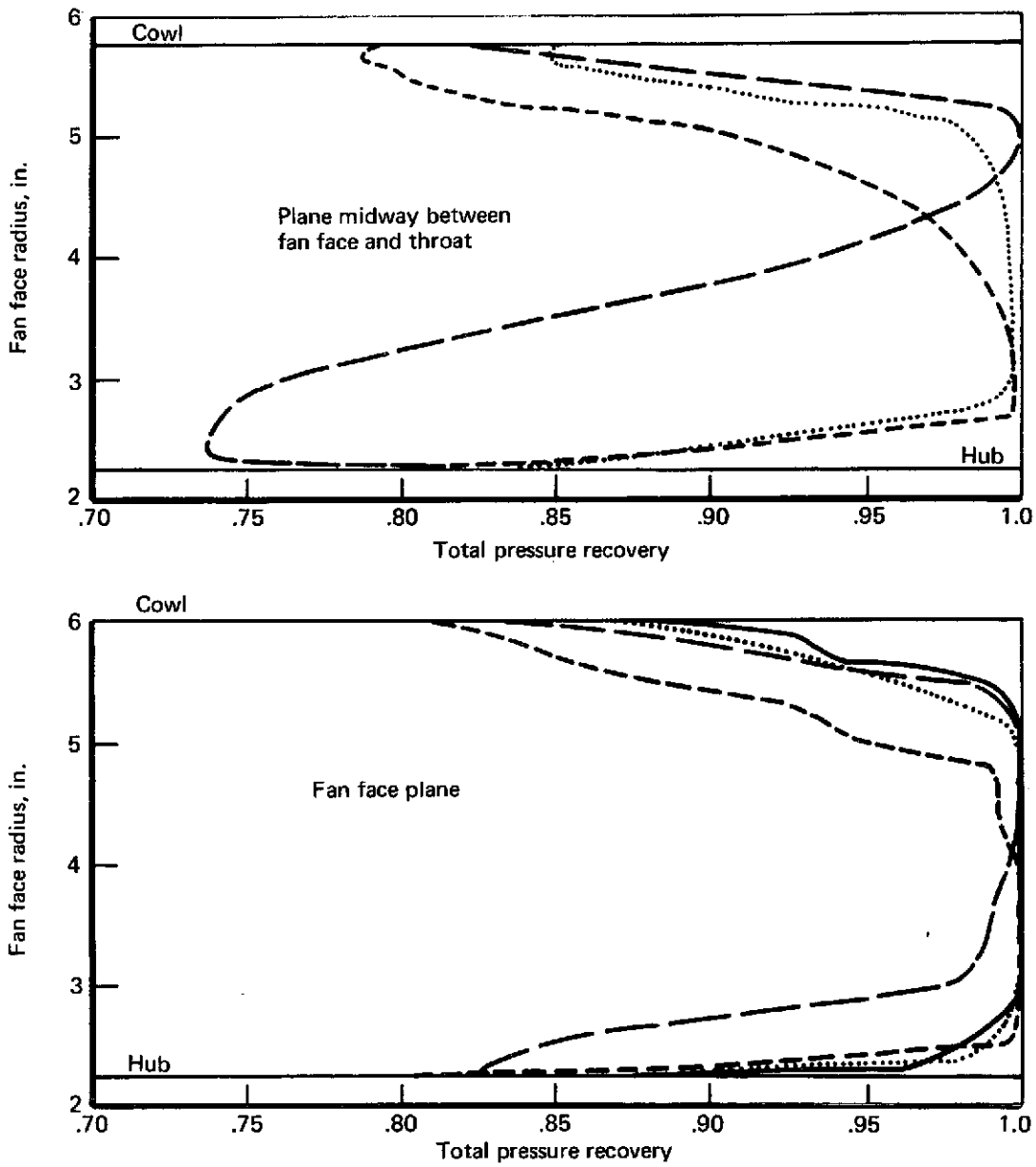


*FIGURE 131.–RECOVERY PROFILE COMPARISON–RUNS 4, 101, 102, AND 10; MODELS 3, 3A, 3B AND 3C*

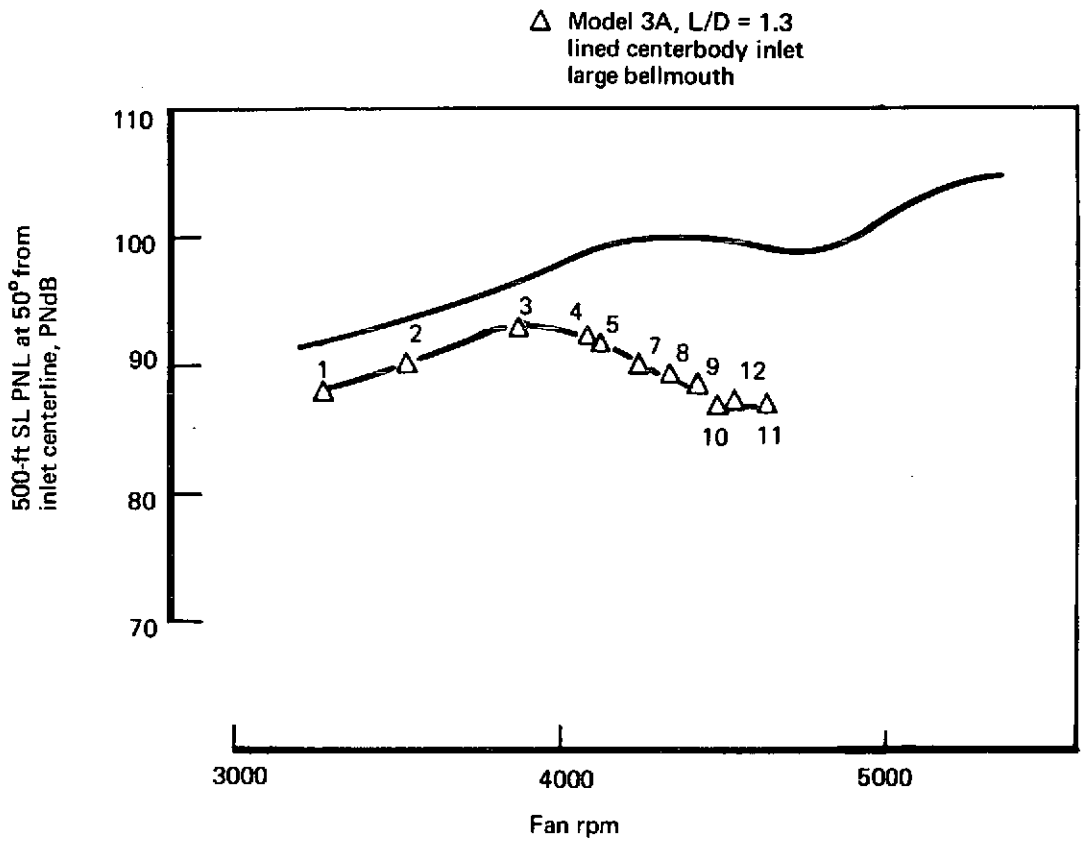


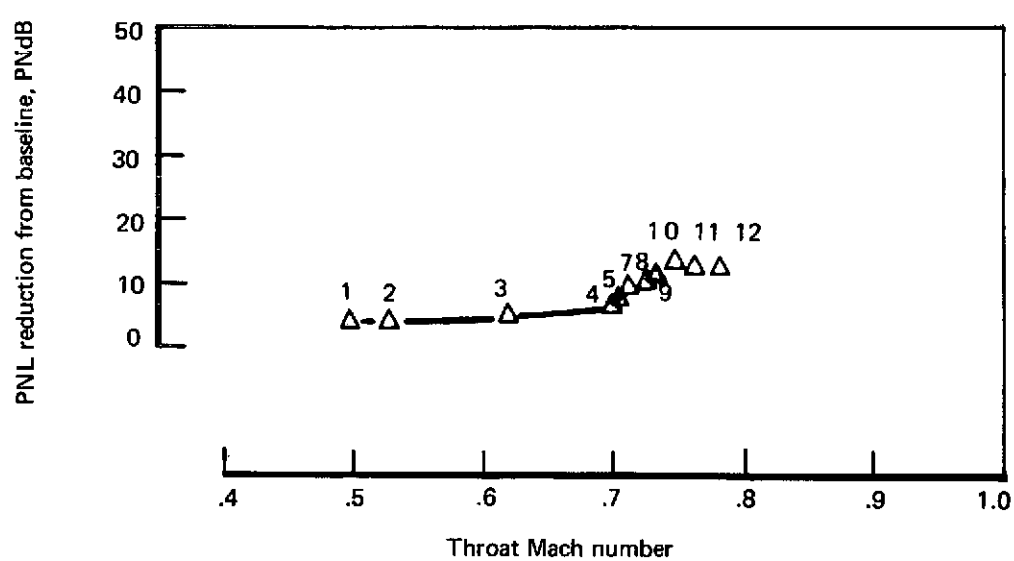


*FIGURE 132.—PNL VS FAN RPM AND PNL REDUCTION VS THROAT MACH NUMBER (APPROACH), SCALED-UP DATA—RUN 101, MODEL 3A*

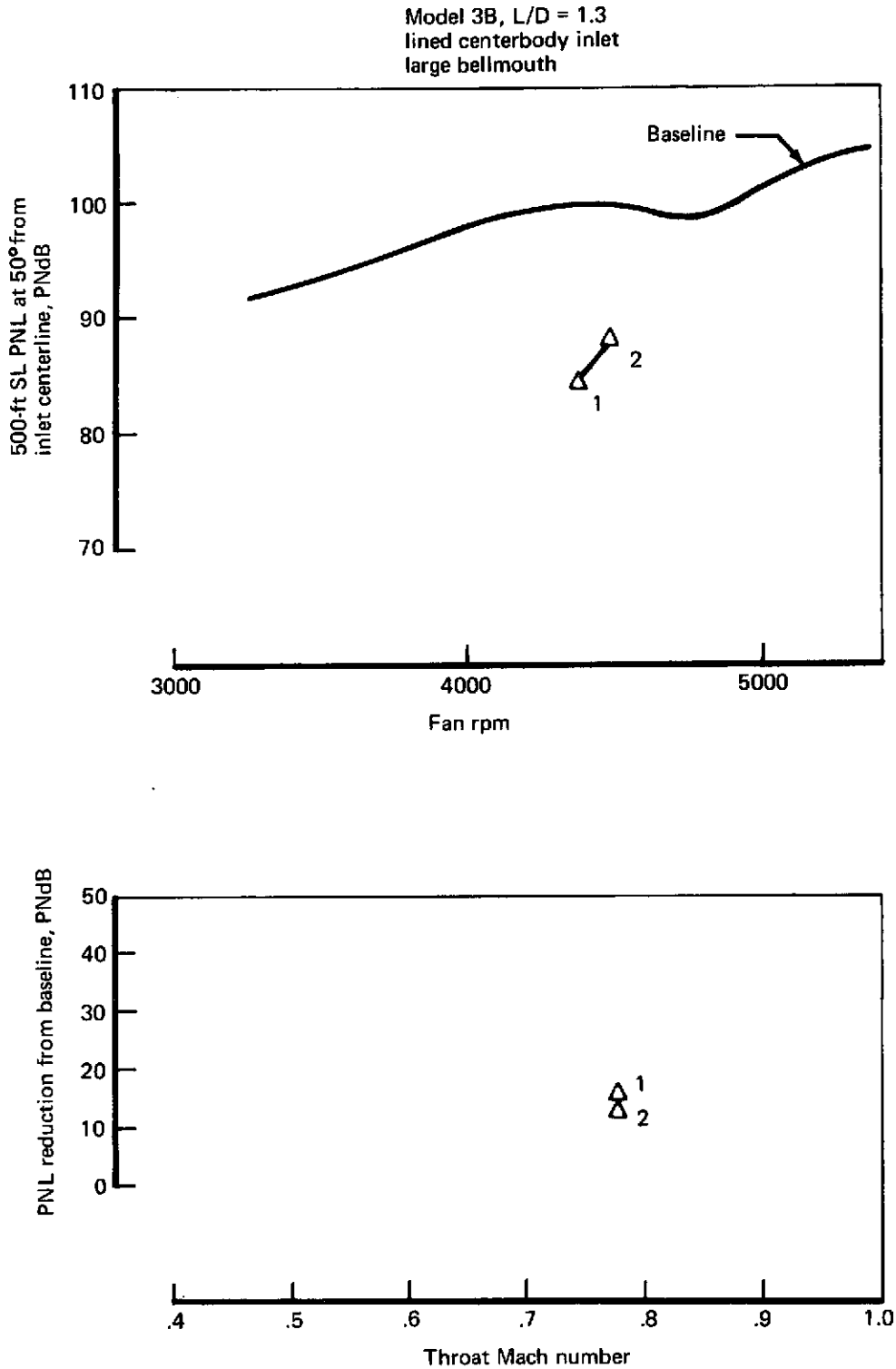


*FIGURE 133.–PNL VS FAN RPM AND PNL REDUCTION VS THROAT MACH NUMBER (APPROACH), SCALED-UP DATA–RUN 102, MODEL 3B*

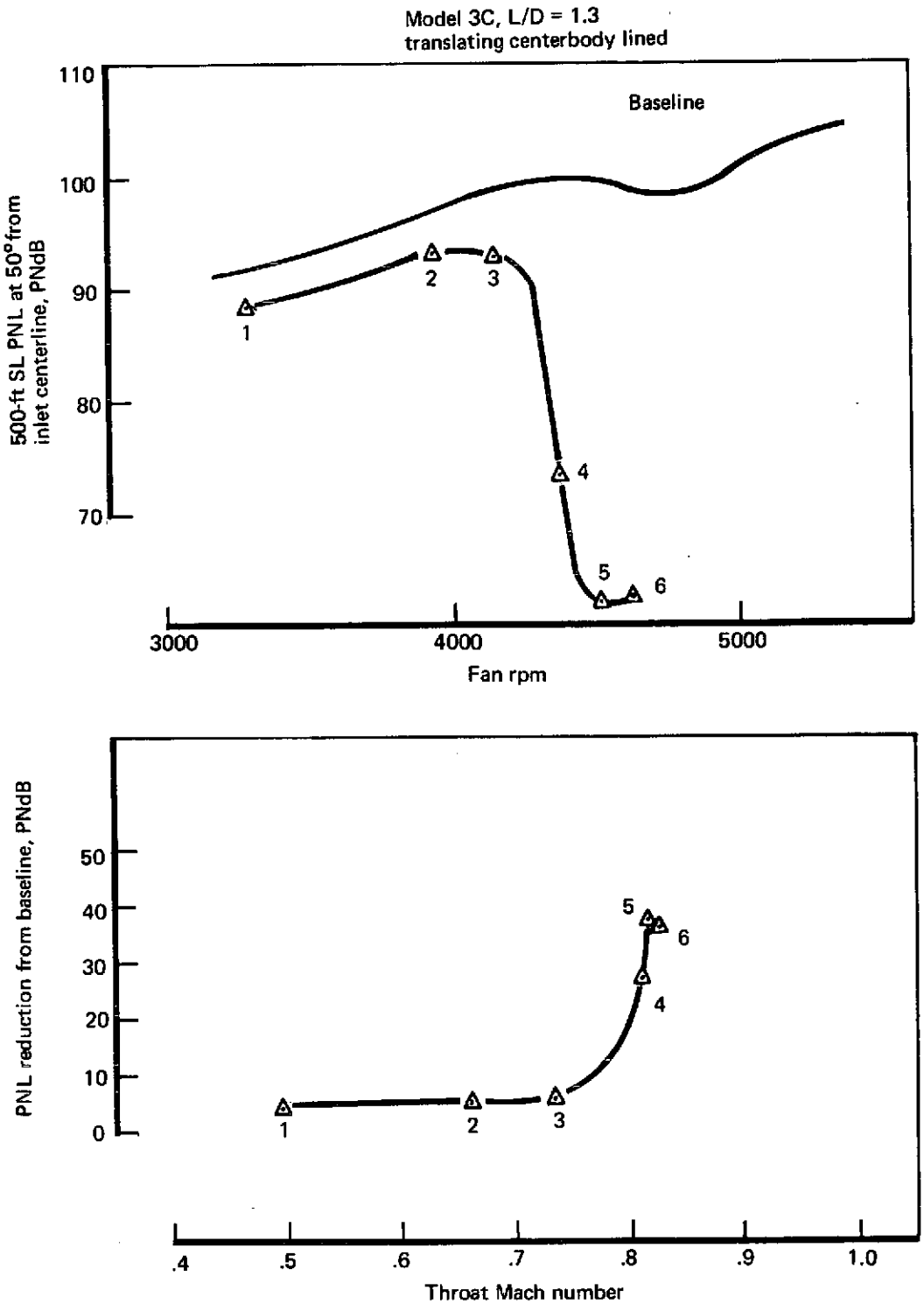


*FIGURE 134.—PNL VS FAN RPM AND PNL REDUCTION VS THROAT MACH NUMBER (APPROACH), SCALED-UP DATA—RUN 10, MODEL 3C*

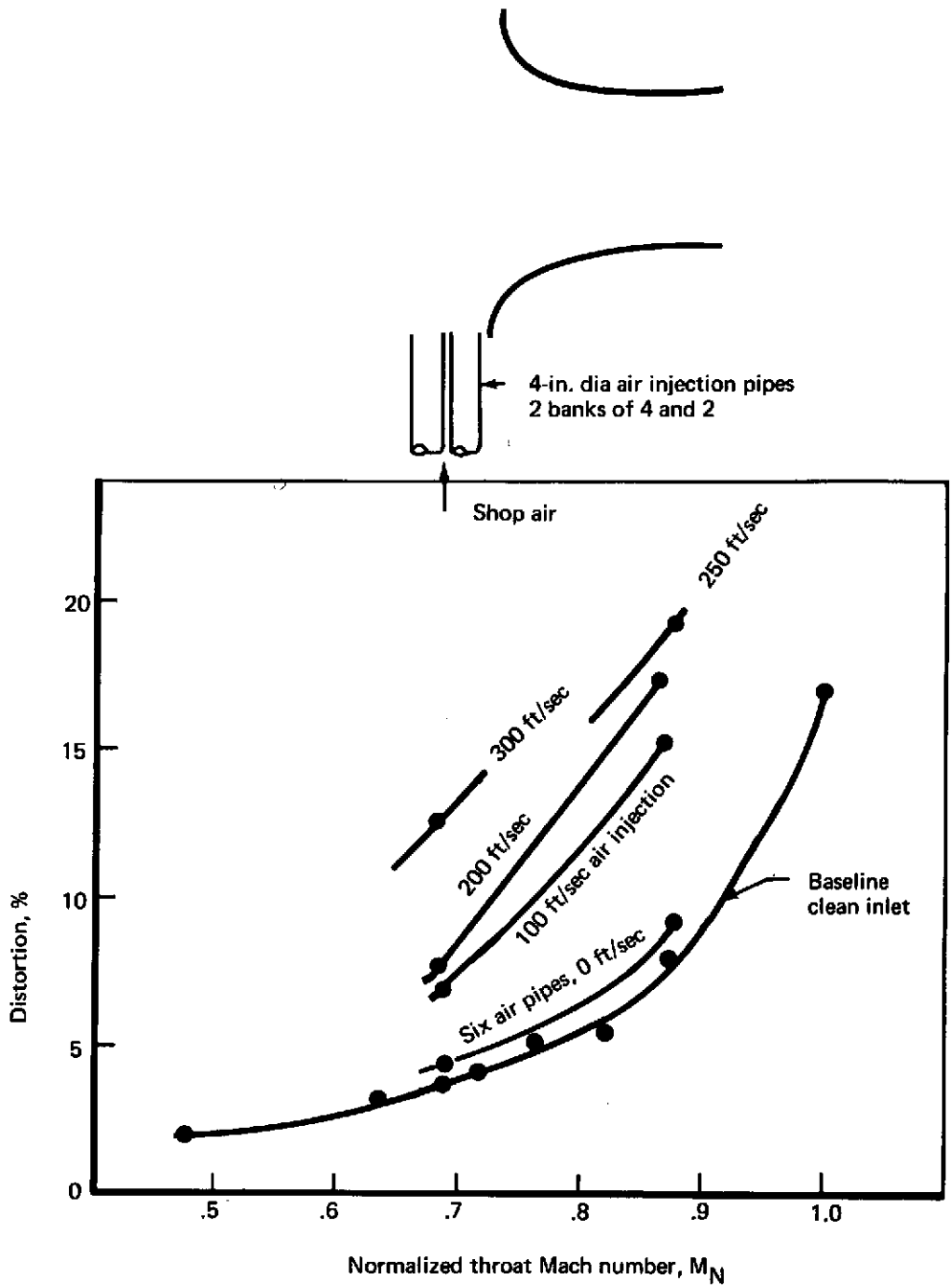


*FIGURE 135.—CROSSWIND DISTORTION SIMULATION, TRANSLATING CENTERBODY (TAKEOFF)—RUN 12, L/D = 1.0*

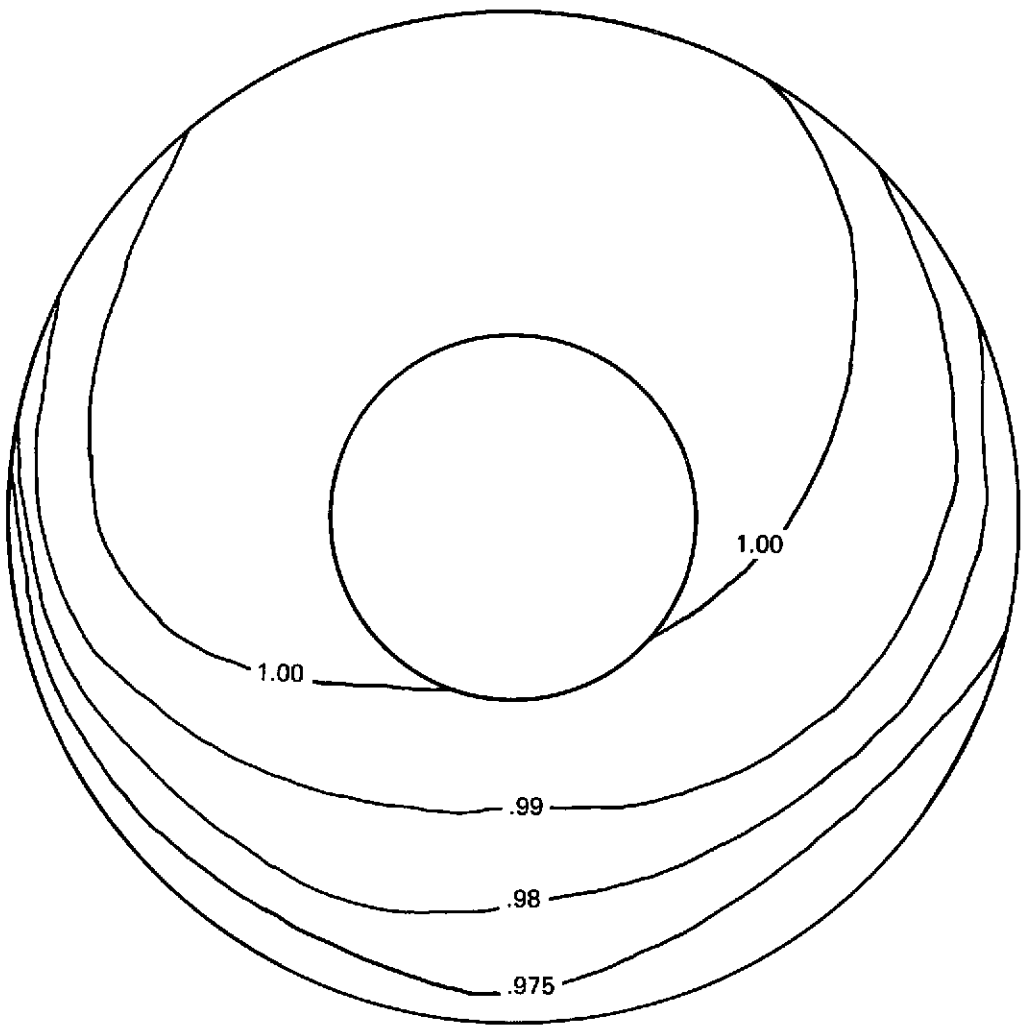


Distortion = 0.026
Recovery = 0.993

Normalized Mach no. = 0.66
Pipes installed

*FIGURE 136.—FAN FACE TOTAL PRESSURE DISTRIBUTION, MACH 0.66, NO CROSSWIND—RUN 11, MODEL 4*

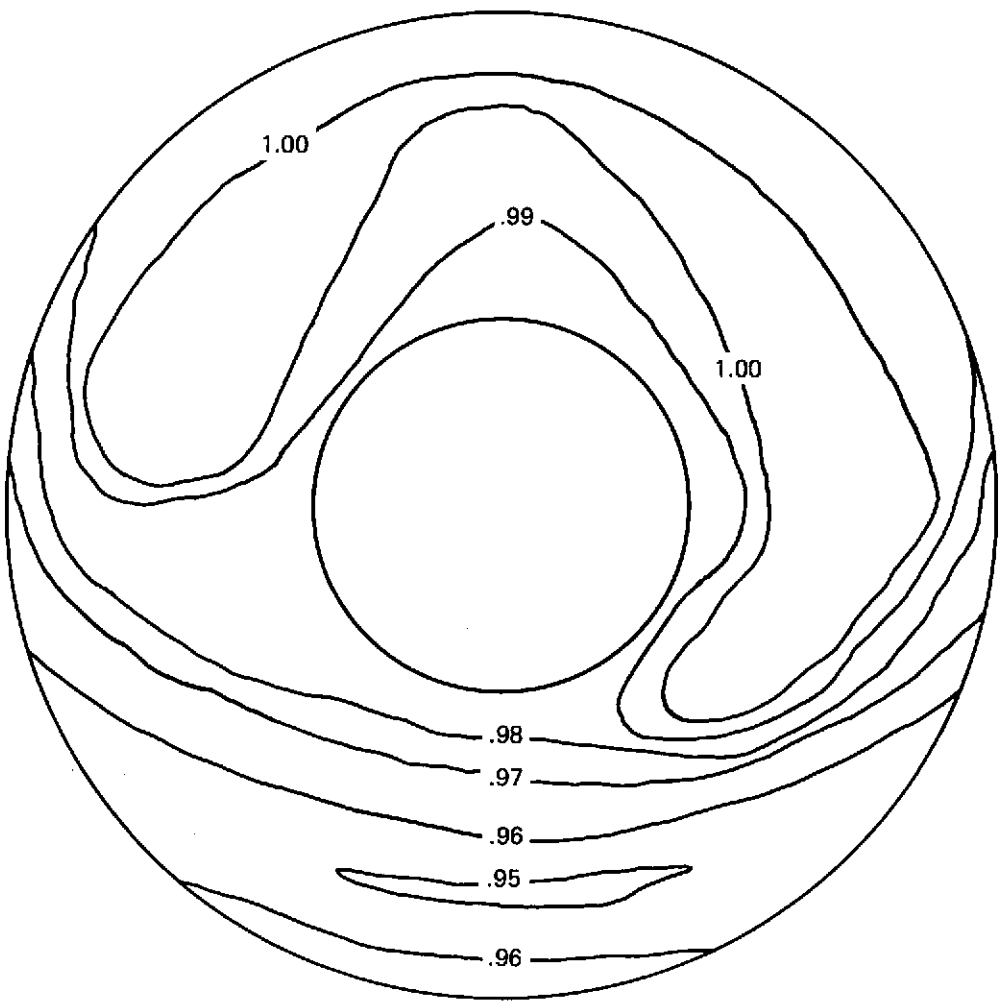


Distortion = 0.046
Recovery = 0.986

Normalized Mach no. = 0.66

*FIGURE 137.—FAN FACE TOTAL PRESSURE DISTRIBUTION, MACH 0.66, 100-FT/SEC CROSSWIND—RUN 11, MODEL 4*

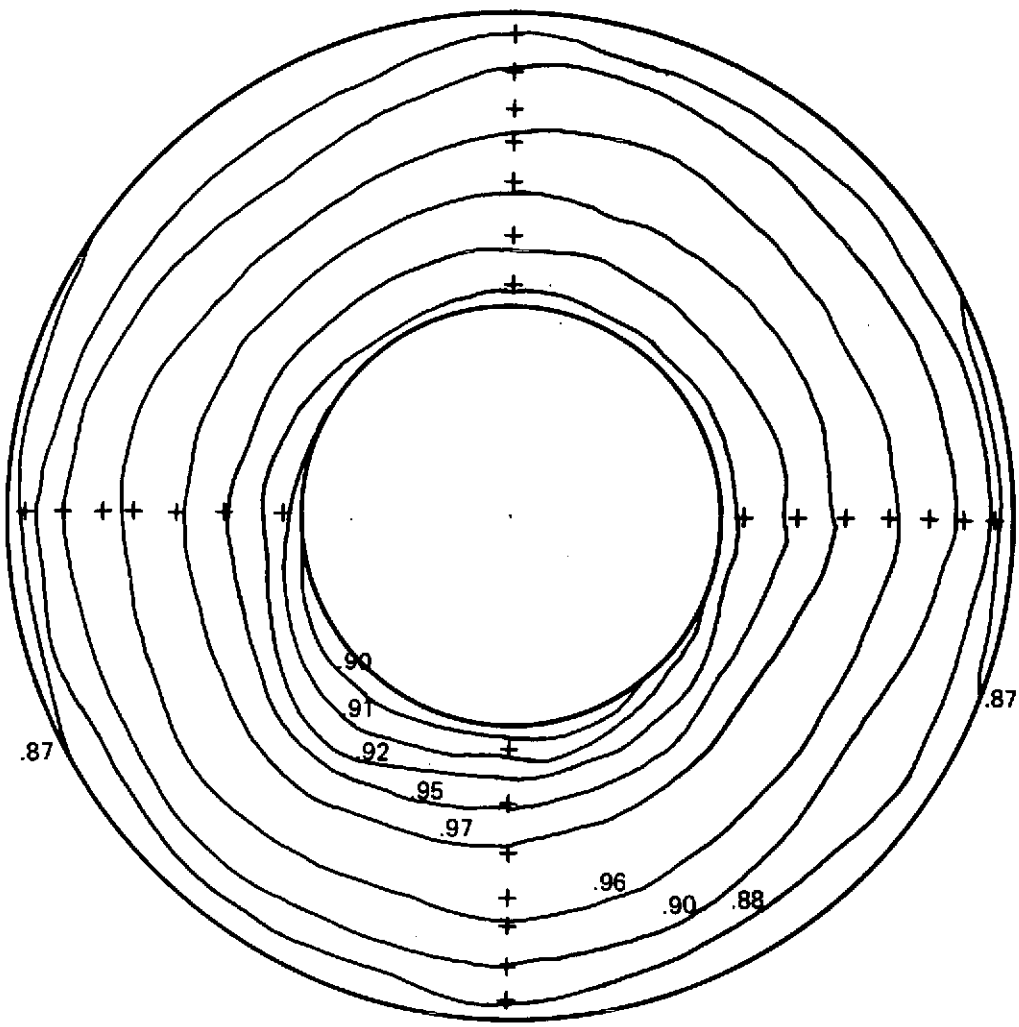


Point No. 11.017
Distortion 0.114
Recovery 0.935

Normalized Mach no. = 1.00
No air pipes

*FIGURE 138.–FAN FACE TOTAL PRESSURE DISTRIBUTION, MACH 1.00, NO CROSSWIND, MODEL 4, RUN 11*

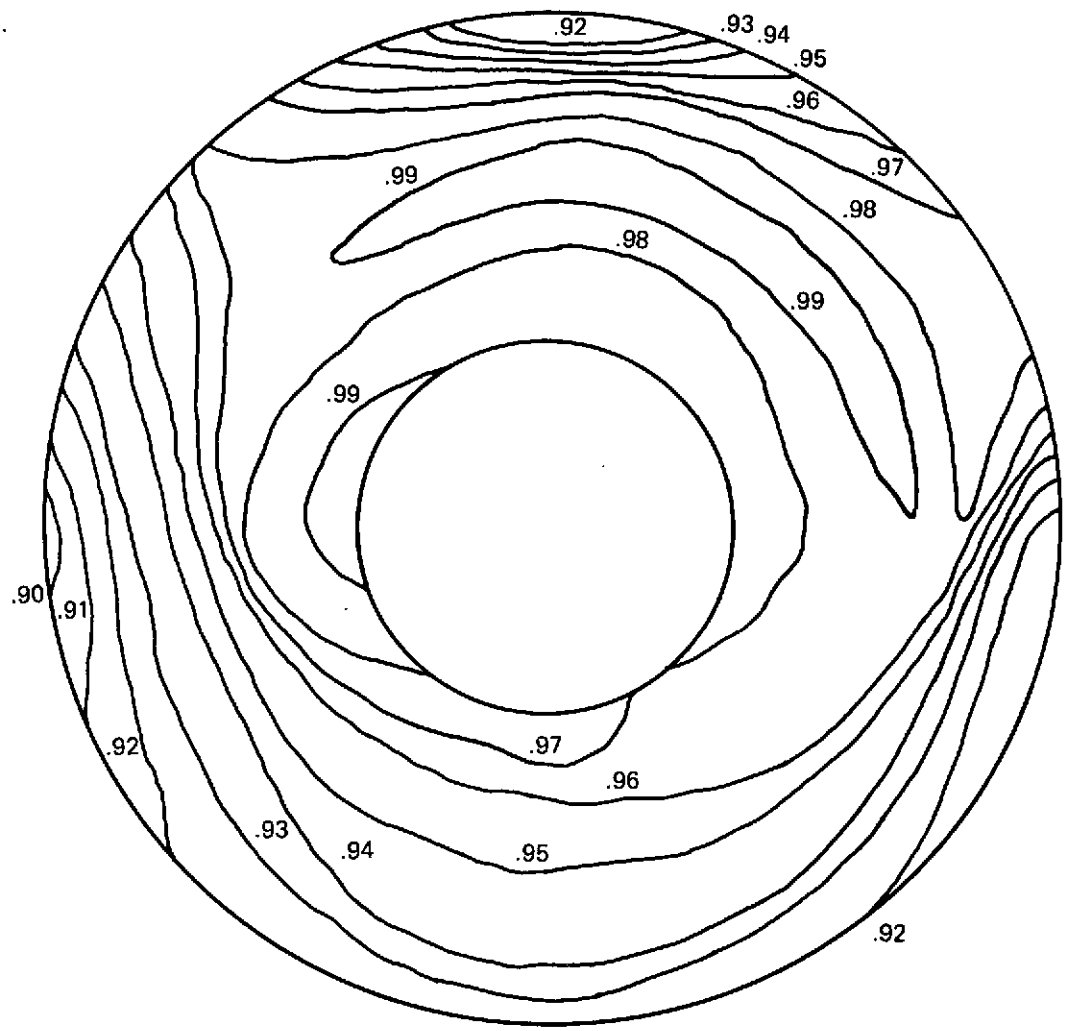


Normalized Mach no. = 0.92

Distortion = 0.093
Recovery = 0.962

*FIGURE 139.—FAN FACE TOTAL PRESSURE DISTRIBUTION, MACH 0.92, 100-FT/SEC CROSSWIND—RUN 11, MODEL 4*

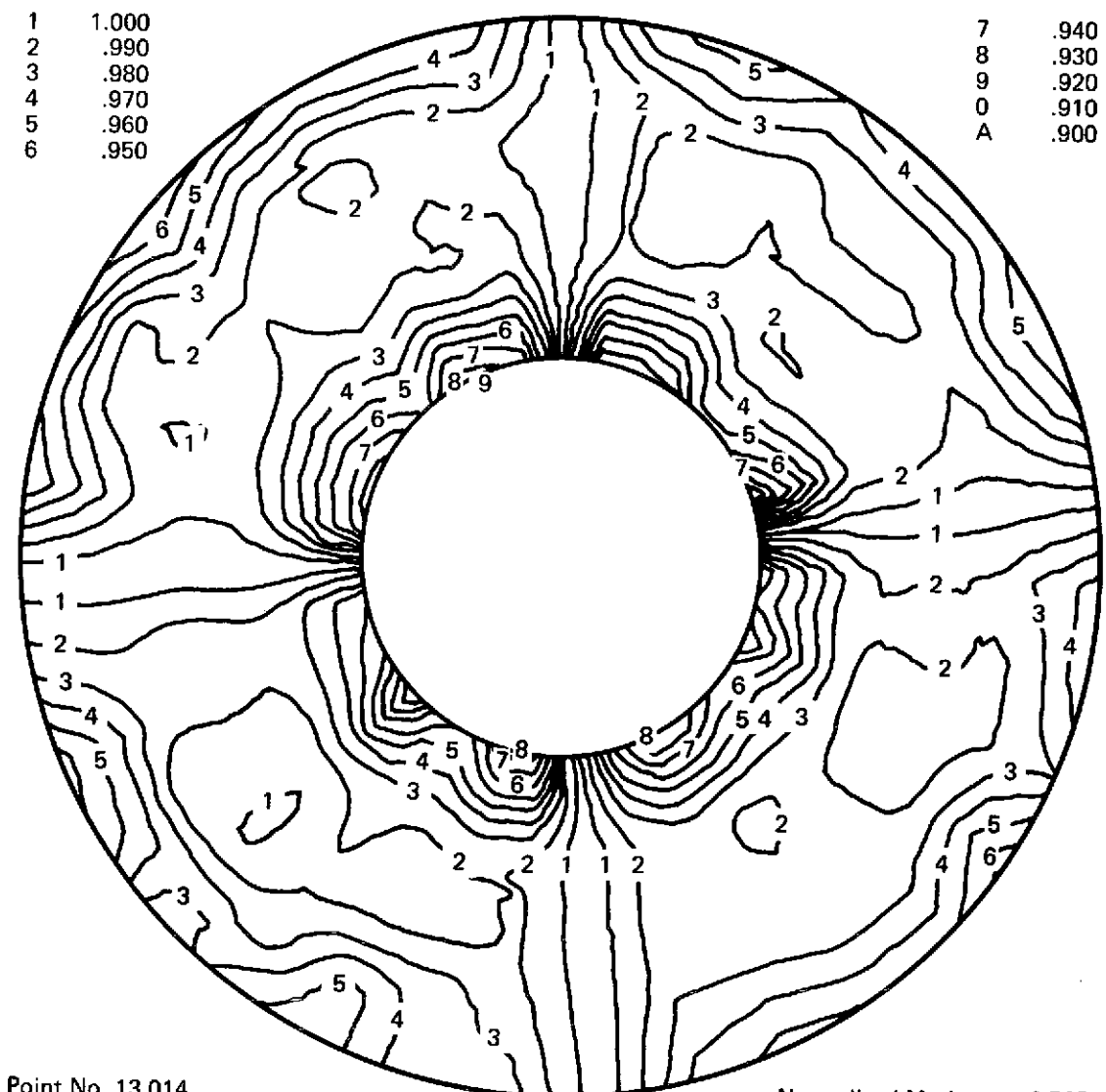


*FIGURE 140.—FAN FACE TOTAL PRESSURE DISTRIBUTION, MACH 0.735, NO CROSSWIND—RUN 13, MODEL 3*


Point no. 13.015
Distortion = 0.0658
Recovery = 0.975

Normalized Mach no. = 0.735

*FIGURE 141.–FAN FACE TOTAL PRESSURE DISTRIBUTION, MACH 0.735, 100-FT/SEC CROSSWIND–RUN 13, MODEL 3*

| | |
|---|---|
| 1 | 1.000 |
| 2 | .990 |
| 3 | .980 |
| 4 | .970 |
| 5 | .960 |
| 6 | .950 |

| | |
|---|---|
| 7 | .940 |
| 8 | .930 |
| 9 | .920 |
| 0 | .910 |
| A | .900 |

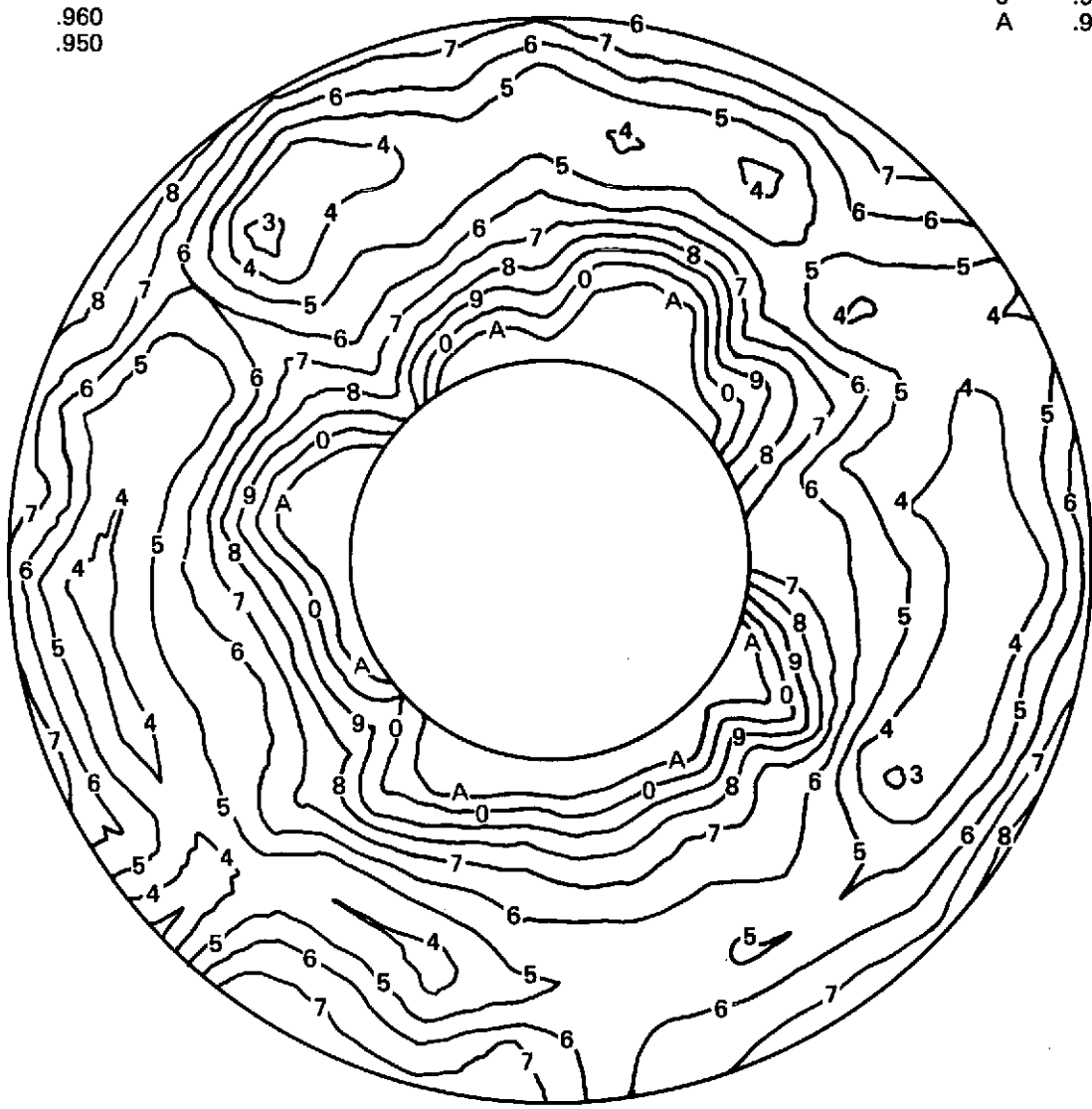

Point No. 13.018
Distortion = 0.1078
Recovery = 0.945

Normalized Mach no. = 0.910
Pipes installed

*FIGURE 142.–FAN FACE TOTAL PRESSURE DISTRIBUTION, MACH 0.910, NO CROSSWIND–RUN 13, MODEL 3*

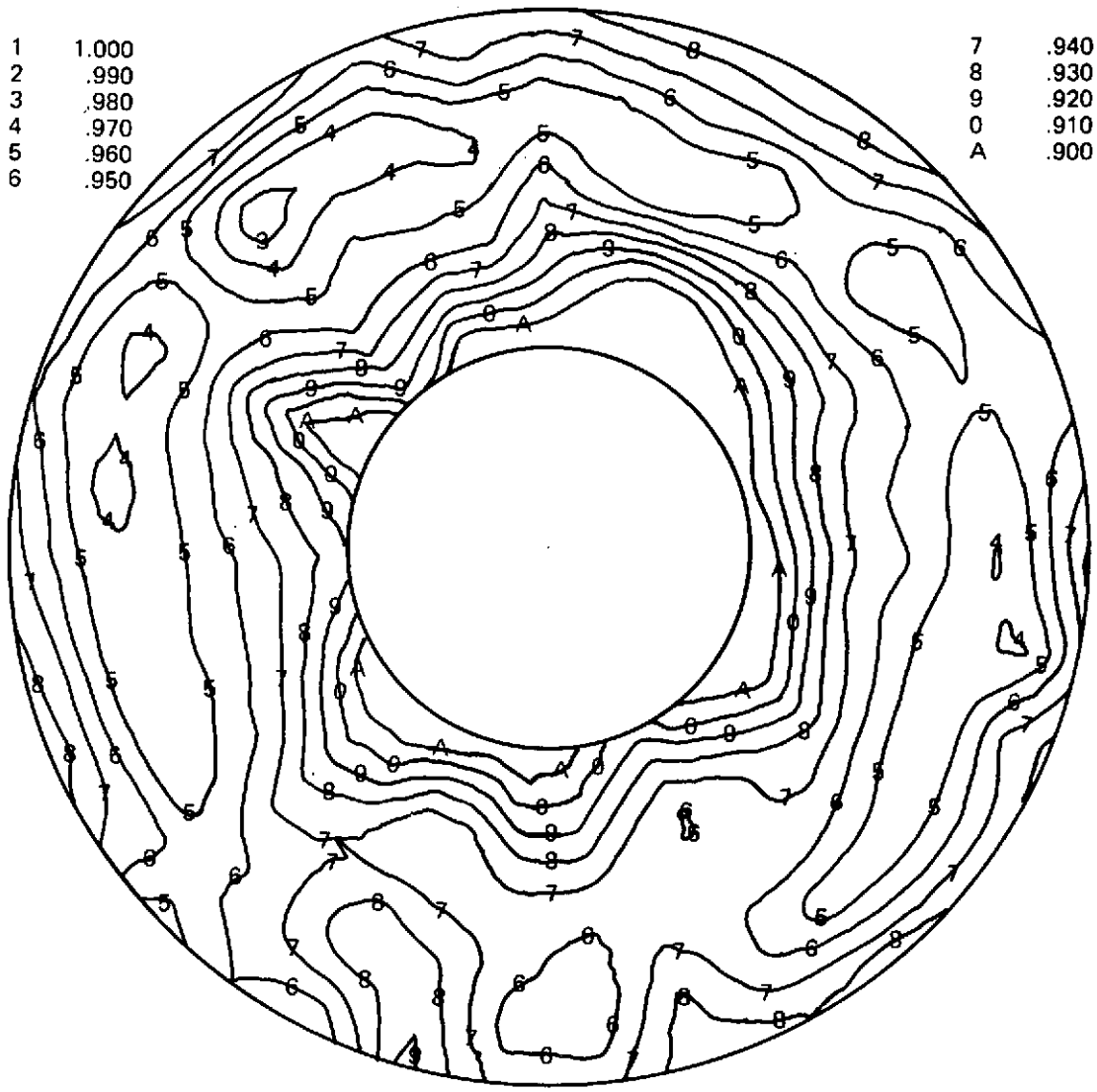


*FIGURE 143.–FAN FACE TOTAL PRESSURE DISTRIBUTION, MACH 0.910, 100-FT/SEC CROSSWIND–RUN 13, MODEL 3*

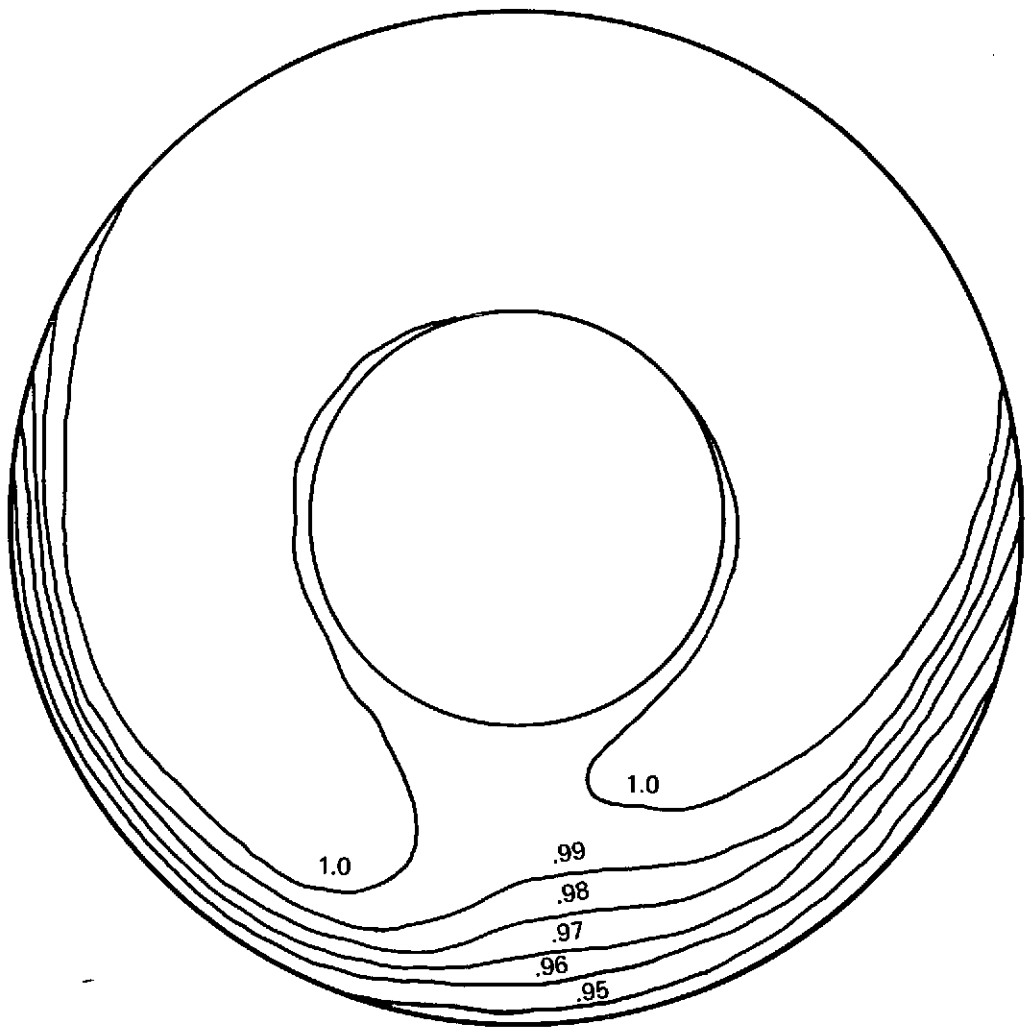


Point no. 12.014
Distortion 0.045
Recovery 0.993

Normalized Mach no. = 0.69
Six pipes installed

*FIGURE 144.—FAN FACE TOTAL PRESSURE DISTRIBUTION, MACH 0.69, NO CROSSWIND —RUN 12, MODEL 4*

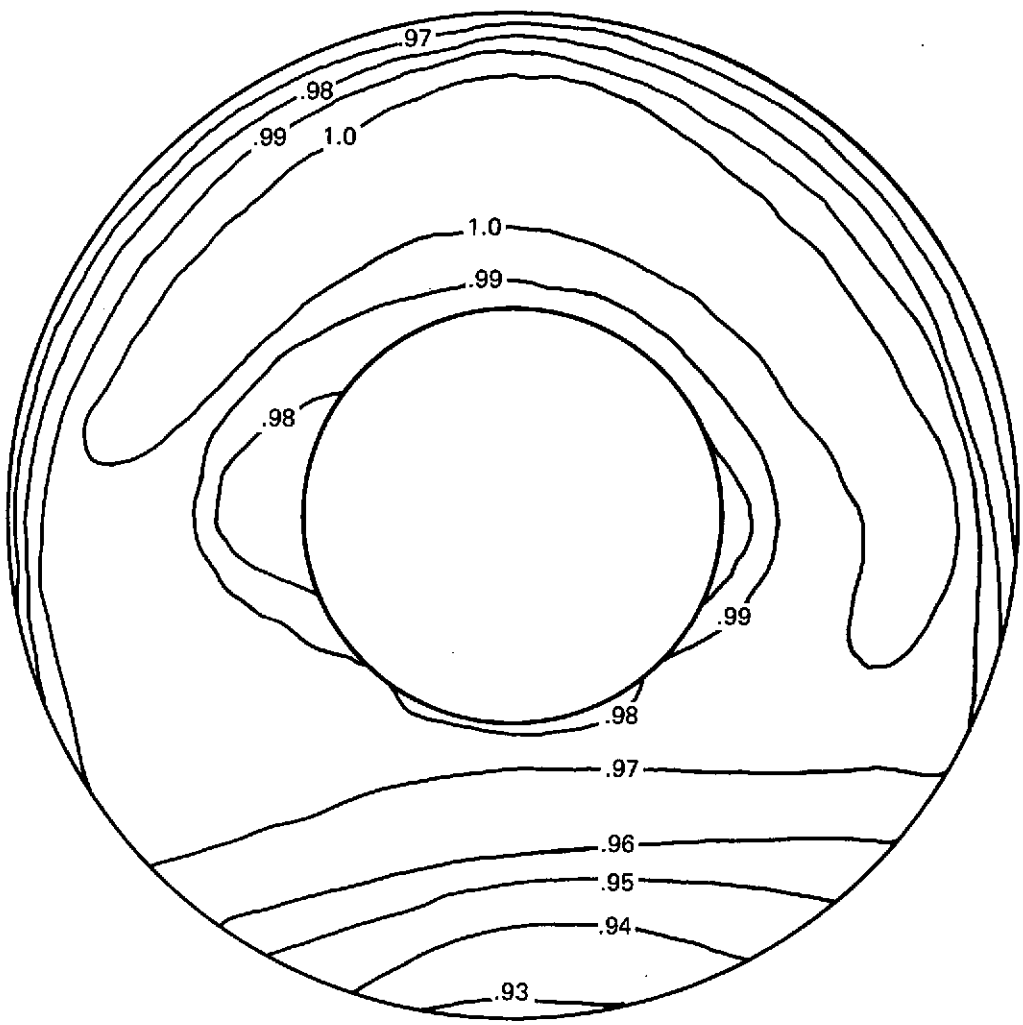


Point no. 12.015
Distortion = 0.071
Recovery = 0.982

Normalized Mach no. = 0.69

*FIGURE 145.–FAN FACE TOTAL PRESSURE DISTRIBUTION, MACH 0.69, 100-FT/SEC CROSSWIND–RUN 12, MODEL 4*

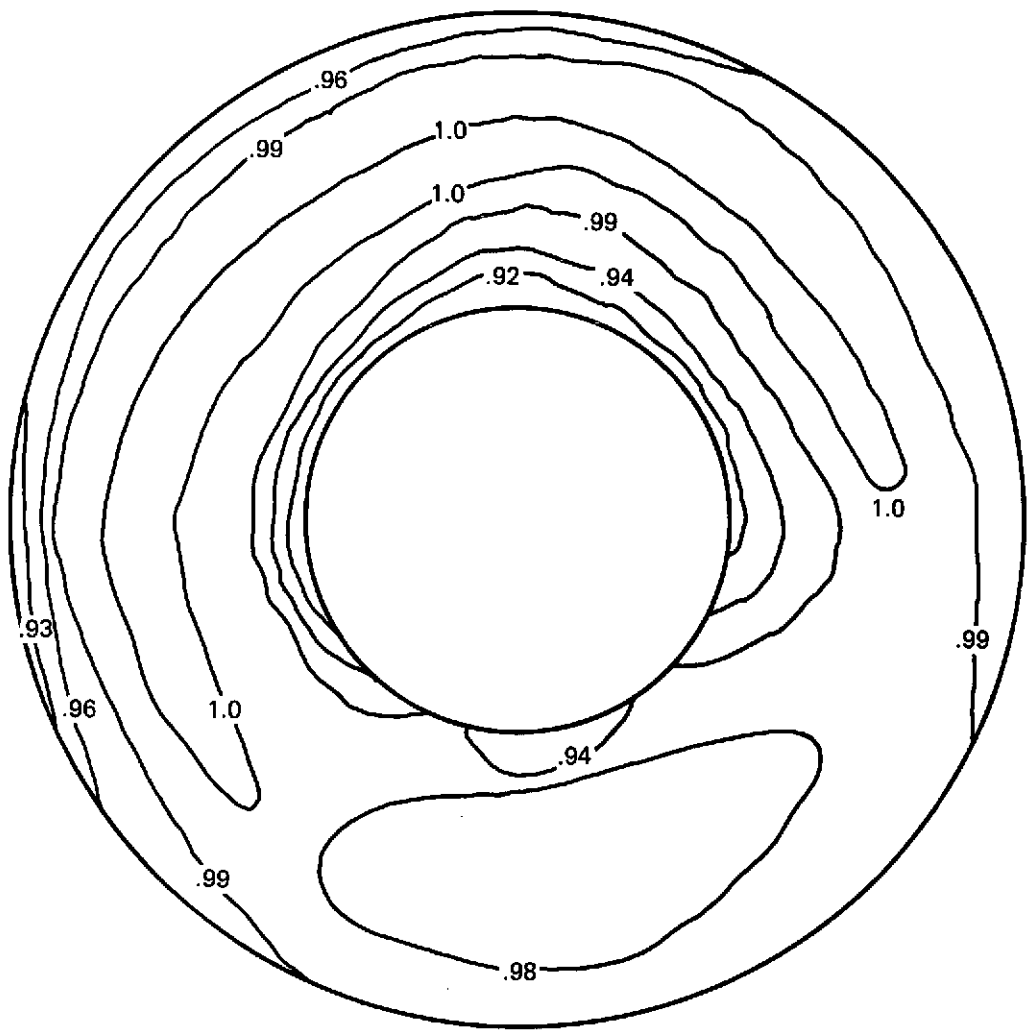


Point no. 12.018
Distortion = 0.091
Recovery = 0.977

Normalized Mach no. = 0.875
Six air pipes installed

*FIGURE 146.—FAN FACE TOTAL PRESSURE DISTRIBUTION, MACH 0.875, NO CROSSWIND—RUN 12, MODEL 4*

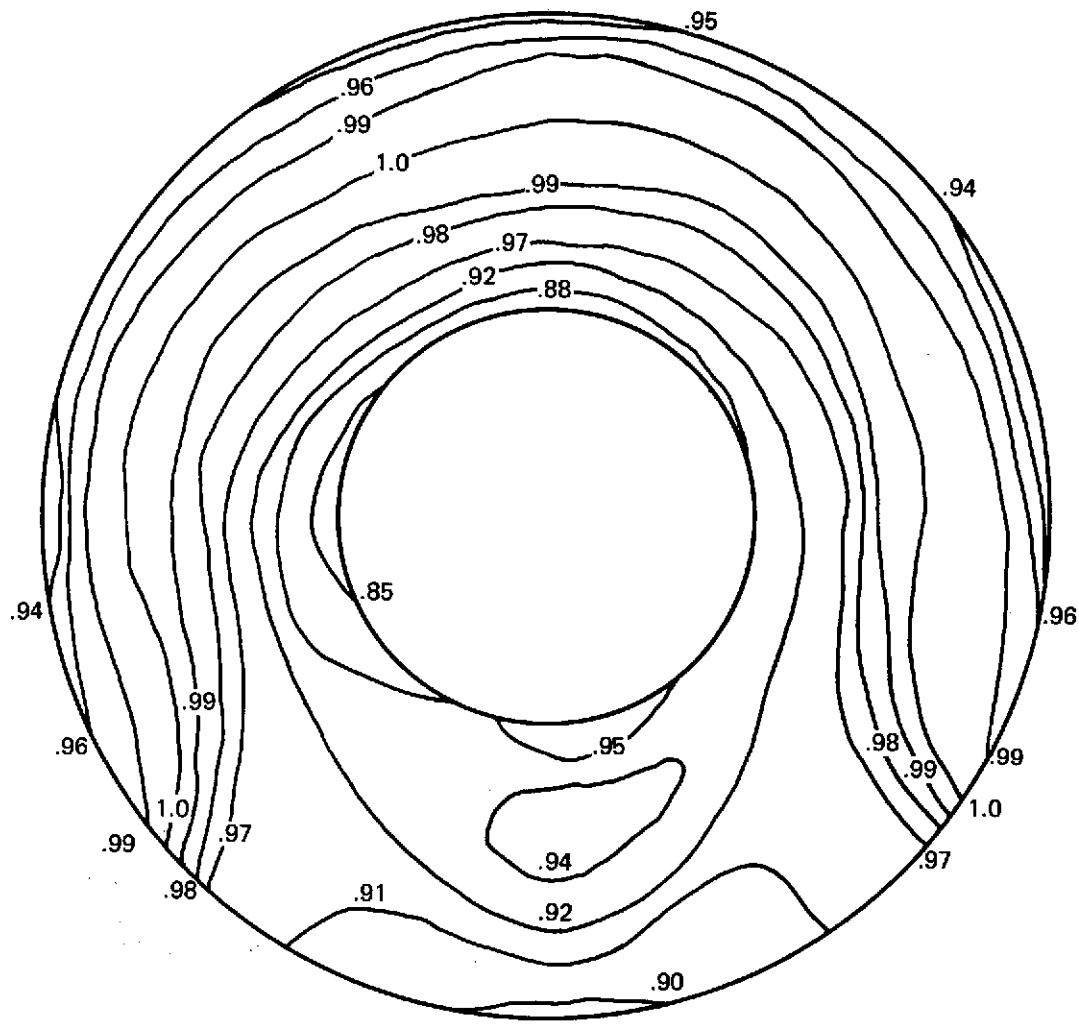


*FIGURE 147.—FAN FACE TOTAL PRESSURE DISTRIBUTION, MACH 0.875, 100-FT/SEC CROSSWIND—RUN 12, MODEL 4*

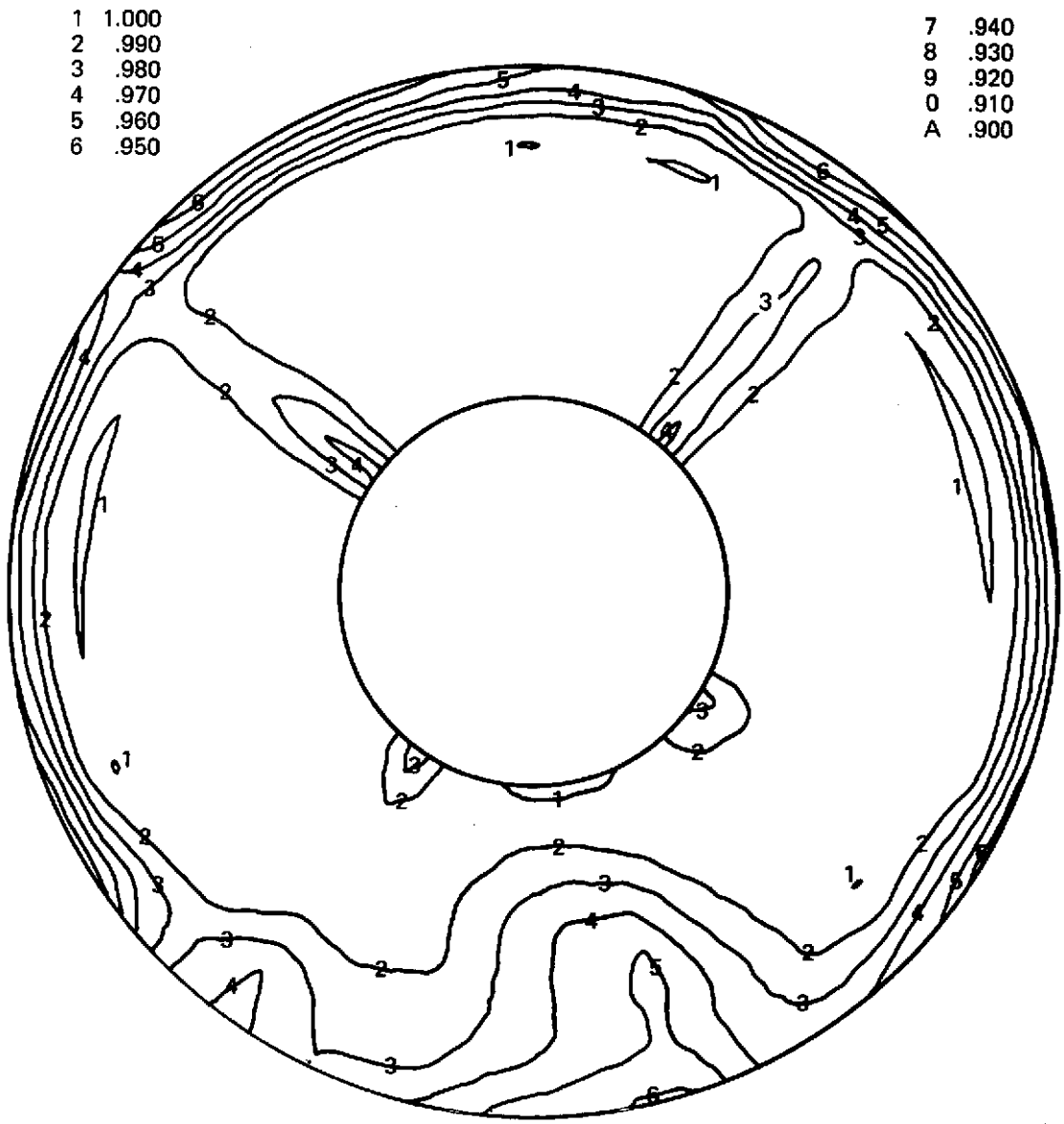


*FIGURE 148.–FAN FACE TOTAL PRESSURE DISTRIBUTION, MACH 0.67, NO CROSSWIND–RUN 14, MODEL 4*

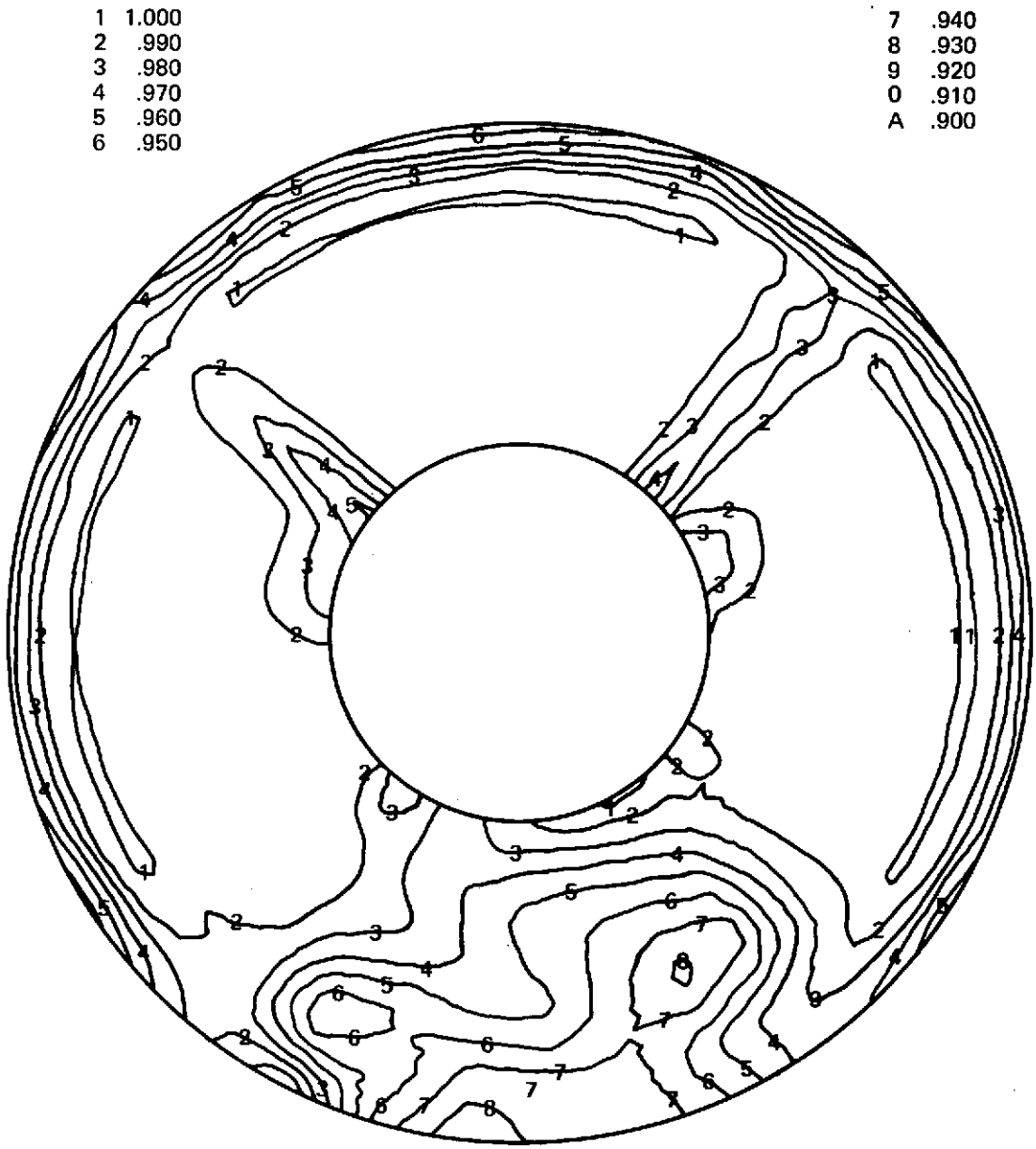


*FIGURE 149.—FAN FACE TOTAL PRESSURE DISTRIBUTION, MACH 0.66, 100-FT/SEC CROSSWIND—RUN 14, MODEL 4*

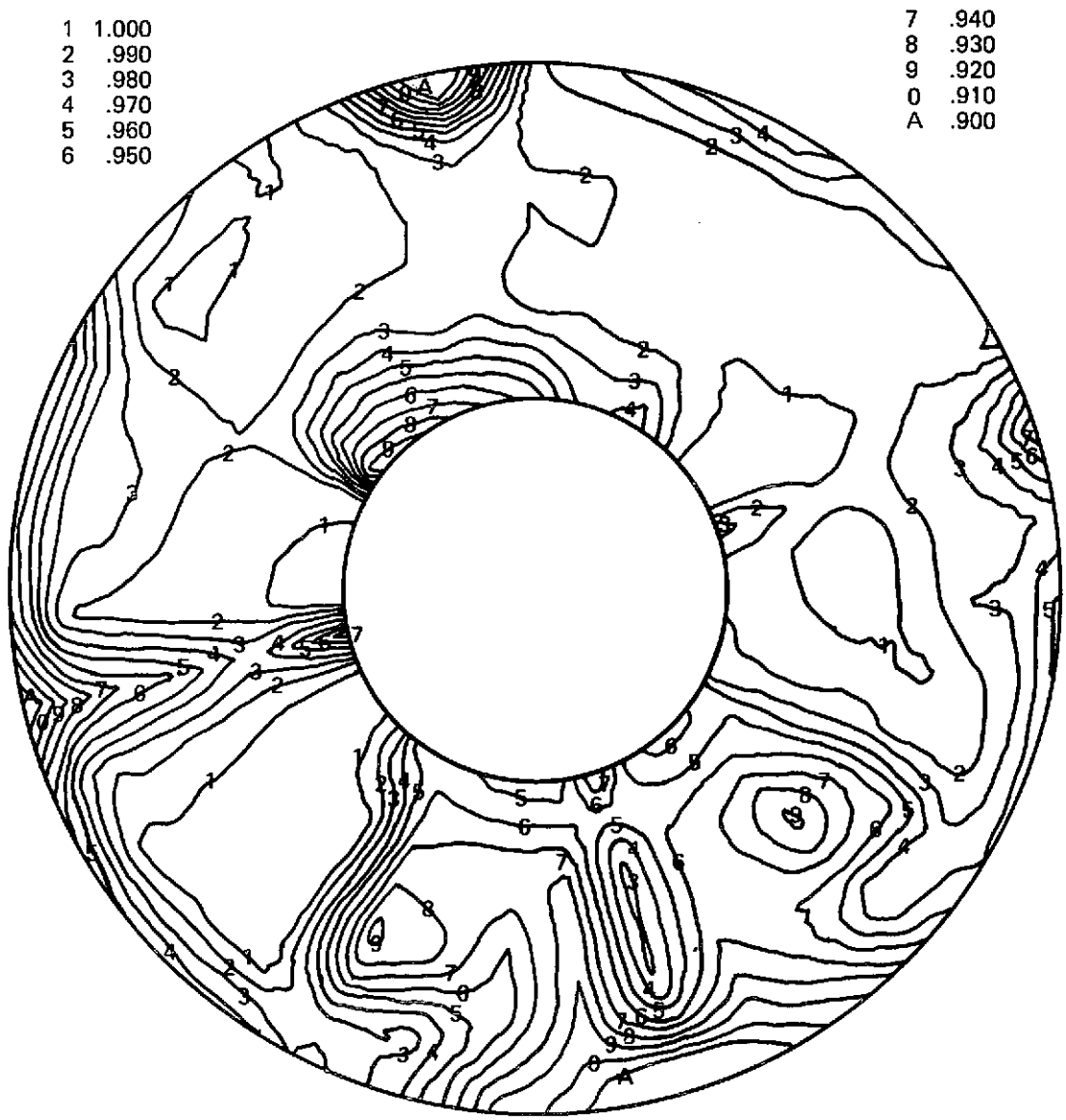


*FIGURE 150.–FAN FACE TOTAL PRESSURE DISTRIBUTION, MACH 0.915, NO CROSSWIND–RUN 14, MODEL 4*

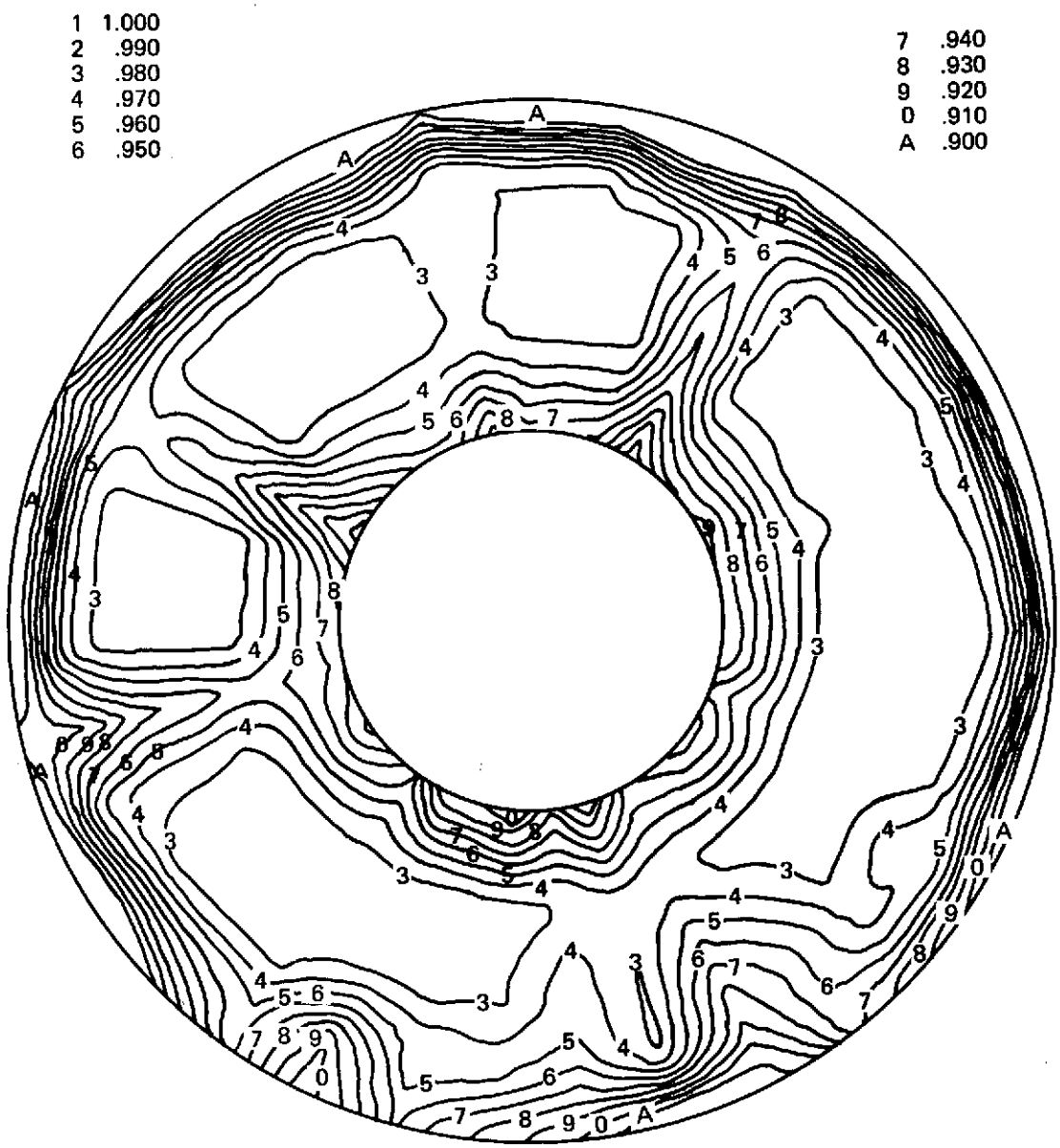


Point no. 14.019
Distortion = 0.093
Recovery = 0.957

Normalized Mach no. = 0.885

*FIGURE 151.—FAN FACE TOTAL PRESSURE DISTRIBUTION, MACH 0.885, 100-FT/SEC CROSSWIND—RUN 14, MODEL 4*

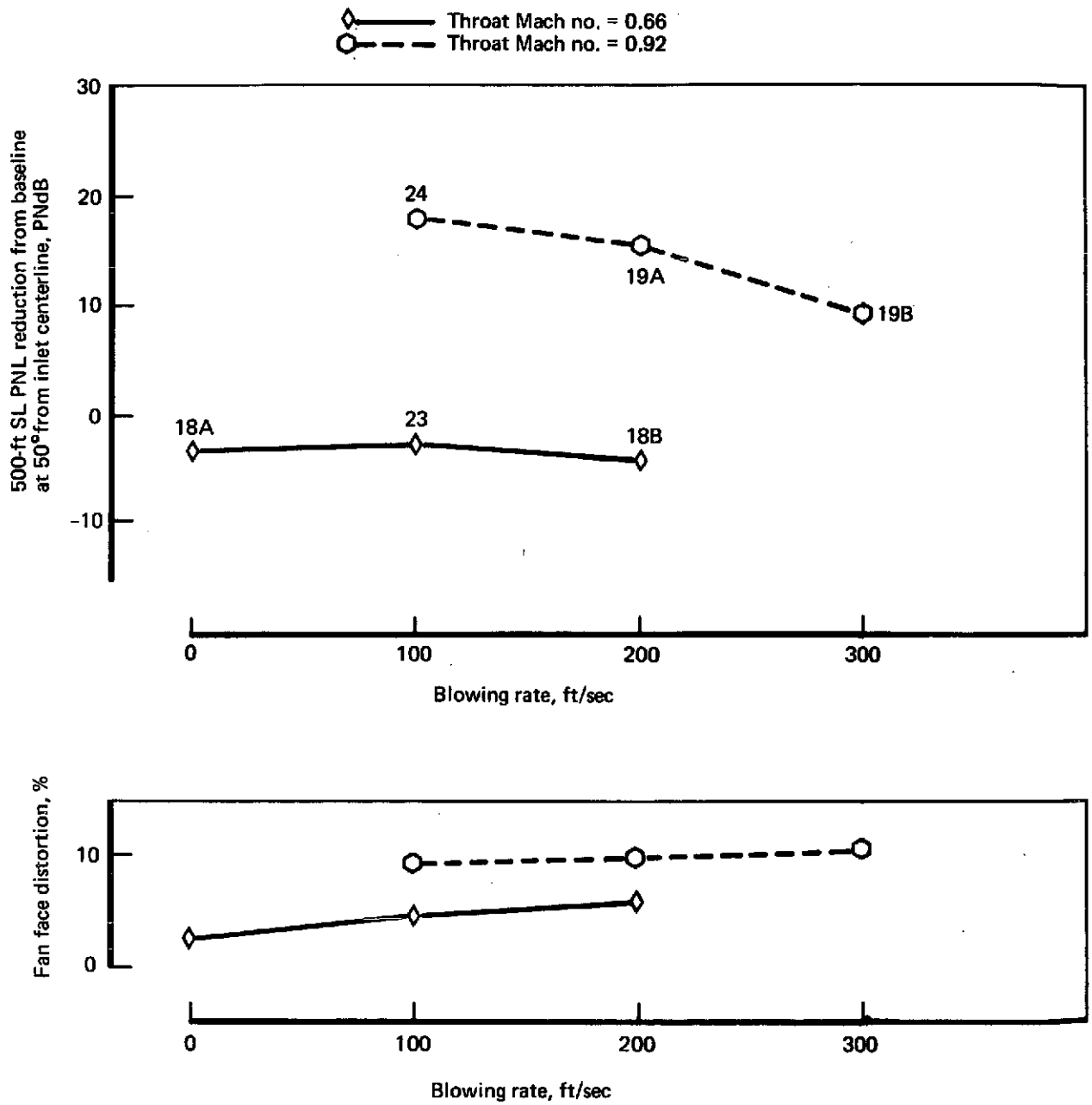


*FIGURE 152.–PNL REDUCTION FROM BASELINE AND PERCENT FAN FACE DISTORTION VS BLOWING RATE (APPROACH)–RUN 11, MODEL 4*

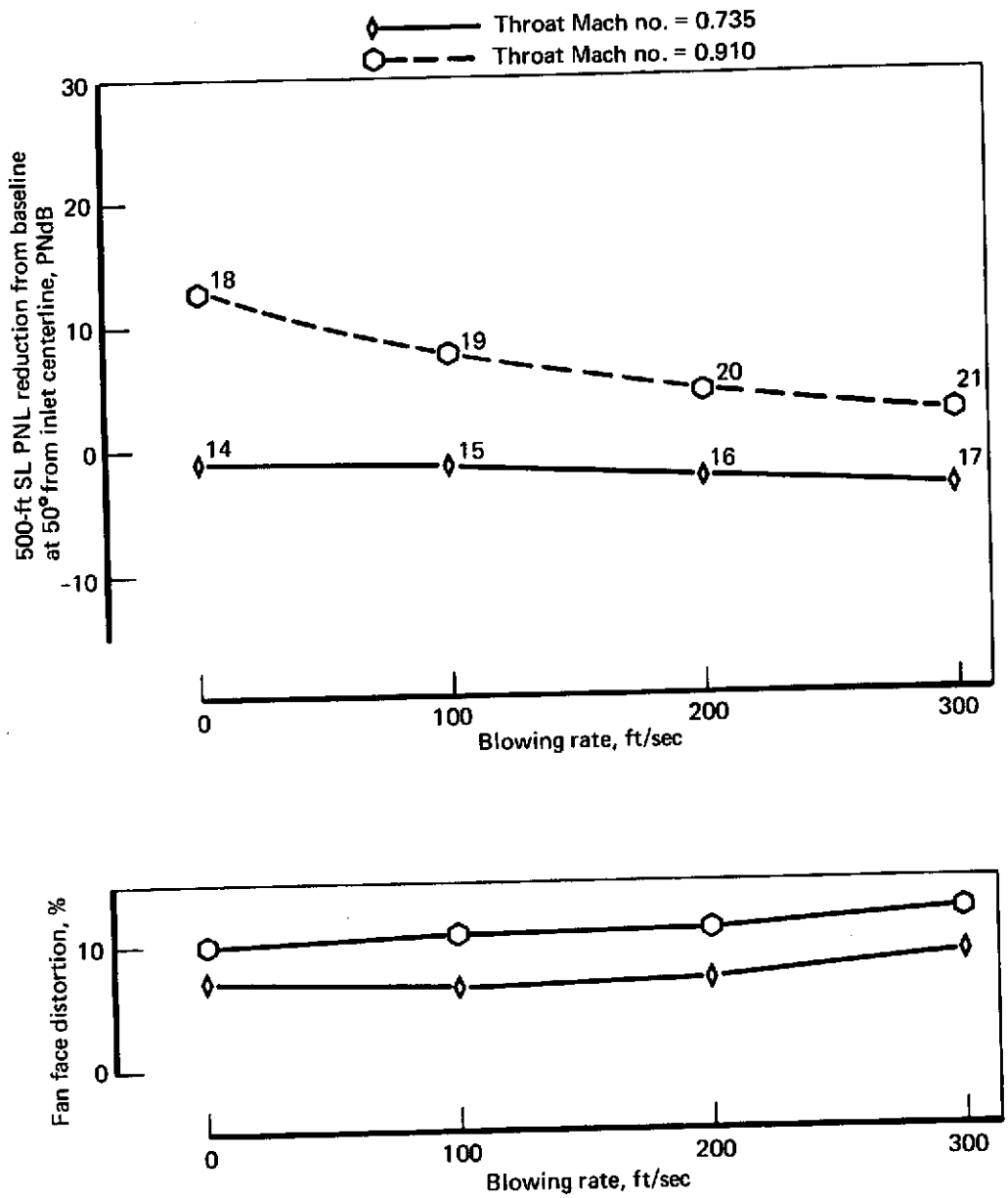


*FIGURE 153.–PNL REDUCTION FROM BASELINE AND PERCENT FAN FACE DISTORTION VS BLOWING RATE (APPROACH)RUN 13, MODEL 5B*

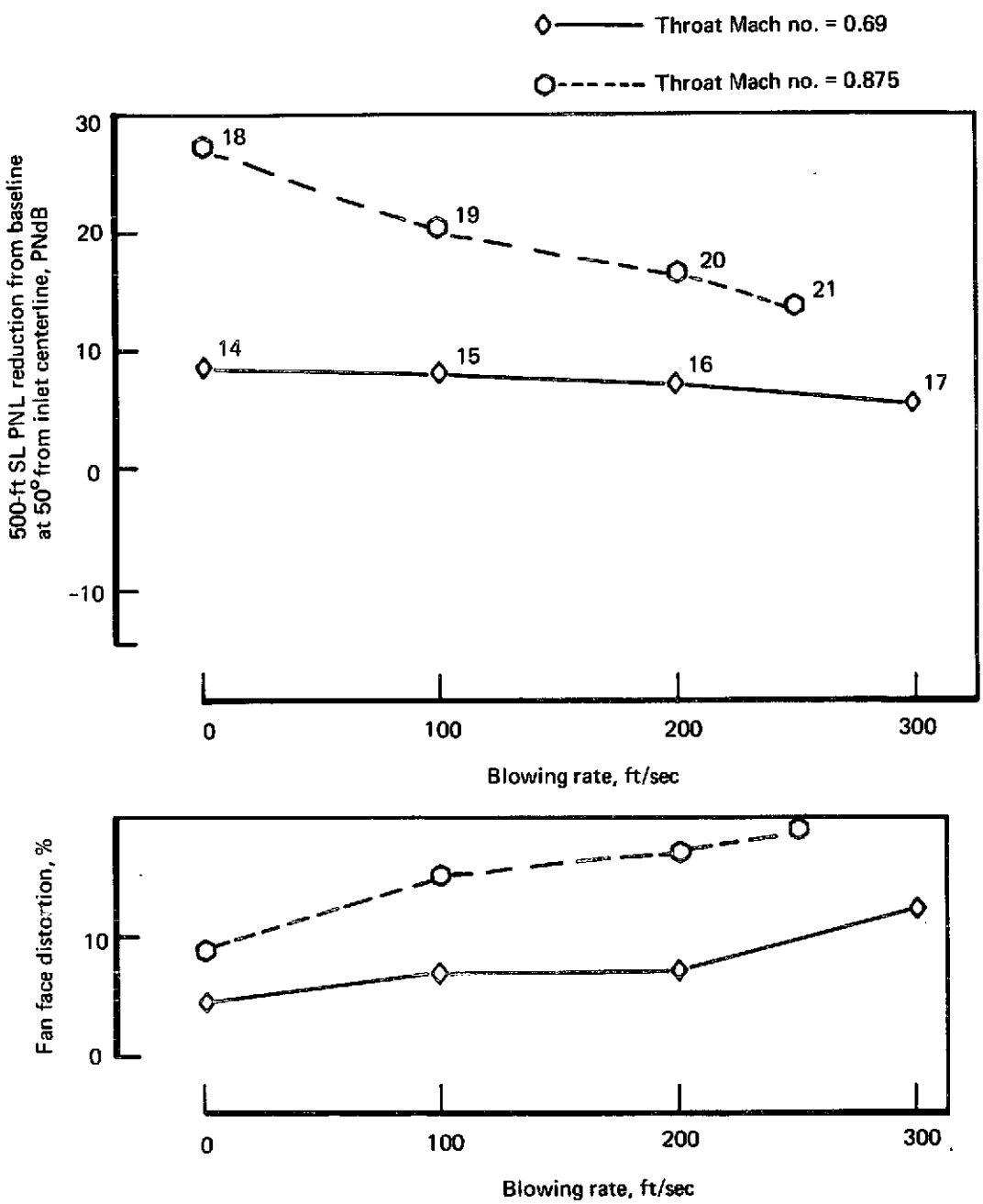


*FIGURE 154.–PNL REDUCTION FROM BASELINE AND PERCENT FAN FACE DISTORTION VS BLOWING RATE (TAKEOFF)–RUN 12, MODEL 4*

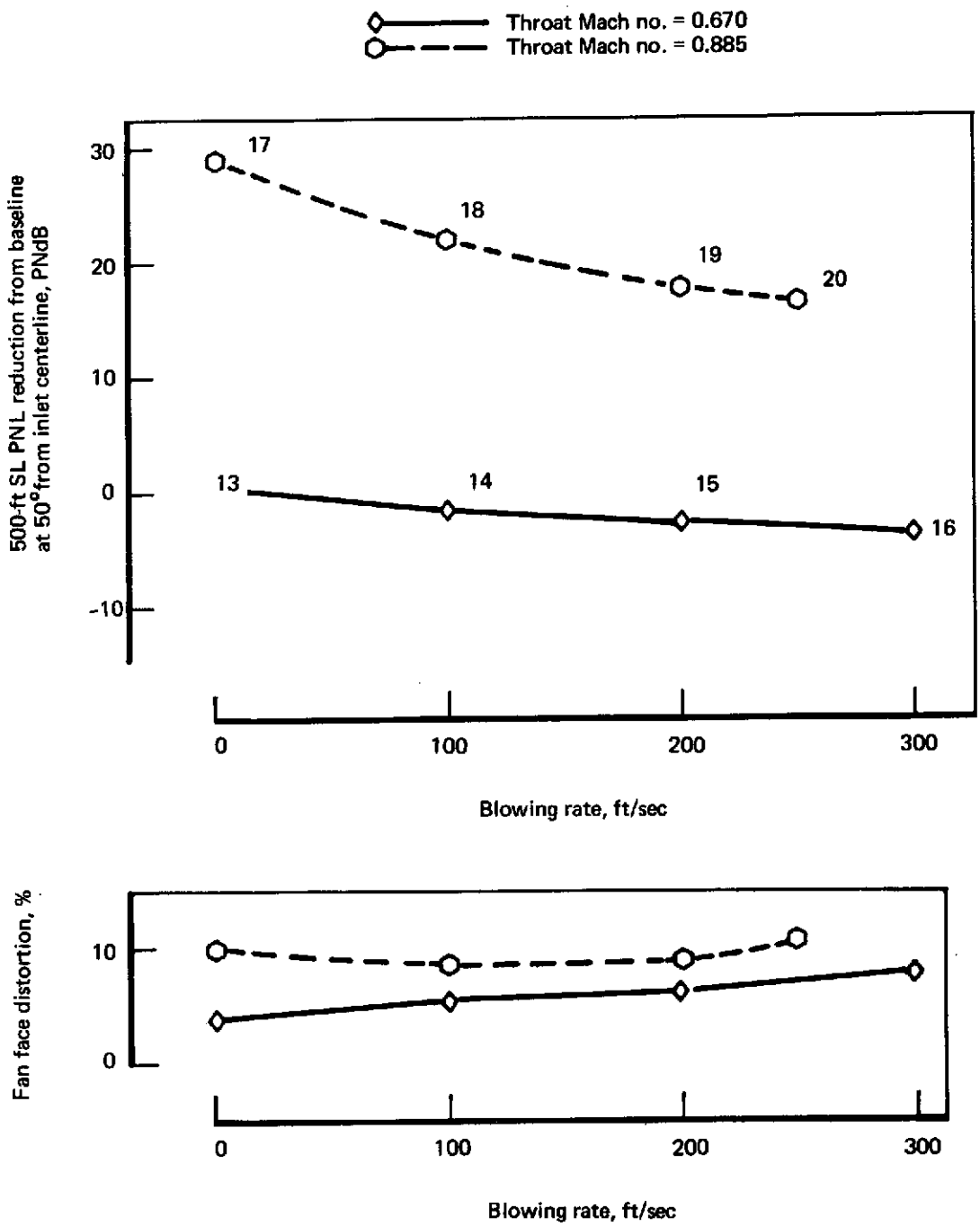


*FIGURE 155.–PNL REDUCTION FROM BASELINE AND PERCENT FAN FACE DISTORTION VS BLOWING RATE (TAKEOFF)–RUN 14, MODEL 5B*

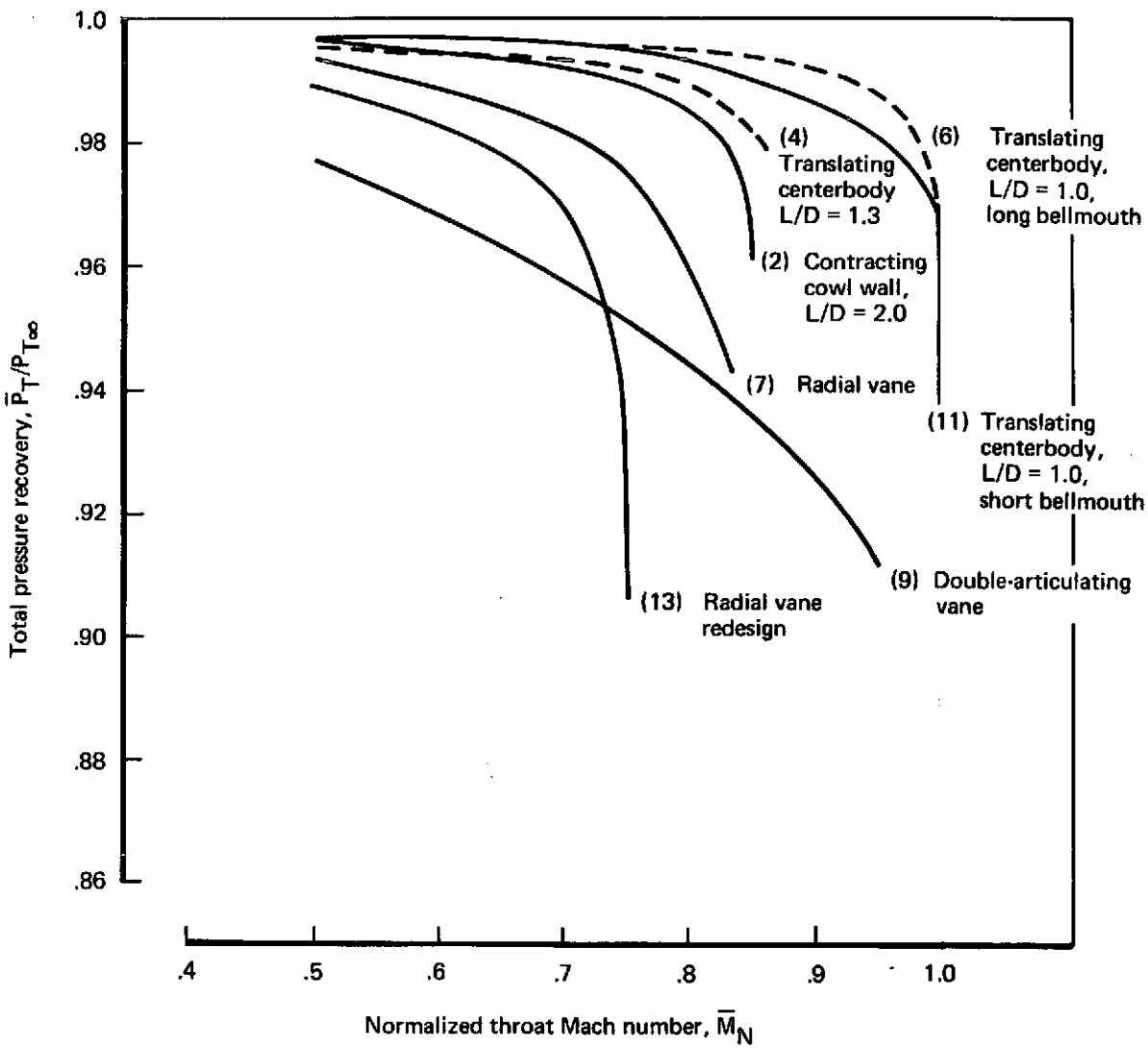


*FIGURE 156.—COMPARISON OF INLET RECOVERY VS MASS-FLOW-DERIVED THROAT MACH NUMBER (APPROACH)*

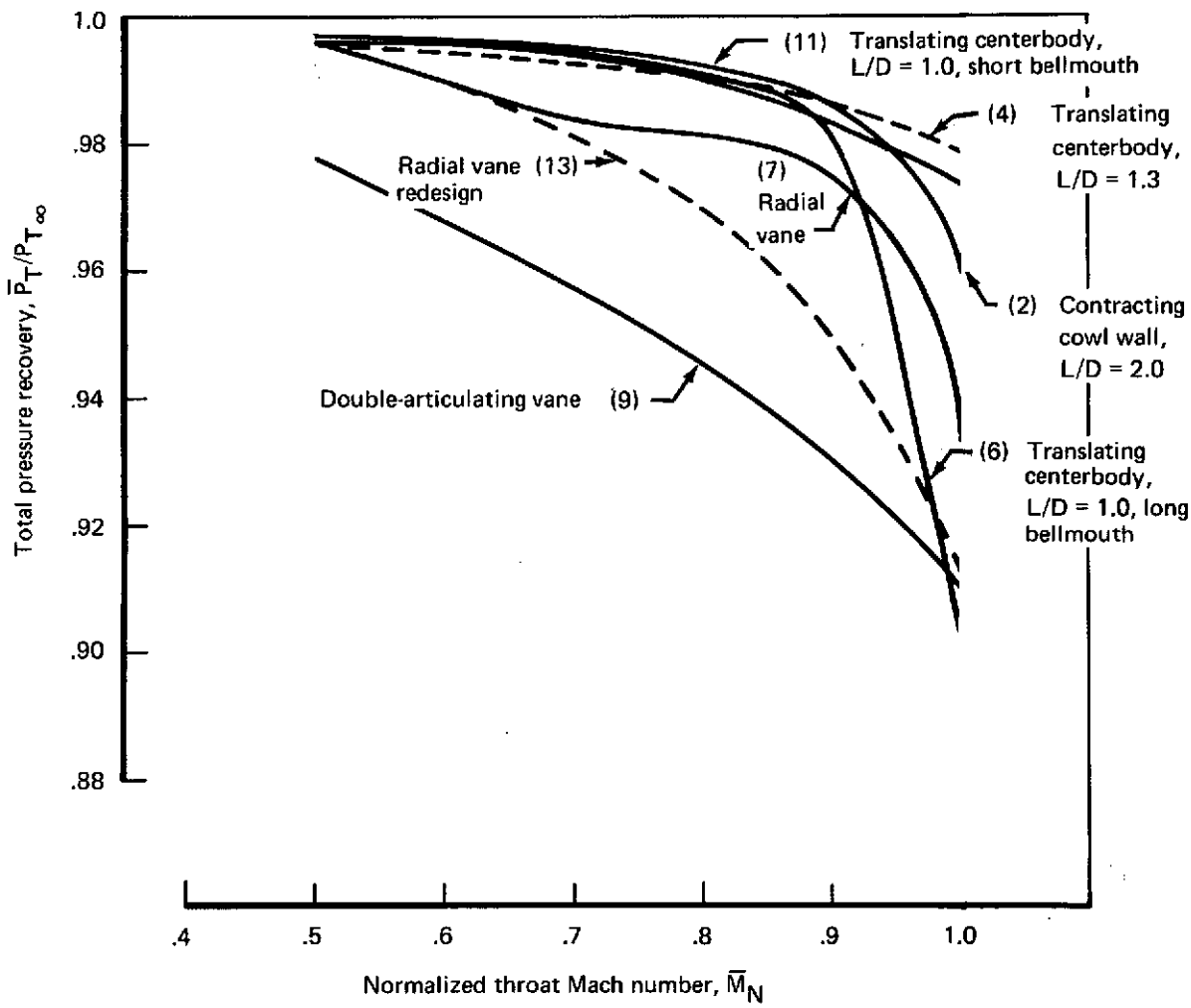


*FIGURE 157.—COMPARISON OF INLET RECOVERY VS NORMALIZED THROAT MACH NUMBER (APPROACH)*

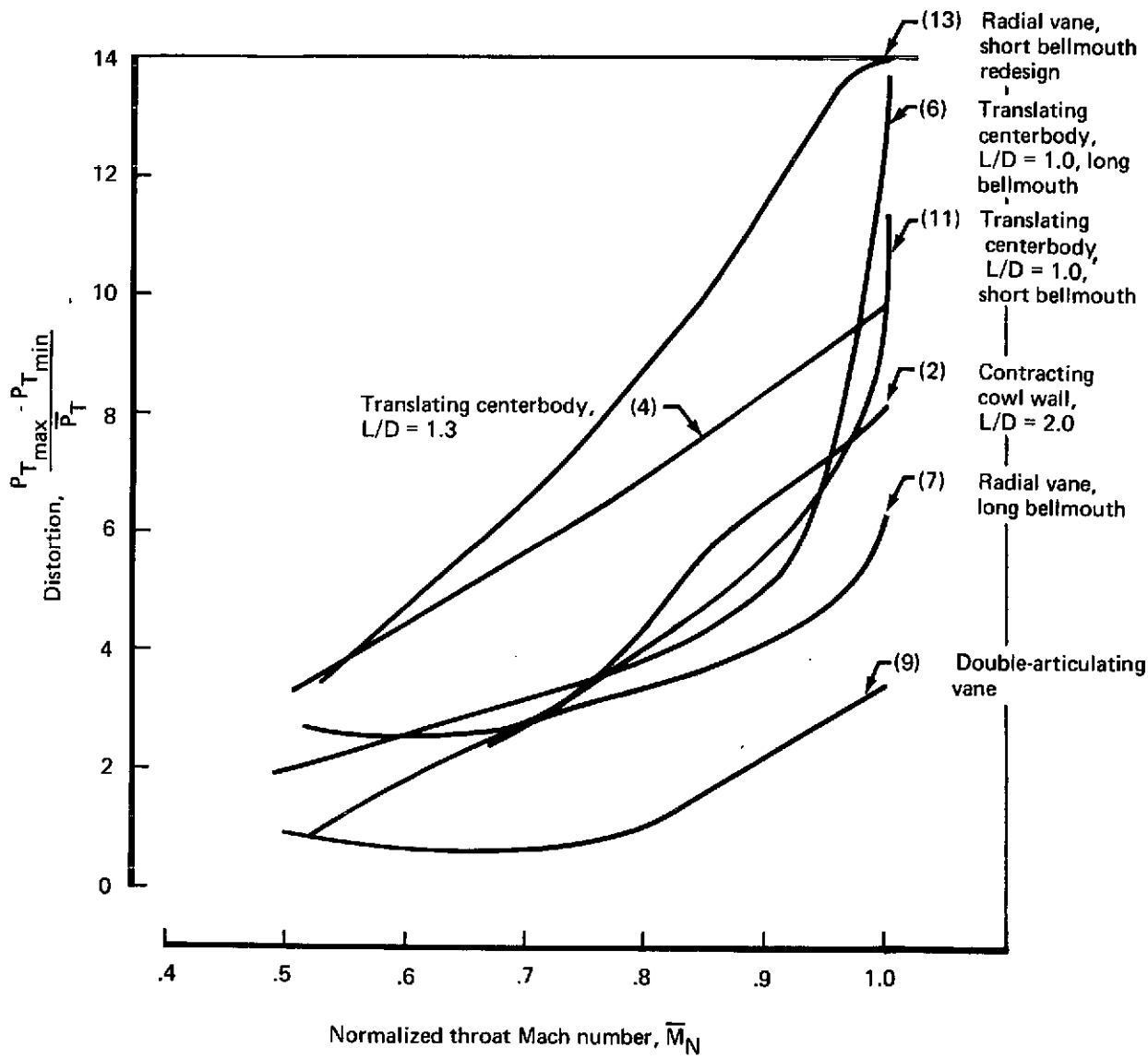


*FIGURE 158.—COMPARISON OF INLET DISTORTION VS NORMALIZED THROAT MACH NUMBER (APPROACH)*

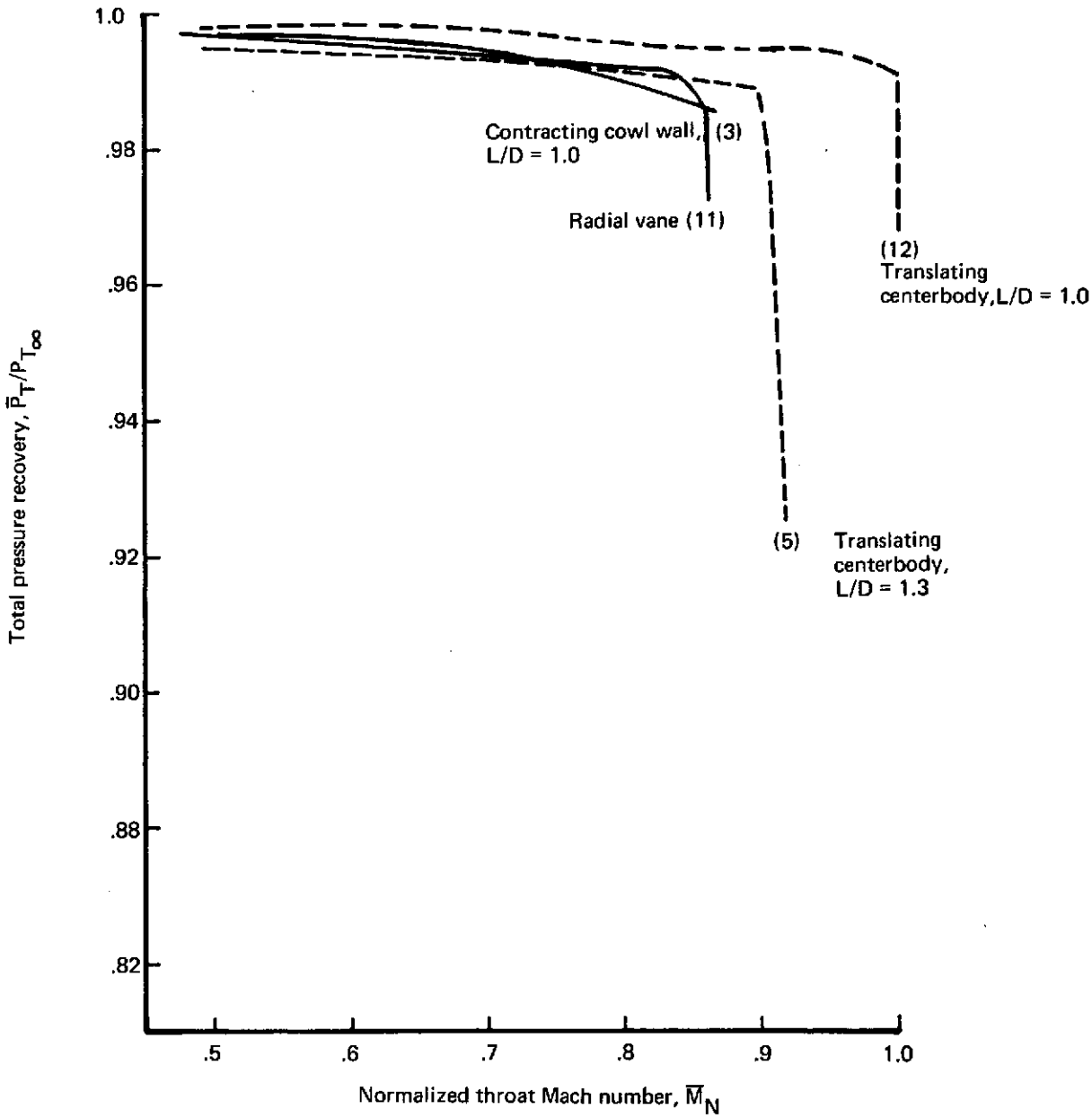


*FIGURE 159.–COMPARISON OF INLET RECOVERY VS MASS-FLOW DERIVED MACH NO. TAKE-OFF CONFIGURATION*

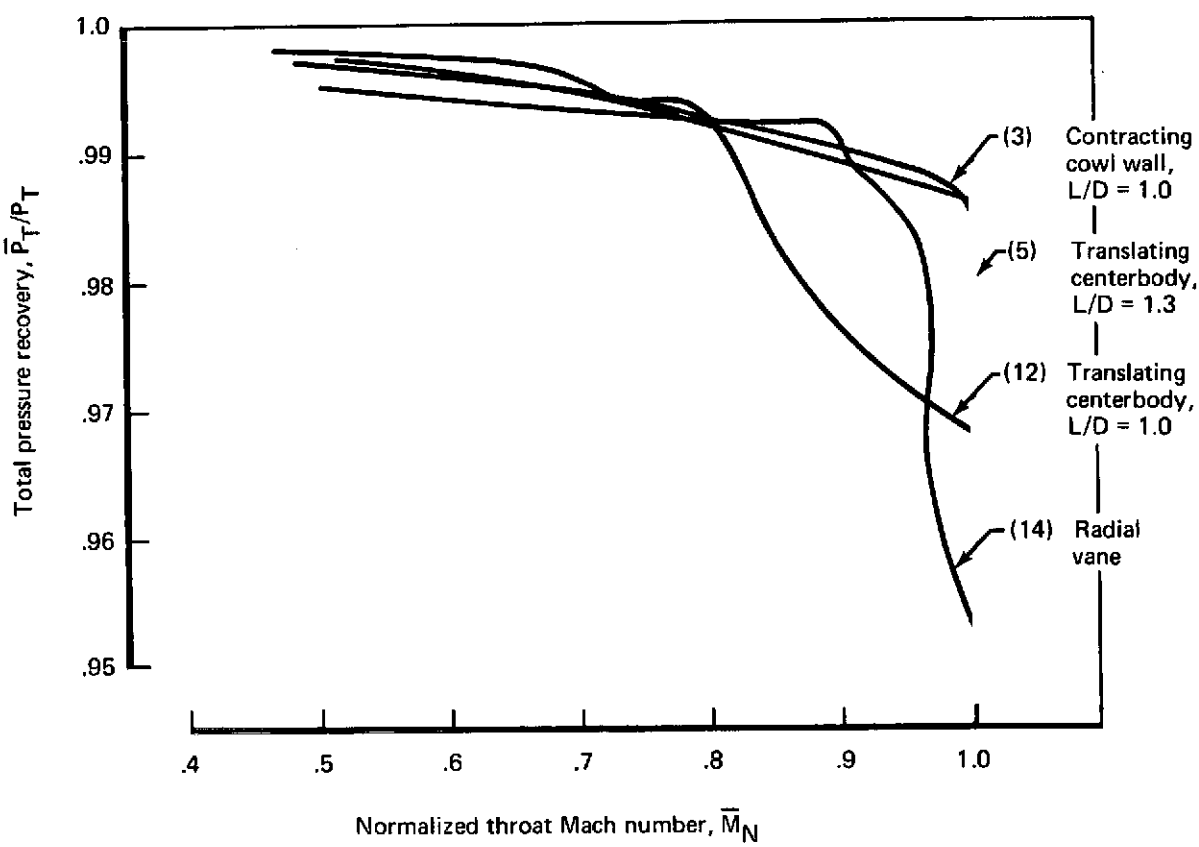


*FIGURE 160.—COMPARISON OF INLET RECOVERY VS NORMALIZED THROAT MACH NUMBER (TAKEOFF)*

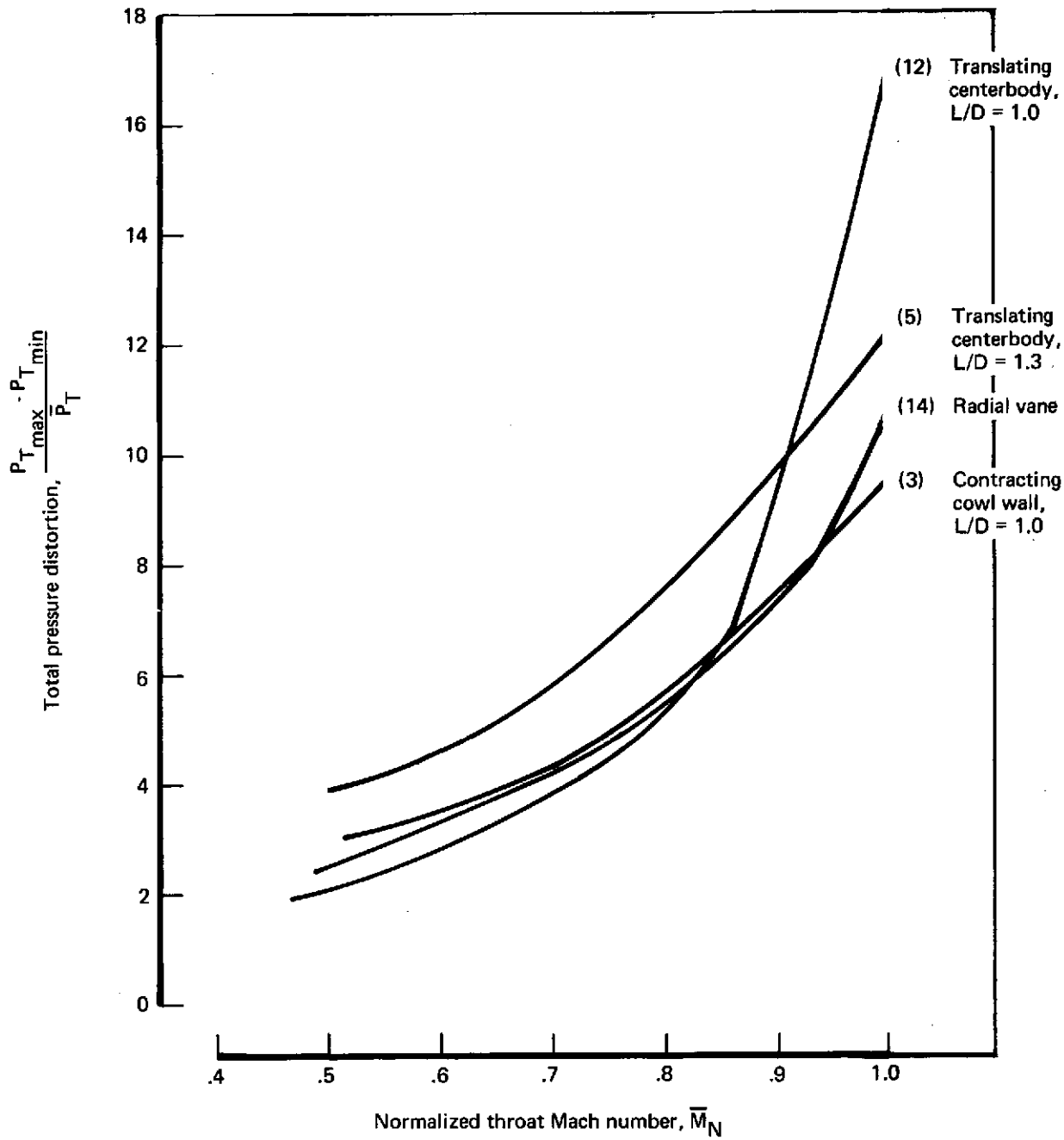


*FIGURE 161.—COMPARISON OF INLET DISTORTION VS NORMALIZED THROAT MACH NUMBER (TAKEOFF)*

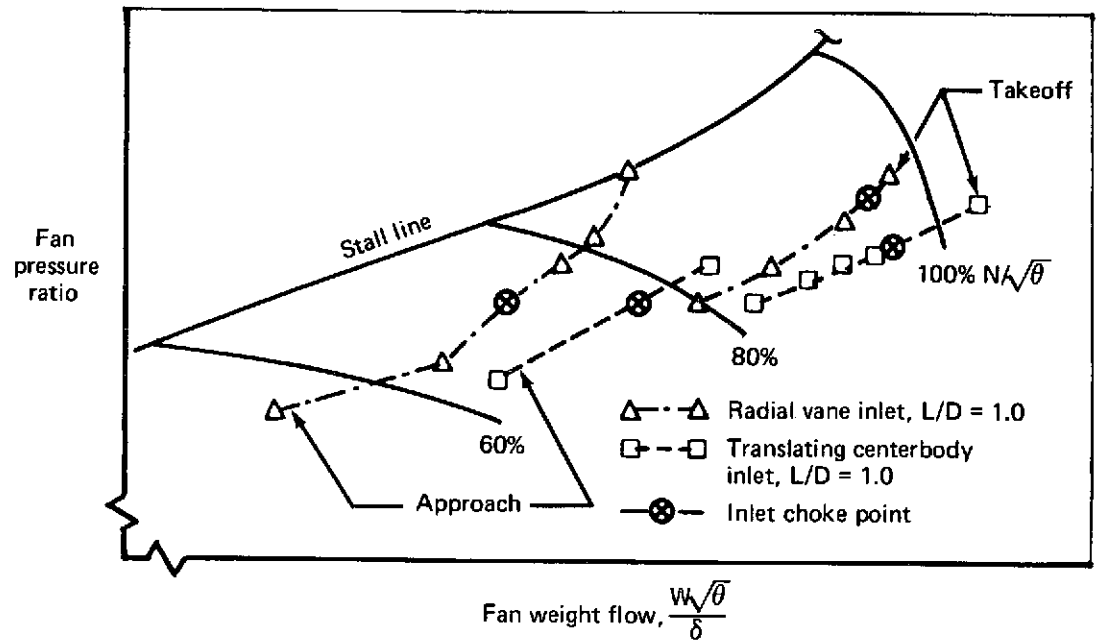


*FIGURE 162.–FAN OPERATING LINES WITH SONIC INLETS*

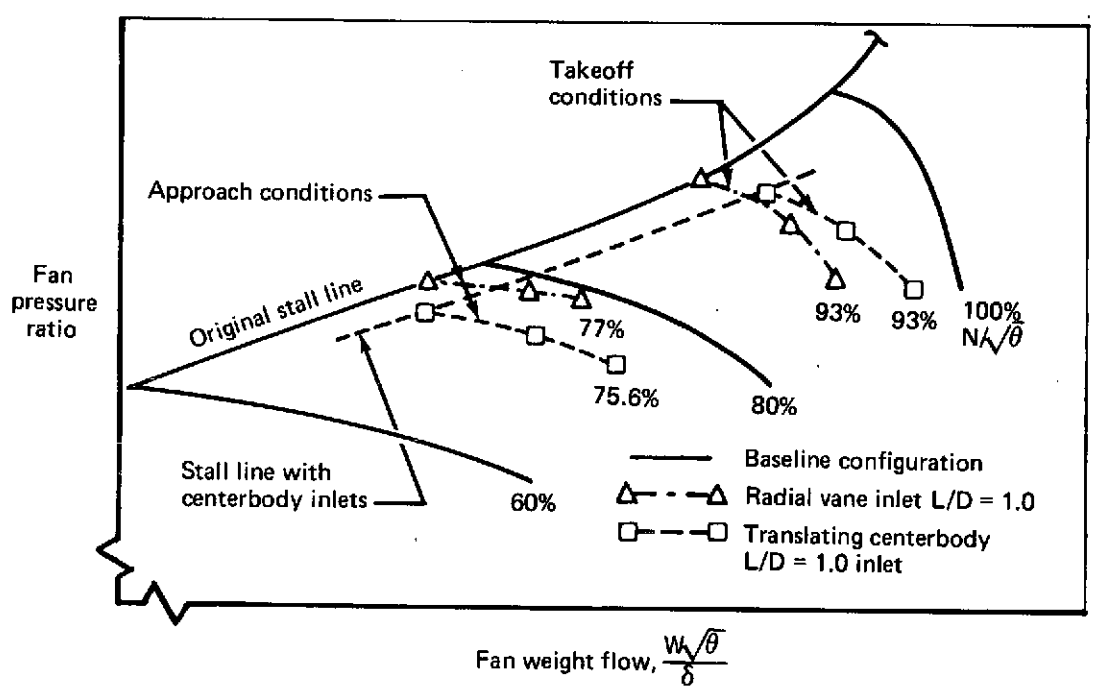


*FIGURE 163.–EFFECT OF SONIC INLETS ON FAN STALL LINE*

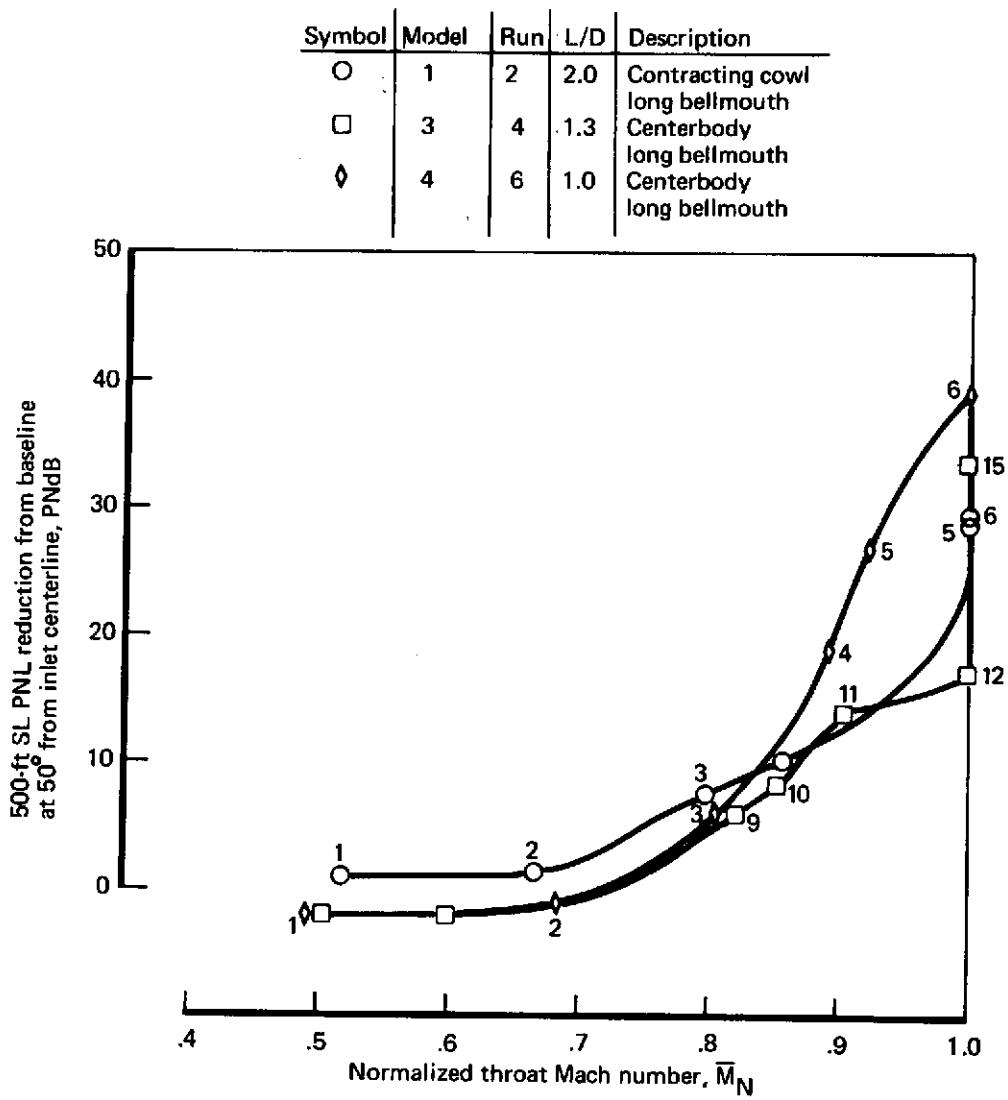


*FIGURE 164.—PNL REDUCTION FROM BASELINE VS NORMALIZED THROAT MACH NUMBER, SINGLE-PASSAGE INLETS (APPROACH)*

| Symbol | Model | Run | L/D | Description |
|---|---|---|---|---|
| O | 1 | 2 | 2.0 | Contracting cowl long bellmouth |
| D | 3 | 4 | 1.3 | Centerbody long bellmouth |
| Δ | 4 | 6 | 1.0 | Centerbody long bellmouth |

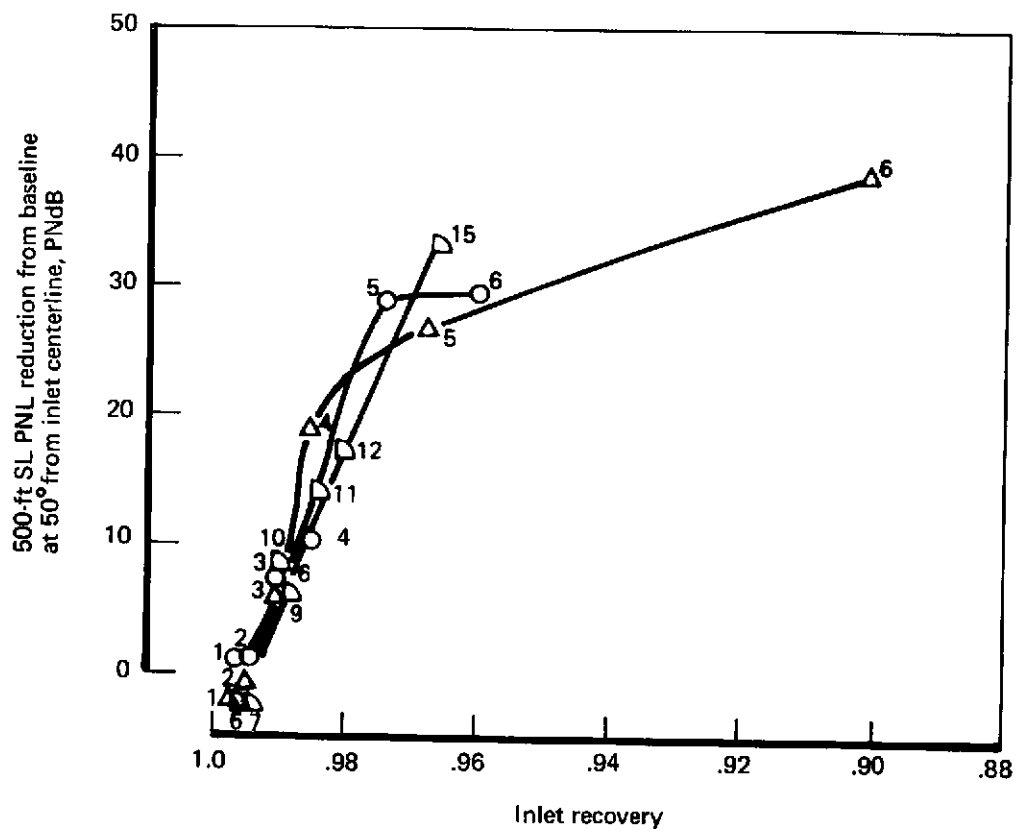


*FIGURE 165.—PNL REDUCTION VS INLET RECOVERY, SINGLE-PASSAGE INLETS (APPROACH), SCALED-UP DATA*

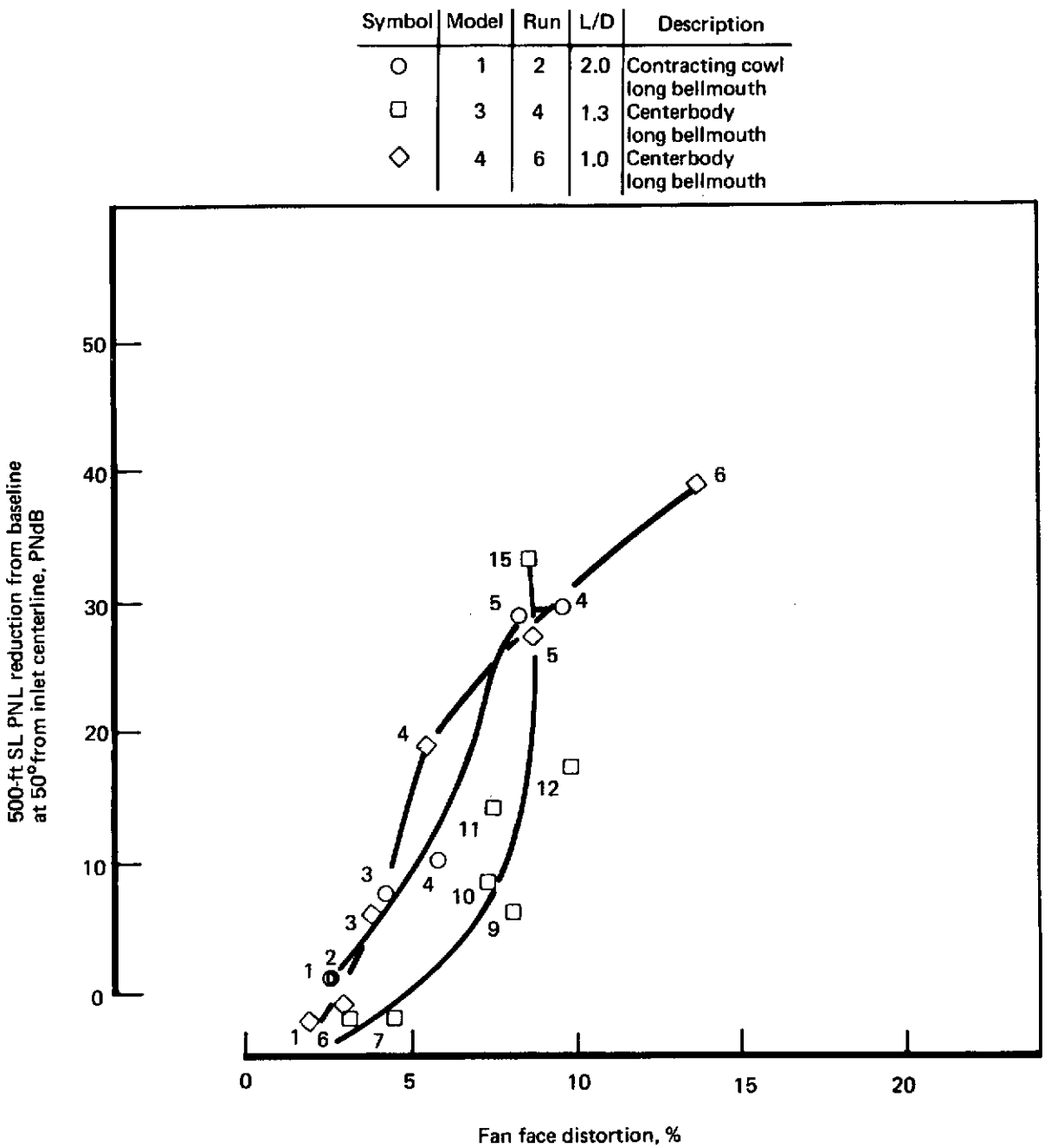


*FIGURE 166.—PNL REDUCTION VS PERCENT FAN FACE DISTORTION, SINGLE-PASSAGE INLETS (APPROACH) SCALED-UP DATA*

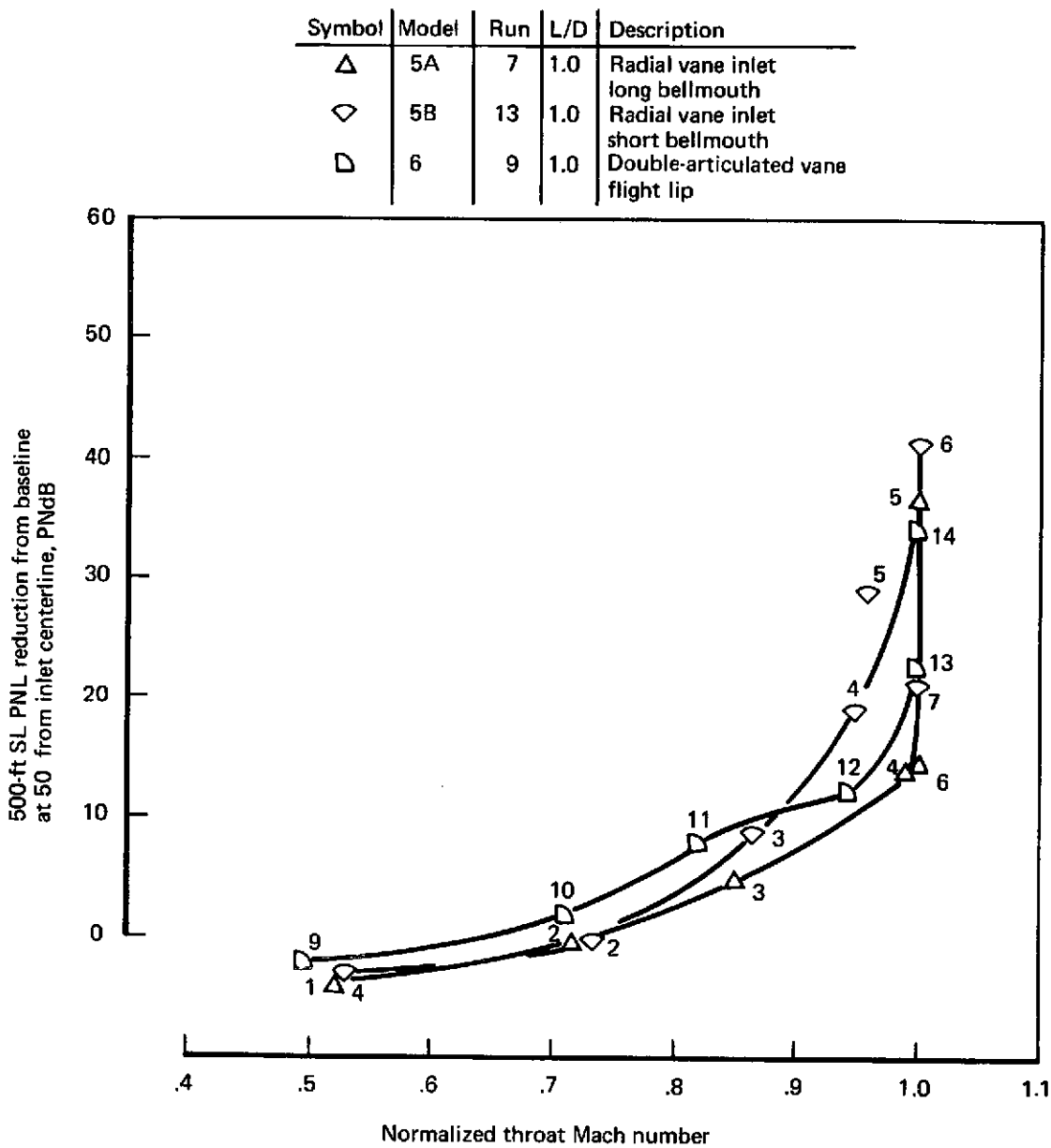


*FIGURE 167.—PNL REDUCTION FROM BASELINE VS NORMALIZED THROAT MACH NUMBER, MULTIPASSAGE INLETS (APPROACH), SCALED-UP DATA*

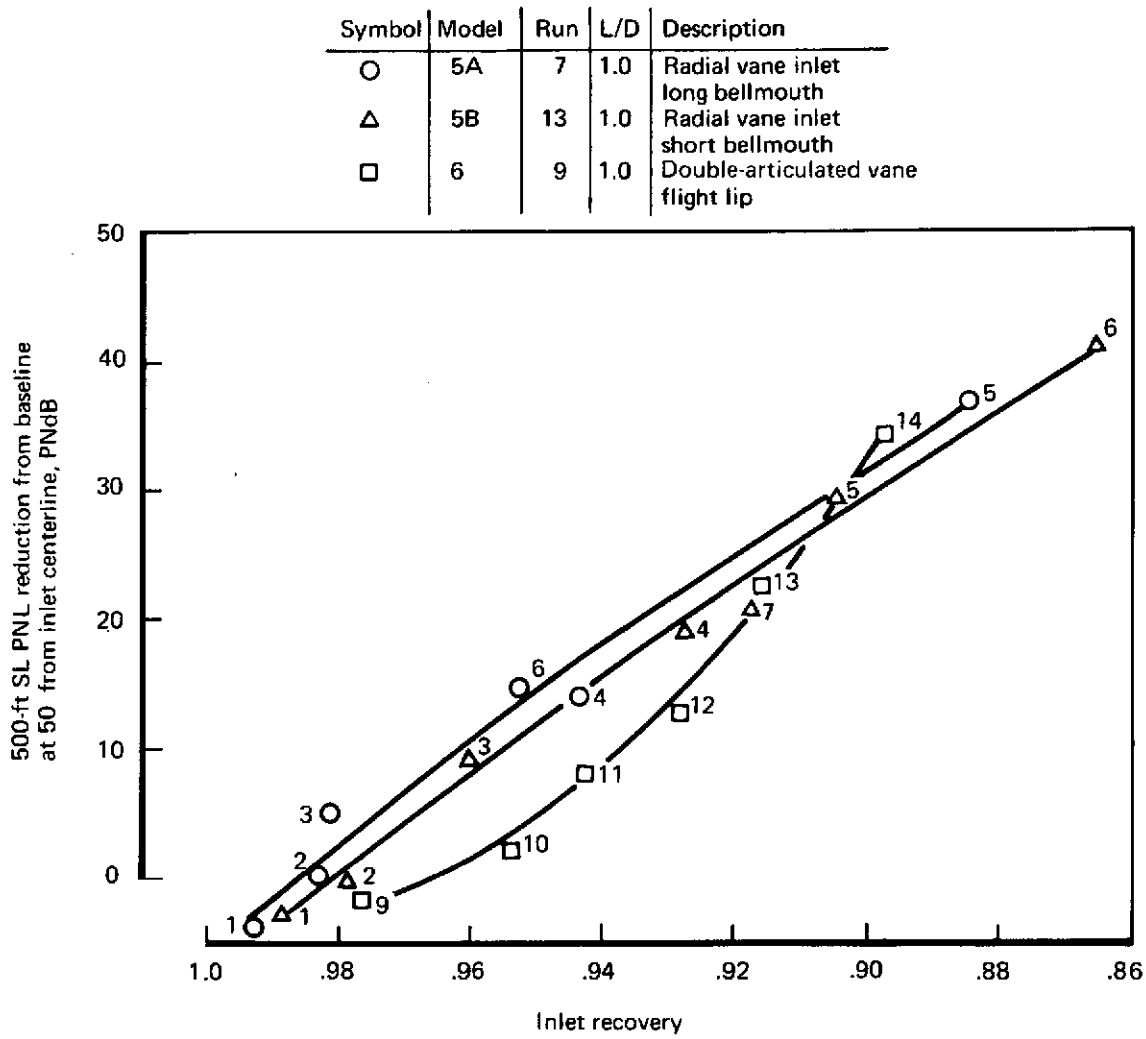


*FIGURE 168.–PNL REDUCTION VS INLET RECOVERY, MULTIPASSAGE INLETS (APPROACH), SCALED-UP DATA*

| Symbol | Model | Run | L/D | Description |
|---|---|---|---|---|
| ○ | 5A | 7 | | Radial vane inlet long bellmouth |
| □ | 5B | 13 | | Radial vane inlet short bellmouth |
| ◊ | 6 | 9 | | Double-articulated vane flight lip |

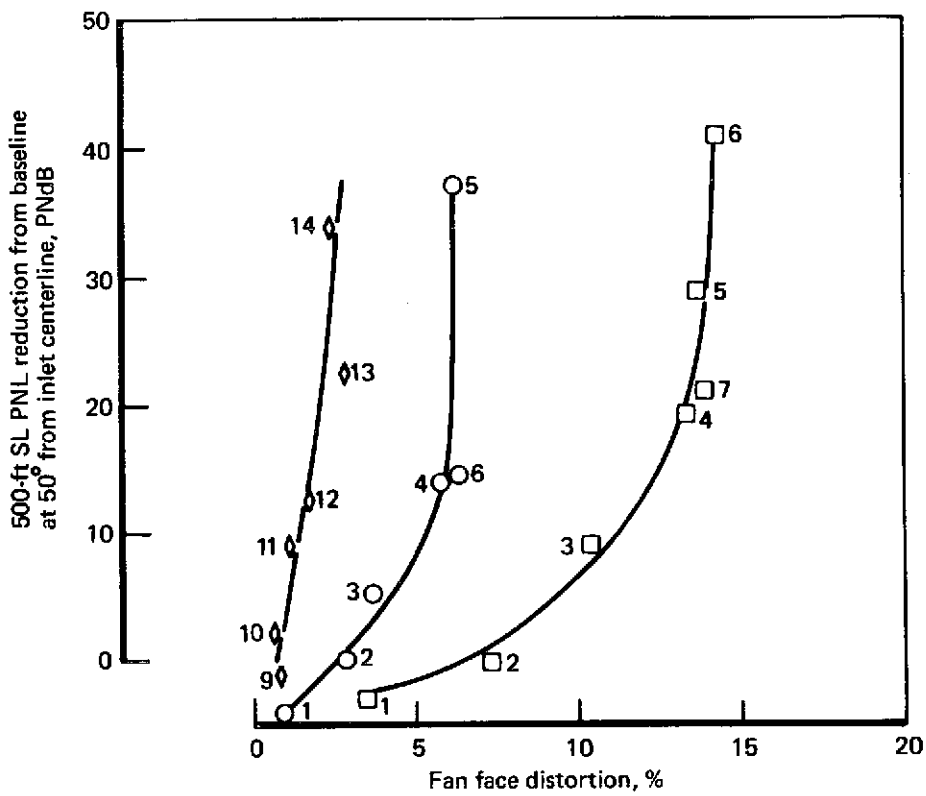


*FIGURE 169.– PNL REDUCTION VS PERCENT FAN FACE DISTORTION, MULTIPASSAGE INLETS (APPROACH), SCALED-UP DATA*

| Symbol | Model | Run | L/D | Description |
|---|---|---|---|---|
| △ | 3 | 4 | 1.3 | Unlined |
| ◊ | 3A | 101 | 1.3 | Lining added to internal surfaces |
| □ | 3B | 102 | 1.3 | Lining added to internal cowl surface and diffuser section of centerbody |
| ○ | 3C | 10 | 1.3 | Lining added to diffuser section only |

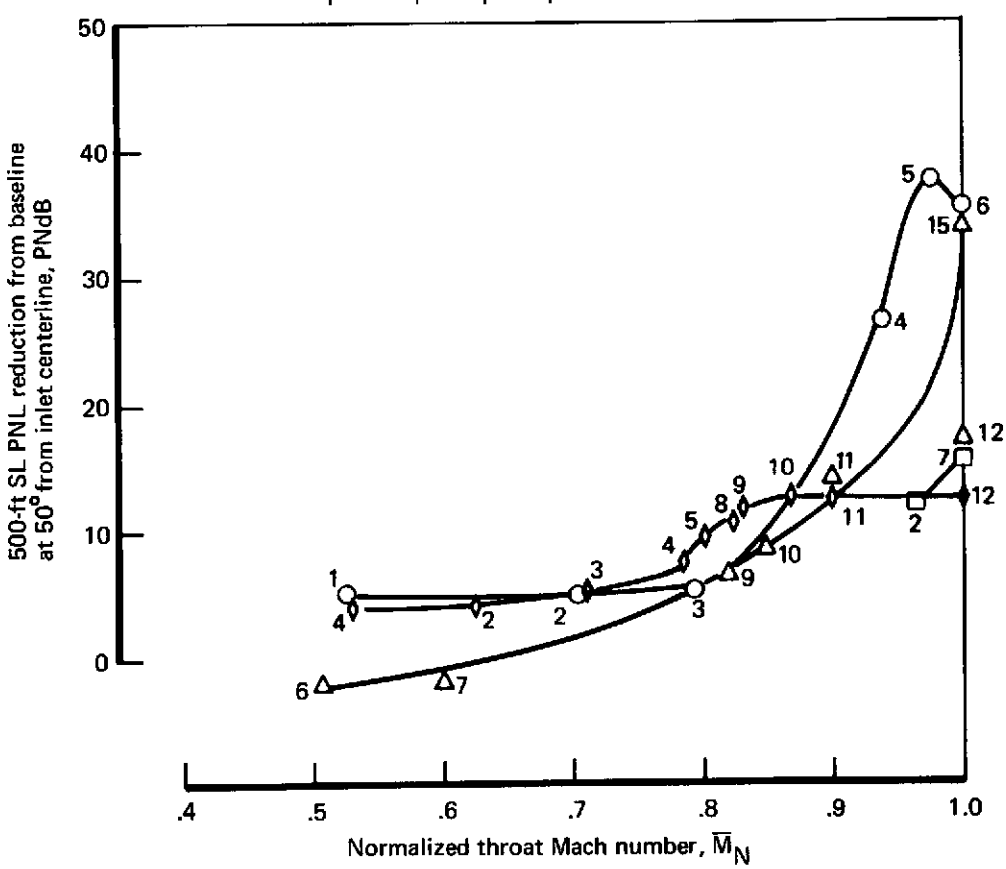


*FIGURE 170.— PNL REDUCTION FROM BASELINE VS NORMALIZED THROAT MACH NUMBER, ACOUSTICALLY TREATED INLETS (APPROACH), SCALED-UP DATA*

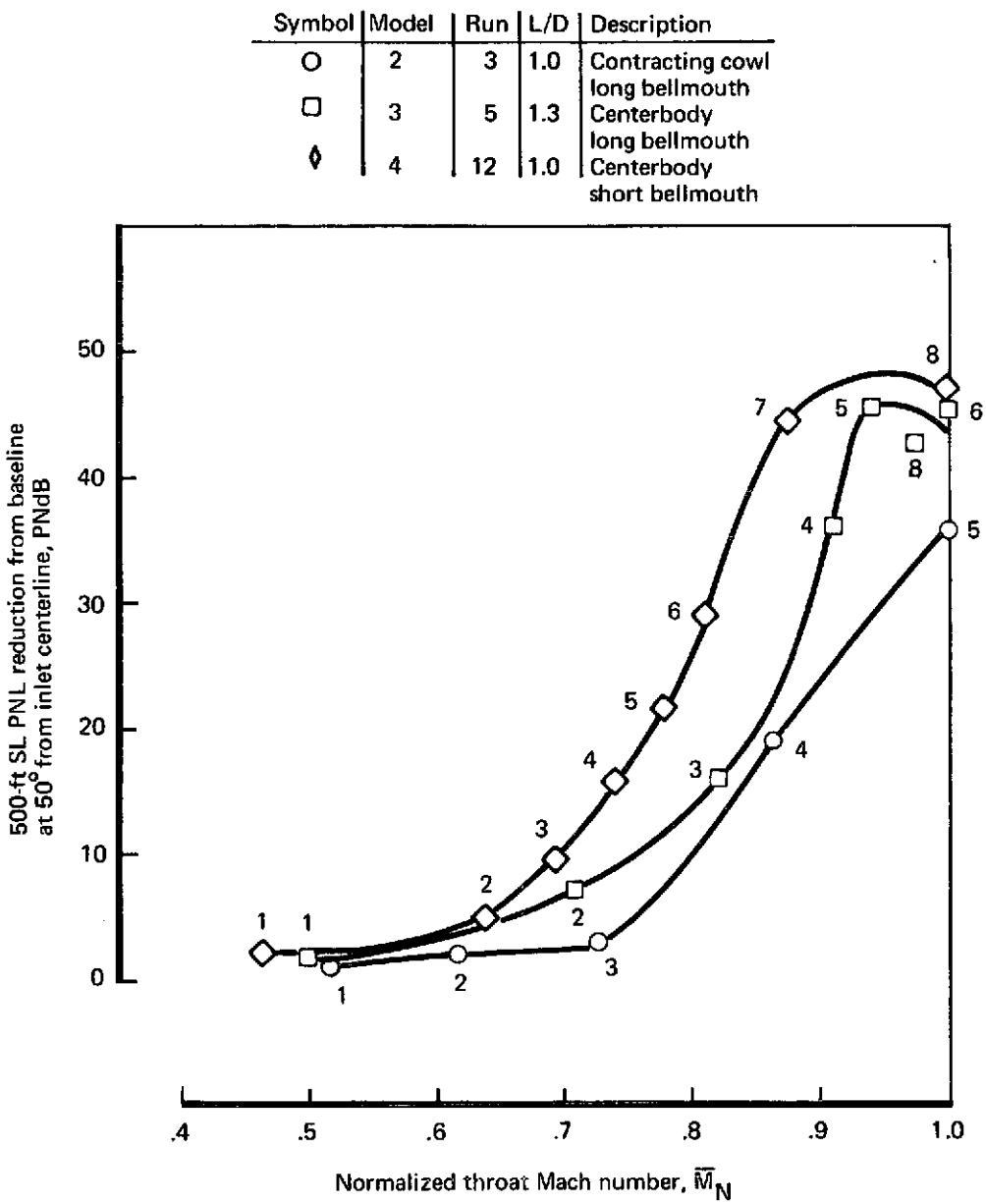


*FIGURE 171.—PNL REDUCTION FROM BASELINE VS NORMALIZED THROAT MACH NUMBER, SINGLE-PASSAGE INLETS (TAKEOFF), SCALED-UP DATA*

| Symbol | Model | Run | L/D | Description |
|---|---|---|---|---|
| ○ | 2 | 3 | 1.0 | Contracting cowl long bellmouth |
| △ | 3 | 5 | 1.3 | Centerbody long bellmouth |
| □ | 4 | 12 | 1.0 | Centerbody short bellmouth |

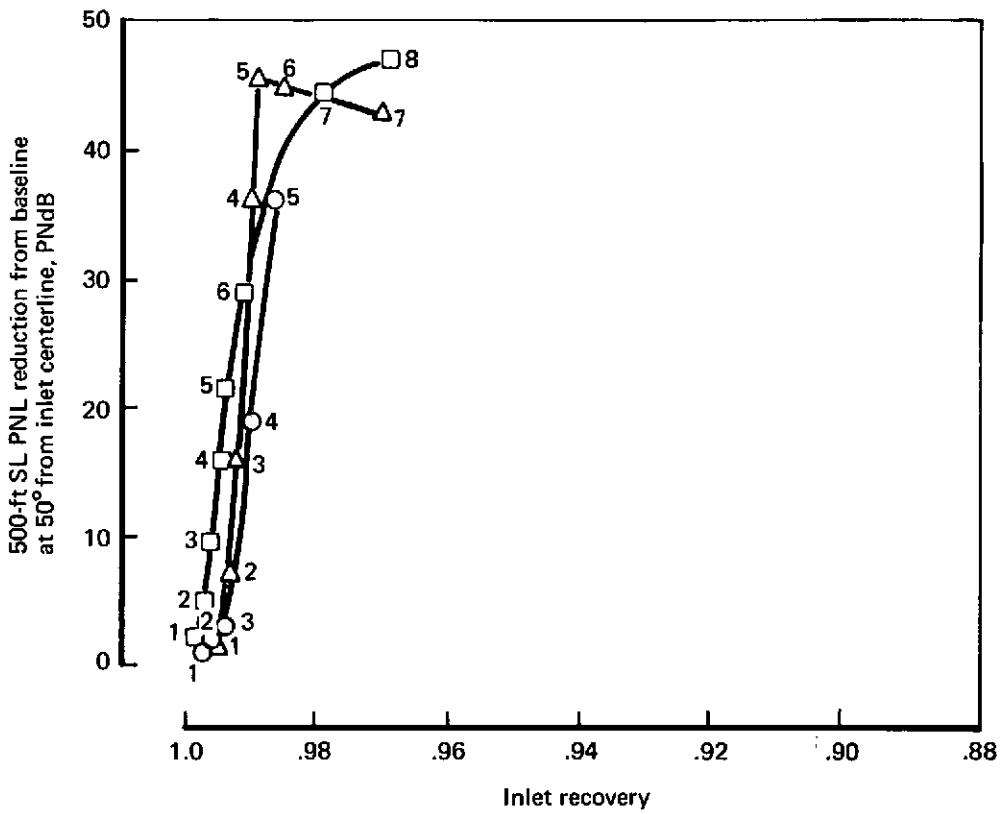


*FIGURE 172.—PNL REDUCTION VS INLET RECOVERY, SINGLE-PASSAGE INLETS (TAKEOFF), SCALED-UP DATA*

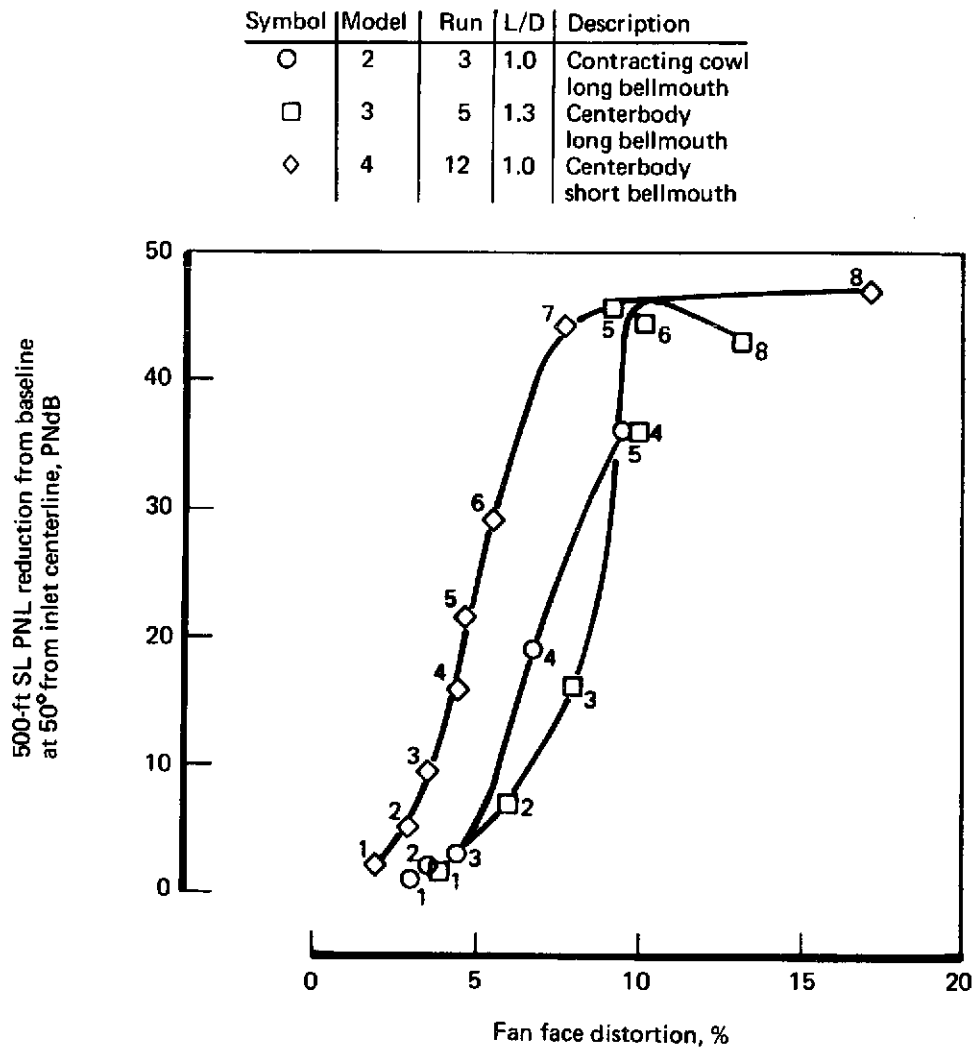


*FIGURE 173.– PNL REDUCTION VS PERCENT FAN FACE DISTORTION, SINGLE-PASSAGE INLETS (TAKEOFF), SCALED-UP DATA*

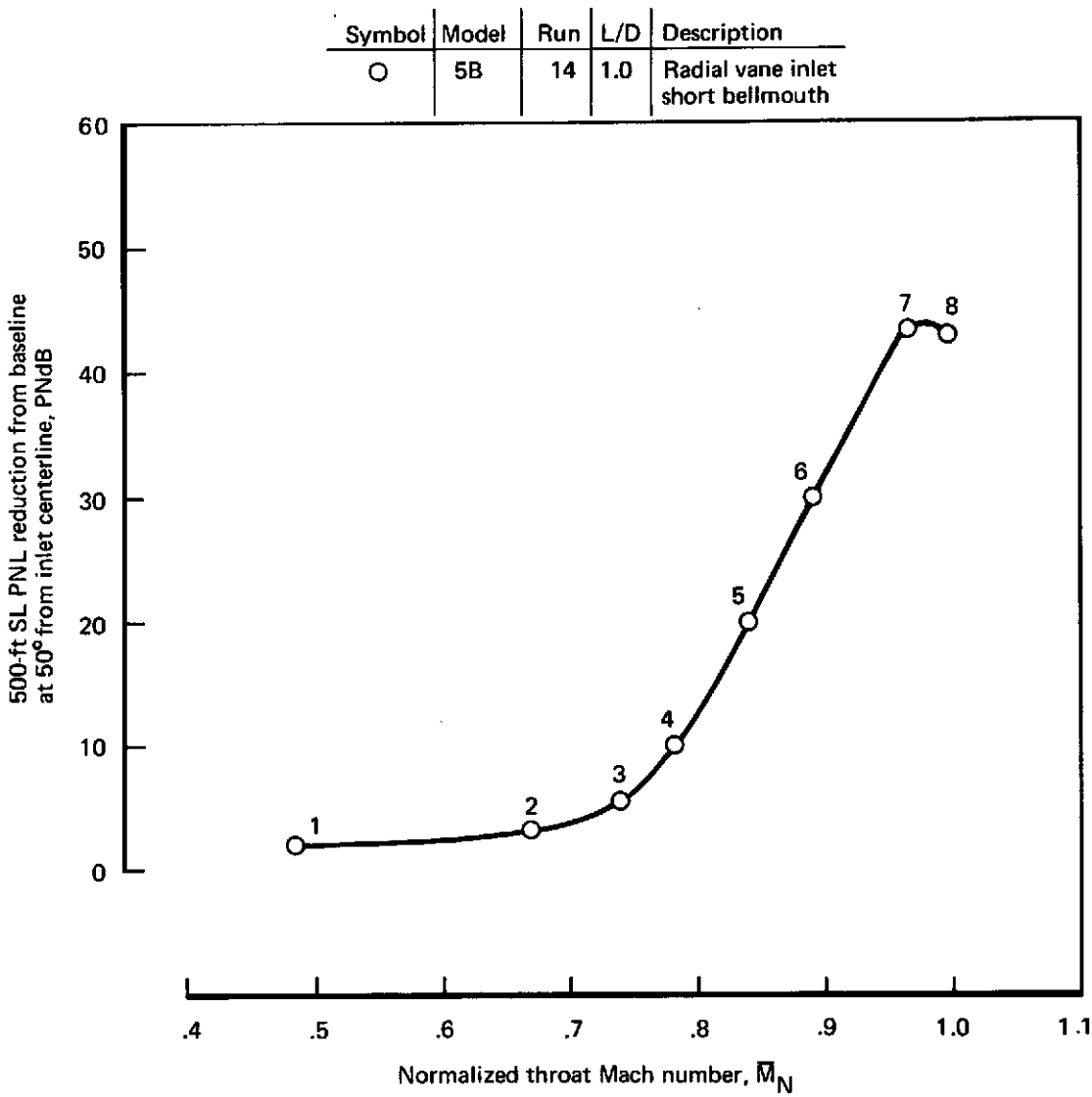


*FIGURE 174.– PNL REDUCTION FROM BASELINE VS NORMALIZED THROAT MACH NUMBER, MULTIPASSAGE INLETS (TAKEOFF), SCALED-UP DATA*

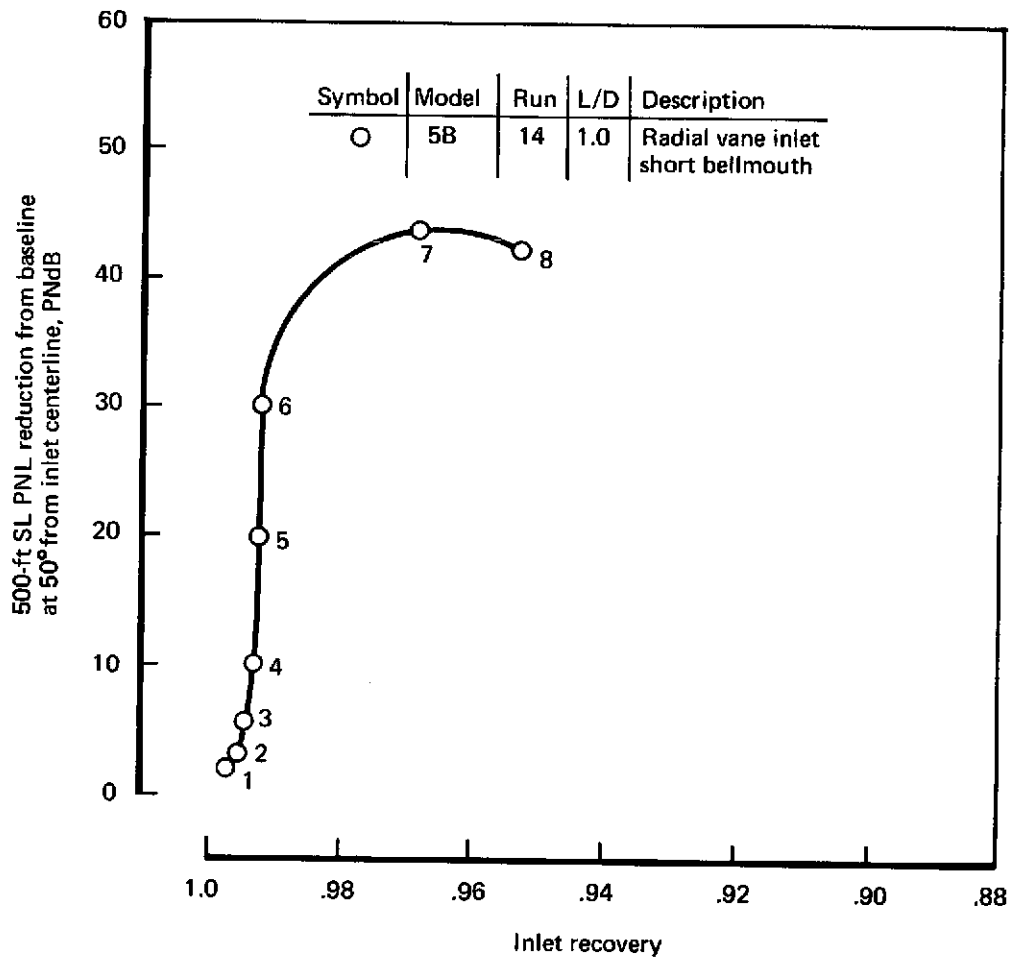


*FIGURE 175.– PNL REDUCTION VS INLET RECOVERY, MULTIPASSAGE INLETS (TAKEOFF), SCALED–UP DATA*

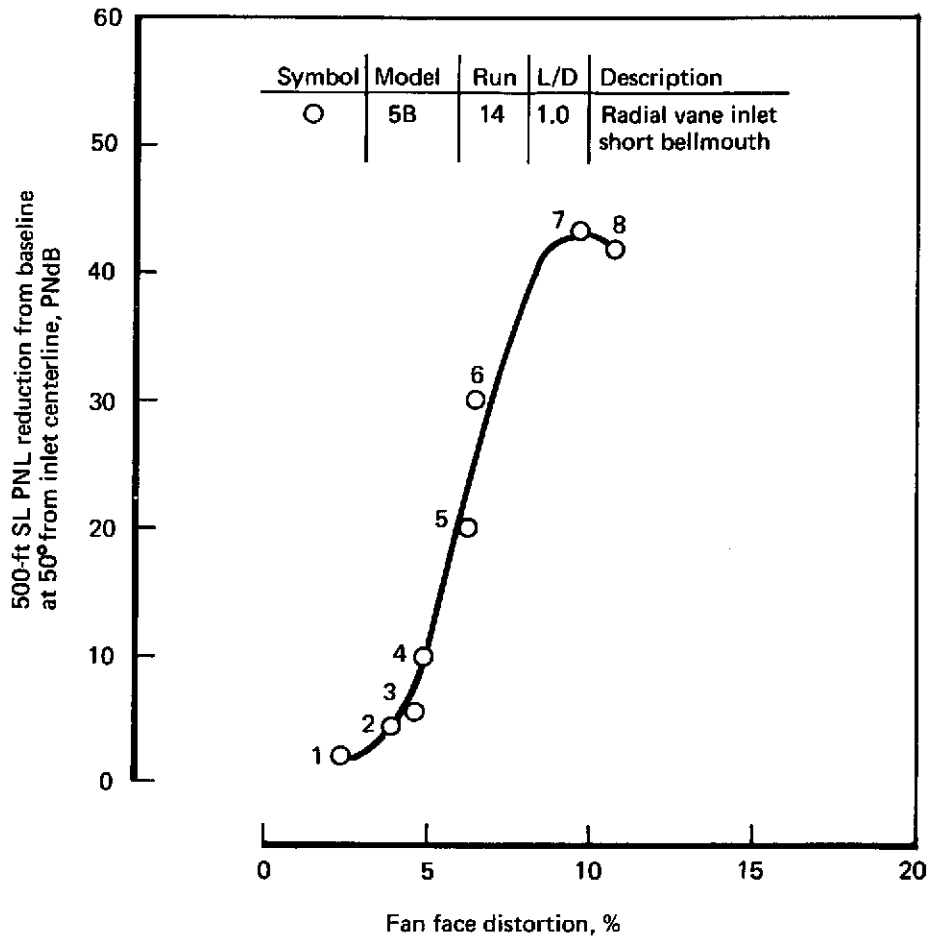


*FIGURE 176.—PNL REDUCTION VS PERCENT FAN FACE DISTORTION, MULTIPASSAGE INLETS (TAKEOFF), SCALED-UP DATA*

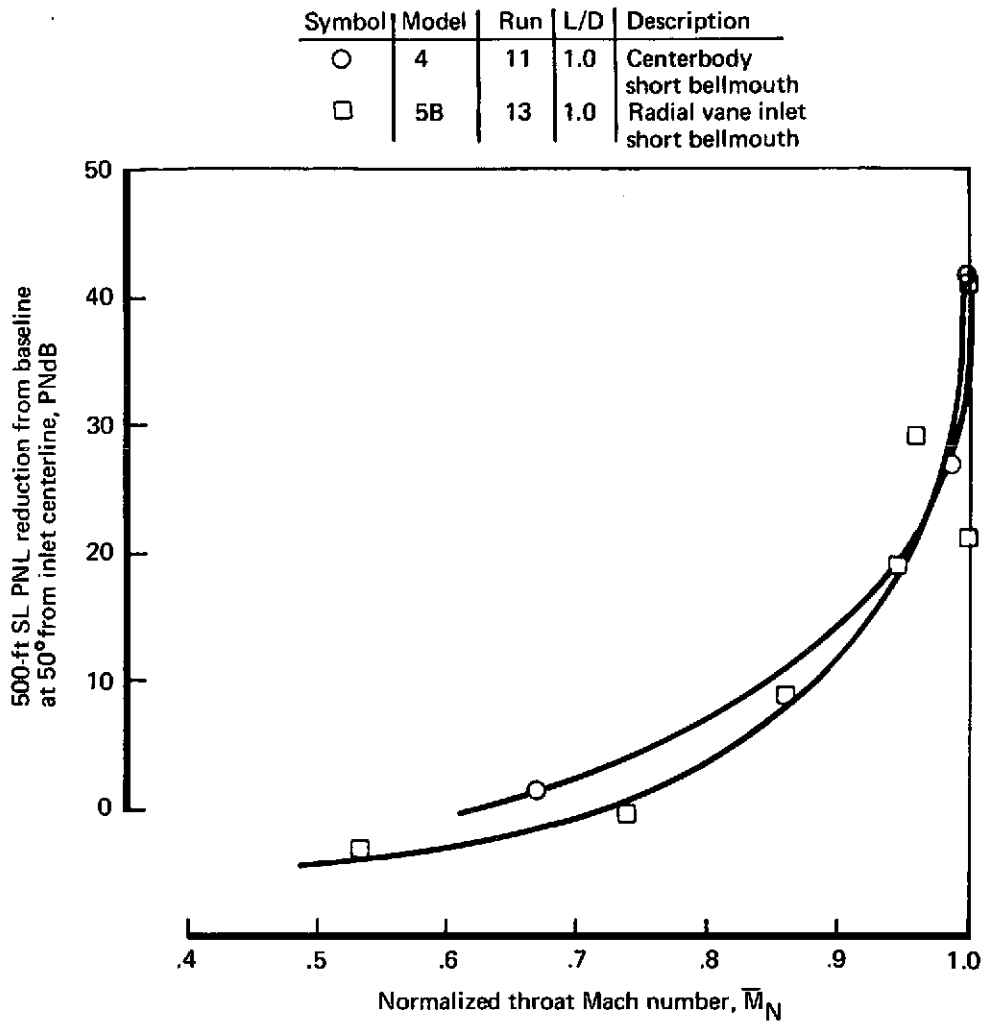


*FIGURE 177.– PNL REDUCTION FROM BASELINE VS NORMALIZED THROAT MACH NUMBER, FINAL CONCEPTS COMPARISONS APPROACH, SCALED-UP DATA*

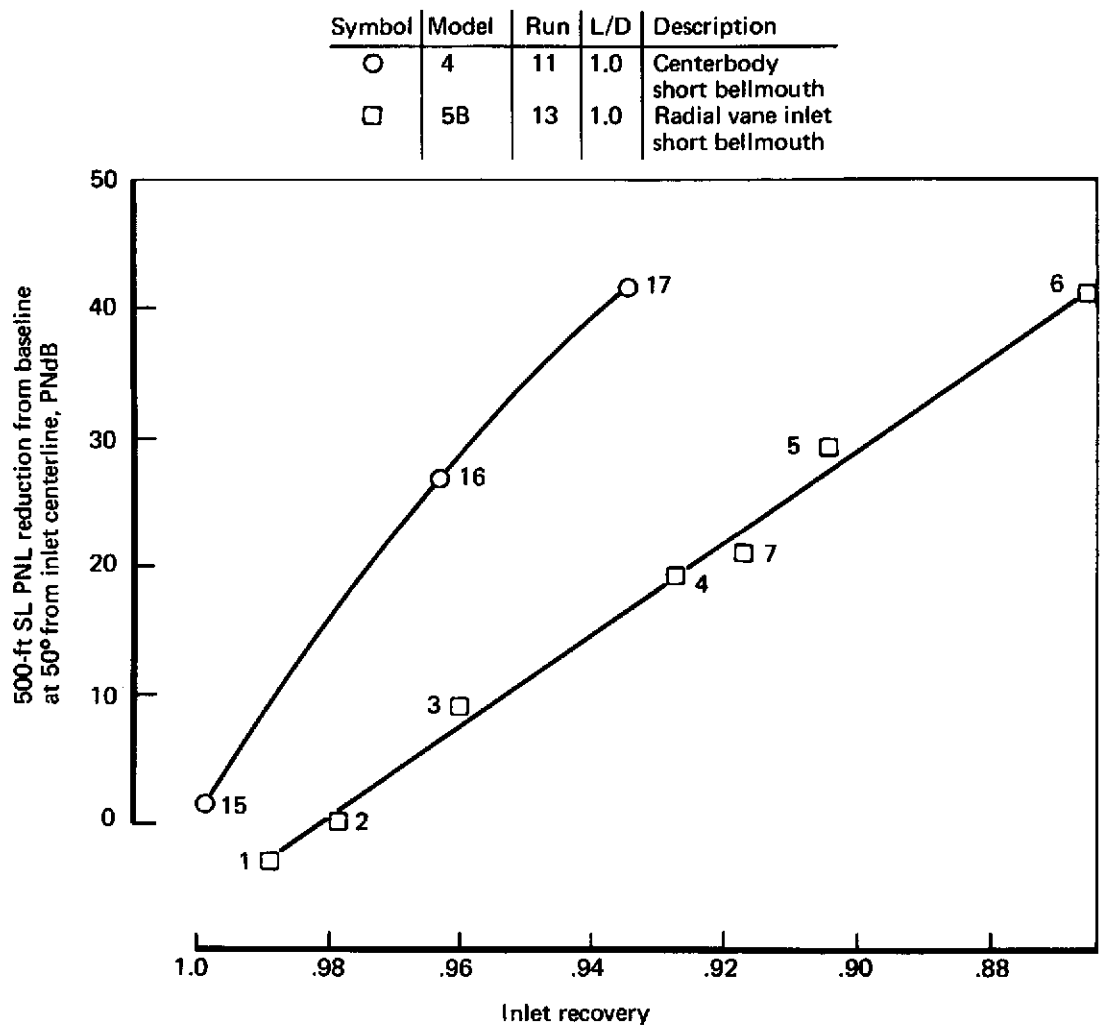


*FIGURE 178.– PNL REDUCTION FROM BASELINE VS INLET RECOVERY, FINAL CONCEPTS COMPARISONS (APPROACH), SCALED-UP DATA*

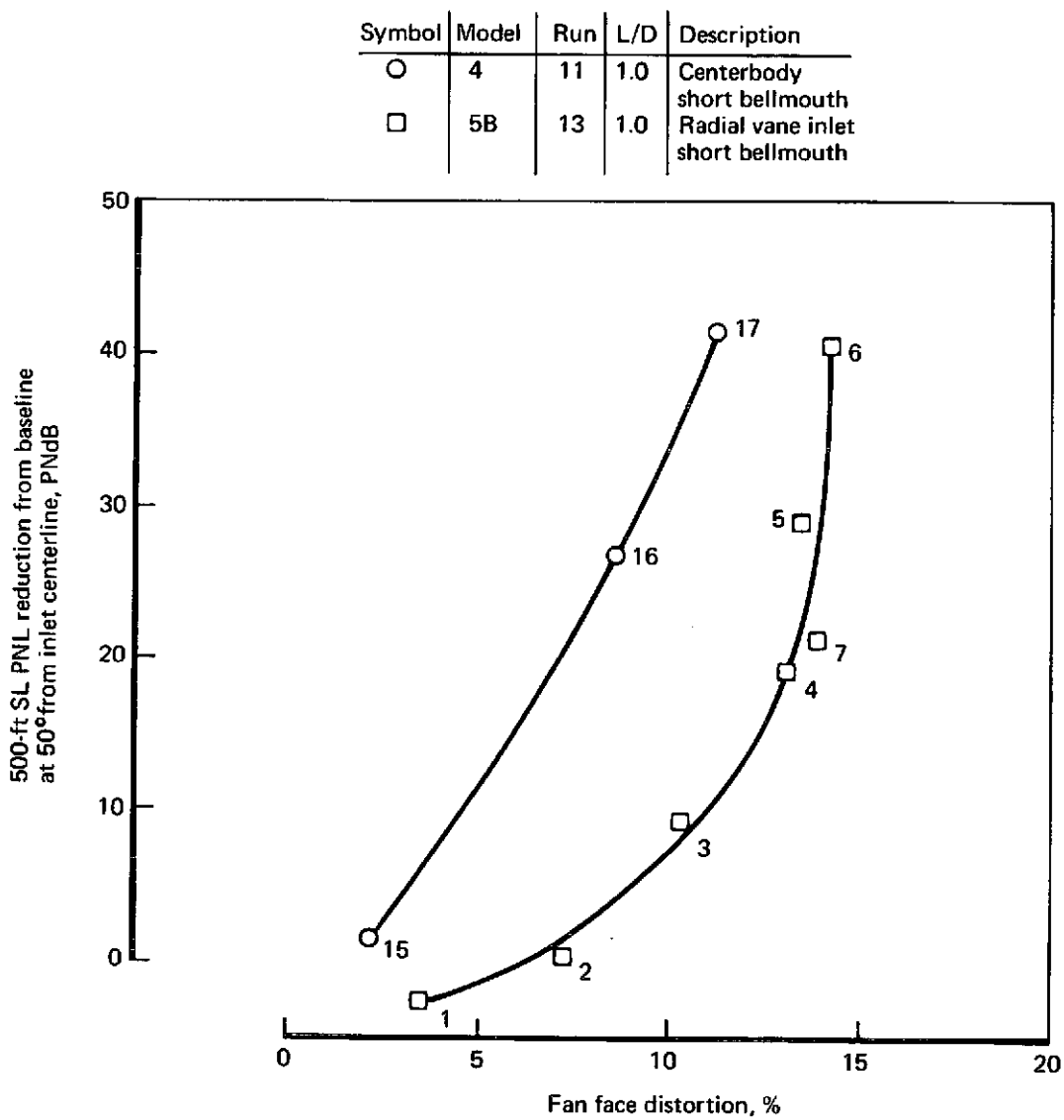


*FIGURE 179.– PNL REDUCTION VS PERCENT FAN FACE DISTORTION, FINAL CONCEPTS COMPARISONS (APPROACH), SCALED-UP DATA*

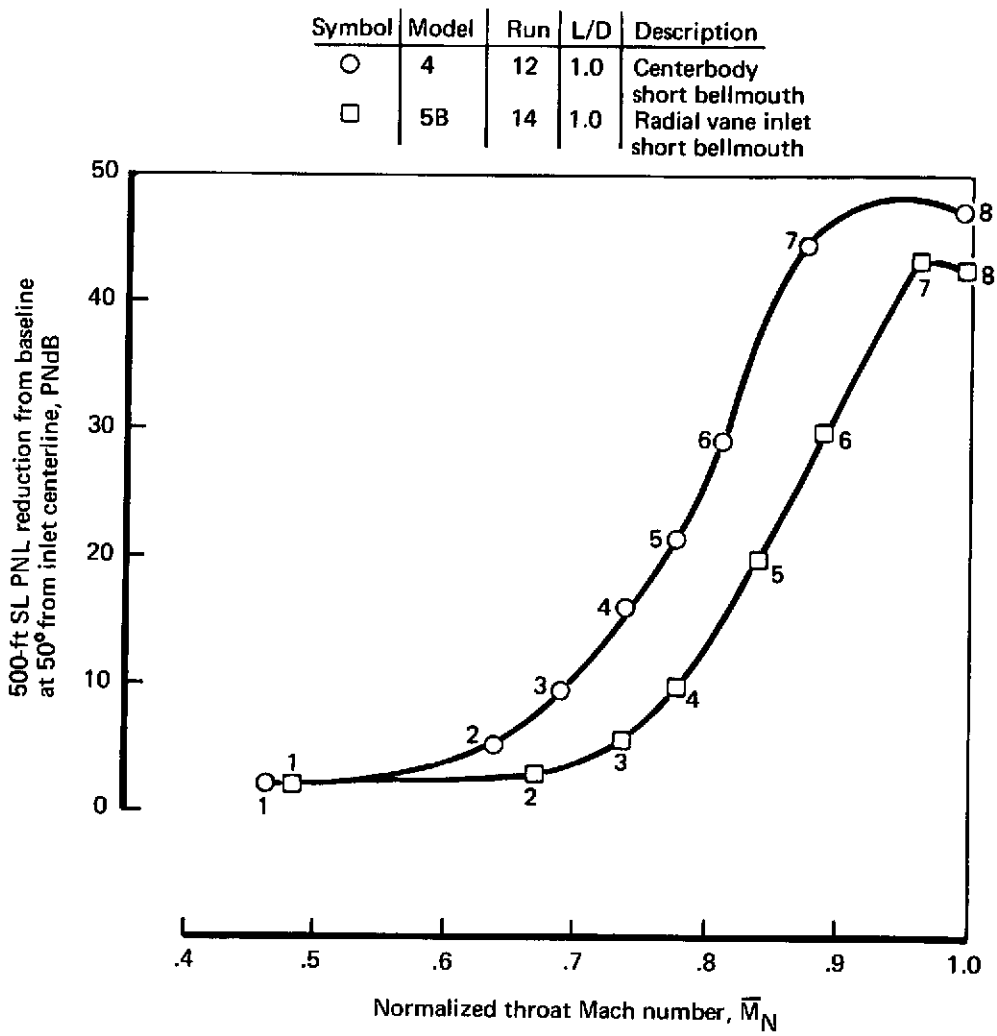


*FIGURE 180.– PNL REDUCTION FROM BASELINE VS NORMALIZED THROAT MACH NUMBER, FINAL CONCEPTS COMPARISONS (TAKEOFF), SCALED-UP DATA*

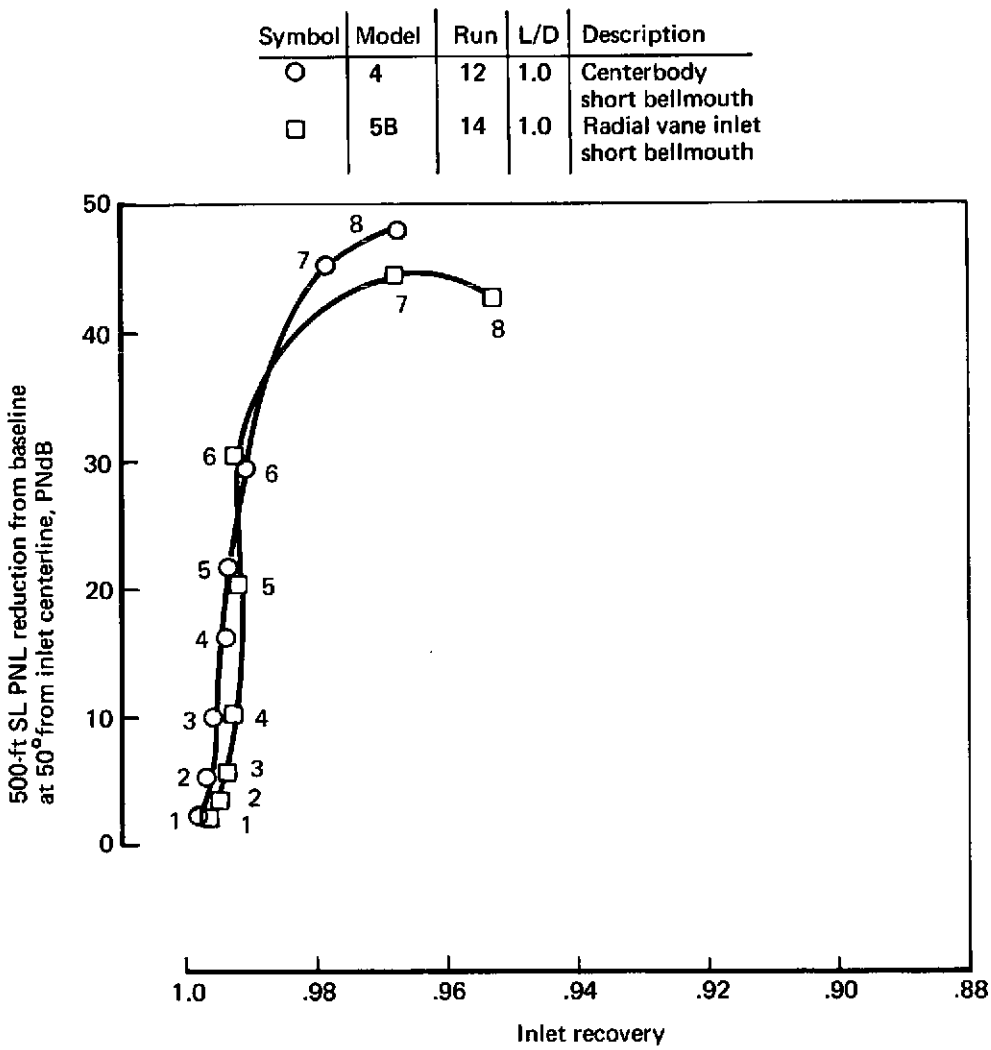


*FIGURE 181.– PNL REDUCTION FROM BASELINE VS INLET RECOVERY, FINAL CONCEPTS COMPARISONS (TAKEOFF), SCALED-UP DATA*

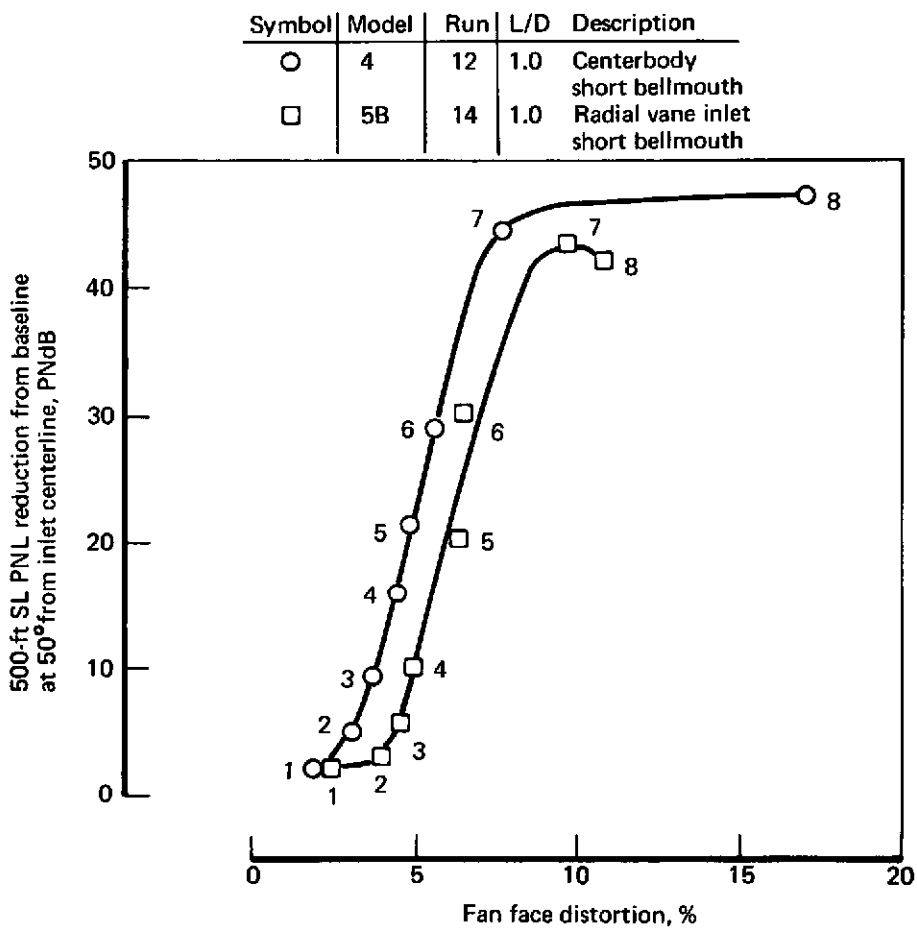


*FIGURE 182.– PNL REDUCTION VS PERCENT FAN FACE DISTORTION, FINAL CONCEPTS COMPARISONS (TAKEOFF), SCALED-UP DATA*

## NOMENCLATURE

| | |
|---|---|
| D | Fan face diameter (inches) |
| DIST | Distortion, $(P_{T_{max}} - P_{T_{min}})/\bar{P}_T$ |
| L | Distance from fan face to highlight plane (inches) |
| M | Mach number |
| M | Average Mach number |
| 1/3 OB | One third octave band (cycles per second) |
| P | Pressure (pounds per square inch) |
| $\bar{P}$ | Average pressure (pounds per square inch) |
| PNL | Perceived noise level (PNdB) |
| REC | Average total pressure recovery, $\bar{P}_T/P_{T_\infty}$ |
| rpm | Fan revolutions per minute |
| SPL | Sound pressure level (dB) |

Subscripts

| | |
|---|---|
| Amb | Ambient (Anechoic chamber) |
| Max | Maximum |
| Min | Minimum |
| N | Normalized |
| T | Total |
| x | Longitudinal distance form highlight plane (inches) |
| $\infty$ | Ambient conditions (Anechoic chamber) |